ASSESSING SECTORAL AND PRIMARY EMISSION CONTRIBUTIONS TO $PM_{2.5}$ POLLUTION OVER NORTH INDIA USING REGIONAL AIR QUALITY MODELLING

INDRANIL NANDI



CENTRE FOR ATMOSPHERIC SCIENCES
INDIAN INSTITUTE OF TECHNOLOGY DELHI
APRIL 2026

©Indian Institute of Technology Delhi (IITD), New Delhi, 2026

Assessing Sectoral and Primary Emission Contributions to $PM_{2.5}$ Pollution over North India Using Regional Air Quality Modelling

By

INDRANIL NANDI

Centre for Atmospheric Sciences

Submitted

In fulfilment of the requirements for the degree of

Doctor of Philosophy

to the



INDIAN INSTITUTE OF TECHNOLOGY DELHI

APRIL 2026

This thesis is dedicated to my inspiration of life, my beloved

Maternal Grandfather & Grandmother

Late Kalicharan Nayak

&

Late Ramarani Nayak

CERTIFICATE

This is to certify that the thesis entitled **"Assessing Sectoral and Primary Emission Contributions to $PM_{2.5}$ Pollution over North India Using Regional Air Quality Modelling"** being submitted by **Mr. Indranil Nandi** to the Indian Institute of Technology Delhi for the award of the degree of **DOCTOR OF PHILOSOPHY**, is a record of his original, bonafide research work. Mr. Indranil Nandi has worked under my guidance and supervision and has fulfilled the requirements for the submission of this thesis. The results presented in this thesis have not been submitted, in part or in full, to any University or Institution for the award of any degree or diploma.

Professor Dilip Ganguly
Centre for Atmospheric Sciences
Indian Institute of Technology Delhi
Hauz Khas, New Delhi-110016, India

New Delhi
April 2026

ACKNOWLEDGEMENTS

I am deeply grateful for the support and encouragement I have received throughout my doctoral journey. This thesis would not have been possible without the guidance, assistance, and inspiration provided by numerous individuals. First and foremost, I offer my sincerest gratitude to my family for their unwavering support throughout all my academic endeavours. Their love, patience, and constant encouragement have been the foundation of my achievements.

I express my deepest sense of obligation and heartfelt gratitude to my supervisor, Prof. Dilip Ganguly, for being a continuous source of inspiration. His expertise, patience, and steadfast guidance have been instrumental in shaping this thesis. Without his support and belief in my abilities, it would have been impossible to overcome the many challenges encountered during my Ph.D. research. My words of appreciation would be incomplete without acknowledging Prof. Sagnik Dey, Head of the Centre whose constant support significantly helped me throughout my Ph.D. journey. I deeply admire his ability to interpret simple statistical curves in meaningful real-world contexts. His guidance in atmospheric processes will continue to inspire my future academic pursuits.

I am also indebted to Prof. Somnath Baidya Roy, former Head of the Centre, and to my SRC committee members Prof. Krishna AchutaRao and Prof. Gazala Habib for their valuable suggestions, time, and encouragement. I sincerely thank the IIT Delhi HPC facility for providing essential computational resources. I am grateful to Prof. Chandra Venkataraman from IIT Bombay for providing the SMoG-COALESCE emission inventory data and for her constructive feedback on my thesis chapters. I also extend my sincere thanks to all faculty members of CAS, IIT Delhi, for their support throughout my coursework.

My warm regards go to all staff members of CAS, IIT Delhi, including the Ph.D. course coordinators, CRC, and DRC, for their timely assistance in every possible way. I would also like to thank my colleagues and friends whose moral support has been a constant source of motivation. I am particularly indebted to Dr. Namita Sinha, Dr. Amit Sharma, and Dr. Pawan Vats for introducing me to Linux and IIT Delhi high-performance computing facility in the initial days of my research. My heartfelt appreciation goes to my dear friends and well-wishers Dr. Sushovan Ghosh, Dr. Subhojit Ghoshal Chowdhury, Dr. Payel Kundu, Alok Kumar, Fahad Imam, Dr. Arshitha Anand K. A., Mukul Kumar, Dr. Vasu Singh, Dr. Shreya Srivastava, Dr. Sankar Prasad

Lahiri, Dr. Chiranjit Das, Dr. Jivesh Dixit, Dr. Ekta Chaudhary, Dr. Deepshikha, Dr. Shiwansha Mishra, Dr. Puneet Sharma, Dr. Sanya Narbar and many others. I extend special gratitude to Manpreet Singh, Sachin Sharma, Vijay Kumar, Mrs. Sushila, and all other staff members at CAS for their constant help and support. Their kindness, encouragement, and friendship have been a true source of joy and confidence.

A special note of thanks is due to Dr. Aheli Das, who supported me immensely during the early stages of my Ph.D., especially during coursework and assignments. I express my deepest gratitude to my parents Tapan Kumar Nandi & Bandana Nandi, my brother Dr. Subhanil Nandi, his wife Mampi Maity Nandi, my wife Suparna Sarkar Nandi, my in laws Prabir Sarkar and Subhashi Sarkar, and especially my daughters Shrinika Nandi & Krittika Nandi, who lovingly sacrificed precious time with her father while he worked tirelessly on his "little television" (laptop). Their understanding and love have been my greatest strength.

I would also like to acknowledge the MERRA-2, Aqua/AIRS, and WRF-Chem science teams for providing aerosol datasets, and the ECMWF science team for the ERA-5 cloud and meteorological variables. I am grateful to IMD and CPCB for the ground-based observational datasets used in this study. I sincerely acknowledge IIT Delhi for providing the Institute Assistantship, without which this research would not have been possible. I am also thankful to the external examiners for their constructive and timely feedback, which greatly improved the quality of this thesis.

Last but certainly not least, I offer my deepest gratitude to the Almighty for being the guiding light throughout this journey. To everyone who played a role directly or indirectly in the successful completion of my Ph.D., I extend my heartfelt thanks. I sincerely apologize for any names I could not mention individually.

New Delhi

April 2026

Indranil Nandi

ABSTRACT

Ambient air pollution is among the most serious environmental health risks worldwide, contributing to nearly seven million premature deaths each year. In India, long-term exposure to fine particulate matter ($PM_{2.5}$) constitutes a major component of this burden, with an estimated 1.67 million deaths in 2019 (≈17.8% of total mortality). The spatiotemporal variability of $PM_{2.5}$, along with its chemical composition and associated exposure risk, is governed by tightly coupled interactions among emission source strength and timing, atmospheric chemical transformation (including secondary aerosol formation), transport and mixing, and boundary-layer meteorology. These couplings are particularly pronounced over the Indo-Gangetic Plain (IGP), a densely populated and economically critical region that frequently experiences severe haze, with short-term $PM_{2.5}$ often exceeding 500 μg m^{-3} during extreme events. The National Capital Territory (NCT) of Delhi, situated in the northwestern IGP, consistently ranks among the most polluted megacities globally, with present-day $PM_{2.5}$ concentrations far above the World Health Organization (WHO) 2021 guideline. Post-monsoon and winter pollution episodes are systematically reinforced by shallow boundary layers, weak winds, persistent temperature inversions, and efficient regional inflow from upwind source regions, highlighting the need for modelling systems that can resolve emission-chemistry-meteorology interactions at the airshed scale rather than within administrative boundaries alone.

The present thesis develops and applies a high-resolution, observation-evaluated WRF-Chem framework to address three linked objectives: (i) reduce dominant sources of uncertainty in $PM_{2.5}$ simulations through systematic evaluation of meteorological and chemical configurations, emission inventories, and nudging strategies; (ii) quantitatively disentangle emission-driven and meteorology-driven contributions to observed $PM_{2.5}$ changes during a major real-world perturbation; and (iii) attribute severe $PM_{2.5}$ over North India, especially the NCT-Delhi airshed, to emission sectors, chemical components, and controlling processes, and assess mitigation pathways consistent with ongoing policy instruments.

First, a coordinated sensitivity analysis across two contrasting meteorological regimes, monsoon (August 2018) and winter (January 2019), demonstrates that WRF-Chem performance over India is strongly configuration dependent, with meteorological boundary conditions exerting first-order control on pollutant realism through their influence on ventilation, precipitation, and boundary-layer evolution. The optimized setup integrates ERA5 meteorological forcing, the YSU

planetary boundary layer scheme, Lin microphysics, the MOZART-MOSAIC chemistry mechanism (including VBS-based SOA representation), the high-resolution SMoG-COALESCE emission inventory, and moderate grid nudging (0.0005 s^{-1}) above the boundary layer. This configuration improves key meteorological drivers (e.g., vertical temperature structure, boundary-layer depth, winds, and rainfall) and the associated pollutant fields relative to reanalysis and satellite constraints, thereby providing a defensible modelling baseline for subsequent attribution and mitigation experiments.

Second, the nationwide COVID-19 lockdown (24 February-30 June 2020) is leveraged as a quasi-experimental perturbation to separate emission and meteorological influences on $PM_{2.5}$. At the national scale, $PM_{2.5}$ decreased by ~29% during the lockdown period; however, the incremental decline relative to preceding years is explained primarily by meteorological variability, while curtailed emissions account for only ~8-9% on average. Sectoral changes were strongly asymmetric: reductions in transport- and activity-linked sectors were partly offset by increased residential emissions during the strict lockdown phase, reflecting intensified household energy use. These results demonstrate that short-term controls concentrated on mobility and industrial activity cannot be expected to deliver sustained compliance with air-quality standards unless persistent, spatially diffuse sources, especially residential combustion and open burning, are mitigated, and they highlight the necessity of explicit meteorological normalization when interpreting apparent air-quality "improvements."

Third, high-resolution simulations for the severe pollution season (September 2019-January 2020) quantify sectoral contributions, chemical composition, and policy-relevant mitigation outcomes for the NCT-Delhi airshed. Crop-residue burning (CRB) is identified as a dominant episodic driver during October-November, contributing ~50% of surface $PM_{2.5}$ in Punjab, ~36% in Haryana, and ~13% in Delhi-NCR, with strong downwind impacts under prevailing north-westerly flow. During winter, secondary aerosol formation is a major contributor to $PM_{2.5}$ over NCT-Delhi, with secondary $PM_{2.5}$ comprising ~57% of total mass, indicating that effective mitigation must target precursor gases (NO_x, SO_2, NH_3, and VOCs) alongside primary particulate emissions. Scenario analysis reveals the limits of city-only interventions: a CRB ban confined to Delhi-NCR yields only ~2-3% reduction in $PM_{2.5}$ over NCT-Delhi, whereas extending CRB mitigation across the full airshed (Punjab–Haryana–Delhi-NCR) yields ~9-10% reduction. A strengthened, policy-consistent package, combining complete CRB elimination with ~50% reductions in residential emissions (via programmes such as PMUY, NCAP, Unnat Chulha Abhiyan, and Saubhagya) and additional transport and industrial controls, reduces wintertime

$PM_{2.5}$ over NCT-Delhi by ~30-40% and remains effective even under stagnant winter conditions, demonstrating that structural emission reductions can substantially lower both baseline concentrations and episode severity.

Overall, this thesis advances a mechanistic and policy-relevant understanding of $PM_{2.5}$ over North India by establishing an optimized WRF-Chem configuration for Indian conditions, demonstrating that meteorology can dominate short-term $PM_{2.5}$ variability during large emission shocks, and quantifying how sectoral emissions, secondary formation, and regional transport jointly sustain severe post-monsoon and winter pollution. The results provide strong evidence that durable improvements in NCT-Delhi air quality require coordinated, multi-sector, airshed-scale strategies that explicitly account for seasonal meteorology and transport pathways, rather than interventions confined to administrative boundaries.

सारांश

परिवेशी वायु प्रदूषण विश्व-भर में सबसे गंभीर पर्यावरणीय स्वास्थ्य जोखिमों में से एक है, जो प्रत्येक वर्ष लगभग 70 लाख समयपूर्व मृत्यु का कारण बनता है। भारत में सूक्ष्म कण पदार्थ ($PM_{2.5}$) के दीर्घकालिक संपर्क से यह बोझ विशेष रूप से अधिक है; वर्ष 2019 में इसके कारण अनुमानित 16.7 लाख मौतें हुईं (कुल मृत्यु का लगभग 17.8%)। $PM_{2.5}$ की स्थानिक-कालिक परिवर्तनशीलता, उसका रासायनिक संघटन तथा उससे जुड़ा संपर्क जोखिम, उत्सर्जन स्रोतों की तीव्रता और समय, वायुमंडलीय रासायनिक रूपांतरण (जिसमें द्वितीयक एरोसोल निर्माण शामिल है), परिवहन व मिश्रण प्रक्रियाएँ तथा सीमांत-परत मौसम विज्ञान के बीच घनिष्ठ रूप से जुड़े अंतःक्रियाओं द्वारा नियंत्रित होते हैं। ये अंतःक्रियाएँ विशेष रूप से इंडो-गैंगेटिक प्लेन (IGP) में अत्यंत प्रबल हैं यह क्षेत्र अत्यधिक जनसंख्या घनत्व और आर्थिक महत्व वाला है तथा यहाँ अक्सर गंभीर धुंध की घटनाएँ होती हैं, जिनमें अल्पकालिक $PM_{2.5}$ चरम स्थितियों में 500 $\mu g\ m^{-3}$ से भी अधिक हो जाता है। IGP के उत्तर-पश्चिमी भाग में स्थित राष्ट्रीय राजधानी क्षेत्र (NCT) दिल्ली निरंतर विश्व के सर्वाधिक प्रदूषित महानगरों में शामिल रहता है, जहाँ वर्तमान $PM_{2.5}$ स्तर विश्व स्वास्थ्य संगठन (WHO) की 2021 की मार्गदर्शक सीमा से कहीं अधिक हैं। मानसूनोत्तर और शीतकालीन प्रदूषण घटनाएँ उथली सीमांत-परत, कमजोर पवनें, स्थायी ताप-उलटाव तथा पवनोन्मुख स्रोत क्षेत्रों से प्रभावी क्षेत्रीय प्रवाह के कारण व्यवस्थित रूप से सुदृढ़ होती हैं। यह तथ्य इस बात पर बल देता है कि केवल प्रशासनिक सीमाओं तक सीमित न रहकर, उत्सर्जन–रसायन–मौसम विज्ञान की अंतःक्रियाओं को वायु-क्षेत्र (airshed) स्तर पर सुलझाने में सक्षम मॉडलिंग प्रणालियों की आवश्यकता है।

यह शोधप्रबंध एक उच्च-रिज़ॉल्यूशन, प्रेक्षण-आधारित मूल्यांकनित WRF-Chem ढाँचे का विकास और अनुप्रयोग करता है, ताकि तीन परस्पर संबद्ध उद्देश्यों को संबोधित किया जा सके: (i) मौसमीय एवं रासायनिक विन्यासों, उत्सर्जन इन्वेंटरी तथा नजिंग रणनीतियों के व्यवस्थित मूल्यांकन के माध्यम से $PM_{2.5}$ सिमुलेशनों में प्रमुख अनिश्चितताओं को कम करना; (ii) एक प्रमुख वास्तविक-दुनिया व्यवधान के दौरान देखे गए $PM_{2.5}$ परिवर्तनों में उत्सर्जन-प्रेरित और मौसम-प्रेरित योगदानों को मात्रात्मक रूप से अलग करना; तथा (iii) उत्तर भारत, विशेषकर NCT-दिल्ली वायु-क्षेत्र में गंभीर $PM_{2.5}$ के लिए उत्सर्जन क्षेत्रों, रासायनिक घटकों और नियंत्रक प्रक्रियाओं का आरोपण (attribution) करना तथा प्रचलित नीतिगत उपकरणों के अनुरूप शमन मार्गों का आकलन करना।

प्रथम, दो परस्पर भिन्न मौसमीय अवस्थाओं मानसून (अगस्त 2018) और शीतकाल (जनवरी 2019)-में किए गए समन्वित संवेदनशीलता विश्लेषण से यह प्रदर्शित होता है कि भारत में WRF-Chem का प्रदर्शन

विन्यास पर अत्यधिक निर्भर है, तथा मौसमीय सीमा-स्थितियाँ प्रदूषक यथार्थता पर प्रथम-क्रम का नियंत्रण रखती हैं, क्योंकि वे वेंटिलेशन, वर्षा और सीमांत-परत के विकास को प्रभावित करती हैं। अनुकूलित विन्यास में ERA5 मौसमीय फोर्सिंग, YSU ग्रहणीय सीमांत-परत योजना, Lin माइक्रोफिज़िक्स, MOZART-MOSAIC रसायन तंत्र (जिसमें VBS-आधारित SOA निरूपण शामिल है), उच्च-रिज़ॉल्यूशन SMoG-COALESCE उत्सर्जन इन्वेंटरी तथा सीमांत-परत के ऊपर मध्यम ग्रिड नजिंग ($0.0005\ s^{-1}$) सम्मिलित हैं। यह विन्यास प्रमुख मौसमीय चालकों (जैसे ऊर्ध्वाधर ताप संरचना, सीमांत-परत की गहराई, पवनें और वर्षा) तथा उनसे संबद्ध प्रदूषक क्षेत्रों में पुनर्विश्लेषण और उपग्रह सीमाओं की तुलना में सुधार करता है, जिससे आगे के आरोपण और शमन प्रयोगों के लिए एक विश्वसनीय मॉडलिंग आधार प्राप्त होता है।

द्वितीय, राष्ट्रव्यापी COVID-19 लॉकडाउन (24 फ़रवरी-30 जून 2020) को एक अर्ध-प्रायोगिक व्यवधान के रूप में उपयोग किया गया, ताकि $PM_{2.5}$ पर उत्सर्जन और मौसम के प्रभावों को अलग किया जा सके। राष्ट्रीय स्तर पर लॉकडाउन अवधि के दौरान $PM_{2.5}$ में लगभग 29% की कमी आई; किंतु पूर्ववर्ती वर्षों की तुलना में अतिरिक्त गिरावट मुख्यतः मौसमीय परिवर्तनशीलता से समझाई जाती है, जबकि उत्सर्जन में कटौती का औसत योगदान केवल ~8-9% रहा। क्षेत्रवार परिवर्तन अत्यंत असममित थे: परिवहन और गतिविधि-संबद्ध क्षेत्रों में कटौती को कड़े लॉकडाउन चरण में आवासीय उत्सर्जनों में वृद्धि ने आंशिक रूप से संतुलित कर दिया, जो घरेलू ऊर्जा उपयोग में वृद्धि को दर्शाता है। ये निष्कर्ष दर्शाते हैं कि केवल गतिशीलता और औद्योगिक गतिविधि पर केंद्रित अल्पकालिक नियंत्रण वायु-गुणवत्ता मानकों के स्थायी अनुपालन को सुनिश्चित नहीं कर सकते, जब तक कि स्थायी और व्यापक स्रोत-विशेषकर आवासीय दहन और खुले दहन-का शमन न किया जाए; साथ ही ये वायु-गुणवत्ता में दिखने वाले "सुधारों" की व्याख्या में स्पष्ट मौसमीय सामान्यीकरण की आवश्यकता को रेखांकित करते हैं।

तृतीय, गंभीर प्रदूषण मौसम (सितंबर 2019-जनवरी 2020) के लिए उच्च-रिज़ॉल्यूशन सिमुलेशनों के माध्यम से NCT-दिल्ली वायु-क्षेत्र में क्षेत्रीय योगदान, रासायनिक संघटन और नीति-प्रासंगिक शमन परिणामों का मात्रात्मक आकलन किया गया। फसल-अवशेष दहन (CRB) को अक्टूबर–नवंबर के दौरान प्रमुख प्रासंगिक चालक के रूप में पहचाना गया, जो पंजाब में सतही $PM_{2.5}$ का ~50%, हरियाणा में ~36% और दिल्ली-NCR में ~13% योगदान देता है, तथा प्रचलित उत्तर-पश्चिमी प्रवाह के तहत मजबूत पवनोत्तर प्रभाव उत्पन्न करता है। शीतकाल के दौरान NCT-दिल्ली में द्वितीयक एरोसोल निर्माण $PM_{2.5}$ का एक प्रमुख घटक है; द्वितीयक $PM_{2.5}$ कुल द्रव्यमान का लगभग ~57% है, जो संकेत देता है कि प्रभावी शमन के लिए प्राथमिक कण उत्सर्जनों के साथ-साथ अग्रदूत गैसों (NO_x, SO_2, NH_3 और VOCs) को भी लक्षित करना होगा। परिदृश्य विश्लेषण शहर-केवल हस्तक्षेपों की सीमाएँ उजागर करता है: यदि CRB प्रतिबंध केवल दिल्ली-NCR तक

सीमित हो, तो NCT-दिल्ली में $PM_{2.5}$ में मात्र ~2-3% की कमी आती है; जबकि पूरे वायु-क्षेत्र (पंजाब-हरियाणा-दिल्ली-NCR) में CRB शमन को विस्तारित करने पर ~9-10% की कमी प्राप्त होती है। एक सुदृढ़, नीति-संगत पैकेज-जिसमें CRB का पूर्ण उन्मूलन, आवासीय उत्सर्जनों में ~50% की कमी (PMUY, NCAP, उन्नत चूल्हा अभियान और सौभाग्य जैसी योजनाओं के माध्यम से), तथा अतिरिक्त परिवहन और औद्योगिक नियंत्रण शामिल हैं-NCT-दिल्ली में शीतकालीन $PM_{2.5}$ को ~30-40% तक कम करता है और ठहरी हुई शीतकालीन परिस्थितियों में भी प्रभावी बना रहता है। यह दर्शाता है कि संरचनात्मक उत्सर्जन कटौतियाँ आधारभूत सांद्रताओं और प्रकरण-तीव्रता दोनों को उल्लेखनीय रूप से घटा सकती हैं।

समग्र रूप से, यह शोधप्रबंध भारतीय परिस्थितियों के लिए एक अनुकूलित WRF-Chem विन्यास स्थापित कर, बड़े उत्सर्जन झटकों के दौरान अल्पकालिक $PM_{2.5}$ परिवर्तनशीलता में मौसम विज्ञान के प्रभुत्व को प्रदर्शित कर, तथा क्षेत्रीय परिवहन, द्वितीयक निर्माण और क्षेत्रीय उत्सर्जनों की संयुक्त भूमिका को मात्रात्मक रूप से स्पष्ट कर, उत्तर भारत में $PM_{2.5}$ के प्रति एक यांत्रिक और नीति-प्रासंगिक समझ को आगे बढ़ाता है। परिणाम सशक्त प्रमाण प्रदान करते हैं कि NCT-दिल्ली की वायु-गुणवत्ता में टिकाऊ सुधार के लिए प्रशासनिक सीमाओं तक सीमित हस्तक्षेपों के बजाय, मौसमी मौसम विज्ञान और परिवहन मार्गों को स्पष्ट रूप से ध्यान में रखते हुए, बहु-क्षेत्रीय और वायु-क्षेत्र-स्तरीय समन्वित रणनीतियों की आवश्यकता है।

Contents

CERTIFICATE ..... **i**
ACKNOWLEDGEMENTS ..... **ii**
ABSTRACT ..... **iv**
सारांश ..... **vii**
GLOSSARY ..... **xiii**
List of Figures ..... **xvi**
List of Tables ..... **xxvii**
Chapter 1: Introduction, Motivation, Research Questions & Thesis Objectives **1**
1.1 Introduction **2**
1.1.1 Air Pollution and Particulate Matter Pollution **3**
1.1.2 Vertical Structure of the Atmosphere, Atmospheric Boundary Layer and Diurnal Cycle of Atmospheric Boundary Layer **5**
1.1.3 Environmental and Geographical Significance of India: A Northern Perspective **8**
1.1.4 Principles and Applications of Online Chemical Transport Models: Focus on WRF-Chem **11**
1.2 Motivation, Knowledge Gaps and Scope of the Thesis **16**
1.3 Research Questions **21**
1.4 Thesis Objectives **22**
1.5 Structure of the Thesis **22**
Chapter 1: Introduction **22**
Chapter 2: Improving Regional $PM_{2.5}$ Modelling over North India **23**
Chapter 3: Drivers of $PM_{2.5}$ Changes during the COVID-19 Period **23**
Chapter 4: Sectoral and Species Drivers of Surface $PM_{2.5}$ in Delhi Airshed **23**
Chapter 5: Toward Improving Regional $PM_{2.5}$ in the NCT Delhi Airshed **24**
Chapter 6: Summary and Scope for Future Work **24**
Chapter 2: Improving Regional $PM_{2.5}$ Modelling over North India: A WRF-Chem Configuration and Sensitivity Study **25**
2.1 Introduction **26**
2.2 Methodology **28**
2.2.1 Model Configuration **28**
2.2.2 Sensitivity Experiments **31**
2.2.2.1 Meteorological Initial and Boundary Conditions **31**
2.2.2.2 Planetary Boundary Layer (PBL) Schemes **32**
2.2.2.3 Microphysics Schemes **33**
2.2.2.4 Chemical Mechanisms **34**
2.2.2.5 Emission Inventories **34**

2.2.2.6 Grid Nudging **36**
2.2.3 Validation Datasets **37**
2.3 Results and Discussion **39**
2.3.1 Meteorological Sensitivity Simulations **39**
2.3.2 PBL and Microphysics Scheme Sensitivity **46**
2.3.3 Chemical Mechanism and Emission Inventory Sensitivity ..... Error! Bookmark not defined.
2.3.4 Grid Nudging Sensitivity **58**
2.4 Summary and Conclusions **64**
Chapter 3: Drivers of $PM_{2.5}$ Changes over North India during the COVID-19 Period: Emissions Controls versus Meteorology **67**
3.1 Introduction **68**
3.2 Datasets and Methodology **70**
3.2.1 Model Description and Simulation Details **70**
3.2.2 Satellite-$PM_{2.5}$ database **73**
3.2.3 Validation and Quantification of Contributions Process **76**
3.2.3.1 Validation using CPCB measurements and MERRA-2 reanalysis **79**
3.2.3.2 Analysis for using the 2015-2019 Average to Estimate Meteorology-Driven Variability in 2020 ..... **85**
3.3 Results and Discussion **91**
3.3.1 Pre-Lockdown Conditions and Initial Lockdown-Driven Changes **91**
3.3.2 Quantifying the Relative Contributions of Emission Reductions and Meteorological Variations **93**
3.3.3 Normalized Anomaly and Ventilation Coefficient Analysis: Seasonal and Spatial Heterogeneity **98**
3.4 Summary and Conclusions **102**
Chapter 4: Disentangling Sectoral and Species Drivers of Surface $PM_{2.5}$ in the NCT Delhi Airshed **105**
4.1 Introduction **106**
4.2 Methodology **110**
4.2.1 Model Description **110**
4.2.2 Simulation Details **114**
4.2.3 Validation of WRF-Chem simulated $PM_{2.5}$ concentrations **117**
4.3 Results and Discussion **117**
4.3.1 Validation using satellite-derived $PM_{2.5}$, CPCB measurements and MERRA-2 reanalysis **117**

4.3.2 Sectoral Contributions and Chemical Composition of $PM_{2.5}$ in the NCT-Delhi Airshed 123
4.3.2.1 Sectoral Influences and Seasonal Structure of the Airshed Burden 123
4.3.2.2 Primary versus Secondary $PM_{2.5}$: Dominance of Secondary Formation in Winter 127
4.3.2.3 Regional heterogeneity and the role of CRB in extreme episodes 128
4.3.2.4 Comparison of Results with earlier literature and interpretation of residual mass 130
4.4 Summary and Conclusions 132
Chapter 5: Toward Improving Regional $PM_{2.5}$ in the NCT Delhi Airshed: A Comparative Evaluation of Control Strategies 136
5.1 Introduction 137
5.2 Datasets and Methodology 141
5.2.1 Model Description and Simulation Details 141
5.2.2 Policy Context and Design of Mitigation Scenarios 145
5.2.2.1 Indian Government Policies to Reduce Residential Sector Air Pollutant Emissions 146
5.2.2.2 Indian Government Policies to Reduce Transport Sector Air Pollutant Emissions 147
5.2.2.3 Indian Government Policies to Reduce Industrial Sector Air Pollutant Emissions 149
5.3 Results and Discussion 150
5.3.1 Impact of Delhi-NCR Only Mitigation on Air Quality in NCT-Delhi 150
5.3.2 Benefits of Airshed-Scale Mitigation for NCT-Delhi Air Quality 163
5.3.3 Role of Meteorology in Modulating $PM_{2.5}$ and Mitigation Effectiveness 166
5.4 Summary and Conclusions 174
Chapter 6: Summary and Scope for Future Work 177
6.1 Summary 178
6.2 Limitations of the Presented Study 181
6.3 Future scope of work 181
References 183
List of Publication 211
Curriculum Vitae 212

GLOSSARY

1	Adjustment Factors **(AFs)**	**26**	Emissions Database for Global Atmospheric Research version 5 **(EDGAR-v5)**
2	Advanced Research WRF **(ARW)**	**27**	Emissions Database for Global Atmospheric Research version 6.1 **(EDGAR-v6.1)**
3	Aerosol Optical Depth **(AOD)**	**28**	Emission Factors **(EFs)**
4	Agricultural Waste Burning **(AWB)**	**29**	European Centre for Medium-Range Weather Forecasts **(ECMWF)**
5	Air Pollution Index **(API)**	**30**	Fast Tropospheric Ultraviolet–Visible **(FTUV)**
6	Air Quality Index **(AQI)**	**31**	Faster Adoption and Manufacturing of Hybrid and Electric Vehicles **(FAME)**
7	Ammonia **(NH_3)**	**32**	Fine Particulate Matter **($PM_{2.5}$)**
8	Ammonium **(NH_4^+)**	**33**	Fire Inventory of the National Center for Atmospheric Research **(FINN-v2.5)**
9	Argon **(Ar)**	**34**	Flue Gas Desulfurization **(FGD)**
10	Atmospheric Boundary Layer **(ABL)**	**35**	Four-Dimensional Data Assimilation **(FDDA)**
11	Atmospheric Infrared Radiation Sounder **(Aqua/AIRS)**	**36**	Global Burden of Disease **(GBD)**
12	Bharat Stage **(BS)** Emission Norms	**37**	Graded Response Action Plan **(GRAP)**
13	Biomass Burning **(BB)**	**38**	Gridded Population of World Version 4 **(GPW-v4)**
14	Biomass Burning Organic Aerosol **(BBOA)**	**39**	Helium **(He)**
15	Black Carbon **(BC)**	**40**	High Resolution Time of Flight Aerosol Mass Spectrometer **(HR-ToF-AMS)**
16	Boundary Layer Height **(BLH)**	**41**	Hydrocarbon like Organic Aerosol **(HOA)**
17	Carbon Bond Mechanism version Z - Model for Simulating Aerosol Interactions and Chemistry **(CBMZ-MOSAIC)**	**42**	Hydrocarbons **(HC)**
18	Carbon Dioxide **(CO_2)**	**43**	Hydroxyl radical **(OH)**
19	Carbon Monoxide **(CO)**	**44**	Indo Gangetic Plain **(IGP)**
20	Central Financial Assistance **(CFA)** for Rooftop Solar **(RTS)**	**45**	Indian Council of Medical Research **(ICMR)**
21	Central Pollution Control Board **(CPCB)**	**46**	Indian National Air Quality Standards **(INAQS)**
22	Chloride **(Cl^-)**	**47**	Krypton **(Kr)**
23	Clean India Mission **(CIM)**	**48**	Liquefied Natural Gas **(LNG)**
24	Coefficient of Determination **(r^2)**	**49**	Mean Absolute Error **(MAE)**
25	COvid-19 adjustmeNt Factors fOR eMissions **(CONFORM)**	**50**	Methane **(CH_4)**

51	Commission for Air Quality Management **(CAQM)**	**78**	Model of Emissions of Gases and Aerosols from Nature **(MEGAN)**
52	Compressed Natural Gas **(CNG)**	**79**	Pearson Correlation Coefficient **(r)**
53	Continuous Emission Monitoring Systems **(CEMS)**	**80**	Piped Natural Gas **(PNG)**
54	Coronavirus Disease 2019 **(COVID-19)**	**81**	Planetary Boundary Layer **(PBL)**
55	Crop Residue Burning **(CRB)**	**82**	Polycyclic Aromatic Hydrocarbons **(PAHs)**
56	Eastern Indo-Gangetic Plain **(EIGP)**	**83**	Pollutant Standards Index **(PSI)**
57	Emissions Database for Global Atmospheric Research – Hemispheric Transport of Air Pollution version 3 **(EDGAR-HTAPv3)**	**84**	Pradhan Mantri Sahaj Bijli Har Ghar Yojana **(Saubhagya Scheme)**
58	Model for OZone And Related chemical Tracers - Model for Simulating Aerosol Interactions and Chemistry **(MOZART-MOSAIC)**	**85**	Pradhan Mantri Ujjwala Yojana **(PMUY)**
59	Model for Simulating Aerosol Interactions and Chemistry **(MOSAIC)**	**86**	Primary Organic Aerosol **(POA)**
60	Modal Aerosol Dynamics Model for Europe - Secondary Organic Aerosol Model **(MADE-SORGAM)**	**87**	Root Mean Square Error **(RMSE)**
61	National Ambient Air Quality Standards **(NAAQS)**	**88**	Secondary Inorganic Aerosol **(SIA)**
62	National Air Quality Index **(NAQI)**	**89**	Secondary Organic Aerosol **(SOA)**
63	Delhi National Capital Region **(Delhi-NCR)**	**90**	Sodium **(Na^+)**
64	National Capital Territory of Delhi **(NCT-Delhi)**	**91**	Solid Fuel Combustion Organic Aerosol **(SFC-OA)**
65	National Clean Air Program **(NCAP)**	**92**	Speciated Multi-Pollutant Generator version 2 **(SMOG-v2)**
66	Neon **(Ne)**	**93**	Sulfur Dioxide **(SO_2)**
67	Nitrate **(NO_3^-)**	**94**	Sulfate **(SO_4^{2-})**
68	Nitrogen **(N_2)**	**95**	Time of Flight Aerosol Chemical Speciation Monitor **(ToF-ACSM)**
69	Nitrogen Oxides **(NO_x)**	**96**	Ultrafine Particles **(UFPs)**
70	Nitrous Oxide **(N_2O)**	**97**	Ventilation Coefficient **(VC)**
71	Non-Methane Hydrocarbons **(NMHCs)**	**98**	Visible Infrared Imaging Radiometer Suite **(VIIRS)**
72	North India **(NI)**	**99**	Volatile Organic Compounds **(VOCs)**
73	Northeast India **(NEI)**	**100**	Volatility Basis Set **(VBS)**
74	Numerical Weather Prediction **(NWP)**	**101**	Weather Research and Forecasting **(WRF)** Model
75	Organic Aerosol **(OA)**	**102**	Weather Research and Forecasting model coupled with Chemistry **(WRF-Chem)**
76	Organic Carbon **(OC)**	**103**	West India **(WI)**
77	Organic Matter **(OM)**	**104**	Whole Atmosphere Community Climate Model **(WACCM)**

105	Oxygen **(O_2)**	**109**	Particulate Matter **(PM)**
106	Ozone **(O_3)**	**110**	Thermal Power Plants **(TPPs)**
107	Parts Per Billion by volume **(ppb)**	**111**	World Health Organization **(WHO)**
108	Parts Per Million by volume **(ppm)**	**112**	Xenon **(Xe)**

List of Figures

Chapter 1

Figure 1.1: Vertical Structure of the Earth's Atmosphere adapted from Schlatter, 2010……..006

Figure 1.2: Daily Evolution of the Atmospheric Boundary Layer adapted from Stull, 1988……008

Figure 1.3: India Region with Simulated Topographic Height (left) and 2020 Population Density from Gridded Population of World Version 4 (GPWv4) (right)……....009

Figure 1.4: North India Region with 2020 Population Density from GPWv4……..010

Figure 1.5: WRF-Chem Modelling System Flow Chart adapted from Zhang et al., 2021……....012

Figure 1.6: Monthly active Fire Locations from the Visible Infrared Imaging Radiometer Suite (VIIRS) for 2019, with the Total Fire Count across India displayed within the plot……..015

Chapter 2

Figure 2.1: WRF-Chem simulation domain overlaid with Topographic Height (first panel) and different Indian states that have been used for validating the model performance (second panel) are shown, overlaid with CPCB measurement sites available for 2018, 2019. This setup was used to examine the WRF-Chem model performance with multiple sensitivity choices over the Indian region……...029

Figure 2.2: Spatial distribution of surface temperature observed by Aqua/AIRS over the Indian region, and the difference in simulated temperature from various WRF-Chem meteorology sensitivity simulations (top panel). Inset values report the domain-mean ± spatial standard deviation ($\mu \pm 1\sigma$) over the Indian landmass, along with Mean Bias Error (MBE) relative to Aqua/AIRS. Daily mean time series comparison of surface relative humidity for various Indian states from different WRF-Chem meteorology and grid nudging sensitivity simulations with CPCB measurements and MERRA2 (bottom panel). Temporal mean ± SD ($\mu \pm 1\sigma$) and correlation coefficient (r) of Nudged03 indicated within the panel…….040

Figure 2.3: Spatial distribution of surface relative humidity observed by Aqua/AIRS over the Indian region, and the corresponding differences from various WRF-Chem meteorology sensitivity simulations. Inset values report the domain-mean ± spatial standard deviation ($\mu \pm 1\sigma$) computed over the Indian landmass, along with Mean Bias Error (MBE) relative to Aqua/AIRS……....041

Figure 2.4: Daily mean time series comparison of surface temperature and surface wind speed for selected Indian states from different WRF-Chem meteorology and grid-nudging sensitivity simulations against CPCB measurements and MERRA2 reanalysis. Temporal mean ± standard deviation ($\mu \pm 1\sigma$), together with correlation coefficient (r) and RMSE of Nudged03, are indicated within each panel……..042

Figure 2.5: Spatial distribution of 850 hPa (top panel) and surface (bottom panel) wind speed from MERRA2 reanalysis over the Indian region and corresponding differences from various WRF-Chem meteorology sensitivity simulations. Inset values show domain-mean ± spatial SD (μ ± 1σ) and Mean Bias Error (MBE) computed over the Indian landmass……043
Figure 2.6: Spatial distribution of accumulated rainfall measured by the IMD over the Indian region and corresponding differences from various WRF-Chem microphysics sensitivity simulations. Inset statistics report domain-mean ± spatial SD (μ ± 1σ) and Mean Bias Error (MBE) over the Indian landmass……..045
Figure 2.7: Vertical temperature profile comparison between MERRA2 reanalysis, Aqua/AIRS observed with different WRF-Chem PBL and grid nudging sensitivity simulations over the entire Indian region (top panel). Profiles are accompanied by domain-mean ± SD statistics over India. Spatial distribution of PBL height by MERRA2 reanalysis over the Indian region, and the difference in simulated PBL height from various WRF-Chem PBL sensitivity simulations (bottom panel). Inset values show domain-mean ± spatial SD (μ ± 1σ), Mean Bias Error (MBE) and Mean Absolute Error (MAE) of Nudged03 computed over the Indian landmass……...046
Figure 2.8: Spatial distribution of 850 hPa temperature observed by Aqua/AIRS over the Indian region, and the difference in simulated temperature from various WRF-Chem PBL sensitivity simulations. Domain-mean ± spatial SD (μ ± 1σ) and Mean Bias Error (MBE) over the Indian landmass are reported within the panels……...…047
Figure 2.9: Spatial distribution of AOD from MERRA2 reanalysis and the difference in simulated AOD from various WRF-Chem emission inventory sensitivity simulations over the Indian region (top panel). Inset values show domain-mean ± spatial SD (μ ± 1σ) and MBE over the Indian landmass. Spatial distribution of surface $PM_{2.5}$ concentration by MERRA2 over the Indian region, and the difference in simulated surface $PM_{2.5}$ from various WRF-Chem emission inventory sensitivity simulations (middle panel), with domain-mean ± SD (μ ± 1σ) and MBE reported within the panel. Daily mean time series comparison of surface SO_2 distribution for various Indian states from different WRF-Chem emission inventory sensitivity simulations with CPCB measurements and MERRA2 reanalysis (bottom panel). Temporal mean ± SD (μ ± 1σ) and RMSE (μg m-3) of Nudged03 are indicated……048
Figure 2.10: Spatial distribution of cloud fraction observed by Aqua/AIRS over the Indian region, and the difference in simulated cloud fraction from various WRF-Chem microphysics sensitivity simulations. Panels include domain-mean ± spatial SD (μ ± 1σ) and Mean Bias Error (MBE) computed over the Indian landmass……..049
Figure 2.11: Spatial distribution of 850 hPa CO concentration by Aqua/AIRS over the Indian region, and the difference in simulated 850 hPa CO from various WRF-Chem emission inventory

sensitivity simulations (top panel). Spatial distribution of surface PM_{10} concentration by MERRA2 over the Indian region, and the difference in simulated surface PM_{10} from various WRF-Chem emission inventory sensitivity simulations (bottom panel). For both panels, domain-mean ± spatial SD (μ ± 1σ) and Mean Bias Error (MBE) over the Indian landmass are reported within the plots…….050

Figure 2.12: Spatial distribution of 850 hPa O3 distribution observed by Aqua/AIRS, MERRA2 and the difference in simulated 850 hPa O3 from different WRF-Chem chemical mechanism sensitivity simulations. Inset values show domain-mean ± spatial SD (μ ± 1σ) and Mean Bias Error (MBE) relative to observations……....052

Figure 2.13: Bar charts showing 5-days mean time series comparison of surface SO4 distribution for various Indian states from different WRF-Chem chemical mechanism sensitivity simulations with MERRA2 reanalysis (top panel). Bars represent mean ± SD over the averaging window. Bar charts illustrating the diurnal variation in the difference of 4-hourly mean surface NOx distributions for various Indian states, derived from different WRF-Chem chemical mechanism sensitivity simulations compared with CPCB measurements (bottom panel). Temporal mean ± SD (μ ± 1σ), Mean Absolute Error (MAE) and correlation coefficient (r) for CBMZWRF and Nudged03 are indicated respectively within the panel to facilitate quantitative comparison……053

Figure 2.14: Daily mean time series comparison of surface $PM_{2.5}$ for selected Indian states from different WRF-Chem chemical mechanism and emission inventory sensitivity simulations against CPCB measurements. Temporal mean ± standard deviation (μ ± 1σ), together with RMSE of Nudged03, are indicated within each panel……..055

Figure 2.15: Daily mean time series comparison of surface PM10 for selected Indian states from different WRF-Chem chemical mechanism and emission inventory sensitivity simulations against CPCB measurements. Temporal mean ± standard deviation (μ ± 1σ), together with RMSE of Nudged03, are indicated within each panel……..056

Figure 2.16: Bar charts showing the monthly total and sectoral emission comparison over India from different emission inventories used in the WRF-Chem emission inventory sensitivity simulations for various primary anthropogenic chemical species for August and January (left panel). The right panel represents the relative contribution of different emission sectors to the total emissions over the Indian region for the respective chemical species and period……..…057

Figure 2.17: Bubble plot representation of statistical comparisons for various surface and 850 hPa pollutants over the Indian region against MERRA2 and Aqua/AIRS for different WRF-Chem nudging coefficient sensitivity simulations for August 2018. Bubble size represents RMSE, colour indicates various experiments, and inset values show Coefficients of determination (r^2)……..…059

Figure 2.18: Bubble plot representation of statistical comparisons for various surface and 850 hPa pollutants over the Indian region against MERRA2 and Aqua/AIRS for different WRF-Chem nudging coefficient sensitivity simulations for January 2019. Bubble size represents RMSE, colour indicates various experiments, and inset values show Coefficients of determination (r^2)……..…060
Figure 2.19: A statistical comparison of preferred WRF-Chem-simulated meteorological parameters and pollutant concentrations with CPCB measurements is shown for various Indian states with available continuous monitoring data (see Fig. 2.1) for August 2018. Panels report state-wise regression statistics (MAE, RMSE, and r^2) indicated in parentheses, enabling direct quantitative assessment of model skill across regions……..061
Figure 2.20: A statistical comparison of preferred WRF-Chem-simulated meteorological parameters and pollutant concentrations with CPCB measurements is shown for various Indian states with available continuous monitoring data (see Fig. 2.1) for January 2019. Panels report state-wise regression statistics (MAE, RMSE, and r^2) indicated in parentheses, enabling direct quantitative assessment of model skill across regions……..063

Chapter 3

Figure 3.1: WRF-Chem simulation domain with topographic height (left) and 2020 population density from GPWv4 (centre). The right panel shows the seven Indian geographical regions North India (NI), Northeast India (NEI), Central India (CI), South India (SI), West India (WI), Eastern Indo-Gangetic Plain (EIGP), and Western Indo-Gangetic Plain (WIGP) alongside CPCB measurement sites active in 2020. This configuration was used to assess the effects of emission changes and meteorological variability during the COVID-19 lockdown across the Indian region……...070
Figure 3.2: Spatial distributions of total $PM_{2.5}$ emissions in 2020 and their changes relative to the non-COVID-19 (pre-lockdown) period over the entire study timeframe……..073
Figure 3.3: Spatial distribution of ambient $PM_{2.5}$ concentrations ($\mu g\ m^{-3}$) over India during the pre-lockdown, four lockdown phases, and unlock period, from satellite data (top) and WRF-Chem simulations (bottom)……079
Figure 3.4: Comparison of 24-hour satellite-derived $PM_{2.5}$ and WRF-Chem simulated $PM_{2.5}$ concentrations against CPCB observations (top panel) from continuous monitoring stations and MERRA-2 surface $PM_{2.5}$ data (bottom panel) across various Indian regions (see Fig. 3.1). The regression statistics, including the slope-intercept form of the equation of a straight line, are explicitly displayed within the plot……...080
Figure 3.5: Comparison of 24-hour satellite-derived $PM_{2.5}$ and WRF-Chem simulated $PM_{2.5}$ concentrations against CPCB observations (top panel) from continuous monitoring stations and

MERRA-2 surface $PM_{2.5}$ data (bottom panel) for the entire pre-lockdown to unlock period across India. The regression statistics, including the slope-intercept form of the equation of a straight line, are explicitly displayed within the plot……..…081
Figure 3.6: Spatial distribution of surface $PM_{2.5}$ concentrations over India during the pre-lockdown, four lockdown phases, and unlock period, based on satellite data, WRF-Chem simulations, and MERRA-2…….082
Figure 3.7: Differences in $PM_{2.5}$ concentrations across lockdown and unlock phases derived from satellite data, WRF-Chem simulations, and MERRA-2 reanalysis……..……082
Figure 3.8: Daily mean time-series comparison of surface $PM_{2.5}$ concentrations ($\mu g\ m^{-3}$) from the pre-lockdown to unlock period in 2020 for Delhi, Bihar, Rajasthan, Haryana, Gujarat, Madhya Pradesh, West Bengal, Karnataka, Tamil Nadu, Uttar Pradesh, Maharashtra, and Punjab……084
Figure 3.9: Daily mean time-series comparison of surface temperature (top) and 2-meter air temperature (bottom) from the pre-lockdown to unlock period in 2020 over the entire Indian region, based on ERA5 reanalysis data. The left panels show the comparison for individual years from 2015 to 2020 along with the 2015-2019 multi-year mean. The right panels compare the 2020 time series with the 2015-2019 mean. The shaded area represents ±1σ of the 2015-2019 multi-year mean…….086
Figure 3.10: Spatial distribution of 2-meter air temperature over India during the pre-lockdown period, four lockdown phases, and the unlock period, based on individual years from 2015 to 2020, along with the 2015-2019 multi-year mean……..087
Figure 3.11: Daily mean time-series comparison of 10-meter wind speed (top) and boundary layer height (bottom) from the pre-lockdown to unlock period in 2020 over the entire Indian region, based on ERA5 reanalysis data. The left panels show the comparison for individual years from 2015 to 2020 along with the 2015-2019 multi-year mean. The right panels compare the 2020 time series with the 2015-2019 mean. The shaded area represents ±1σ of the 2015-2019 multi-year mean…….088
Figure 3.12: Spatial distribution of 10-meter wind speed over India during the pre-lockdown period, four lockdown phases, and the unlock period, based on individual years from 2015 to 2020, along with the 2015-2019 multi-year mean……..088
Figure 3.13: Spatial distribution of boundary layer height over India during the pre-lockdown period, four lockdown phases, and the unlock period, based on individual years from 2015 to 2020, along with the 2015-2019 multi-year mean……..089
Figure 3.14: Daily mean time-series comparison of relative humidity (top) and specific humidity (bottom) from the pre-lockdown to unlock period in 2020 over the entire Indian region, based on ERA5 reanalysis data. The left panels show the comparison for individual years from 2015 to 2020

along with the 2015-2019 multi-year mean. The right panels compare the 2020 time series with the 2015-2019 mean. The shaded area represents ±1σ of the 2015-2019 multi-year mean…...…090
Figure 3.15: Spatial distribution of total cloud cover over India during the pre-lockdown period, four lockdown phases, and the unlock period, based on individual years from 2015 to 2020, along with the 2015-2019 multi-year mean……090
Figure 3.16: Bar chart illustrating the relative changes in $PM_{2.5}$ emissions from various sectors, as well as the total anthropogenic and biomass burning (FINN-v2.5) emissions, across different lockdown and unlock phases compared to the pre-lockdown baseline for all of India……..…093
Figure 3.17: Grouped bar chart showing the total relative changes in ambient $PM_{2.5}$ concentrations across India during each lockdown and unlock phase, compared to the pre-lockdown baseline. Each bar distinguishes the contributions of meteorology-induced variations from those resulting from activity-restricted emission reductions……094
Figure 3.18: Spatial distribution of total relative changes in ambient $PM_{2.5}$ (top), and the separate contributions from meteorology (middle) and activity restrictions (bottom) during each lockdown and unlock phase, compared to pre-lockdown conditions. Results are based on satellite-derived $PM_{2.5}$ data. Mean values are explicitly displayed within the plot……...……...095
Figure 3.19: Spatial distributions of total relative changes in ambient $PM_{2.5}$ (top), and the separate contributions from meteorology (middle) and activity restrictions (bottom) during each lockdown and unlock phase, relative to pre-lockdown conditions, based on WRF-Chem simulations. Mean values are explicitly displayed within the plot……..096
Figure 3.20: Grouped bar chart showing total relative changes in ambient $PM_{2.5}$ concentrations and the contributions from meteorology and activity restrictions during each lockdown and unlock phase, compared to the pre-lockdown baseline, across seven Indian regions……...097
Figure 3.21: Spatial distribution of normalized $PM_{2.5}$ anomalies (top), time series of zone-wise normalized $PM_{2.5}$ anomalies from satellite data (bottom left) and WRF-Chem simulations (bottom right) for the entire lockdown period (March 25-May 31, 2020). The ventilation coefficient (VC) and VIIRS fire counts are shown (middle left) for pre-lockdown, each lockdown phase, and the unlock period across seven regions. ERA5 850 hPa wind speeds for the last two lockdown phases are presented (middle right) for all of India……..099
Figure 3.22: Normalized $PM_{2.5}$ anomalies from satellite data and WRF-Chem simulations for different lockdown phases over India……...100
Figure 3.23: Spatial distribution of the Ventilation Coefficient (VC) from ERA5 (top) ($m^2\ s^{-1}$) and VIIRS fire counts (bottom) over India during the pre-lockdown, phased lockdown, and unlock periods……..100

Figure 3.24: Time-series comparison of normalized $PM_{2.5}$ anomalies (top) from satellite data and WRF-Chem simulations, and 850 hPa ERA5 wind speed (bottom) over the study period across India……..…101

Chapter 4

Figure 4.1: Model domains and regional context: The top-left panel shows the WRF-Chem outer and inner simulation domains overlaid with 2020 population density from GPWv4. The top-right panel provides a zoomed-in view of the high-resolution inner domain with highlighted Delhi-NCR region. The middle-left panel maps NCT-Delhi, its administrative districts, and CPCB monitoring stations active during 2019-2020. The middle-right panel depicts the NCT-Delhi airshed for October-November (Kumar et al., 2025) (Punjab, Haryana, and Delhi-NCR), overlaid with simulated WRF-Chem wind flow patterns. The bottom panel presents monthly simulated surface and 850-hPa wind speeds and flow directions across North India, highlighting seasonal changes in regional transport……..111

Figure 4.2: Sectoral contributions to $PM_{2.5}$ emissions from the SMoG-COALESCE inventory. The pie chart displays the mean percentage contribution from each sector, illustrating the relative importance of major emission sources across the study region…….113

Figure 4.3: Stacked bar chart showing the sectoral contributions to $PM_{2.5}$ emissions derived from the SMoG-COALESCE inventory, highlighting the relative magnitude and variability of emissions from major source sectors…….114

Figure 4.4: Monthly spatial distributions of surface $PM_{2.5}$ over North India from satellite-derived estimates and the WRF-Chem control simulation, along with the corresponding spatial bias fields illustrating areas of model underestimation and overestimation……...118

Figure 4.5: Comparison of 24-hour satellite-derived $PM_{2.5}$ concentrations with corresponding values from the WRF-Chem control simulation across NCT-Delhi, Delhi-NCR, Haryana, and Punjab for the entire study period. The slope-intercept form of the linear regression fit and associated statistical metrics are shown within each panel……...119

Figure 4.6: Daily mean time-series of surface $PM_{2.5}$ concentrations ($\mu g\ m^{-3}$) over the study period, comparing CPCB observations, satellite-derived estimates, the WRF-Chem control simulation, and MERRA-2 reanalysis for NCT-Delhi, Delhi-NCR, Haryana, and Punjab…….....119

Figure 4.7: Daily mean time-series comparison of surface Black Carbon (BC) concentrations ($\mu g\ m^{-3}$) from the WRF-Chem control simulation and MERRA-2 reanalysis for NCT-Delhi, Delhi-NCR, Haryana, and Punjab over the full study period……..120

Figure 4.8: Daily mean time-series comparison of surface Organic Carbon (OC) concentrations ($\mu g\ m^{-3}$) from the WRF-Chem control simulation and MERRA-2 reanalysis for NCT-Delhi, Delhi-NCR, Haryana, and Punjab over the full study period……..122
Figure 4.9: Daily mean time-series comparison of surface sulfate (SO_4^{2-}) concentrations ($\mu g\ m^{-3}$) from the WRF-Chem control simulation and MERRA-2 reanalysis for NCT-Delhi, Delhi-NCR, Haryana, and Punjab across the entire study period……..122
Figure 4.10: Monthly spatial distribution of surface $PM_{2.5}$ concentrations over northern India from the WRF-Chem control simulation (left panel). The middle panel shows monthly pie charts of sectoral contributions to surface $PM_{2.5}$ across four agriculturally and economically significant northern Indian states, derived from the emission-perturbed WRF-Chem simulations. The right panel presents corresponding monthly pie charts of $PM_{2.5}$ chemical composition from the control simulation. Mean percentage contributions for each sector or chemical species are indicated within the respective charts……125
Figure 4.11: Monthly chemical composition of surface $PM_{2.5}$ across the selected northern Indian states, presented as bar charts and derived from the WRF-Chem control simulation……126
Figure 4.12: Monthly sectoral contributions to surface $PM_{2.5}$ concentrations across four agriculturally and economically significant states in northern India, illustrated through bar charts and derived from the suite of WRF-Chem emission-perturbed simulations……126
Figure 4.13: Monthly stacked bar charts showing the relative contributions of primary and secondary $PM_{2.5}$ to surface $PM_{2.5}$ concentrations over NCT-Delhi, Delhi-NCR, Punjab, and Haryana, based on the WRF-Chem control simulation. Mean contributions ($\mu \pm 1\sigma$) for each component are indicated within the bars……...127
Figure 4.14: Monthly stacked bar charts showing sectoral contributions and chemical composition of surface $PM_{2.5}$ from WRF-Chem control and emission-perturbed simulations for the period September 2019-January 2020……128
Figure 4.15: Spatial comparison of September-January mean emissions of major VOCs, Benzene, Toluene, Formaldehyde, Acetone, and Ethylene, from EDGAR-v5 (2015), alongside key gaseous precursors, NO_x, SO_2, and NH_3, from SMoG-COALESCE (2019). The top panels show the emission distributions across the broader North India domain, while the bottom panels present a zoomed-in view over the inner study region……132

Chapter 5

Figure 5.1: WRF-Chem simulation domain overlaid with 2019 $PM_{2.5}$ mean emission from SMoG-COALESCE emission inventory (left). The right panel illustrates the NCT-Delhi airshed region

for October-November (Kumar et al., 2025), overlaid with WRF-Chem simulated wind flow directions……..141
Figure 5.2: Monthly spatial distribution of SMoG-COALESCE $PM_{2.5}$ emissions (top panel) and active fire locations detected by MODIS and VIIRS (middle panel) across the study region, together with their cumulative distribution over the full analysis period. The bottom panel shows daily time series of surface $PM_{2.5}$ emissions from FINN-v2.5, MODIS and VIIRS fire counts, and IMD accumulated rainfall (mm day-1) for NCT-Delhi, Delhi-NCR, Punjab, and Haryana throughout the study period……..145
Figure 5.3: Multi-panel summary of surface $PM_{2.5}$ responses over NCT-Delhi from emission-perturbed WRF-Chem simulations for the full study period. Panel (a) shows the daily time series of $PM_{2.5}$ concentrations, panel (b) presents the corresponding monthly mean $PM_{2.5}$ concentrations as bar plots, and panel (c) illustrates the relative reductions under sector-specific emission-perturbation scenarios. In panels (a-c), the left sub-panels represent mitigation limited to Delhi-NCR (city-centric scenario), while the right sub-panels show responses under the broader NCT-Delhi airshed mitigation strategy (Punjab, Haryana, and Delhi-NCR), together with the nationwide regulatory scenario with emission controls implemented across India. The baseline simulation is included for reference, and observations from Central Pollution Control Board monitoring sites are shown in panel (b) for comparison. The bottom panel presents the overall change in the relative frequency of NAQI-defined polluted days across all scenarios……...…153
Figure 5.4: Daily time series of surface $PM_{2.5}$ concentrations over Delhi-NCR, Punjab, and Haryana for the full study period, derived from emission-perturbed WRF-Chem simulations. The left panel shows $PM_{2.5}$ responses under mitigation applied only within Delhi-NCR (city-centric scenario), while the right panel shows responses under the broader NCT-Delhi airshed mitigation strategy (Punjab, Haryana, and Delhi-NCR), along with the nationwide regulatory scenario with emission controls applied across India. The baseline scenario is included in both panels for reference……...154
Figure 5.5: Bar plot of monthly mean surface $PM_{2.5}$ concentrations over Delhi-NCR, Punjab, and Haryana for the full study period, derived from emission-perturbed WRF-Chem simulations. The left panel presents $PM_{2.5}$ responses under mitigation limited to Delhi-NCR (city-centric scenario), whereas the right panel shows responses under the broader NCT-Delhi airshed mitigation strategy (Punjab, Haryana, and Delhi-NCR), together with the nationwide regulatory scenario with emission controls implemented across India. The baseline simulation and observed $PM_{2.5}$ concentrations from CPCB monitoring sites are included in both panels for comparison…….155
Figure 5.6: Bar charts illustrating the relative reductions in surface $PM_{2.5}$ over Delhi-NCR, Punjab, and Haryana under sector-specific emission-perturbation scenarios derived from WRF-

Chem simulations. The left panel shows reductions resulting from mitigation confined to Delhi-NCR (city-centric scenario), while the right panel presents the corresponding reductions under the broader NCT-Delhi airshed mitigation strategy (Punjab, Haryana, and Delhi-NCR), as well as the nationwide regulatory scenario with emission controls implemented across India……...156
Figure 5.7: Frequency of polluted-day occurrences over NCT-Delhi, Delhi-NCR, Punjab, and Haryana, classified according to the National Air Quality Index (NAQI) and derived from emission-perturbed WRF-Chem simulations. The left panel shows occurrences under mitigation restricted to Delhi-NCR (city-centric scenario), while the right panel presents corresponding changes under the broader NCT-Delhi airshed mitigation strategy (Punjab, Haryana, and Delhi-NCR), along with the nationwide regulatory scenario with emission controls implemented across India. The baseline simulation and observed frequencies from CPCB monitoring stations are included in both panels for comparison……157
Figure 5.8: Stacked bar charts showing changes in the relative frequency of polluted-day categories, based on the National Air Quality Index (NAQI), across NCT-Delhi, Delhi-NCR, Punjab, and Haryana for all emission-perturbed WRF-Chem simulations……...159
Figure 5.9: Daily time series of surface $PM_{2.5}$ over NCT-Delhi showing the occurrence of polluted-day categories (National Air Quality Index, NAQI) across all emission-perturbed simulations for the full study period……..…160
Figure 5.10: Daily time series of surface $PM_{2.5}$ over Delhi-NCR, showing the occurrence of polluted-day categories (National Air Quality Index, NAQI) across all emission-perturbed simulations for the full study period……..…160
Figure 5.11: Daily time series of surface $PM_{2.5}$ over Punjab, showing the occurrence of polluted-day categories (National Air Quality Index, NAQI) across all emission-perturbed simulations for the full study period……..161
Figure 5.12: Daily time series of surface $PM_{2.5}$ over Haryana, showing the occurrence of polluted-day categories (National Air Quality Index, NAQI) across all emission-perturbed simulations for the full study period……..….161
Figure 5.13: Monthly spatial distribution of surface $PM_{2.5}$ concentrations over northern India from the WRF-Chem emission-perturbed simulations for the full study period, illustrating the regional impacts of sector-specific and CRB-related mitigation scenarios…….....…164
Figure 5.14: Daily time series of surface $PM_{2.5}$ from WRF-Chem, satellite retrievals, and CPCB observations, along with major meteorological variables over NCT-Delhi (top panels). The lower panels depict reductions in $PM_{2.5}$ under five emission-perturbation scenarios, grouped by meteorological-variable ranges for the study period……..…168

Figure 5.15: Daily time series of surface $PM_{2.5}$ over Delhi-NCR from the WRF-Chem control simulation, satellite-derived estimates, and CPCB observations, shown alongside key meteorological variables for the full study period (top two panels). The bottom two panels present the relative reductions in surface $PM_{2.5}$ achieved under five targeted emission-perturbation scenarios, stratified by ranges of selected meteorological conditions over the same period…….169
Figure 5.16: Daily time series of surface $PM_{2.5}$ over Punjab from the WRF-Chem control simulation, satellite-derived estimates, and CPCB observations, shown together with key meteorological variables for the full study period (top two panels). The bottom two panels depict the relative reductions in surface $PM_{2.5}$ under five targeted emission-perturbation scenarios, stratified by ranges of selected meteorological conditions over Punjab during the same period……...…170
Figure 5.17: Daily time series of surface $PM_{2.5}$ over Haryana from the WRF-Chem control simulation, satellite-derived estimates, and CPCB observations, shown alongside key meteorological variables for the full study period (top two panels). The bottom two panels present the relative reductions in surface $PM_{2.5}$ achieved under five targeted emission-perturbation scenarios, stratified by different ranges of meteorological conditions over Haryana during the same period……...171
Figure 5.18: Daily time-series analysis of key meteorological variables over NCT-Delhi and Delhi-NCR for the full study period, comparing the responses simulated under the different emission-perturbed WRF-Chem scenarios……...172
Figure 5.19: Daily time-series analysis of Aerosol Optical Depth (AOD) over NCT-Delhi, Delhi-NCR, Punjab, and Haryana for the entire study period, comparing the response across the different emission-perturbed WRF-Chem simulations……...173
Figure 5.20: Daily time-series analysis of key meteorological variables over Punjab and Haryana for the full study period, comparing their evolution across the different emission-perturbed WRF-Chem simulations…….173

List of Tables

Chapter 1

Table 1.1: Concentration (with respect to dry air) of major gaseous elements present in the atmosphere up to an elevation of 105 km adapted from Jacob, 1999……003

Chapter 2

Table 2.1: Summary of WRF-Chem model sensitivity simulations setup details…….038

Table 2.2: Regression statistics for various meteorological variables over the Indian region from different meteorological and PBL sensitivity simulations for both study periods, evaluated against Aqua/AIRS and MERRA-2 observational datasets……..044

Table 2.3: Regression statistics for surface temperature, surface wind speed, surface relative humidity, cloud fraction and accumulated rainfall between various WRF-Chem microphysics sensitivity simulations with Aqua/AIRS observations, MERRA2 reanalysis, and IMD measurements over the Indian region for both study periods……051

Table 2.4: Regression statistics for AOD, Surface $PM_{2.5}$, Surface PM10 and 850 hPa CO over the Indian region from different WRF-Chem Emission Inventory sensitivity simulations for both study periods, evaluated against Aqua/AIRS and MERRA-2 observational datasets……....054

Table 2.5: Regression statistics Surface $PM_{2.5}$, PM_{10}, SO_2 and SO_4 over the Entire Indian region from different WRF-Chem chemical mechanism, grid-nudging, grid-nudging strength and approach sensitivity simulations for both study periods, evaluated against MERRA-2 observational datasets……..058

Chapter 3

Table 3.1: WRF-Chem model simulations setup……..072

Table 3.2: Quantifying the contributions of emission reductions and meteorological variability……...……..074

Table 3.3: Central Pollution Control Board Sites with measurement data available from February 24 to June 30, 2020……...077

Table 3.4: Regression statistics comparing satellite-derived and WRF-Chem simulated $PM_{2.5}$ with CPCB and MERRA-2 surface $PM_{2.5}$ across the geographical regions shown in Fig. 3.1 and different phases of lockdown and unlock period……...083

Table 3.5: Population-weighted ambient $PM_{2.5}$ concentrations ($\mu g\ m^{-3}$) across India and its seven geographical regions during the entire study period in 2020 ($\mu \pm 1\sigma$) (Values are pixel means)….091

Table 3.6: Population-weighted total relative changes in ambient $PM_{2.5}$ concentrations (%) across India and its seven geographical regions during each lockdown and unlock phase, compared to the pre-lockdown baseline, along with the contributions of meteorology-induced variations and activity-restricted emission reductions. The reported values represent pixel-level means……095

Chapter 4

Table 4.1: WRF-Chem model setup for source apportionment of $PM_{2.5}$…….116
Table 4.2: Monthly sectoral contributions and chemical composition of surface $PM_{2.5}$ derived from the WRF-Chem control simulation over NCT-Delhi……....125
Table 4.3: Monthly sectoral contributions and chemical composition of surface $PM_{2.5}$ derived from the WRF-Chem control simulation over Haryana……129
Table 4.4: Monthly sectoral contributions and chemical composition of surface $PM_{2.5}$ derived from the WRF-Chem control simulation over Delhi-NCR…….....130
Table 4.5: Monthly sectoral contributions and chemical composition of surface $PM_{2.5}$ derived from the WRF-Chem control simulation over Punjab……...130

Chapter 5

Table 5.1: WRF-Chem model setup for analysing emission control strategies……142
Table 5.2: Monthly reduction in surface $PM_{2.5}$ from emission-perturbed WRF-Chem simulations, relative to the control simulation……..152
Table 5.3: Frequency of polluted-day categories, as defined by the National Air Quality Index (NAQI), over the 153-day study period for each emission-perturbed simulation…….158

Chapter 1: Introduction, Motivation, Research Questions & Thesis Objectives

1.1 Introduction

The Earth's atmosphere is a thin yet highly dynamic envelope of gases that contains variable amounts of water vapour, clouds, and suspended particulate matter (aerosols), collectively sustaining life, governing weather and circulation, and regulating the Earth's climate system. By volume, the dry atmosphere is composed of approximately 78.09% nitrogen (N_2), 20.95% oxygen (O_2), 0.93% argon (Ar), with the remaining fraction contributed by trace constituents and other noble gases. Among the noble gases, argon is most abundant, followed by neon (Ne), helium (He), krypton (Kr), and xenon (Xe). Together, nitrogen and oxygen constitute nearly 99% of the total atmospheric volume (Pinti, 2021). Water vapour is another critical atmospheric constituent, but unlike the major gases it exhibits pronounced spatiotemporal variability. It contributes ~0.25% of the atmospheric mass on average, ranging from ~10 parts per million (ppm by volume) in the coldest regions to ~4% under warm and humid conditions (Wallace et al., 2006). As water vapour varies strongly in space and time, the concentrations of other gases are typically reported with respect to dry air (Table 1.1).

Species present in very small abundances are commonly termed trace gases, comprising roughly ~0.03% of the atmosphere. Despite their low concentrations, trace gases are central to atmospheric chemistry, air quality, and climate forcing. Key trace constituents include carbon dioxide (CO_2), ozones (O_3), nitrogen oxides (NO_x), carbon monoxide (CO), sulfur dioxide (SO_2), methane (CH_4), non-methane hydrocarbons (NMHCs), and nitrous oxide (N_2O). These species participate in processes that underpin major environmental challenges, including global warming, ozone chemistry, and photochemical smog formation (Afifa et al., 2024; Seinfeld et al., 1998). Their atmospheric burdens vary substantially across regions and seasons because they are controlled by a combination of sources, chemical transformation pathways, and meteorology.

Trace gases, and aerosols originate from diverse natural and anthropogenic sources. Natural contributions include volcanic activity, forest fires, lightning, soil emissions, windblown dust, sea spray, and biogenic emissions from vegetation and microbial activity. Anthropogenic sources, such as fossil fuel combustion, industrial processes, vehicular emissions, and domestic biomass burning, often dominate pollutant loading in densely populated and industrialized regions (Tie et al., 2001). In addition to local emissions, long-range transport can redistribute pollutants over continental scales, influencing air quality far from their source regions (Seinfeld et al., 1998; Zhang et al., 2010).

Once emitted, atmospheric pollutants are shaped by coupled physical and chemical processes that determine their lifetime, spatial footprint, and impacts. Oxidation is a primary sink for many reactive pollutants, and the hydroxyl radical (OH) is considered the most important atmospheric oxidant, initiating the degradation of numerous trace gases and thereby controlling their lifetimes (Lelieveld et al., 2016; Levy, 1971). Alongside gases, atmospheric aerosols, suspensions of solid or liquid particles spanning orders of magnitude in size and composition, introduce additional complexity. Aerosols may be emitted directly (primary aerosols) or formed in situ through chemical transformation of precursor gases (secondary aerosols) (Putaud et al., 2010; Samset et al., 2018). Through their interactions with radiation and clouds, aerosols influence the Earth's energy balance, cloud microphysics, and hydrological cycle, and they are therefore central to both air quality and climate research (Kirkevåg et al., 2018). The degradation of air quality due to elevated concentrations of gaseous and particulate has severe societal consequences. Exposure to polluted air increases hospital admissions for exacerbates respiratory diseases such as asthma and pneumonia, and it contributes to premature mortality (Cohen et al., 2017). Continuous air quality monitoring and scientifically grounded attribution of pollutant sources are therefore essential for quantifying health risks and designing effective mitigation strategies.

Table 1.1: Concentration (with respect to dry air) of major gaseous elements present in the atmosphere up to an elevation of 105 km adapted from Jacob, 1999.

Gas	**Concentration by Volume (%)**	**Gas**	**Concentration by Volume (%)**
Nitrogen (N_2)	78.08	Methane (CH_4)	1.75 (ppm)
Oxygen (O_2)	20.95	Krypton (Kr)	1 (ppm)
Argon (Ar)	0.93	Hydrogen (H_2)	0.5 (ppm)
Carbon Dioxide (CO_2)	0.038	Nitrogen Dioxide (NO_2)	0.02 (ppm)
Water Vapour (H_2O)	0.01 - 4	Xenon (Xe)	0.009 (ppm)
Neon (Ne)	18 (ppm)	Ozone (O_3)	0 - 0.1 (ppm)
Helium (He)	5 (ppm)		

1.1.1 Air Pollution and Particulate Matter Pollution

Air pollution refers to the presence of chemical, physical, or biological substances in the atmosphere at concentrations that harm human health, ecosystems, materials, or the climate system. The World Health Organization (WHO) defines air pollution as contamination of the

indoor or outdoor environment by any agent that modifies the natural characteristics of the atmosphere (WHO, 2021). Major ambient pollutants include particulate matter (PM), sulfur dioxide (SO_2), nitrogen oxides (NO_x), carbon monoxide (CO), ozone (O_3), volatile organic compounds (VOCs), and ammonia (NH_3) (Seinfeld et al., 1998; Zhang et al., 2010). Importantly, these pollutants do not exist in isolation, instead, they interact through atmospheric chemistry and physics, often producing secondary pollutants. For example, tropospheric ozone and secondary aerosols are formed through photochemical reactions involving NO_x, VOCs, and SO_2 in the presence of sunlight (Finlayson et al., 2000).

Air pollution is a leading environmental risk factor and contributes to millions of premature deaths annually, primarily through cardiovascular and respiratory disease pathways (Cohen et al., 2017; Lelieveld et al., 2015). Beyond human health, air pollutants reduce visibility, damage vegetation, and crops, and influence regional-to-global climate through direct and indirect radiative effects (Rogelj et al., 2018). Within the pollutant mixture, particulate matter (PM) is of particular concern because it embodies a chemically complex, size-resolved mixture of solids and liquid droplets suspended in air. PM spans from nanometre-scale particles to coarse particles tens of micrometres in diameter and is commonly categorized by aerodynamic diameter: PM_{10} ($\leq$ 10 μm), $PM_{2.5}$ ($\leq$ 2.5 μm), and ultrafine particles (UFPs $\leq$ 0.1 μm). PM composition varies by source and atmospheric processing and typically includes sulfate, nitrate, ammonium, organic carbon, elemental carbon (soot), mineral dust, sea salt, and trace metals (Putaud et al., 2010; Zhang et al., 2017).

Particulate matter arises from both primary and secondary sources. Primary PM is directly emitted by sources such as fossil fuel combustion, industrial activities, vehicular exhaust, biomass burning, windblown dust, and sea spray. Secondary PM forms in the atmosphere through chemical reactions involving precursor gases such as SO_2, NO_x, NH_3, and VOCs, leading to sulfate, nitrate, and secondary organic aerosols (SOA) production (Jimenez et al., 2009). In urban environments, anthropogenic activities, transportation, energy production, and industry, often dominate $PM_{2.5}$ burdens, whereas natural sources such as dust storms, sea salt, and episodic events can dominate in some remote or arid regions (Samset et al., 2018). After emission, particles evolve through coagulation, condensation, nucleation, and heterogeneous reactions, processes that modify their size distribution, chemical composition, hygroscopicity, and optical properties (Jacob, 1999). Long-range transport allows aerosols to travel thousands of kilometres, coupling regional air quality to synoptic circulation and influencing climate and deposition far from emission regions (Zhang et al., 2020).

Aerosols affect the Earth's radiative balance through direct interactions with solar radiation (scattering and absorption) and through indirect effects on clouds (changes in cloud droplet number, cloud albedo, lifetime, and precipitation efficiency) (Jia et al., 2019). These aerosol–radiation and aerosol-cloud interactions contribute substantially to uncertainties in radiative forcing and climate projections. From a public health perspective, fine $PM_{2.5}$ is the most harmful fraction because it penetrates deep into the lungs and can enter the bloodstream. Chronic and acute exposure is linked to cardiovascular disease, lung cancer, asthma, and premature mortality (Dockery, 2006). The Global Burden of Disease (GBD) study estimated that exposure to ambient $PM_{2.5}$ caused over 4 million premature deaths globally in 2019 (GDB, 2020). Environmentally, particulate pollution reduces visibility, damages vegetation, contributes to ecosystem acidification through deposition, and can influence surface radiation ("global dimming") (Andreae et al., 2008). Consequently, monitoring and mitigation of PM pollution remain central goals of air quality management.

India faces an especially severe air pollution challenge driven by rapid urbanization, industrial development, growth in vehicle fleets, biomass burning, and construction activity (Ghude et al., 2020). Elevated $PM_{2.5}$, PM_{10}, NO_x, SO_2, CO, and ground-level ozone concentrations adversely affect health, ecosystems, and agricultural productivity and impose substantial economic costs (Cohen et al., 2015; Mahapatra et al., 2018). Nearly the entire population is exposed to $PM_{2.5}$ concentrations exceeding the World Health Organization (WHO) guideline of 5 $\mu g\ m^{-3}$, and approximately three-fourths live in regions exceeding the National Ambient Air Quality Standards (NAAQS) of 40 $\mu g\ m^{-3}$ (Balakrishnan et al., 2019a). In response, the Government of India launched the National Clean Air Programme (NCAP) in 2019, targeting a 20-30% reduction in $PM_{2.5}$ levels by 2024 in 131 non-attainment cities.

1.1.2 Vertical Structure of the Atmosphere, Atmospheric Boundary Layer and Diurnal Cycle of Atmospheric Boundary Layer

The atmosphere vertically stratified into layers that reflect the thermal structure produced by radiative absorption, emission, and dynamical mixing. The lowest layer, the troposphere, extends from the surface to ~15 km and is characterized by decreasing temperature with height, it contains most of the atmospheric mass and essentially all-weather phenomena. The troposphere is capped by the tropopause, above which lies the Stratosphere (~15-50 km). In the stratosphere, temperature increases with altitude due to the absorption of ultraviolet (UV) radiation by ozone (O_3), producing radiative heating. Above the stratosphere, the mesosphere (~50-90 km) exhibits

decreasing temperature with height and is bounded above by the mesopause. The thermosphere (~90-120 km) follows, where temperature rises sharply due to photodissociation and ionization of O_2 and N_2 by short-wavelength radiation. For air quality, the most consequential region is the lowest troposphere where pollutants are emitted, mixed, transformed, and removed: the *Atmospheric Boundary Layer* (ABL), also called the *Planetary Boundary Layer* (PBL) (Stull, 1988) (Fig. 1.1).

The Earth's surface forms the lower boundary of the atmosphere and continuously exchanges heat, moisture, and momentum with the air above. The ABL is the portion of the troposphere that responds to these surface fluxes on timescales of an hour or less (Stull, 1988). Turbulence in the ABL is generated primarily by surface heating (buoyancy production) and vertical wind shear (mechanical production), and it governs the vertical mixing that controls near-surface pollutant concentrations. Consequently, boundary-layer depth and stability strongly modulate air quality. The ABL height varies widely in time and space, from tens of metres under stable conditions to several kilometres under deep daytime convection, depending on surface forcing, synoptic setting, land-atmosphere coupling, and mesoscale circulations (Markowski et al., 2010). During daytime, solar heating promotes convection and vigorous turbulent mixing, typically producing a deeper, well-mixed boundary layer. In summer, stronger insolation and enhanced convection can deepen the PBL to several kilometres in many regions, accelerating dilution and vertical redistribution of pollutants. In contrast, subsidence under high-pressure conditions often favours temperature inversions that suppress mixing, trap pollutants near the surface, and increase exposure.

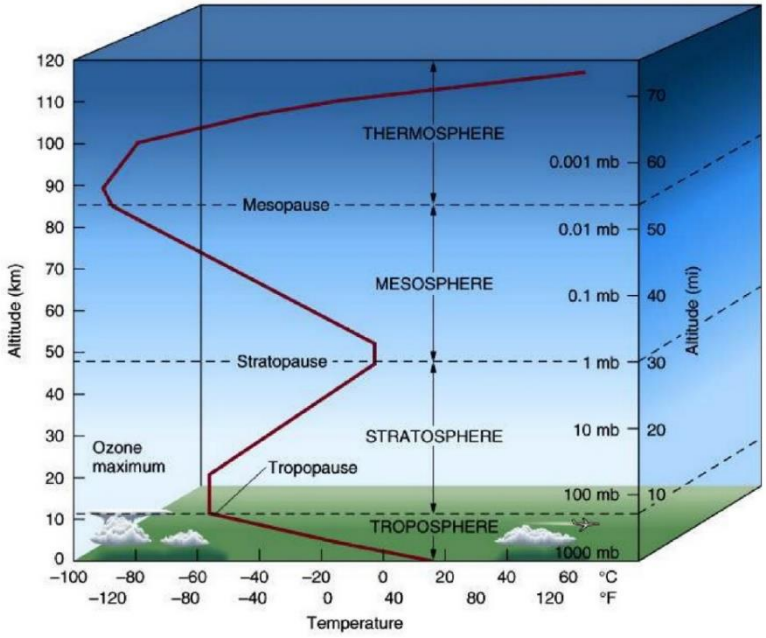


Figure 1.1: Vertical Structure of the Earth's Atmosphere adapted from Schlatter, 2010.

The diurnal cycle of the boundary layer is driven by the day–night contrast in surface energy balance. During daytime, positive sensible heat flux destabilizes the lower atmosphere, generating convective turbulence and upward transport. Rising thermals and convective eddies can homogenize temperature, moisture, and tracer concentrations within the mixed layer, and in some cases convective plumes may overshoot the boundary layer top into the more stable free troposphere. Over this period, pollutants emitted near the surface are rapidly mixed through the boundary layer depth, often yielding relatively uniform vertical profiles within the mixed layer. In comparison, exchange between the boundary layer and the free troposphere is typically slower and can require several days under many conditions. After sunset, radiative cooling of the surface produces a stable temperature stratification, reduces buoyancy-driven turbulence, and rapidly collapses the mixed layer into a shallow Stable Boundary Layer (SBL) or Nocturnal Boundary Layer (NBL) (Fig. 1.2).

Under these stable conditions, vertical mixing is weak and pollutants accumulate near the surface, producing strong gradients and elevated concentrations (Brown et al., 1994). The daily evolution commonly exhibits a maximum boundary-layer height in the late afternoon, followed by progressive shallowing overnight as surface cooling strengthens stability. At night, turbulence is maintained mainly by wind shear, and it is sensitive to topography, local circulations, and weak-wind regimes (Salmond et al., 2005). Weak winds can further suppress turbulence, enhance near-surface cooling, and intensify stability (Duarte et al., 2015). Above the stable nocturnal layer, a residual layer often persists as a remnant of the previous daytime mixed layer, retaining relatively homogeneous thermodynamic and pollutant properties. These boundary-layer processes are fundamental for interpreting observed $PM_{2.5}$ variability and for accurately simulating pollutant accumulation and dispersion in regional models.

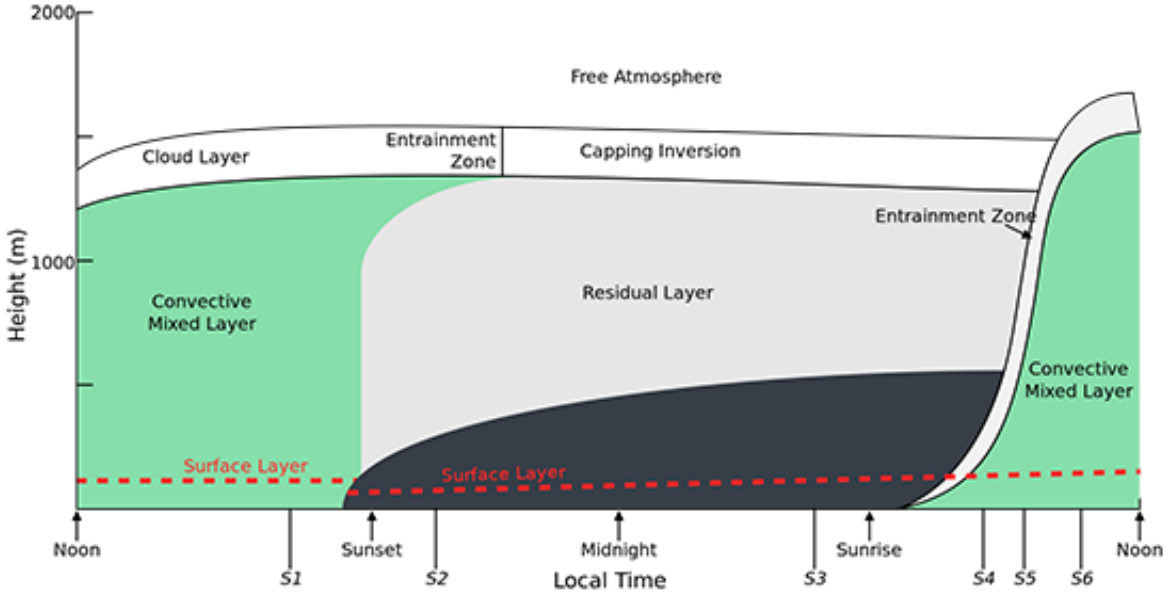


Figure 1.2: Daily Evolution of the Atmospheric Boundary Layer adapted from Stull, 1988.

1.1.3 Environmental and Geographical Significance of India: A Northern Perspective

India is the second most populous country globally and the seventh largest in geographical area. It lies on the northern portion of the Indo Australian Plate (Indian Plate) and extends from 8°4'-37°6' N and 68°7'-97°25' E. It is bounded by the Indian Ocean to the south, the Bay of Bengal to the east, and the Arabian Sea to the west, and shares orders with Pakistan to the west, China, Nepal, and Bhutan to the north and northeast, and Bangladesh and Myanmar (Burma) to the east. Sri Lanka lies to the south of the Palk Strait, and the Andaman and Nicobar Islands extend toward southeast Asia.

India comprises of 29 states and seven union territories (New Delhi, Chandigarh, Dadra and Nagar Haveli, Daman and Diu, Puducherry, Andaman and Nicobar Islands, and Lakshadweep), spanning diverse physiography and climatic regimes. The subcontinent is broadly divided into six major physiographic regions: the Northern Mountain Region, Indo Gangetic Plain (IGP), Thar Desert, Peninsular Plateau, Coastal Plains, and Island systems. The Northern Mountain Region includes the Himalayas and associated valleys and plateaus that exert strong dynamical control on circulation and precipitation. The IGP one of the world's largest alluvial plains is shaped by the Indus, Ganga, and Brahmaputra river systems and is often subdivided into the Bhabhar, Terai, Bangar, and Khadir belts based on depositional and soil characteristics. The Thar Desert spans much of Rajasthan and extends into adjoining regions of Gujarat, Punjab, and

Haryana. The Peninsular Plateau is the oldest geological unit, consisting mainly of crystalline igneous and metamorphic rocks, separated from the IGP by ranges including the Aravalli, Vindhya, Maikal, and Ajanta. The Coastal Plains lie along the western and eastern margins, with major east-flowing rivers (Mahanadi, Godavari, Krishna, and Kaveri) draining into the Bay of Bengal and shorter rivers and backwaters characterizing the west coast. The Lakshadweep archipelago includes ~35 islands and islets, while the Andaman and Nicobar system includes ~572 islands (Fig. 1.3).

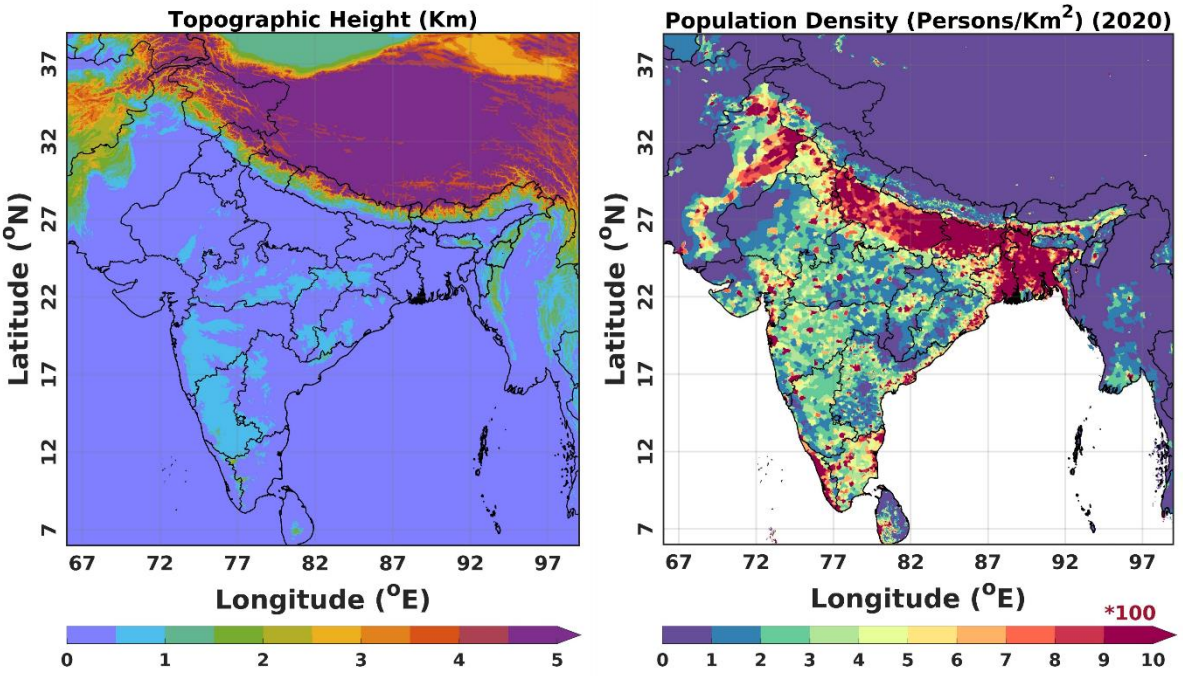


Figure 1.3: India Region with Simulated Topographic Height (left) and 2020 Population Density from Gridded Population of World Version 4 (GPWv4) (right).

India's climatic diversity is exceptional, ranging from arid desert climates to alpine conditions and humid tropical regimes. The country is commonly described as experiencing four seasons: Winter (December-February), Spring (March-May), Summer (June-August), and Autumn (September-November). The Himalayas form a major climatic barrier, reducing intrusion of cold continental air in winter and modulating large-scale circulation. The Indian monsoon is a defining feature of regional climate and is commonly separated into Pre-Monsoon (March-May), Monsoon (June-August), and Post-Monsoon (September-November) phases. During summer, stronger land heating relative to surrounding oceans produces a low-pressure region that draws moist south-westerly flow, generating widespread rainfall. In winter, the land-sea thermal contrast reverses, northeasterly flow dominates, and most of India experiences drier conditions except parts of the southern peninsula.

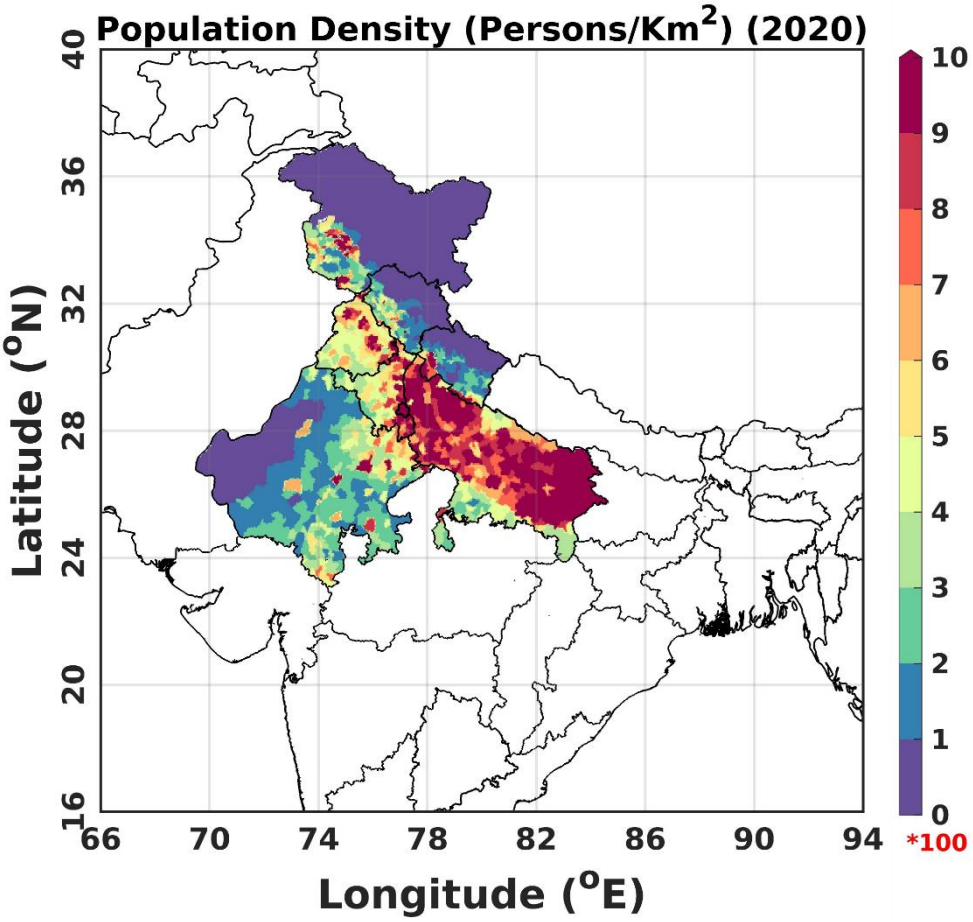


Figure 1.4: North India Region with 2020 Population Density from GPWv4.

The spatial distribution of air pollution across India is strongly heterogeneous because it reflects the interplay of emissions, topography, and meteorology. Northern India (Fig. 1.4), particularly the Indo Gangetic Plain and the National Capital Territory (NCT) of Delhi, experiences some of the most severe and persistent pollution episodes globally. Annual mean $PM_{2.5}$ concentrations in Delhi (~140 µg m^{-3}) exceed the WHO (2021) guideline by nearly thirtyfold (Bhattu et al., 2024). Such episodes reflect both intense local emissions and substantial regional transport from surrounding states, including Punjab and Haryana (Ambulkar et al., 2025). Post-harvest crop residue burning during October-November often coincides with low wind speeds, frequent temperature inversions, and seasonal circulation changes, which collectively favour pollutant accumulation (Singh et al., 2020; Lalchandani et al., 2022; Nagar et al., 2017). India burns ~116 Tg yr^{-1} of agricultural residue, contributing ~9-13% of national $PM_{2.5}$ emissions (Yin et al., 2019). Achieving sustained air quality improvement over Delhi and the broader IGP therefore requires integrated, multi-sectoral, and regionally coordinated mitigation strategies that account for both local sources (transport, industry, domestic fuel use) and regional transport processes, supported by scientifically robust assessments using regional air quality models.

1.1.4 Principles and Applications of Online Chemical Transport Models: Focus on WRF-Chem

Chemical Transport Models (CTMs) are essential tools for investigating the atmospheric distribution, transformation, and removal of trace gases and aerosols across scales. A key advantage of online CTMs is their explicit representation of feedbacks between meteorology and chemistry, enabling chemically active species and aerosols to evolve consistently with boundary-layer dynamics, clouds, radiation, and precipitation (Grell et al., 2004). CTMs simulate the transport and evolution of species through resolved advection, convection, and PBL mixing, along with chemical production and loss and wet and dry deposition. Model simulations generally depend on meteorological analysis datasets and on emission inventories that provide surface fluxes of anthropogenic and natural sources. CTMs are widely used in combination with observations to examine atmospheric processes that shape pollutant concentrations (Emmons, 2003; Jacob et al., 2005; Mao et al., 2010), to quantify source-receptor relationships (Cook et al., 2007), and to estimate atmospheric budgets over regional to global domains (Duncan et al., 2007).

A widely used online CTM is the Weather Research and Forecasting model coupled with Chemistry (WRF-Chem), which is employed in this thesis to assess sectoral and primary emission contributions to $PM_{2.5}$ and to understand the coupled chemical and transport processes governing $PM_{2.5}$ over India. The overarching goal in CTM applications is to reproduce pollutant concentrations alongside key meteorological fields (temperature, humidity, winds, pressure) because these jointly control emissions, chemistry, transport, and deposition. WRF-Chem is built upon a fully compressible, non-hydrostatic, Eulerian framework that solves the governing equations for mass, momentum, and energy along with the ideal gas law, while simultaneously integrating chemical continuity equations for gaseous and particulate species. This architecture enforces consistency between atmospheric physics and chemistry at each model time step.

WRF-Chem is based on the Advanced Research WRF (ARW) dynamical core (Skamarock et al., 2019) (Fig. 1.5), designed for flexibility and computational efficiency on parallel architectures. The model supports a broad range of applications from operational forecasts to research simulations at mesoscale, regional, and local scales. It employs Runge-Kutta second- and third-order time integration and uses horizontal and vertical advection schemes spanning second to sixth order. Prognostic variables include three-dimensional wind components (u, v, w), perturbation potential temperature, geopotential, and surface pressure, with optional prognostic fields such as turbulent kinetic energy (TKE), water vapour, cloud condensate, and precipitation

mixing ratios. Physical parameterizations include cloud microphysics schemes, land surface models ranging from simple thermal formulations to coupled vegetation soil moisture systems, boundary-layer schemes (TKE-based or non-local K approaches), and longwave/shortwave radiation parameterizations. The vertical coordinate system is terrain-following hydrostatic pressure (Kumar et al., 2012). In online-coupled mode, meteorology, chemistry, emissions, and transport are computed on a common grid at each time step using consistent parameterizations (Grell et al., 2011).

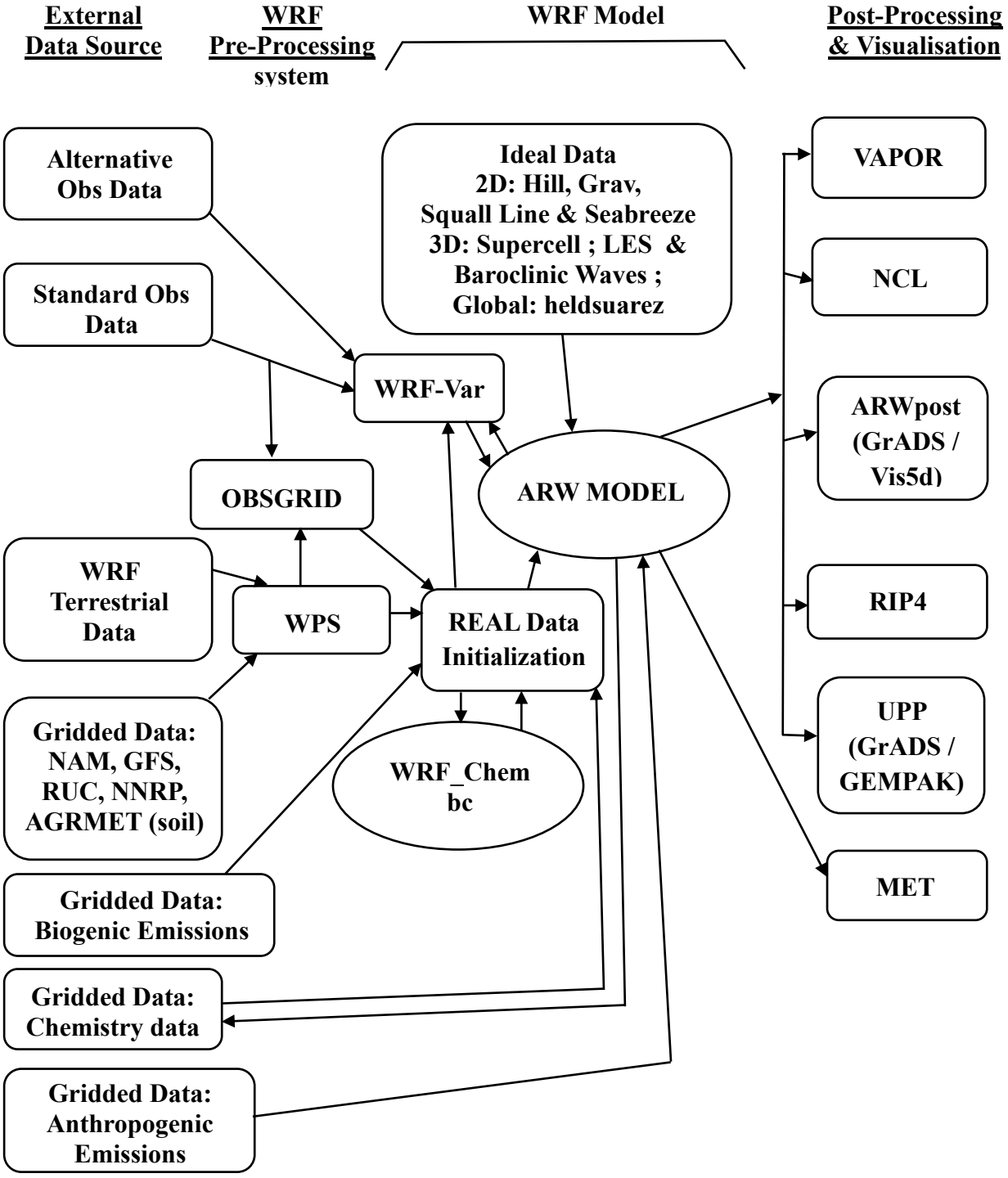


Figure 1.5: WRF-Chem Modelling System Flow Chart adapted from Zhang et al., 2021.

Emission inventories are a central input and a major source of uncertainty in CTM simulations, and uncertainties in emission magnitudes, temporal profiles, and chemical speciation can strongly influence simulated concentrations and composition (Smith et al., 2011; Zhao et al., 2011). Emissions are typically characterized into anthropogenic and natural sources. Anthropogenic emissions arise from industrial activity, power generation, transportation, agriculture residue burning**,** and waste related processes. Natural emissions include biogenic VOC emissions from vegetation, soil emissions, wildfires, volcanoes, and lightning. Natural emissions are strongly modulated by meteorology (temperature, radiation, precipitation) and land-surface characteristics (vegetation type, leaf area index, land use), and they are often considered the most uncertain component of total emissions (Zhang, 2008). Emission estimates are commonly constructed using emission factors (EFs) combined with activity data to quantify fluxes from specific source categories.

Within WRF-Chem, biogenic emissions are often estimated using the Model of Emissions of Gases and Aerosols from Nature (MEGAN) (Guenther, Karl, Harley, Wiedinmyer, Palmer, & Geron, 2006), which computes emissions for each Plant Functional Type (PFT) as functions of radiation and temperature. The WRF-Chem emission module converts point, area, and mobile sources into gridded, temporally resolved emissions consistent with model resolution and chemical mechanism via temporization, speciation, and gridding steps. This produces hourly gridded fluxes of major species such as CO, NO, NO_2, SO_2, HNO_2, and various volatile organic compounds (VOCs). Biomass burning emissions can be prescribed using products such as FINN (Fire INventory from NCAR), which provides daily varying emissions based on MODIS fire detections (Wiedinmyer et al., 2011).

Biomass burning exhibits pronounced seasonal variability in India, with peak emissions observed during spring due to open-field crop residue burning (Venkataraman et al., 2006) (Fig. 1.6). MEGAN is used to simulate isoprene and monoterpene emissions from vegetation, providing location and time-dependent net fluxes to the atmosphere. Improving emission inventories is therefore a key pathway to reducing uncertainty in regional air quality modelling, strengthening the evidentiary basis for pollution control strategies, and improving confidence in assessments of health and environmental impacts.

India’s air pollution problem is intensified by the diversity of sources interacting with strong seasonal meteorological contrasts, including monsoon-driven removal, winter stagnation and inversions, and episodic dust transport. Numerical frameworks such as WRF-Chem are

therefore indispensable for simultaneously representing emissions, transport, chemical transformation, and deposition (Shrivastava et al., 2014). Model sensitivity to physical parameterizations, land-surface schemes, and emission inventories is particularly important over India because seasonal meteorological regimes strongly modulate pollutant accumulation and removal (Gunwani et al., 2021; Mohan et al., 2018). The COVID-19 lockdown in 2020 provided a unique "natural experiment" in which abrupt reductions in industrial, transportation, and construction activities produced measurable declines in primary and secondary pollutants, while also exposing the dominant role of meteorology (e.g., boundary layer height, winds, precipitation) in shaping observed $PM_{2.5}$ variability (Xie et al., 2024). These outcomes reinforce the need for fully coupled modelling approaches such as WRF-Chem to represent real-world emission-chemistry-meteorology interactions and to support reliable attribution of air quality changes.

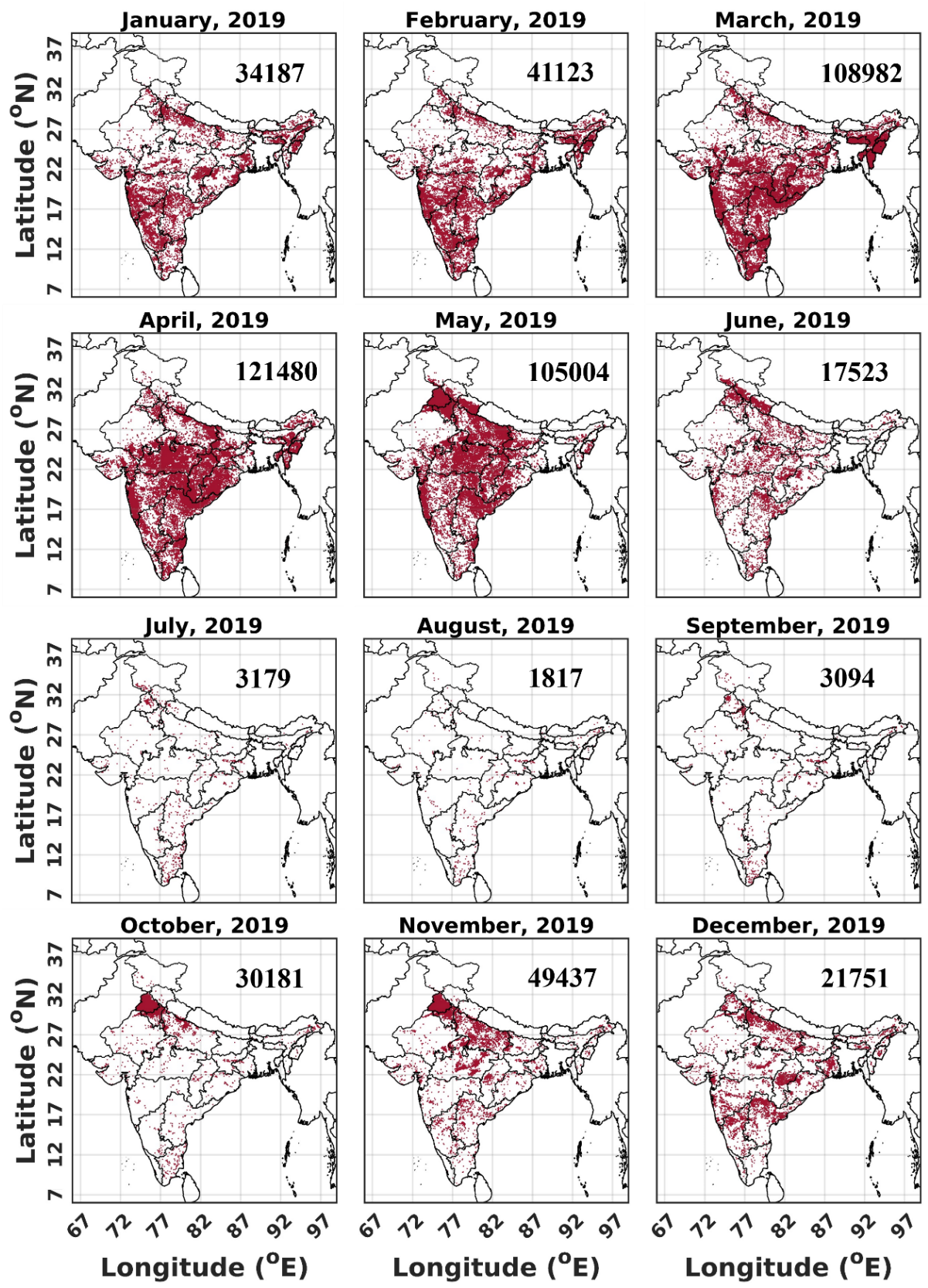


Figure 1.6: Monthly active Fire Locations from the Visible Infrared Imaging Radiometer Suite (VIIRS) for 2019, with the Total Fire Count across India displayed within the plot.

1.2 Motivation, Knowledge Gaps and Scope of the Thesis

Numerical Weather Prediction (NWP) and regional atmospheric models are increasingly used to study and forecast extreme pollution episodes, but achieving credible simulations requires careful region-specific configuration and parameterization. Models represent key sub-grid processes, radiation, surface fluxes, turbulence, cloud microphysics, and convective transport, through parameterizations that can strongly influence boundary-layer structure, dispersion, cloud–precipitation processes, and hence pollutant concentrations (Shrivastava et al., 2014). The WRF modelling system has become a widely used and flexible regional framework for understanding meteorological processes and their coupling with severe air pollution episodes. The WRF modelling system has become a widely used and flexible regional framework for understanding meteorological processes and their coupling with severe air pollution. However, WRF offers multiple physics and chemistry choices, and selecting an optimal combination is non-trivial and often case-dependent (Patil et al., 2016).

Globally, numerous sensitivity studies have evaluated how WRF physical parameterizations simulated meteorology. PBL schemes have been tested in settings ranging from typhoon environments over the Northwest Pacific Ocean (Di et al., 2019) to urban and regional domains such as Greater Athens (Banks et al., 2016), Southern Italy (Avolio et al., 2017), Texas (Hu et al., 2010), and the Iberian Peninsula (Borge et al., 2008), with a focus on near-surface variables and PBL height. Several studies have also examined combined sensitivities, demonstrating that interactions among PBL, cumulus, and microphysics options can modify rainfall and boundary-layer evolution (Liu et al., 2020; Zeyaeyan et al., 2017).

Over India, many studies have sought to improve WRF performance for meteorology and associated applications (Gunwani et al., 2017; Sathyanadh et al., 2017). For example, Sathyanadh et al. (2017) evaluated six PBL schemes (MYJ, BouLac, UW, YSU, and ACM2) at 1 km resolution over Barkachha (25.06°N, 82.59°E) and found that MYNN produced more realistic boundary-layer height variability. Hariprasad et al. (2014) tested seven PBL schemes (MYJ, MYNN, QNSE, YSU, ACM2, BL, and UW) over Kalpakkam and reported that MYNN and YSU best captured observed PBL characteristics. Madala et al. (2014) examined five PBL schemes (YSU, MYJ, MYNN2, MRF, ACM2) and three cumulus schemes (KF, BMJ, GD) for a severe thunderstorm over Gadanki and suggested that the MYJ-GD combination performed best. Panda et al. (2012) investigated PBL schemes (MYJ, YSU, MRF) and land-surface options (Noah, RUC, THD) over

northern India and reported improved surface and boundary-layer predictions with the Noah-MYJ combination. Patil et al. (2016) analyzed sensitivity to microphysics schemes during Western Disturbances over northwestern India and concluded that the NSSL one-moment microphysics with Kain-Fritsch cumulus, YSU PBL, RRTM longwave, and Dudhia shortwave options produced the best results. Over Delhi, Mohan et al. (2011) found that MM5-YSU improved wind speed estimates, while Pleim-ACM improved temperature and moisture predictions. Gunwani et al. (2017) tested five PBL schemes (YSU, MYJ, ACM2, QNSE, MYNN) and reported ACM2 as most suitable for simulating a broad set of meteorological parameters.

Collectively, these studies highlight that parameterization performance is highly region-, season-, and event-specific. Therefore, physics choices optimized for one domain or synoptic regime may not generalize to another because of differences in domain size, resolution, simulation period, synoptic forcing, land-atmosphere coupling, and topography. NWP modelling has become indispensable for understanding meteorology across scales and for applications spanning climate, agriculture, disaster management, energy forecasting, and urban meteorology (Warner, 2010). Depending on domain extent and resolution, models are often categorized into global and regional systems. Global models provide short- to medium-range forecasts (~10-15 days), whereas regional models typically provide higher-resolution simulations over shorter ranges (~1-3 days) (Eugenia Kalnay, 2002).

The WRF model has also been widely applied to floods (Jabbari et al., 2018; Karki et al., 2018; Mahoney et al., 2018; Sikder et al., 2s019), urban heat islands (Mohan et al., 2013; Morini et al., 2017; Ramamurthy et al., 2023; Wang et al., 2016), air pollution (Balakrishnan et al., 2019; Mohan et al., 2018; Nandi et al., 2020, 2025; Upadhyay et al., 2018), and fog formation (Upadhyay et al., 2018). These applications all depend on parameterizations that represent unresolved processes such as evaporation, condensation, friction, radiation, and turbulent exchanges (Kalnay, 2002). As model complexity grows, so does the need for careful and defensible selection of physics and chemistry options. WRF includes a broad suite of parameterizations (PBL, microphysics, cumulus, radiation, land-surface, shallow convection, surface layer, urban canopy, and ocean processes), and sensitivity analyses over India have documented the importance of choosing schemes that are appropriate for the region and season (Gunwani et al., 2021, 2017). Microphysics options have similarly been tested for simulating cloud processes and precipitation over India (Rajesh et al., 2017; Mohan et al., 2018; Singh et al., 2018; Srinivas et al., 2018).

Against this modelling backdrop, India's air pollution burden has intensified with rapid urbanization and industrial expansion (Karambelas et al., 2018). WHO assessments have reported multiple Indian cities among the most polluted globally (WHO, 2018), and air pollution has contributed to substantial premature mortality and ecological and agricultural damages (Balakrishnan et al., 2019; Lal et al., 2017). Although emission control initiatives, such as clean fuel transitions under the Clean India Mission (CIM), have been implemented, both long-term and short-term strategies have often been insufficient to achieve sustained compliance with ambient standards (Banerjee et al., 2017; Purohit et al., 2019). The COVID-19 pandemic created an unexpected opportunity to assess the consequences of abrupt emission reductions. In India, after the first confirmed case on 30 January 2020, a nationwide lockdown began on 24 March and was extended through 30 June. While these restrictions helped mitigate viral spread (Anderson et al., 2020; Pai et al., 2020), they also sharply reduced emissions by suspending industrial, transport, and construction activities (Chintalapudi ets al., 2020; Dantas et al., 2020).

Many studies documented conspicuous decreases in pollutant concentrations during lockdown periods (Gautam, 2020; Isaifan, 2020). $PM_{2.5}$ reductions of up to ~50% were reported across India (Mahato et al., 2020; Sharma et al., 2020). In contrast, increases in ground-level ozone were observed in multiple regions (Sicard et al., 2020), and severe pollution episodes still occurred under unfavourable meteorology (Wang et al., 2020). Evidence also suggests that the realized improvements were sometimes smaller than expected from emission reductions alone, highlighting the importance of chemical and meteorological controls (Bekbulat et al., 2020). Regional assessments reported sharp improvements in India's National Air Quality Index (NAQI) during early lockdown, especially over Delhi (Mahato et al., 2020), and substantial decreases in primary pollutants across major cities (Kumari et al., 2022; Srivastava et al., 2020). Selvam et al. (2020) reported a 58% AQI improvement in Gujarat during March-April 2020 relative to 2019. Satellite analyses indicated record-low aerosol levels (Gautam, 2020), and large $PM_{2.5}$ reductions across the IGP were also reported (Das et al., 2021; Kabiraj et al., 2020). However, many of these studies relied primarily on surface observations and often did not explicitly separate meteorological influences from emission-driven changes or represent chemical processing pathways (Sahu et al., 2020). Further, limited monitoring coverage and uneven station distribution introduce spatial bias in observation-only evaluations.

Delhi, often cited as the second-largest megacity globally (Tickell et al., 2018), has experienced rapid population growth and intensified economic activity, amplifying emissions from transport, industry, and power generation. Rising vehicle sales, increased transport demand

(projected to grow by 200% between 2015 and 2030; Amann et al., 2017), and growth in traffic volume and energy use have contributed to persistent air quality deterioration (Gulia et al., 2018; Kanawade et al., 2020). WHO assessments have repeatedly placed Delhi among the world's most polluted cities (WHO, 2016, 2018), with $PM_{2.5}$ far exceeding NAAQS (Kumar et al., 2017). The resulting health burden includes elevated risks of asthma, pneumonia, and other respiratory outcomes (Heal et al., 2012; Rizwan et al., 2013). In 2017, ICMR declared a community health emergency in the National Capital Region (Chowdhury et al., 2019). Nationally, air pollution has been identified as a leading driver of premature mortality, with a large fraction of deaths in India associated with air pollution exposure (WHO, 2014; Dandona et al., 2017).

The economic burden of pollution-related health impacts is also substantial; in many developing contexts where public expenditure supports healthcare, welfare costs associated with air pollution have been estimated to approach ~8% of GDP (Lim et al., 2012). Regulatory and policy interventions in Delhi and nationally have included restrictions on highly polluting industries, tighter vehicle emission standards, adoption of compressed natural gas (CNG) for public transport, conversion of coal-based plants to natural gas (CPCB, 2011), heavy vehicle bans, and the odd-even traffic policy (Kumar et al., 2017). Yet, pollution levels remain critically high, raising questions about the effectiveness of existing measures and the need for regionally coordinated, multi-sectoral strategies. The COVID-19 lockdown provided a rare opportunity to evaluate air quality response to large-scale emission reductions; CPCB reported sharp declines across multiple cities within days of lockdown onset (Sharma et al., 2020). Such a "natural experiment" is valuable for diagnosing emission-meteorology interactions and for assessing whether targeted reductions could achieve meaningful and sustained benefits.

To quantify and communicate air quality, multiple indices have been proposed over time, including the Air Pollution Index (API), Pollutant Standards Index (PSI), and Air Quality Index (AQI) (Shenfeld, 1970). These indices differ in pollutant selection and aggregation methods (Qian et al., 2004). CPCB subsequently revised the National Air Quality Index (NAQI) using the Maximum Operator approach to address limitations and improve alignment with Indian National Ambient Air Quality Standards (INAQS), and NAQI is now widely adopted for real-time air quality reporting in India. Overall, the lockdown period highlights that a comprehensive, quantitative evaluation, explicitly separating emission changes from meteorological variability, is essential to uncover the controlling mechanisms and to inform realistic, durable policy interventions for megacities such as Delhi.

Emission inventories for Delhi and South Asia identify transportation, industrial emissions, roadside dust, domestic fuel use, and biomass burning as major contributors to $PM_{2.5}$ (Conibear et al., 2018; Guo et al., 2018). Considerable progress has been made using receptor-based source apportionment and high-resolution measurements (Lalchandani et al., 2021; Reyes-Villegas et al., 2021). Advanced aerosol mass spectrometry has revealed important features of urban aerosol composition and sources. Tobler et al. (2020) and Lalchandani et al. (2021), using ToF-ACSM and HR-ToF-AMS, identified a solid fuel combustion organic aerosol (SFC-OA) factor, chemically similar to biomass burning organic aerosol (BBOA) but enriched in aromatic compounds and polycyclic aromatic hydrocarbons (PAHs). SFC-OA contributed ~20-35% of total organic aerosol (OA) at suburban and urban sites in Faridabad (Haryana) and Delhi, respectively. Rai et al. (2020) similarly identified an SFC-related factor using highly time-resolved measurements of atmospheric metals. Additional primary OA sources have also been quantified: Bhandari et al. (2020) reported that hydrocarbon-like organic aerosol (HOA), typically associated with vehicular emissions, contributes ~16% of total PM burden, while Singh et al. (2021) found BBOA accounts for ~50% of brown carbon absorption during winter. Goel et al. (2021) concluded that biomass burning is a major post-monsoon pollution source based on BC measurements.

Despite these advances, uncertainties persist regarding the magnitude and mechanisms by which biomass burning drives haze over Delhi and across the IGP, partly due to limited multi-species observations, inadequate vertical profiling, and insufficient characterization of boundary-layer structure and evolution. These limitations restrict understanding of dispersion, entrainment, and long-range transport processes that are central to interpreting episodic pollution and evaluating control strategies. Seasonal haze across northern India is strongly influenced by open burning of post-harvest agricultural residues (Patel et al., 2021; Rastogi et al., 2014), a practice also documented as an important pollution source globally (Cao et al., 2017; Zhang et al., 2017). Venkataraman et al. (2006) estimated ~116 Tg yr^{-1} of crop residue burning in India, contributing ~25% of national BC, organic matter (OM), and CO emissions, and ~9-13% of $PM_{2.5}$ emissions, with negligible SO_2 contribution. Dual-carbon isotope fingerprinting suggests ~42 ± 17% of total BC over Delhi originates from regional biomass burning (Bikkina et al., 2019). Agricultural burning also emits VOCs that can form SOA through oxidation (Li et al., 2014) and increases in reactive gases following burning events have been observed downwind in northwestern India (Kumar et al., 2018). Nevertheless, the quantitative contribution of agricultural residue burning to Delhi's post-monsoon $PM_{2.5}$ remains uncertain due to limited spatiotemporal coverage, chemical speciation constraints, and inadequate boundary-layer observations.

In summary, despite extensive research on $PM_{2.5}$ pollution over India and its impacts, several key modelling and attribution gaps remain. (i) Many WRF-Chem and related modelling studies have explored individual factors (e.g., PBL schemes or inventories) in isolation; integrated sensitivity assessments across India's highly contrasting meteorological regimes remain limited. This is critical because monsoon conditions feature strong convection, high humidity, and efficient wet removal, whereas winter conditions feature shallow stable layers, inversions, and strong accumulation. (ii) Many lockdown-era studies focused only on the strict lockdown phase and did not extend to unlock phases when emissions resumed; further, meteorological normalization and chemistry-aware interpretation were often limited, and observation-only assessments were constrained by sparse and non-uniform monitoring networks. (iii) The lockdown period demonstrated that emission reductions alone do not fully explain observed $PM_{2.5}$ changes; meteorology can dominate short-term variability, highlighting the need for long-term, sector-specific, regionally coordinated strategies informed by coupled modelling.

This thesis is designed to address these gaps through systematic regional air quality modelling, targeted sensitivity experiments, and sectoral emission perturbation approaches, with a particular emphasis on North India and the NCT Delhi airshed.

1.3 Research Questions

This thesis addresses the above knowledge gaps through the following key research questions:

1. How sensitive are the simulated concentrations of major air pollutants over India to variations in parameterization schemes, emission inventories, and meteorological configurations in the WRF-Chem model?
2. To what extent did changes in emissions and meteorological conditions individually contribute to variations in air quality during the COVID-19 period?
3. What are the relative contributions of different emission sectors and chemical species to surface $PM_{2.5}$ levels over major North Indian states within the NCT Delhi airshed region?
4. How effective are sector-specific versus multi-sectoral emission control strategies in improving air quality across the National Capital Region within the NCT Delhi airshed?

1.4 Thesis Objectives

To systematically answer these questions, this thesis employs regional air quality modelling to quantify sectoral and primary emission contributions to $PM_{2.5}$ pollution over North India. By integrating model sensitivity experiments with emission perturbation and attribution analyses, the study disentangles the relative roles of emissions and meteorology in driving severe pollution episodes. The outcomes are intended to provide actionable scientific evidence for designing multi-sectoral, regionally coordinated mitigation strategies, particularly for NCT-Delhi and the broader Indo Gangetic Plain.

The key research objectives of this thesis are:

1. Investigation of the sensitivity of major air pollutant levels simulated by the WRF-Chem to different parameterization schemes, emission inventories, and meteorological options over India.
2. To quantify and distinguish the impacts of changing emissions and meteorological conditions on air quality levels over India during the COVID-19 period.
3. To estimate the contributions of emission sectors and chemical species to surface $PM_{2.5}$ over North Indian states within the NCT Delhi airshed region.
4. Evaluation of the relative effectiveness of sector-specific and multi-sectoral emission control strategies over the Delhi NCR and NCT Delhi airshed in improving regional air quality across the NCT Delhi.

1.5 Structure of the Thesis

This thesis comprises of six chapters, including four working chapters aligned with four objectives described above. A brief is provided below:

Chapter 1: Introduction

This chapter presents an overview of atmospheric composition, the distribution and transformation of air pollutants, and the fundamental concepts governing atmospheric aerosols. It emphasizes aerosols as a key component of the Earth–atmosphere system and discusses aerosol lifecycles, spatial-temporal variability, and the factors controlling atmospheric burdens, as documented in previous studies. The sources and sinks of surface particulate matter (PM) and their

implications for human activity and environmental systems are reviewed. The chapter introduces Chemical Transport Models (CTMs), focusing on the online-coupled WRF-Chem framework and its operating principles and applications. It then reviews previous work on $PM_{2.5}$ pollution over India, with emphasis on modelling studies over North India during severe pollution episodes and highlights the strengths and limitations of aerosol-related parameterizations in the context of model uncertainty. Finally, the chapter motivates the present thesis, defines the region of interest, identifies key knowledge gaps, and outlines the scope of the study to guide subsequent chapters.

Chapter 2: Improving Regional $PM_{2.5}$ Modelling over North India

This chapter systematically evaluates WRF-Chem sensitivity to meteorological and chemical configurations during two contrasting periods: the monsoon season (August 2018) and winter (January 2019). The objective is to identify an optimal WRF-Chem setup for simulating air pollution under seasonally distinct conditions. The strengths and limitations of commonly used parameterizations and emission inventories are assessed for their influence on model skill. The resulting configuration improves predictive capability and supports more reliable air quality forecasting and mitigation assessment.

Chapter 3: Drivers of $PM_{2.5}$ Changes during the COVID-19 Period

This chapter combines satellite-derived $PM_{2.5}$ data with WRF-Chem simulations to analyse surface $PM_{2.5}$ before, during, and after COVID-19 lockdown phases across India. The analysis isolates meteorology-driven variability from emission-driven changes, improving understanding of air quality response to reduced activity. The results show substantial $PM_{2.5}$ declines during lockdown in many regions, while highlighting continued contributions from less-restricted sectors (notably residential). The chapter also evaluates emission changes during lockdown and subsequent unlock phases to characterize how emissions and meteorology jointly shaped observed air quality.

Chapter 4: Sectoral and Species Drivers of Surface $PM_{2.5}$ in Delhi Airshed

This chapter synthesizes literature on sectoral contributions and chemical composition of $PM_{2.5}$ during post-monsoon and winter, when crop residue burning can strongly affect northern India. Using a high-resolution online-coupled chemistry–transport model with updated emission inventories and real-time biomass burning emissions, the chapter quantifies sectoral contributions over North India and the NCT Delhi airshed. Sectors include agriculture, biomass burning, transport, trash burning, energy production, industry, residential emissions, and natural/biogenic sources (biogenic emissions, aqueous aerosols, natural dust, forest fires, grassland fires). $PM_{2.5}$

composition is analyzed for major components including BC, OA, NO_3^-, SO_4^{2-}, NH_4^+, and other inorganic/aqueous/dust species, enabling identification of dominant sources and key chemical drivers.

Chapter 5: Toward Improving Regional $PM_{2.5}$ in the NCT Delhi Airshed

This chapter provides a quantitative assessment of potential benefits of existing Government of India policies across northern India, emphasizing pathways for reducing pollution and increasing the frequency of good-to-moderate AQI days, particularly over NCT Delhi. Building on the sectoral and compositional analyses, it targets dominant sectors and upwind regions influencing Delhi. The chapter accounts for meteorological controls, circulation patterns, and regional transport, evaluates effectiveness of ongoing initiatives, identifies gaps, and highlights priorities for improved mitigation to achieve cleaner air.

Chapter 6: Summary and Scope for Future Work

The final chapter summarizes the major conclusions of the thesis, discusses limitations, and outlines directions for future research.

Chapter 2: Improving Regional $PM_{2.5}$ Modelling over North India: A WRF-Chem Configuration and Sensitivity Study

2.1 Introduction

Air pollution in India poses an enduring environmental and public health crisis, particularly in rapidly urbanizing and industrializing regions such as Delhi, Mumbai, and Kolkata, where growing vehicular activity, industrial emissions, construction dust, and widespread biomass burning contribute to persistently high pollutant levels (Ghude et al., 2020; Pandey et al., 2014). Concentrations of particulate matter ($PM_{2.5}$ and PM_{10}), nitrogen oxides (NO_x), sulfur dioxide (SO_2), carbon monoxide (CO), and ground-level ozone (O_3) often exceed national and international standards, with substantial implications for human health, ecosystems, visibility, agricultural productivity, and the economy (Cohen et al., 2015). Although urban centres experience the most severe pollution episodes, rural regions are also heavily affected by agricultural residue burning and household biomass fuel use, emphasizing the nationwide extent of the problem. Winter meteorology, marked by strong inversions, weak winds, and shallow boundary layers, frequently exacerbates pollution accumulation near the surface, leading to severe smog events and elevated health risks (Ganguly et al., 2006; Mahapatra et al., 2018; Mohan et al., 2011).

The complexity of India's air pollution arises from the confluence of diverse emission sources and highly heterogeneous meteorological conditions. Numerical weather prediction (NWP) models, particularly the Weather Research and Forecasting model coupled with Chemistry (WRF-Chem), play a central role in simulating these coupled processes (Skamarock et al., 2008). WRF-Chem resolves emissions, transport, chemical transformation, deposition, and meteorology within a unified modelling framework, enabling process-level understanding of pollutant behaviour. However, the accuracy of WRF-Chem simulations is highly sensitive to choices in meteorological initial and boundary conditions, physical and chemical parameterization schemes, and emission inventories (Shrivastava et al., 2014). These sensitivities are especially consequential in India, where monsoonal circulations, winter stagnation, pre-monsoon dust activity, and steep spatial gradients in terrain, from coastal regions to the Himalayas, create complex meteorological regimes that strongly modulate pollutant dispersion and transformation (Gunwani et al., 2017).

Accurate meteorological simulation is particularly vital in India, where extreme events such as heatwaves, lightning, cold surges, and heavy precipitation are key drivers of socioeconomic impacts, with 25% of accidental deaths between 2001 and 2014 linked to such events (Ghoshal Chowdhury et al., 2025; Mahapatra et al., 2018). WRF-Chem applications in the region have expanded rapidly, driven by its ability to represent monsoon dynamics, moisture

fluxes, and convective processes that shape rainfall patterns and pollutant distribution (Ragi et al., 2017; Rajeevan et al., 2013). The selection of planetary boundary layer (PBL) schemes, microphysics schemes, and radiation parameterizations critically influences simulations of temperature, wind speed, turbulence, and pollutant concentrations (Stensrud, 2011). PBL schemes are especially important for resolving diurnal mixing and vertical transport of pollutants, with substantial impacts on surface ozone, PM, and other regulated species (Anand K A et al., 2025; Ghude et al., 2020; Hariprasad et al., 2014; Yerramilli et al., 2012).

Despite major advances, WRF-Chem performance over India continues to exhibit substantial uncertainties, driven by the region's meteorological diversity, complex chemistry, and emission heterogeneity (Sikder et al., 2019). Sensitivity studies have shown that improved model accuracy requires careful combination of parameterization schemes, high-quality meteorological inputs, and region-specific emissions (Gupta et al., 2015). Data assimilation approaches such as Four-Dimensional Data Assimilation (FDDA) or grid nudging can enhance large-scale meteorological realism by constraining model fields toward observations, thereby improving the representation of temperature gradients, wind profiles, and pollutant transport (Liu et al., 2012). Prior studies have also demonstrated that microphysics choices significantly influence rainfall, wet deposition, and cloud-aerosol interactions (Mukhopadhyay et al., 2010; Srinivas et al., 2013), while aerosol schemes such as MADE-SORGAM (Modal Aerosol Dynamics Model for Europe - Secondary Organic Aerosol Model) (Schell et al., 2001) and MOSAIC (Model for Simulating Aerosol Interactions and Chemistry) (Zaveri et al., 2008) can lead to divergent predictions of $PM_{2.5}$ (Balzarini et al., 2015). Boundary layer and land surface schemes similarly modulate surface fluxes and turbulence, affecting pollutant mixing depth and vertical structure (Mohan et al., 2018).

Although numerous studies have examined individual components of WRF-Chem over India, such as boundary layer schemes, chemical mechanisms, or emission inventories, few have performed a comprehensive, multi-component sensitivity assessment spanning contrasting meteorological regimes. This gap limits our understanding of how different modelling choices interact to influence pollutant simulations across India's diverse atmospheric environment. To address this need, the present study systematically evaluates WRF-Chem sensitivity to meteorological and chemical configurations during two distinct periods: the monsoon season (August 2018) , characterized by strong convection, high humidity, and efficient wet deposition; and the winter season (January 2019), dominated by stagnant conditions, shallow PBLs, and pollution buildup (Ganguly et al., 2006; Ghude et al., 2020). Through coordinated perturbations to meteorological initial and boundary conditions, PBL schemes, microphysics schemes, chemical

mechanisms, emission inventories, and grid-nudging strengths, we identify an optimal WRF-Chem configuration capable of more accurately reproducing observed meteorological fields and air pollutant concentrations across India.

This work advances regional air-quality modelling by evaluating the combined effects of physical and chemical modelling choices rather than assessing individual components in isolation. The resulting optimized configuration has substantial implications for air-quality forecasting, long-term air pollution assessments, and policy design. Although the present analysis focuses on August (peak monsoon) and January (peak winter), we recognize that India also experiences distinct pre-monsoon and post-monsoon regimes. Pre-monsoon conditions are characterized by high temperatures, deep daytime boundary layers, and frequent dust transport from western arid regions, while post-monsoon conditions over northern India are often influenced by enhanced stagnation and episodic agricultural biomass burning. These regimes introduce additional sensitivities related to dust emission and transport, aerosol optical properties and mixing state, and the temporal allocation and vertical injection of biomass-burning emissions. A full extension of the present multi-component sensitivity matrix to these seasons would require a substantial additional set of simulations and is therefore beyond the scope of this work. Instead, we use the two most meteorologically contrasting regimes, peak monsoon and peak winter, to provide a stringent test of WRF-Chem meteorology-chemistry coupling and to identify a robust baseline configuration intended for broad air-quality applications across India.

2.2 Methodology

2.2.1 Model Configuration

The Weather Research and Forecasting model coupled with Chemistry (WRF-Chem, v4.2.2) (Grell et al., 2005) was used to simulate meteorological and atmospheric composition over the Indian subcontinent. WRF-Chem integrates prognostic meteorological fields generated by the Weather Research and Forecasting (WRF) model with fully interactive gas-phase chemistry and aerosol processes, enabling the coupled simulation of emissions, transport, chemical transformation, and deposition of atmospheric pollutants within a single modelling system (Skamarock et al., 2008). This fully coupled approach is particularly well suited for India, where

strong interactions between complex emission patterns and highly variable meteorological conditions occur across seasons, and terrain types.

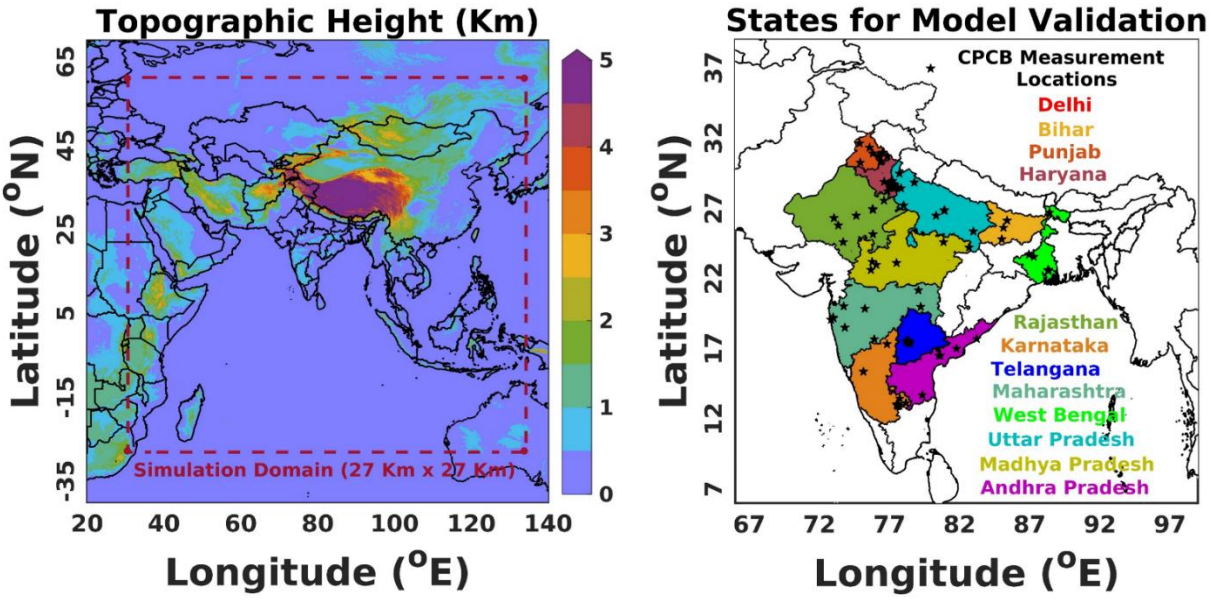


Figure 2.1: WRF-Chem simulation domain overlaid with Topographic Height (first panel) and different Indian states that have been used for validating the model performance (second panel) are shown, overlaid with CPCB measurement sites available for 2018, 2019. This setup was used to examine the WRF-Chem model performance with multiple sensitivity choices over the Indian region.

The model domain spans 60°E to 106°E and 1°N to 46°N, encompassing India and surrounding regions to account for long-range transport influences. The domain is centred over Bilaspur (22.38°N and 82.13°E), providing balanced spatial coverage of India's diverse climatic zones while maintaining computational efficiency. Simulations were conducted at a horizontal resolution of 27 × 27 km using a grid of 321 × 331 points, with 39 vertical levels extending from the surface to 50 hPa (Fig. 2.1). This vertical configuration provides enhanced resolution within the planetary boundary layer (PBL), where pollutant mixing and removal processes dominate, while also allowing realistic representation of free-tropospheric and upper-level dynamical features (Kulkarni et al., 2020; Sharma et al., 2023).

Two simulation periods were selected to represent contrasting meteorological regimes. August 2018 corresponds to the monsoon season, characterized by deep convection, strong moisture transport, high humidity, and frequent wet deposition, whereas January 2019 represents winter conditions marked by weak winds, strong temperature inversions, shallow boundary layers,

and severe pollutant accumulation. A 10-day spin-up period was applied prior to each simulation to minimize initialization effects, and spin-up output was excluded from the analyses.

To systematically assess model sensitivity and identify an optimal configuration for air-quality applications over India, a comprehensive suite of sensitivity experiments was conducted. Seven distinct sensitivity experiment groups were designed to isolate the influence of individual modelling components, including meteorological initial and boundary conditions, physical parameterization schemes, chemical mechanisms, emission inventories, and grid-nudging strategies. These groups collectively comprise a total of 18 WRF-Chem simulations, following a controlled, stepwise experimental design in which one model component is varied at a time while all other settings are held constant. This approach enables a clear attribution of model performance differences to specific configuration choices.

Specifically, the first set of simulations (Control, CFSWRF, and GDASWRF) evaluated sensitivity to meteorological initial and boundary conditions. This was followed by experiments assessing planetary boundary layer and microphysics parameterizations (MYJWRF, MYNWRF, THOMWRF, and MDMWRF) to identify optimal representations of boundary-layer mixing and precipitation processes. Subsequently, Four-Dimensional Data Assimilation (FDDA) was introduced, and model performance was evaluated using two chemical mechanisms (CBMZWRF and Nudged03). Using the best-performing chemical configuration, four anthropogenic emission inventories (CMIPWRF, ED5WRF, ED6WRF, and HTAPWRF) were then tested for their ability to reproduce pollutant concentrations at the surface and 850 hPa. Finally, five additional simulations (Nudged05, Nudged1, NoNudPBL03, NoNudPBL05, and NoNudPBL1) were conducted to examine the sensitivity of model performance to grid-nudging strength and boundary-layer-specific nudging strategies. Details of all simulations, including their physical and chemical configurations, emission inventories, meteorological forcings, and nudging settings, are summarized in Table 2.1, which serves as a comprehensive reference for the experimental design and supports reproducibility of the study.

Unless otherwise stated, all sensitivity experiments are evaluated relative to a common baseline (Control) configuration. The Control simulation employs ERA5 meteorological initial and boundary conditions, the Yonsei University (YSU) planetary boundary layer scheme, Lin microphysics, the MOZART-MOSAIC chemical mechanism, the SMoG-COALESCE anthropogenic emission inventory, and no grid nudging. In each sensitivity experiment, only one

model component is modified relative to this baseline, while all other physical, chemical, emission, and meteorological settings are held fixed.

2.2.2 Sensitivity Experiments

The sensitivity experiments were designed to quantify how WRF-Chem responds to changes in key modelling components that collectively shape the simulation of meteorology, atmospheric chemistry, and pollutant distribution. These components include the selection of meteorological initial and boundary conditions, PBL schemes, microphysics schemes, chemical mechanisms, and emission inventories. Experiments were conducted for August 2018 and January 2019, enabling evaluation under monsoon and winter meteorological regimes, respectively. These seasons represent sharply contrasting atmospheric conditions, allowing a robust assessment of how different configurations influence the model's ability to reproduce observed meteorological variables and pollutant concentrations across India. For each sensitivity test, comparisons are conducted against the baseline configuration described in Section 2.2.1, ensuring that all reported differences arise solely from the targeted model component under investigation.

2.2.2.1 Meteorological Initial and Boundary Conditions

Meteorological initial and boundary conditions exert a dominant influence on model performance because errors or biases introduced at the lateral and initial boundaries propagate throughout the simulation, affecting cloud development, moisture transport, temperature gradients, wind fields, and ultimately pollutant transport and transformation (Anchev et al., 2020). To evaluate this influence, three widely used global meteorological datasets were tested.

ECMWF Reanalysis 5th Generation reanalysis (ERA5), with a horizontal resolution of 31 km, provides high-quality fields capable of resolving synoptic and mesoscale features critical for representing pollutant dispersion and meteorological variability across the Indian region (Govardhan et al., 2015). Its higher resolution and improved representation of monsoonal dynamics, moisture fluxes, and temperature structure offer potential advantages for both monsoon and winter simulations.

The National Centers for Environmental Prediction - Global Data Assimilation System (NCEP-GDAS) Final Analysis (0.25° resolution) offers high-frequency updates that capture rapid

temporal variability but is limited by its coarser horizontal resolution. This can weaken the representation of fine-scale meteorological features such as localized convergence, orographic lifting, or nocturnal low-level jets, which influence pollutant transport and dispersion (E Kalnay et al., 1996).

National Centers for Environmental Prediction Climate Forecast System Version 2 (NCEP CFSv2, 0.5° resolution) is widely used for climate applications, but its relatively coarse horizontal resolution and weaker representation of regional-scale features make it less suitable for resolving important processes such as shallow winter inversions, weak wind regimes, and humidity stratification, which are essential for pollution buildup and persistence (Saha et al., 2011).

The performance of these datasets was assessed by comparing simulated surface temperature, relative humidity, rainfall, and wind fields against observations, satellite products, and reanalysis datasets.

2.2.2.2 Planetary Boundary Layer (PBL) Schemes

The planetary boundary layer governs vertical exchange of heat, momentum, and atmospheric constituents, and thus strongly influences the dispersion, dilution, and near-surface accumulation of pollutants. Accurate representation of PBL processes is therefore critical for air-quality simulations, especially in regions such as northern India where shallow winter boundary layers exacerbate pollution episodes (Sathyanadh et al., 2017). Three PBL schemes were examined to capture the diversity of boundary-layer conditions characteristic of monsoon and winter seasons.

The Yonsei University PBL (YSU) (Hong et al., 2006), a nonlocal first-order closure scheme, is known for effectively representing convective boundary-layer dynamics and has demonstrated strong performance over Indian conditions during both monsoon and winter. Its ability to capture entrainment processes and the diurnal evolution of the PBL makes it a strong candidate for simulating pollutant mixing under varying atmospheric stability. The Mellor-Yamada-Janjic PBL scheme (MYJ) (Janjić, 1994) employs a local 1.5-order turbulence kinetic energy closure and is better suited to representing stable boundary layers. This makes it particularly relevant for winter conditions over regions such as the Indo-Gangetic Plain, where persistent temperature inversions and weak winds trap pollutants near the surface. The Mellor-Yamada-Nakanishi-Niino Level 3 PBL scheme (MYNN3) (Nakanishi et al., 2006) offers an advanced

turbulence parameterization designed for complex terrain and urban environments. It attempts to capture a broader spectrum of turbulent processes and may, in principle, improve pollutant dispersion simulations in heterogeneous landscapes.

These three schemes were evaluated using PBL height (PBLH), vertical temperature profiles, and surface pollutant concentrations illustrating how each scheme influences pollutant accumulation and vertical mixing across regions and seasons.

2.2.2.3 Microphysics Schemes

Microphysics schemes determine the representation of cloud formation, precipitation processes, and wet deposition, all of which exert direct control over atmospheric composition. This influence is especially pronounced during the monsoon, when rainfall is the dominant removal mechanism for aerosol and gas-phase pollutants (Pithani et al., 2019). To evaluate these processes, three microphysics schemes were examined.

The Lin scheme (Chen et al., 2002) is a widely used single-moment scheme that offers computational efficiency while providing reasonable performance for regional-scale meteorological and air-quality applications. Its representation of cloud microphysical processes and precipitation formation is often suitable for capturing large-scale monsoon rainfall patterns. The Thompson scheme (Thompson et al., 2008) is a more advanced double-moment formulation that improves the representation of cloud-aerosol interactions by predicting both mass and number concentrations for hydrometeors. Its enhanced microphysical detail may improve the simulation of cloud fraction, liquid water path, and aerosol-cloud interactions. The Morrison scheme (Morrison et al., 2009), also a double-moment scheme, is designed to capture a broad spectrum of hydrometeor species and is well suited for convective environments. Its ability to represent convective microphysical processes may contribute to improved precipitation fields and enhanced removal of pollutants.

Rainfall distributions, cloud fraction fields, and wet deposition estimate from these schemes were compared using India Meteorological Department (IMD) rainfall observations, Modern-Era Retrospective Analysis for Research and Applications, Version 2 (MERRA2) datasets, and satellite measurements.

2.2.2.4 Chemical Mechanisms

Chemical mechanisms govern the formation, transformation, and removal of gas-phase species and aerosols, including secondary pollutants such as ozone, sulfate, nitrate, and secondary organic aerosols (Knote et al., 2015). Two mechanisms were evaluated to assess their suitability for air-quality simulations over India's complex emission and chemical environments.

The Carbon Bond Mechanism version Z - Model for Simulating Aerosol Interactions and Chemistry (CBMZ-MOSAIC) mechanism (Zaveri et al., 1999) is computationally efficient and widely implemented in regional air-quality studies. However, its simplified representation of secondary chemistry may limit its ability to capture detailed oxidant chemistry and multiphase processes, especially under low-photolysis winter conditions or in regions with complex Volatile Organic Compounds (VOC) and Nitrogen Oxides (NO_x) mixtures. The Model for OZone And Related chemical Tracers - Model for Simulating Aerosol Interactions and Chemistry (MOZART-MOSAIC) mechanism (Emmons et al., 2010) includes more comprehensive representations of Ozone-NO_x-VOC chemistry, aerosol thermodynamics, heterogeneous reactions, and the Volatility Basis Set (VBS) approach for secondary organic aerosol formation (Knote et al., 2014). This richer framework enables improved simulation of secondary pollutant formation, making it more suitable for regions such as northern India where wintertime stagnation and complex emissions contribute to severe pollution episodes. Chemical mechanism performance was evaluated using pollutant concentrations from CPCB monitoring stations, MERRA2 and satellite observations for O_3, SO_4 and NO_x.

2.2.2.5 Emission Inventories

Emission inventories control the spatial and temporal distribution of pollutants entering the atmosphere and remain among the largest sources of uncertainty in chemical transport modelling (Tibrewal et al., 2023). Their accuracy is especially critical for India, where emissions vary sharply across dense urban centres, industrial clusters, rural areas reliant on biofuel combustion, and extensive biomass-burning regions. To evaluate how these uncertainties propagate into air-quality simulations, five widely used emission inventories were examined during both the monsoon and winter simulation periods.

The Coupled Model Intercomparison Project Phase 6 (CMIP6) inventory from Community Emissions Data System (Hoesly et al., 2018), available at a coarser 50 km resolution, is optimized for climate modelling applications rather than urban air-quality forecasting. Its coarse spatial representation tends to smooth strong emission gradients, which can lead to systematic underestimation of pollutant concentrations in densely populated or industrially active regions. Emissions Database for Global Atmospheric Research, Version 5 (EDGARv5) (Crippa et al., 2020), with a resolution of 10 km, supplies global emission coverage and updated sectoral contributions, but its reliance on generalized global activity data limits its ability to capture India's fine-scale urban and industrial emission structures.

Emissions Database for Global Atmospheric Research, Version 6.1 (EDGARv6.1) (Ferrario et al., 2022), also provided at 10 km resolution, incorporates more recent emission factors and activity data, yet still lacks the spatial detail required to characterize the intense but localized sources common in Indian metropolitan regions. Emissions Database for Global Atmospheric Research - Hemispheric Transport of Air Pollution, Version 3 (EDGAR-HTAPv3) (Crippa et al., 2023) provides updated global anthropogenic emissions intended for hemispheric transport assessments but remains limited in its ability to represent the complex emission heterogeneity characteristic of India.

The Speciated Multi-pOllutant Generator - COordinated Aerosol and oLution SOurce Emissions for Chemical Evaluation (SMoG-COALESCE) inventory (Venkataraman et al., 2024) is a recent high-resolution, India-specific dataset (5 km) that provides detailed sectoral emissions and offers the spatial granularity needed to resolve intra-urban gradients and localized emission hotspots. Anthropogenic emissions of $PM_{2.5}$ and its precursors are primarily taken from the Speciated MultipOllutant Generator-India (SMoG-India, 2019) (Lal et al., 2025), which provides sectorally resolved emissions for residential combustion, transportation, industry, energy production, agriculture, waste burning, and several other categories. This comprehensive sectoral breakdown makes SMoG-COALESCE particularly suited for simulating the diverse and spatially heterogeneous emission landscape of India.

Emission inventories that were directly available for the study period were used without modification. For inventories not available for the exact simulation months (August 2018 and January 2019), the most recent year available in the respective database was adopted as a representative proxy. Specifically, when emissions for August 2018 or January 2019 were available, those datasets were used directly; otherwise, the latest available August and January

emissions from that inventory were used to represent the corresponding simulation months. This approach ensures temporal consistency while relying on the most up-to-date emission information available for each inventory. The capability of each inventory to reproduce observed spatial and temporal pollution patterns, including regional gradients and urban pollution hotspots across the Indo-Gangetic Plain and major metropolitan centres, was systematically evaluated. The monthly total and sectoral emission comparisons over India from different emission inventories, used in the WRF-Chem emission inventory sensitivity simulations for major primary anthropogenic species during August and January, have been analyzed. The figure also illustrates the relative contribution of different emission sectors to the total emissions over the Indian region for the corresponding species and months. These comparisons reveal substantial differences in how inventories represent sectoral contributions and spatial variability, which ultimately influence the accuracy of WRF-Chem simulations under contrasting seasonal meteorological conditions.

2.2.2.6 Grid Nudging

Grid nudging was employed to constrain the model toward large-scale meteorological fields, thereby improving atmospheric realism without suppressing local-scale variability. This approach, commonly referred to as Four-Dimensional Data Assimilation (FDDA), enhances the accuracy of temperature, moisture, and wind fields, particularly in extended simulations (Bowden et al., 2012; Zittis et al., 2018). Nudging was applied above the PBL to preserve near-surface turbulence and vertical mixing processes that strongly influence pollutant dispersion (Lucas-Picher et al., 2016). Three nudging strengths, 0.0003 s^{-1}, 0.0005 s^{-1}, and 0.001 s^{-1}, were evaluated.

The effects of nudging on meteorological fields were examined using surface variables, surface temperature and wind speed, and vertical temperature profiles. Particular attention was given to winter simulations, where accurate representation of temperature inversions and stable boundary layers is essential for realistic pollutant accumulation.

2.2.3 Validation Datasets

Model evaluation utilized a diverse suite of observational datasets spanning surface, satellite, and reanalysis products to ensure robust multi-scale validation. Ground-based measurements of $PM_{2.5}$, PM_{10}, NO_x, SO_2, and O_3 were obtained from the publicly available Central Pollution Control Board (CPCB) air quality data repository (https://airquality.cpcb.gov.in/ccr/#/caaqm-dashboard-all/caaqm-landing/caaqm-data-repository), providing high temporal resolution observations of pollutant concentrations across major Indian cities. To address known CPCB data quality issues (Sharma et al., 2022; Vohra et al., 2025), we applied strict quality control by removing outliers and eliminating constant or repetitive values, ensuring reliable daily chemistry and meteorological observations throughout the study period (Singh et al., 2020; Zhou et al., 2024).

Satellite observations from Atmospheric Infrared Sounder (AIRS) instrument aboard NASA's Aqua satellite (Aqua/AIRS) and meteorological reanalysis from Modern-Era Retrospective Analysis for Research and Applications, Version 2 (MERRA2) (https://giovanni.gsfc.nasa.gov/giovanni/) were used to validate surface temperature, humidity, wind speed, and vertical structure. Rainfall was assessed using high-quality India Meteorological Department (IMD) datasets (https://imdpune.gov.in/cmpg/Griddata/Rainfall_25_NetCDF.html) (Pai et al., 2014). These datasets collectively enabled evaluation of the model's capability to capture meteorological conditions, boundary-layer behaviour, and pollutant distributions across India's diverse climate regimes (Govardhan et al., 2015). For spatial panels, we summarize each map using the domain-mean and spatial standard deviation ($\mu \pm 1\sigma$) computed over the Indian landmass (consistent with the land-mask used in the analysis), and these values are reported in the corresponding figure panels/captions. For temporal panels, we report the time-mean and temporal standard deviation ($\mu \pm 1\sigma$) over the evaluation period, also indicated in the relevant figures. In addition, model skill is quantified using mean bias error (MBE), mean absolute error (MAE), root-mean-square error (RMSE), correlation coefficient (r), and coefficient of determination (r^2), computed consistently for each sensitivity experiment against the corresponding observational/reanalysis dataset.

Table 2.1: Summary of WRF-Chem model sensitivity simulations setup details.

SI No.	WRF-Chem model Configuration Details		Simulation Name
Meteorology Sensitivity Simulations		**Common Model Configurations**	
1	ERA5	YSU PBL, Purdue Lin Microphysics, SMoG-COALESCE Emission, MOZART – MOSAIC, No Nudging	**Control**
2	NCEP CFSv2		**CFSWRF**
3	NCEP GDAS		**GDASWRF**
	PBL Sensitivity Simulations		
1	YSU Scheme	ERA5 Meteorology, Purdue Lin Microphysics, SMoG-COALESCE Emission, MOZART – MOSAIC, No Nudging	**Control**
4	MYJ Scheme		**MYJWRF**
5	MYNN3 Scheme		**MYNWRF**
	Microphysics Sensitivity Simulations		
1	Purdue Lin Scheme	ERA5 Meteorology, YSU PBL, SMoG-COALESCE Emission, MOZART – MOSAIC, No Nudging	**Control**
6	New Thompson Scheme		**THOMWRF**
7	Morrison Double-Moment Scheme		**MDMWRF**
	Grid Nudging Approach Sensitivity Simulations		
8	Grid Nudging for Winds, Temperature, and Water Vapor from ERA5	ERA5 Meteorology, YSU PBL, Purdue Lin Microphysics, SMoG-COALESCE Emission, MOZART – MOSAIC, Whole Atmosphere Nudging, Nudging Coeff. 0.0003 s^{-1}	**Nudged03**
	Chemical Mechanism Sensitivity Simulations		
9	CBMZ – MOSAIC (4 bins, DMS, Aqueous)	ERA5 Meteorology, YSU PBL, Purdue Lin Microphysics, SMoG-COALESCE Emission, Whole Atmosphere Nudging, Nudging Coeff. 0.0003 s^{-1}	**CBMZWRF**
8	MOZART – MOSAIC (4 bins, VBS, Aqueous)		**Nudged03**
	Emission Inventory Sensitivity Simulations		
10	CMIP6 (2014)	ERA5 Meteorology, YSU PBL, Purdue Lin Microphysics, MOZART – MOSAIC, Whole Atmosphere Nudging, Nudging Coeff. 0.0003 s^{-1}	**CMIPWRF**
11	EDGARv5 (2015)		**ED5WRF**
12	EDGARv6.1 (2018)		**ED6WRF**
13	EDGAR-HTAPv3 (2018)		**HTAPWRF**
8	SMoG-COALESCE (2019)		**Nudged03**
	Nudging Strength and Approach Sensitivity Simulations		
14	Nudging Coeff. 0.0005 s^{-1}	ERA5 Meteorology, YSU PBL, Purdue Lin Microphysics, SMoG-COALESCE Emission, MOZART – MOSAIC, Whole Atmosphere Nudging	**Nudged05**
15	Nudging Coeff. 0.001 s^{-1}		**Nudged1**
16	Nudging Coeff. 0.0003 s^{-1}	ERA5 Meteorology, YSU PBL, Purdue Lin Microphysics, SMoG-COALESCE Emission, MOZART – MOSAIC, No Nudging within the PBL	**NoNudPBL03**
17	Nudging Coeff. 0.0005 s^{-1}		**NoNudPBL05**
18	Nudging Coeff. 0.001 s^{-1}		**NoNudPBL1**

2.3 Results and Discussion

The WRF-Chem sensitivity simulations conducted for August 2018 (monsoon) and January 2019 (winter) provide a comprehensive framework for evaluating model performance across India's contrasting meteorological regimes. August is dominated by deep convection, strong moisture transport, high humidity, and vigorous wet deposition, whereas January is characterized by stagnant conditions, shallow planetary boundary layers (PBLs), frequent temperature inversions, and weak winds that promote severe pollutant accumulation. These stark meteorological contrasts exert strong controls on transport, dispersion, deposition, aerosol hygroscopicity, and secondary pollutant formation. By systematically evaluating boundary conditions, physical parameterizations, chemical mechanisms, emission inventories, and grid-nudging strengths, and by comparing simulations against CPCB surface measurements, MERRA2 reanalysis, Aqua/AIRS satellite retrievals, and IMD rainfall, we identify an optimized WRF-Chem configuration capable of realistically capturing meteorological and air-quality processes across India. Statistical metrics including Mean Absolute Error (MAE), Mean Bias Error (MBE), Root Mean Square Error (RMSE), correlation coefficient (r), and coefficient of determination (r^2) were used to quantify model skill (Sharma et al., 2023).

2.3.1 Meteorological Sensitivity Simulations

Meteorological initial and boundary conditions had a dominant influence on model performance across both seasons. Simulations driven by ERA5 consistently outperformed those using NCEP GDAS or NCEP CFSv2 for key variables including surface temperature, relative humidity, cloud fields, and near-surface winds. As shown in Fig. 2.2, ERA5 reduced surface temperature biases by up to 2 °C relative to GDAS and CFSv2, particularly across northern and central India. Comparison with Aqua/AIRS surface temperature showed that ERA5 exhibits the best performance over the Indian landmass during August, with an RMSE of 2.09 ^{o}C and a correlation coefficient of 0.97. In contrast, GDAS and CFSv2 showed higher RMSE values of 2.63 ^{o}C and 2.81 ^{o}C, with lower correlation coefficients of 0.91 and 0.89, respectively. This improvement reflects ERA5's finer spatial and temporal resolution, which enables more accurate representation of mesoscale processes such as monsoonal convection, moisture convergence, and weak synoptic disturbances. These improvements are further illustrated in Fig. 2.3, which highlights enhanced spatial temperature distributions important for capturing land-atmosphere interactions.

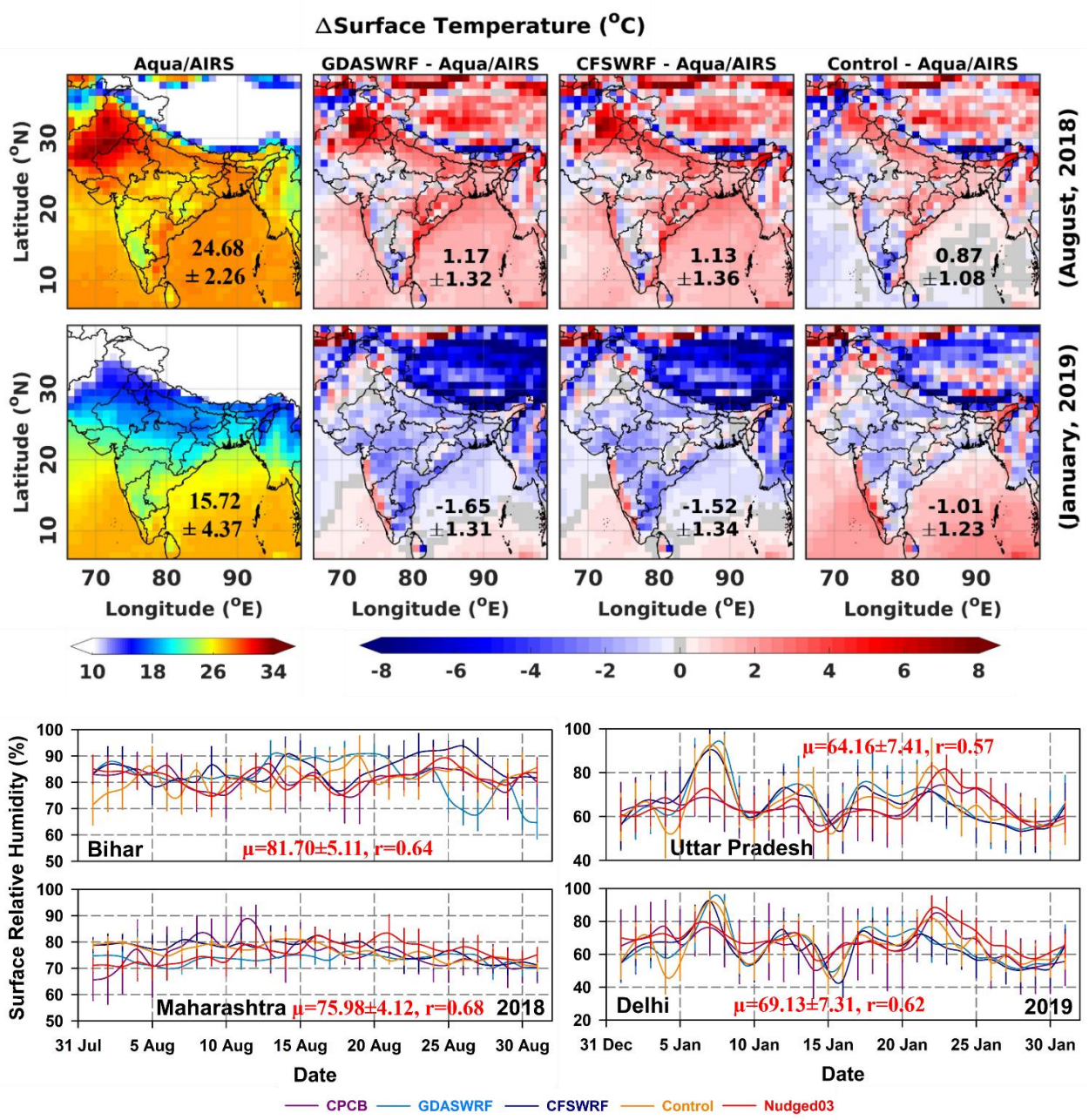


Figure 2.2: Spatial distribution of surface temperature observed by Aqua/AIRS over the Indian region, and the difference in simulated temperature from various WRF-Chem meteorology sensitivity simulations (top panel). Inset values report the domain-mean ± spatial standard deviation (μ ± 1σ) over the Indian landmass, along with Mean Bias Error (MBE) relative to Aqua/AIRS. Daily mean time series comparison of surface relative humidity for various Indian states from different WRF-Chem meteorology and grid nudging sensitivity simulations with CPCB measurements and MERRA2 (bottom panel). Temporal mean ± SD (μ ± 1σ) and correlation coefficient (r) of Nudged03 indicated within the panel.

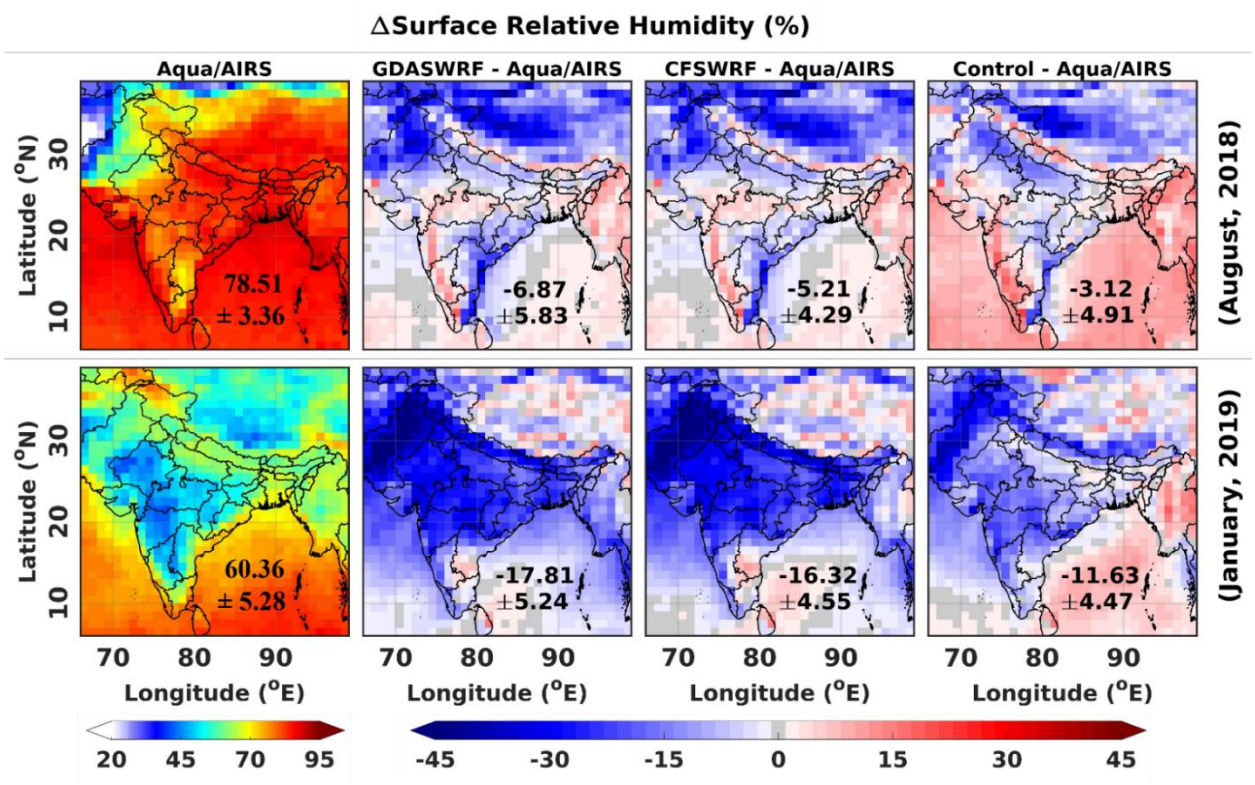


Figure 2.3: Spatial distribution of surface relative humidity observed by Aqua/AIRS over the Indian region, and the corresponding differences from various WRF-Chem meteorology sensitivity simulations. Inset values report the domain-mean ± spatial standard deviation (μ ± 1σ) computed over the Indian landmass, along with Mean Bias Error (MBE) relative to Aqua/AIRS.

Wind speed and wind direction, which are critical determinants of horizontal pollutant transport and dispersion, also exhibited strong sensitivity to the choice of meteorological initial and boundary dataset. Winter simulations forced with GDAS and CFSv2 tended to underestimate weak-wind and stagnation events in the Indo-Gangetic Plain (IGP), whereas ERA5-driven simulations more accurately captured the magnitude, timing, and diurnal cycle of low-level winds. Fig. 2.4 demonstrates ERA5's ability to resolve diurnal wind variability, while Fig. 2.5 shows improved spatial patterns of surface wind speed, both of which are crucial for simulating pollutant accumulation and dispersion during winter (Anchev et al., 2020).

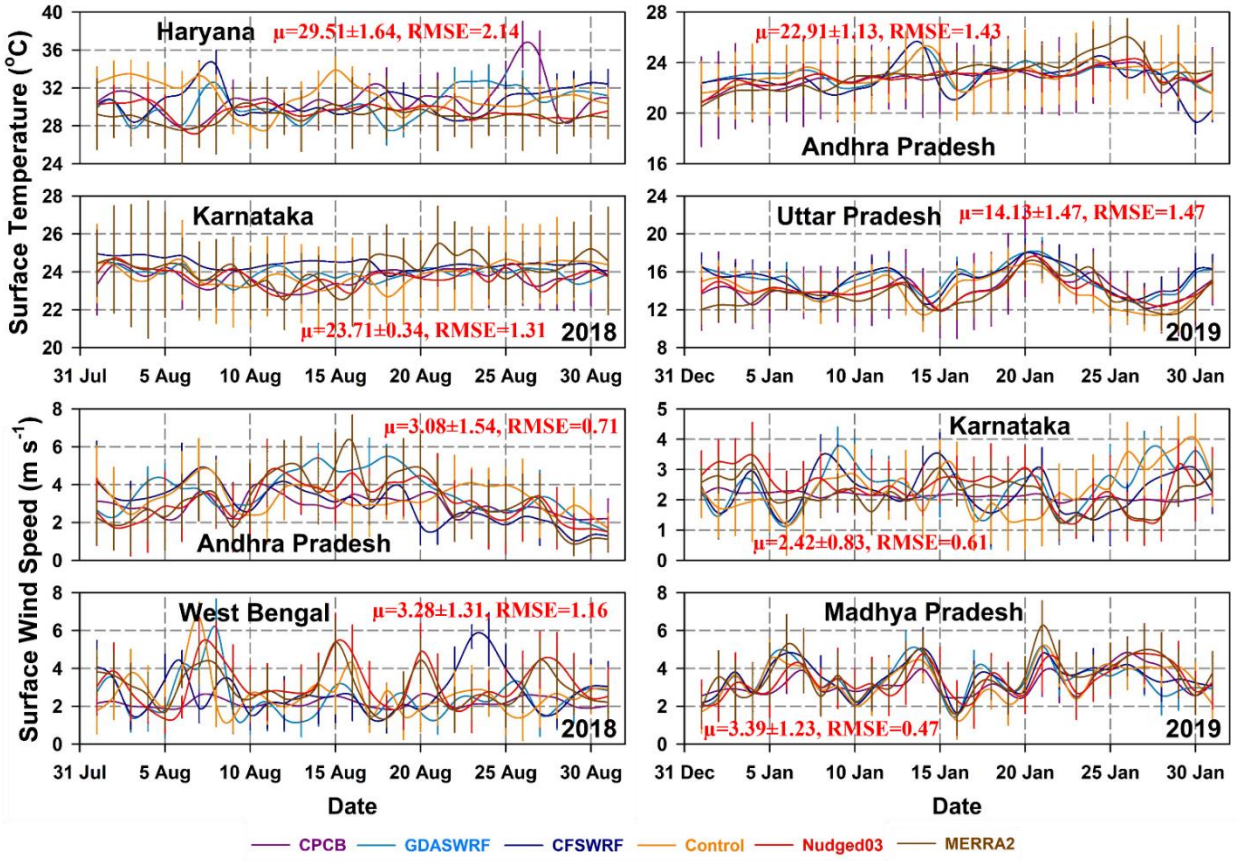


Figure 2.4: Daily mean time series comparison of surface temperature and surface wind speed for selected Indian states from different WRF-Chem meteorology and grid-nudging sensitivity simulations against CPCB measurements and MERRA2 reanalysis. Temporal mean ± standard deviation (μ ± 1σ), together with correlation coefficient (r) and RMSE of Nudged03, are indicated within each panel.

Comparison with MERRA2 850 hPa wind speed showed that ERA5 exhibits the best performance over the Indian landmass during January, with an RMSE of 1.72 m s^{-1} and a correlation coefficient of 0.61. In contrast, GDAS and CFSv2 showed higher RMSE values of 1.81 m s^{-1} and 1.89 m s^{-1}, with lower correlation coefficients of 0.58 and 0.55, respectively. ERA5 also provided a markedly better representation of relative humidity and moisture fields, which influence cloud formation, fog and haze occurrence, and wet deposition. In August, the improved moisture structure led to more realistic rainfall patterns, as evidenced by Fig. 2.3 & 2.6 (accumulated rainfall), enabling a more accurate simulation of aerosol wet scavenging processes. In January, realistic humidity fields improved the representation of fog, haze, and aerosol hygroscopic growth, all of which have strong implications for visibility and particulate matter concentrations. A detailed statistical analysis of ERA5 performance for various meteorological variables has been summarized in Table 2.2.

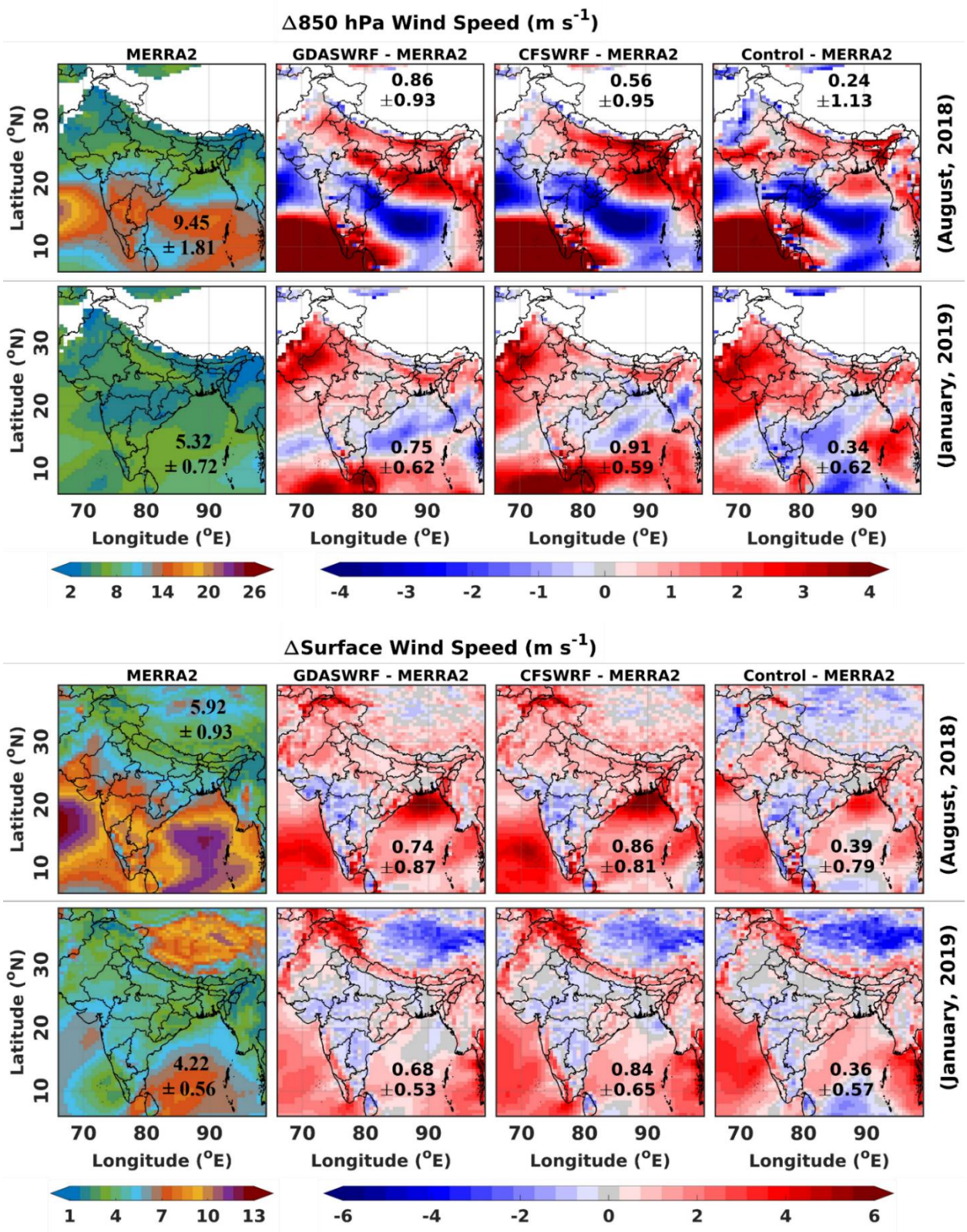


Figure 2.5: Spatial distribution of 850 hPa (top panel) and surface (bottom panel) wind speed from MERRA2 reanalysis over the Indian region and corresponding differences from various WRF-Chem meteorology sensitivity simulations. Inset values show domain-mean ± spatial SD ($\mu \pm 1\sigma$) and Mean Bias Error (MBE) computed over the Indian landmass.

Table 2.2: Regression statistics for various meteorological variables over the Indian region from different meteorological and PBL sensitivity simulations for both study periods, evaluated against Aqua/AIRS and MERRA-2 observational datasets.

Regression Statistics for Surface Temperature between Aqua/AIRS and Different Meteorology Sensitivity Simulations										
		Control			**GDASWRF**			**CFSWRF**		
Common Model Configurations		**YSU PBL, Purdue Lin Microphysics, SMoG-COALESCE Emission, MOZART – MOSAIC, No Nudging**								
Month	**Count**	**MBE**	**r**	**RMSE**	**MBE**	**r**	**RMSE**	**MBE**	**r**	**RMSE**
August 2018	2812	0.87 (ºC)	0.97	2.09 (ºC)	1.17 (ºC)	0.91	2.63 (ºC)	1.13 (ºC)	0.89	2.81 (ºC)
January 2019	3811	-1.01 (ºC)	0.96	2.39 (ºC)	-1.65 (ºC)	0.87	2.53 (ºC)	-1.52 (ºC)	0.88	2.43 (ºC)
Regression Statistics for Surface Relative Humidity between Aqua/AIRS and Diff. Meteorology Sensitivity Simulations										
August 2018	2882	-3.12 (%)	0.49	14.72 (%)	-6.87 (%)	0.54	19.23 (%)	-5.21 (%)	0.58	17.76 (%)
January 2019	3943	-11.63 (%)	0.52	19.35 (%)	-17.81 (%)	0.56	23.26 (%)	-16.32 (%)	0.53	23.01 (%)
Regression Statistics for 850 hPa Wind Speed between MERRA2 and Different Meteorology Sensitivity Simulations										
August 2018	6217	0.24 ($m\ s^{-1}$)	0.57	4.69 ($m\ s^{-1}$)	0.86 ($m\ s^{-1}$)	0.43	4.80 ($m\ s^{-1}$)	0.56 ($m\ s^{-1}$)	0.41	4.61 ($m\ s^{-1}$)
January 2019	6217	0.34 ($m\ s^{-1}$)	0.61	1.72 ($m\ s^{-1}$)	0.75 ($m\ s^{-1}$)	0.58	1.81 ($m\ s^{-1}$)	0.91 ($m\ s^{-1}$)	0.55	1.89 ($m\ s^{-1}$)
Regression Statistics for Surface Wind Speed between MERRA2 and Different Meteorology Sensitivity Simulations										
August 2018	7936	0.39 ($m\ s^{-1}$)	0.61	2.51 ($m\ s^{-1}$)	0.74 ($m\ s^{-1}$)	0.56	2.47 ($m\ s^{-1}$)	0.86 ($m\ s^{-1}$)	0.53	2.44 ($m\ s^{-1}$)
January 2019	7936	0.36 ($m\ s^{-1}$)	0.59	1.37 ($m\ s^{-1}$)	0.68 ($m\ s^{-1}$)	0.54	1.58 ($m\ s^{-1}$)	0.84 ($m\ s^{-1}$)	0.52	1.64 ($m\ s^{-1}$)
Regression Statistics for PBL height between MERRA2 and Different PBL Sensitivity Simulations										
		Control			**MYNWRF**			**MYJWRF**		
August 2018	7936	0.13 (km)	0.45	0.27 (km)	0.16 (km)	0.42	0.36 (km)	0.17 (km)	0.41	0.33 (km)
January 2019	7936	0.11 (km)	0.49	0.18 (km)	0.15 (km)	0.44	0.21 (km)	0.14 (km)	0.38	0.21 (km)
Regression Statistics for 850 hPa Temperature between Aqua/AIRS and Different PBL Sensitivity Simulations										
August 2018	2812	0.32 (ºC)	0.58	2.58 (ºC)	0.86 (ºC)	0.51	3.19 (ºC)	0.41 (ºC)	0.52	3.29 (ºC)
January 2019	3811	0.17 (ºC)	0.61	3.07 (ºC)	-1.72 (ºC)	0.63	2.79 (ºC)	-1.25 (ºC)	0.69	2.40 (ºC)

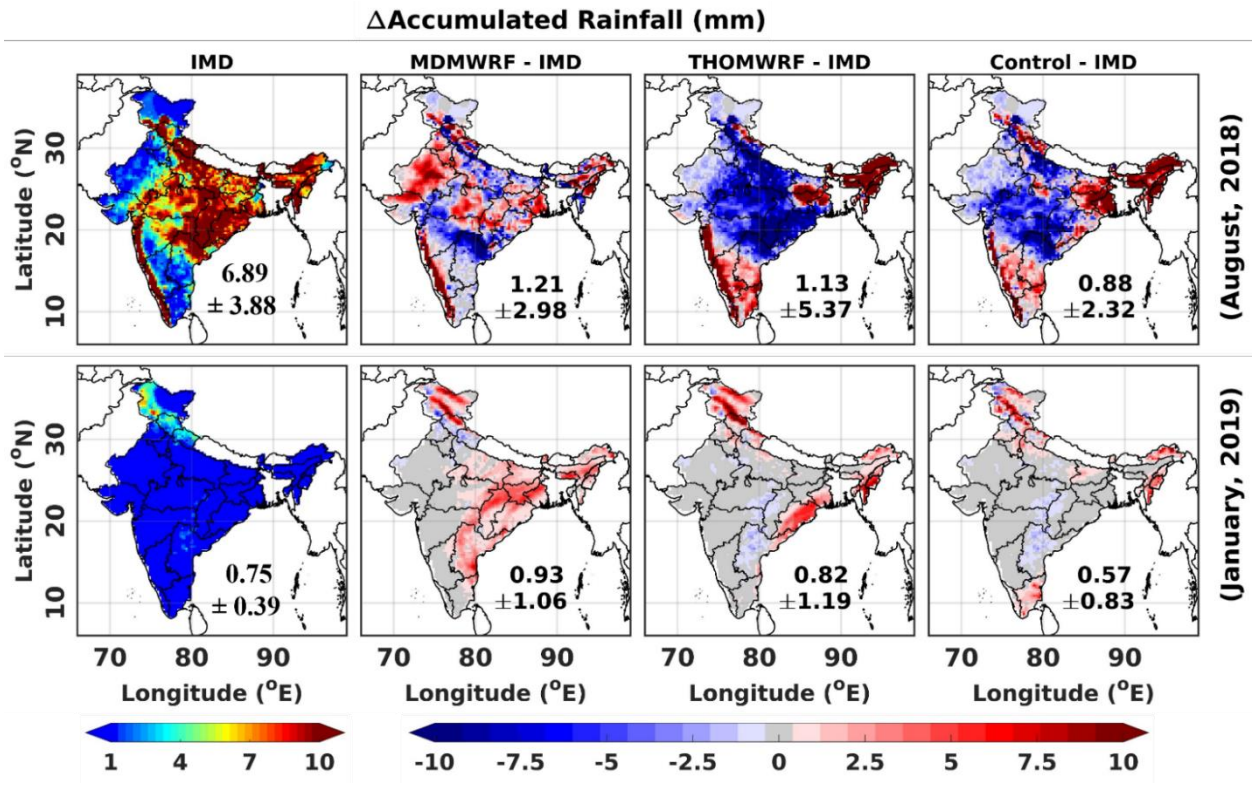


Figure 2.6: Spatial distribution of accumulated rainfall measured by the IMD over the Indian region and corresponding differences from various WRF-Chem microphysics sensitivity simulations. Inset statistics report domain-mean ± spatial SD (μ ± 1σ) and Mean Bias Error (MBE) over the Indian landmass.

The combined improvements in temperature, wind, and humidity fields under ERA5 translated directly into enhanced air-quality simulations. More realistic dispersion and boundary-layer structure led to improved $PM_{2.5}$, NO_x, and CO concentrations. These results confirm ERA5 as the preferred meteorological initial and boundary dataset for WRF-Chem simulations over India, especially in regions affected by complex interactions among synoptic forcing, monsoonal dynamics, inversions, and fog formation. Overall, the use of ERA5 forcing reduced surface temperature RMSE by approximately 20-25% relative to GDAS and CFSv2 during August 2018, while increasing correlation coefficients by up to 0.08. During January 2019, ERA5 improved 850 hPa wind speed skill by reducing RMSE by ~0.1-0.2 m s^{-1} and increasing correlation by ~0.05-0.06. These quantitative improvements highlight the strong dependence of air-quality simulations on the accuracy of large-scale meteorological forcing.

2.3.2 PBL and Microphysics Scheme Sensitivity

The PBL and microphysics schemes are critical components of atmospheric modelling because they govern vertical mixing, pollutant dispersion, cloud formation, precipitation, and wet deposition. Together, these processes strongly influence near-surface pollutant concentrations and therefore the skill of air-quality simulations over India.

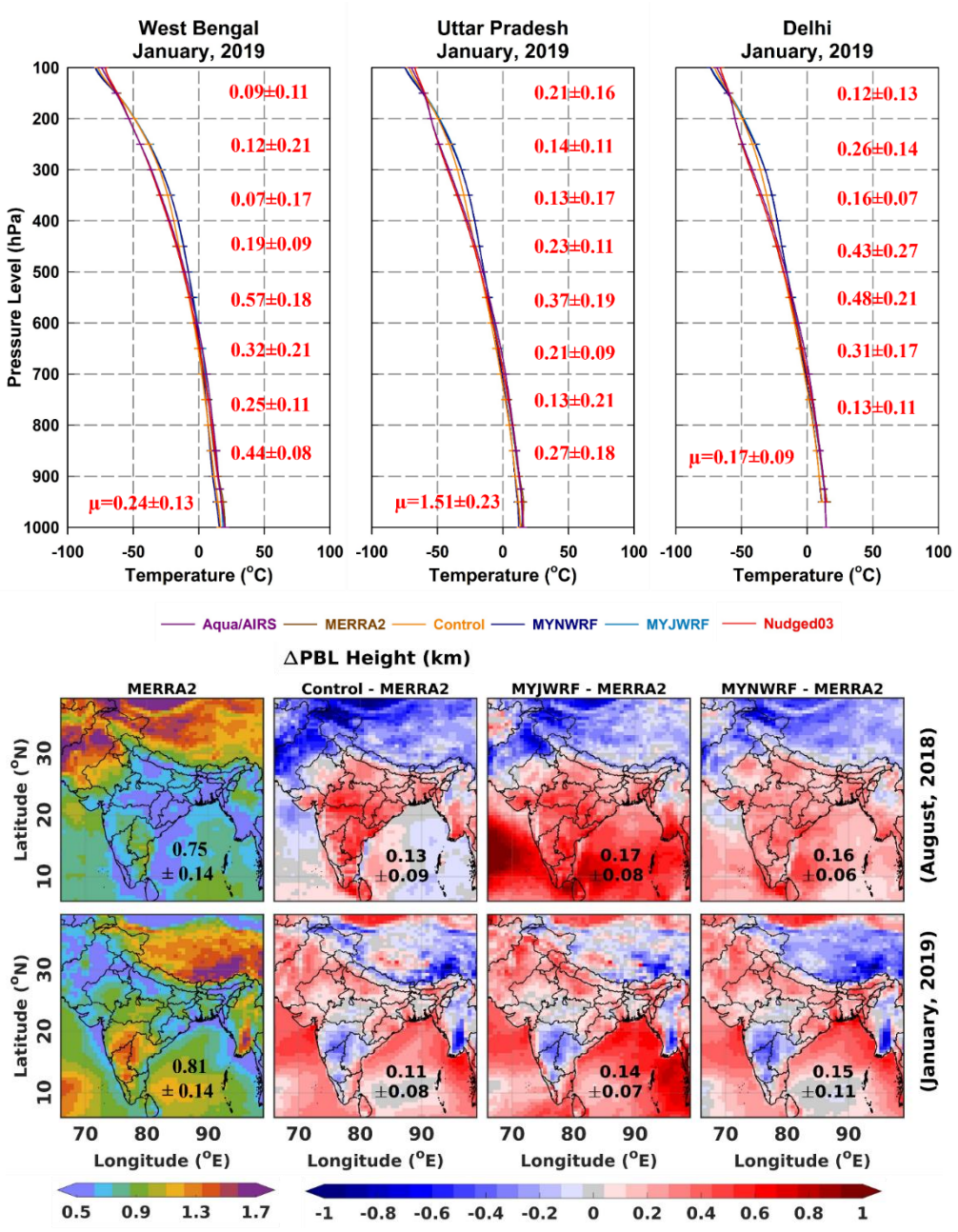


Figure 2.7: Vertical temperature profile comparison between MERRA2 reanalysis, Aqua/AIRS observed with different WRF-Chem PBL and grid nudging sensitivity simulations over the entire Indian region (top panel). Profiles are accompanied by domain-mean ± SD statistics over India. Spatial distribution of PBL height by MERRA2 reanalysis over the Indian region, and the difference in simulated PBL height from various WRF-Chem PBL sensitivity simulations (bottom panel). Inset values show domain-mean ± spatial SD (μ ± 1σ), Mean Bias Error (MBE) and Mean Absolute Error (MAE) of Nudged03 computed over the Indian landmass.

Boundary-layer dynamics exert particularly strong control over pollutant accumulation by determining the depth of vertical mixing and the extent of surface pollutant dilution. Fig. 2.7 shows that the YSU PBL scheme produced the most realistic PBL heights during both monsoon and winter seasons. During January 2019, the ability of YSU to capture shallow nocturnal PBLs and strong inversion layers was essential for simulating wintertime pollution buildup over the IGP. In contrast, MYJ and MYNN3 systematically overestimated PBL height, resulting in excessive vertical mixing and underestimation of $PM_{2.5}$, NO_x, and CO concentrations across the IGP and other polluted urban regions.

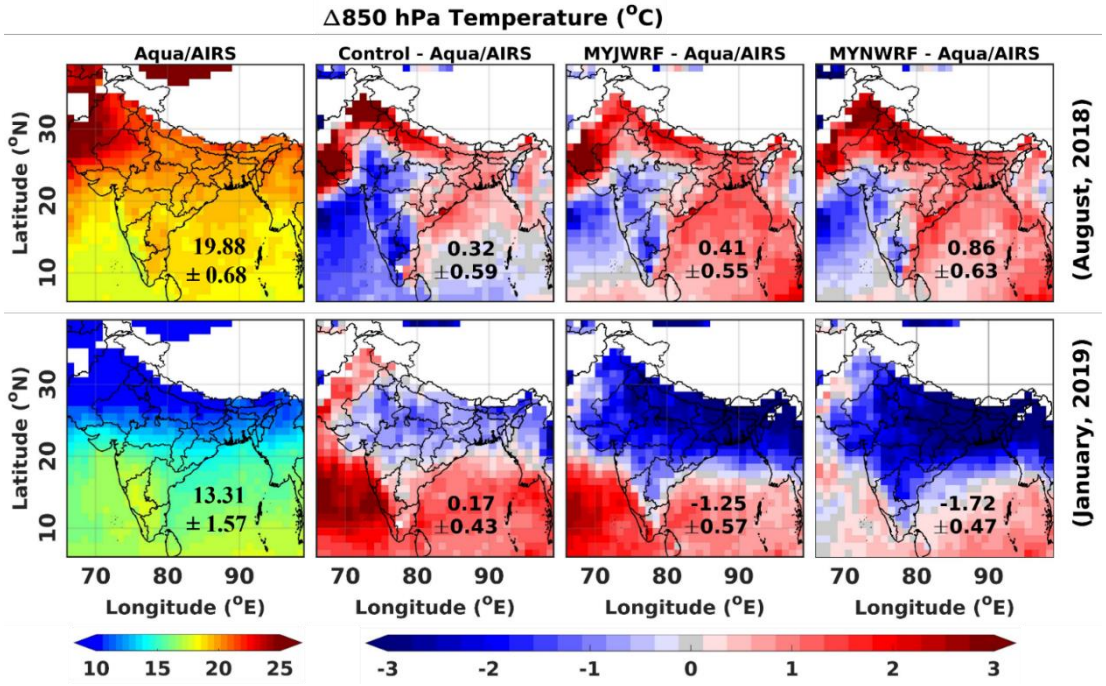


Figure 2.8: Spatial distribution of 850 hPa temperature observed by Aqua/AIRS over the Indian region, and the difference in simulated temperature from various WRF-Chem PBL sensitivity simulations. Domain-mean ± spatial SD (μ ± 1σ) and Mean Bias Error (MBE) over the Indian landmass are reported within the panels.

Evaluation against MERRA2 PBL height indicates that the YSU scheme performs better over the Indian landmass during January, with an RMSE of 0.18 km and a correlation coefficient of 0.49. In comparison, MYJ and MYNN3 show higher RMSE values (0.21 km each) and lower correlations (0.38 and 0.44, respectively). Consistent behaviour is found for August when compared with Aqua/AIRS 850 hPa temperature, where YSU again shows superior performance (RMSE: 2.58 °C; correlation: 0.58), while MYJ and MYNN3 exhibit larger errors (3.29 °C and 3.19 °C) and weaker correlations (0.52 and 0.51, respectively). These findings are consistent with earlier studies demonstrating that YSU effectively represents diurnal boundary-layer dynamics and nonlocal mixing under stable conditions over India (Hariprasad et al., 2014; Hong et al., 2006).

Spatial distributions of $PM_{2.5}$ (Fig. 2.9), together with vertical structure diagnostics (Fig. 2.8), further highlight the YSU scheme's ability to capture pollutant accumulation under stable winter conditions and to improve simulations of surface $PM_{2.5}$, NO_x, and O_3.

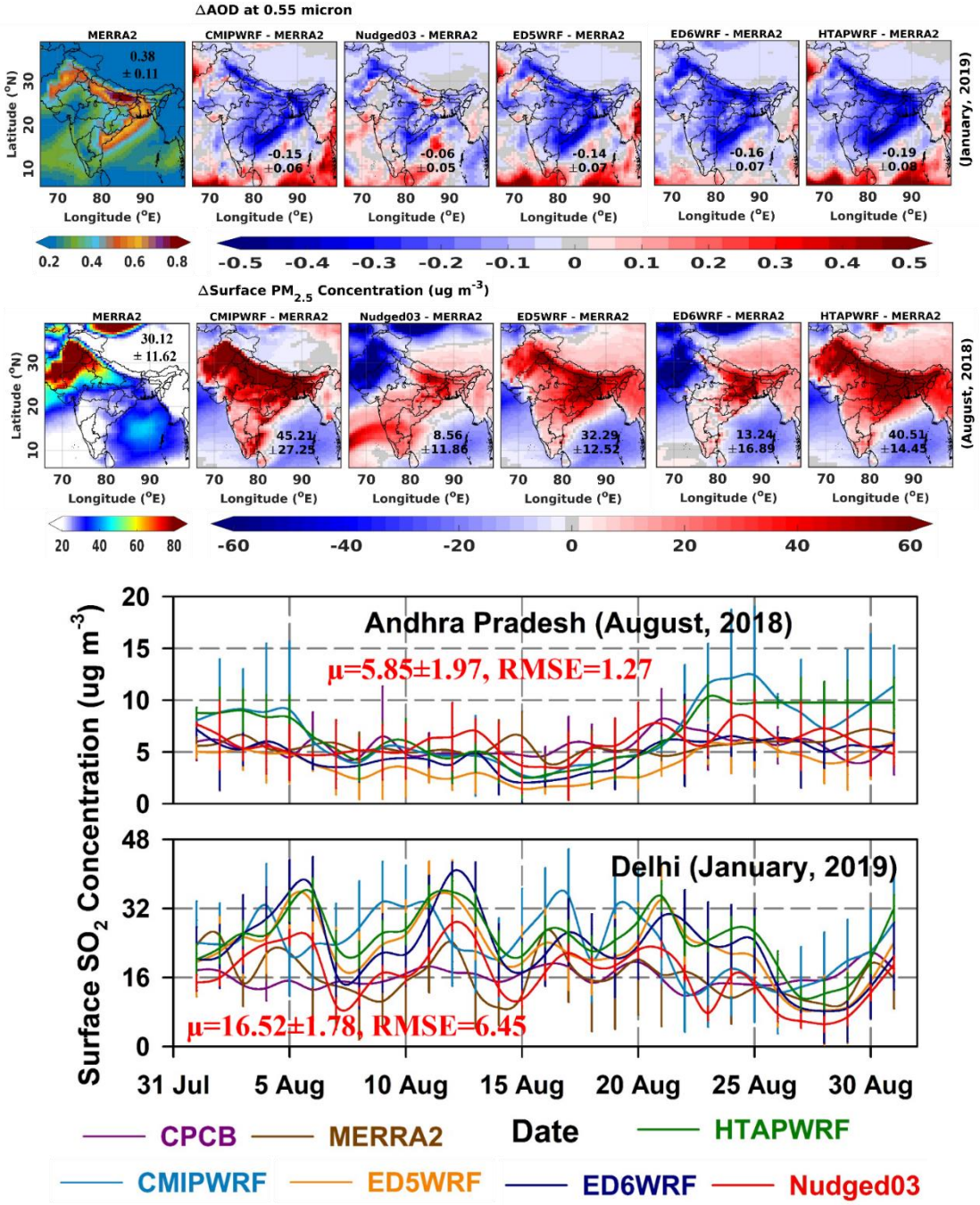


Figure 2.9: Spatial distribution of AOD from MERRA2 reanalysis and the difference in simulated AOD from various WRF-Chem emission inventory sensitivity simulations over the Indian region (top panel). Inset values show domain-mean ± spatial SD (μ ± 1σ) and MBE over the Indian landmass. Spatial distribution of surface $PM_{2.5}$ concentration by MERRA2 over the Indian region, and the difference in simulated surface $PM_{2.5}$ from various WRF-Chem emission inventory sensitivity simulations (middle panel), with domain-mean ± SD (μ ± 1σ) and MBE reported within the panel. Daily mean time series comparison of surface SO_2 distribution for various Indian states from different WRF-Chem emission inventory sensitivity simulations with CPCB measurements and MERRA2 reanalysis (bottom panel). Temporal mean ± SD (μ ± 1σ) and RMSE (μg m^{-3}) of Nudged03 are indicated.

During August, the YSU scheme again performed best by realistically representing deep convective mixing and the diurnal evolution of the boundary layer under monsoon conditions. Accurate simulation of daytime PBL growth is essential for representing pollutant lofting into the free troposphere, while nighttime collapse strongly influences surface accumulation and nocturnal chemistry. The robustness of YSU across both monsoon and winter therefore highlights its suitability for simulating boundary-layer processes and pollutant dispersion in regions characterized by strong seasonal contrasts in stability and pollution levels. A detailed statistical analysis of YSU PBL scheme performance for various meteorological variables has been summarized in Table 2.2. Microphysics schemes introduced additional sensitivity, particularly during the monsoon when rainfall dominates pollutant removal. Microphysics governs cloud processes, precipitation formation, and wet deposition, making it central to both meteorological and air-quality performance (Sathyanadh et al., 2017). Fig. 2.6 compares accumulated rainfall for the Lin, Thompson, and Morrison schemes. The Lin scheme (Chen et al., 2002) produced the most realistic rainfall patterns, especially over central and southern India where convective precipitation dominates during the monsoon season (with IMD RMSE: 12.16 mm and correlation: 0.37). Accurate representation of both stratiform and convective rainfall structures is critical because rainfall intensity, frequency, and spatial distribution determine the efficiency and timing of wet deposition, the primary mechanism for pollutant removal during this period.

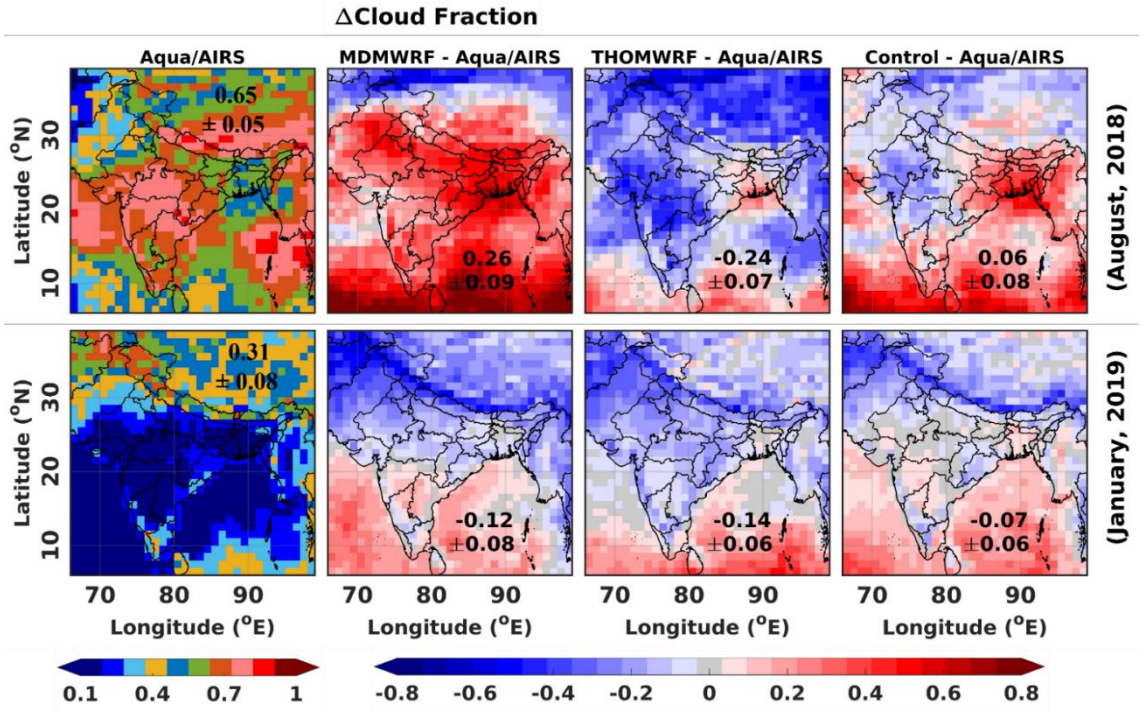


Figure 2.10: Spatial distribution of cloud fraction observed by Aqua/AIRS over the Indian region, and the difference in simulated cloud fraction from various WRF-Chem microphysics sensitivity simulations. Panels include domain-mean ± spatial SD (μ ± 1σ) and Mean Bias Error (MBE) computed over the Indian landmass.

The realistic rainfall fields simulated by the Lin scheme led to improved predictions of pollutant concentrations, particularly for SO_2 and PM_{10}, as demonstrated in Fig. 2.9 & 2.11. In contrast, the Thompson and Morrison schemes tended to overestimate rainfall in several regions, leading to excessive wet scavenging and unrealistically low concentrations of aerosols and trace gases. Furthermore, cloud fraction representation, crucial for radiative transfer, boundary-layer evolution, and photolysis rates, was most accurate in the Lin scheme (Fig. 2.10), enhancing the reliability of pollutant concentration predictions during monsoon conditions (Zhang et al., 2019).

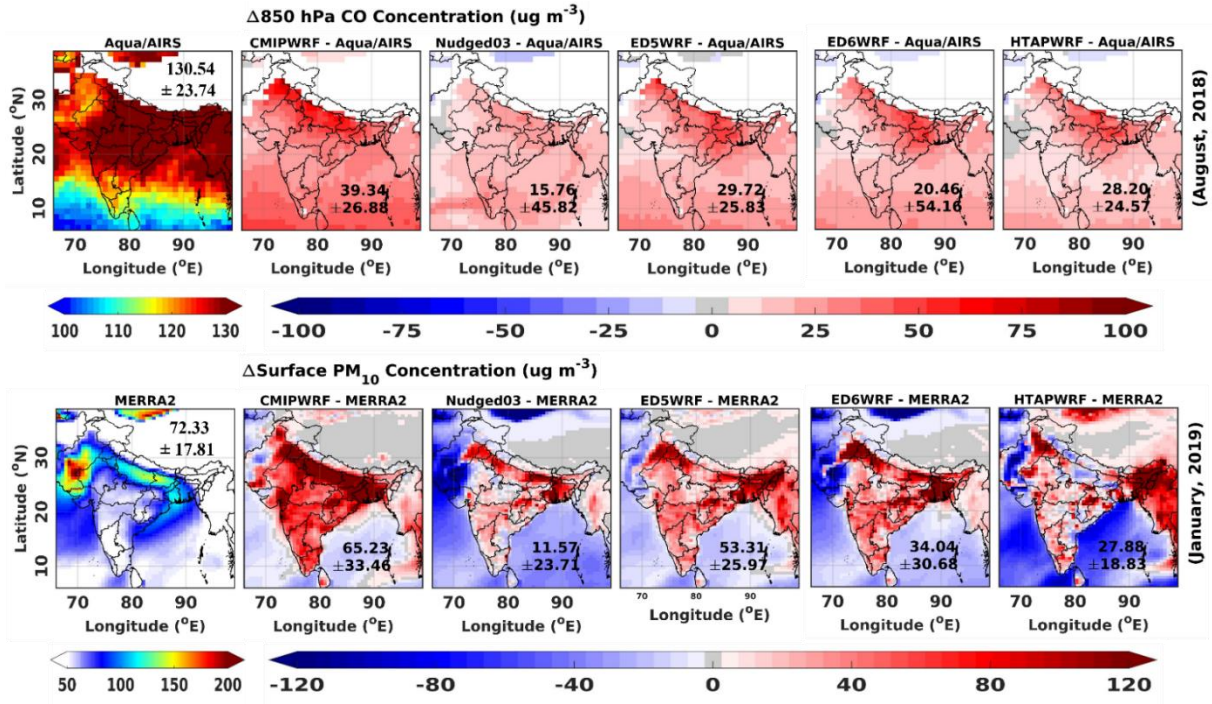


Figure 2.11: Spatial distribution of 850 hPa CO concentration by Aqua/AIRS over the Indian region, and the difference in simulated 850 hPa CO from various WRF-Chem emission inventory sensitivity simulations (top panel). Spatial distribution of surface PM_{10} concentration by MERRA2 over the Indian region, and the difference in simulated surface PM_{10} from various WRF-Chem emission inventory sensitivity simulations (bottom panel). For both panels, domain-mean ± spatial SD ($\mu \pm 1\sigma$) and Mean Bias Error (MBE) over the Indian landmass are reported within the plots.

A comprehensive statistical comparison of surface temperature, wind speed, relative humidity, cloud fraction, and accumulated rainfall against Aqua/AIRS observations, MERRA2 reanalysis, and IMD measurements (Pai et al., 2014) confirms that simulations using ERA5 meteorology coupled with the YSU PBL and Lin microphysics schemes achieved the best overall performance across the Indian region (Table 2.3). The sensitivity analysis therefore highlights the superior performance of the YSU scheme for simulating boundary-layer processes and the Lin scheme for capturing precipitation and pollutant removal mechanisms. Their combined application offers a robust framework for improving meteorological and air-pollution simulations over India, and these schemes are recommended for air-quality modelling in both winter and monsoon periods

to support more accurate forecasts and policy-relevant assessments. Relative to MYJ and MYNN3, the YSU scheme reduced wintertime PBL height RMSE by ~15-20%, resulting in systematically higher near-surface pollutant concentrations that are more consistent with CPCB observations. For microphysics, the Lin scheme reduced monsoon rainfall RMSE by ~30-40% compared to Thompson and Morrison, leading to more realistic wet scavenging and avoiding excessive removal of aerosols and trace gases.

Table 2.3: Regression statistics for surface temperature, surface wind speed, surface relative humidity, cloud fraction and accumulated rainfall between various WRF-Chem microphysics sensitivity simulations with Aqua/AIRS observations, MERRA2 reanalysis, and IMD measurements over the Indian region for both study periods.

Regression Statistics for Surface Temperature between Aqua/AIRS and Different Microphysics Sensitivity Simulations										
		Control			**THOMWRF**			**MDMWRF**		
Common Model Configurations		**ERA5 Meteorology, YSU PBL, SMoG-COALESCE Emission, MOZART – MOSAIC, No Nudging**								
Month	**Count**	**MAE**	**r**	**RMSE**	**MAE**	**r**	**RMSE**	**MAE**	**r**	**RMSE**
August 2018	2812	1.20 (°C)	0.97	2.09 (°C)	3.03 (°C)	0.93	3.67 (°C)	1.77 (°C)	0.94	2.79 (°C)
January 2019	3811	1.72 (°C)	0.96	2.39 (°C)	2.77 (°C)	0.95	3.48 (°C)	2.84 (°C)	0.91	3.45 (°C)
Regression Statistics for Surface Temperature between MERRA2 and Different Microphysics Sensitivity Simulations										
August 2018	2812	1.36 (°C)	0.91	1.83 (°C)	2.48 (°C)	0.89	2.98 (°C)	1.75 (°C)	0.91	2.33 (°C)
January 2019	3811	2.11 (°C)	0.92	2.23 (°C)	2.37 (°C)	0.96	2.32 (°C)	2.41 (°C)	0.87	3.14 (°C)
Regression Statistics for Surface Wind Speed between MERRA2 and Different Microphysics Sensitivity Simulations										
August 2018	7936	1.38 ($m\ s^{-1}$)	0.61	2.51 ($m\ s^{-1}$)	1.81 ($m\ s^{-1}$)	0.61	2.38 ($m\ s^{-1}$)	1.69 ($m\ s^{-1}$)	0.63	2.17 ($m\ s^{-1}$)
January 2019	7936	1.19 ($m\ s^{-1}$)	0.59	1.37 ($m\ s^{-1}$)	1.38 ($m\ s^{-1}$)	0.58	1.89 ($m\ s^{-1}$)	1.45 ($m\ s^{-1}$)	0.39	1.98 ($m\ s^{-1}$)
Regression Statistics for Surface Relative Humidity between Aqua/AIRS and Diff. Microphysics Sensitivity Simulations										
August 2018	2882	11.21 (%)	0.49	14.72 (%)	17.05 (%)	0.56	20.71 (%)	12.17 (%)	0.48	13.51 (%)
January 2019	3943	11.63 (%)	0.52	19.35 (%)	15.83 (%)	0.45	18.64 (%)	14.95 (%)	0.47	18.83 (%)
Regression Statistics for Accumulated Rainfall between IMD and Different Microphysics Sensitivity Simulations										
August 2018	3677	19.63 (mm)	0.37	12.16 (mm)	13.69 (mm)	0.34	18.55 (mm)	14.42 (mm)	0.33	16.28 (mm)
January 2019	307	7.36 (mm)	0.25	3.49 (mm)	6.68 (mm)	0.23	5.88 (mm)	6.71 (mm)	0.21	7.98 (mm)
Regression Statistics for Cloud Fraction between Aqua/AIRS and Different Microphysics Sensitivity Simulations										
August 2018	2882	1.16	0.63	0.21	1.78	0.57	0.29	2.62	0.54	0.37
January 2019	3943	2.14	0.59	0.17	1.68	0.54	0.25	1.41	0.52	0.21

2.3.3 Chemical Mechanism and Emission Inventory Sensitivity

Chemical mechanisms and emission inventories played a crucial role in determining the accuracy of simulated pollutant concentrations. Fig. 2.9 & 2.11 to 2.13 show that the MOZART-MOSAIC mechanism consistently outperformed CBMZ in reproducing O_3, $PM_{2.5}$, SO_2, and CO across India. MOZART-MOSAIC includes detailed ozone-NO_x-VOC chemistry, aerosol thermodynamics, heterogeneous reactions, and VBS-based SOA formation (Emmons et al., 2010; Knote et al., 2015), which together enable a more realistic representation of secondary pollutant formation. This advantage was particularly evident during January 2019, when reduced photolysis rates increase the relative importance of multiphase and heterogeneous processes. Fig. 2.11 & 2.12 highlight the improved representation of pollutant variability across urban, rural, and industrial regions achieved with MOZART-MOSAIC compared to CBMZ.

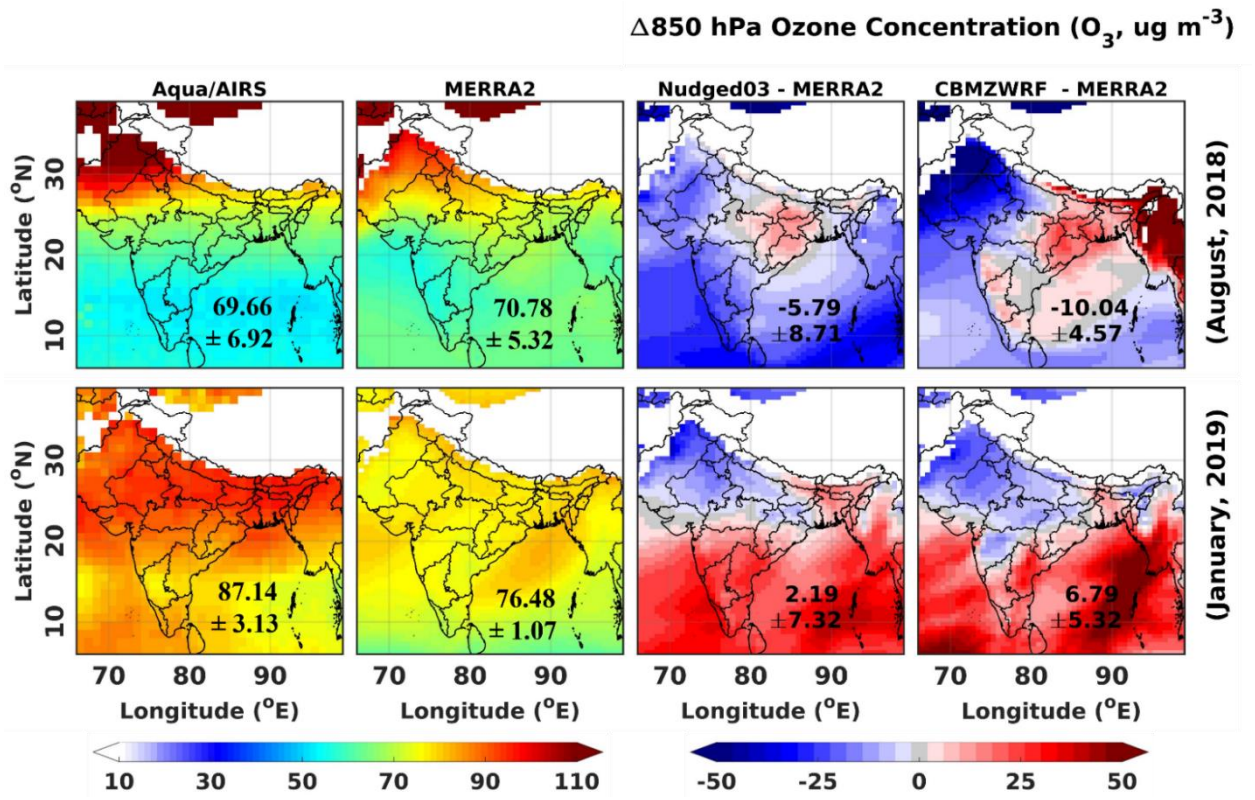


Figure 2.12: Spatial distribution of 850 hPa O_3 distribution observed by Aqua/AIRS, MERRA2 and the difference in simulated 850 hPa O_3 from different WRF-Chem chemical mechanism sensitivity simulations. Inset values show domain-mean ± spatial SD (μ ± 1σ) and Mean Bias Error (MBE) relative to observations.

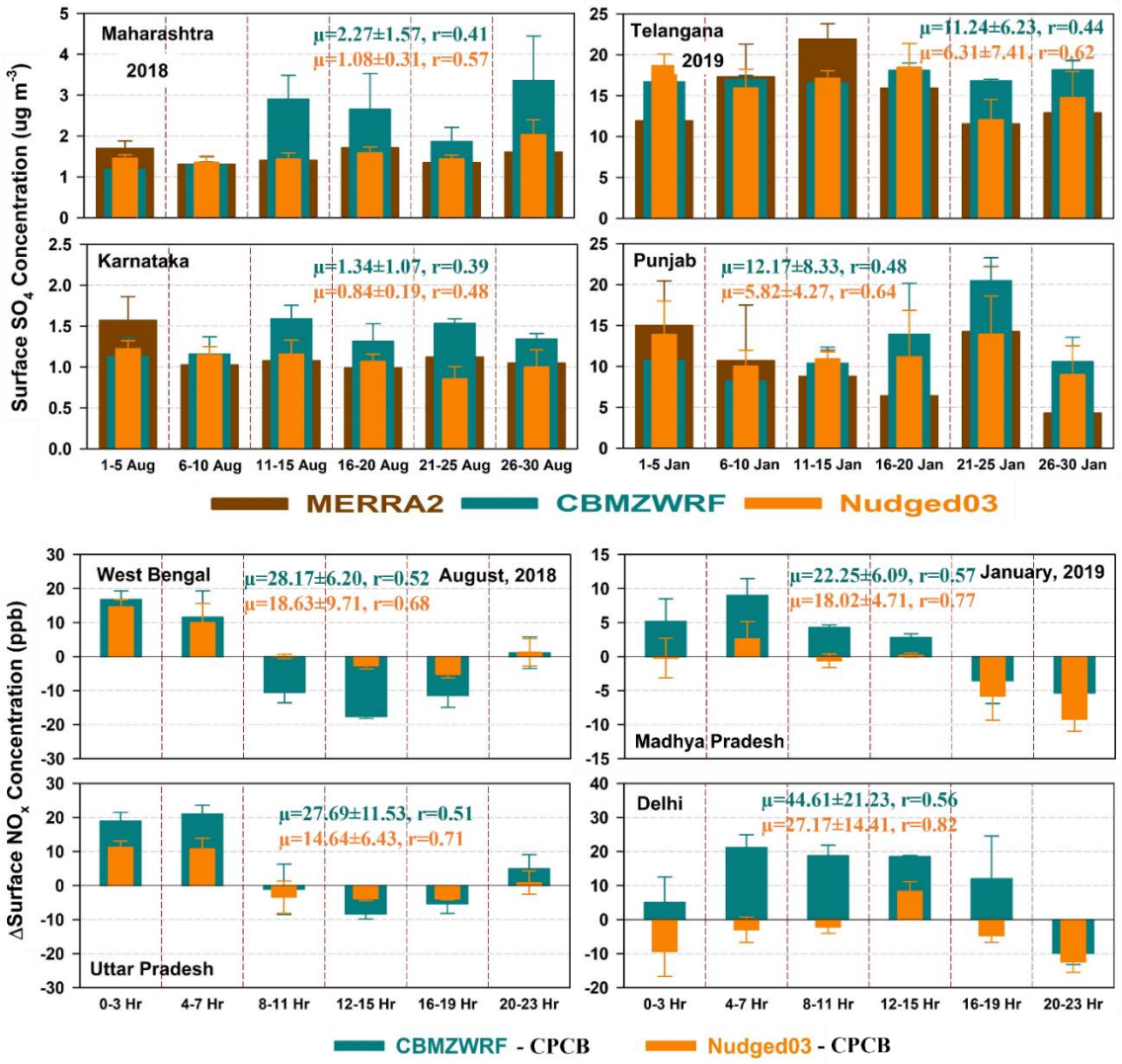


Figure 2.13: Bar charts showing 5-days mean time series comparison of surface SO_4 distribution for various Indian states from different WRF-Chem chemical mechanism sensitivity simulations with MERRA2 reanalysis (top panel). Bars represent mean ± SD over the averaging window. Bar charts illustrating the diurnal variation in the difference of 4-hourly mean surface NO_x distributions for various Indian states, derived from different WRF-Chem chemical mechanism sensitivity simulations compared with CPCB measurements (bottom panel). Temporal mean ± SD (μ ± 1σ), Mean Absolute Error (MAE) and correlation coefficient (r) for CBMZWRF and Nudged03 are indicated respectively within the panel to facilitate quantitative comparison.

Emission inventory choice introduced an additional major source of sensitivity. The SMoG-COALESCE inventory, with its high spatial resolution (5 km) and India-specific sectoral detail (Venkataraman et al., 2024), provided the most accurate representation of pollution distributions during both monsoon and winter. Comparison with MERRA2 surface $PM_{2.5}$ showed that SMoG-COALESCE exhibits better performance over the Indian landmass during January, with an RMSE of 44.46 μg m^{-3} and a correlation coefficient of 0.87. In contrast, EDGARv6.1 and EDGAR-HTAPv3 showed higher RMSE values of ~70 μg m^{-3} for both, with lower correlation

coefficients of 0.80 and 0.41, respectively. Urban regions such as Delhi, Kolkata, and Mumbai showed substantial improvements in simulated pollutant concentrations when SMoG-COALESCE was used, owing to its realistic representation of industrial, transport, and residential emissions (Fig. 2.9). In contrast, coarser global inventories such as EDGARv5, EDGARv6.1, EDGAR-HTAPv3, and CEDS-CMIP6 failed to capture localized emission hotspots and intra-urban gradients, leading to systematic underprediction of pollutant concentrations in densely populated regions and along industrial corridors (Fig. 2.9 & 2.11). A detailed statistical analysis of the performance of all emission inventories for various air pollutants is summarized in Table 2.4.

Table 2.4: Regression statistics for AOD, Surface $PM_{2.5}$, Surface PM_{10} and 850 hPa CO over the Indian region from different WRF-Chem Emission Inventory sensitivity simulations for both study periods, evaluated against Aqua/AIRS and MERRA-2 observational datasets.

Regression Statistics for AOD between MERRA2 and Different Emission Inventory Sensitivity Simulations																
		CMIPWRF			ED5WRF			ED6WRF			HTAPWRF			Nudged03		
Common Model Configurations		ERA5 Meteorology, YSU PBL, Purdue Lin Microphysics, MOZART – MOSAIC, Whole Atmosphere Nudging, Nudging Coeff. 0.0003 s^{-1}														
Month	Count	MBE	r	RMSE	MBE	r	RMSE	MBE	r	RMSE	MBE	r	RMSE	MBE	r	RMSE
August 2018	7936	0.13	0.47	0.39	0.24	0.51	0.40	0.10	0.48	0.26	0.45	0.32	0.62	0.07	0.56	0.27
January 2019	7936	-0.15	0.76	0.17	-0.14	0.74	0.18	-0.16	0.77	0.19	-0.19	0.72	0.22	-0.06	0.83	0.12
Regression Statistics for Surface $PM_{2.5}$ between MERRA2 and Different Emission Inventory Sensitivity Simulations																
August 2018	7936	45.21 ug/m^3	0.63	68.46 ug/m^3	32.29 ug/m^3	0.65	38.07 ug/m^3	13.24 ug/m^3	0.61	35.55 ug/m^3	40.51 ug/m^3	0.56	44.91 ug/m^3	8.56 ug/m^3	0.68	26.76 ug/m^3
January 2019	7936	64.08 ug/m^3	0.79	140.21 ug/m^3	59.38 ug/m^3	0.57	107.97 ug/m^3	29.81 ug/m^3	0.80	66.62 ug/m^3	32.60 ug/m^3	0.41	68.29 ug/m^3	16.52 ug/m^3	0.87	44.46 ug/m^3
Regression Statistics for Surface PM_{10} between MERRA2 and Different Emission Inventory Sensitivity Simulations																
August 2018	7936	32.66 ug/m^3	0.62	79.63 ug/m^3	25.10 ug/m^3	0.65	51.99 ug/m^3	23.74 ug/m^3	0.69	109.17 ug/m^3	21.09 ug/m^3	0.57	48.53 ug/m^3	17.34 ug/m^3	0.71	46.22 ug/m^3
January 2019	7936	65.23 ug/m^3	0.68	92.98 ug/m^3	53.31 ug/m^3	0.66	66.97 ug/m^3	34.04 ug/m^3	0.62	64.19 ug/m^3	27.88 ug/m^3	0.59	51.29 ug/m^3	11.57 ug/m^3	0.77	34.68 ug/m^3
Regression Statistics for 850 hPa CO between Aqua/AIRS and Different Emission Inventory Sensitivity Simulations																
August 2018	2812	39.34 ug/m^3	0.43	72.60 ug/m^3	29.72 ug/m^3	0.52	53.57 ug/m^3	20.46 ug/m^3	0.47	51.38 ug/m^3	28.20 ug/m^3	0.56	57.54 ug/m^3	15.76 ug/m^3	0.63	44.75 ug/m^3
January 2019	3811	35.52 ug/m^3	0.51	84.40 ug/m^3	29.28 ug/m^3	0.53	105.96 ug/m^3	22.82 ug/m^3	0.49	54.92 ug/m^3	27.11 ug/m^3	0.55	60.91 ug/m^3	15.54 ug/m^3	0.61	36.82 ug/m^3

Overall, the combination of the MOZART-MOSAIC chemical mechanism with the SMoG-COALESCE emission inventory provided the most reliable predictions for air quality over India, particularly in urban and industrial regions with complex emission signatures. These results highlight the importance of using both a chemically comprehensive mechanism and a high-resolution, region-specific emission inventory for accurate air-quality simulations (Fig. 2.9 to 2.15). The use of the SMoG-COALESCE inventory reduced $PM_{2.5}$ RMSE by approximately 35-40% relative to global inventories during winter and increased correlation coefficients by up to 0.46 in some regions (Fig. 2.14 & 2.15). These differences highlight the dominant role of emission resolution and sectoral representation in controlling simulated pollution levels over India, particularly under stagnant winter conditions.

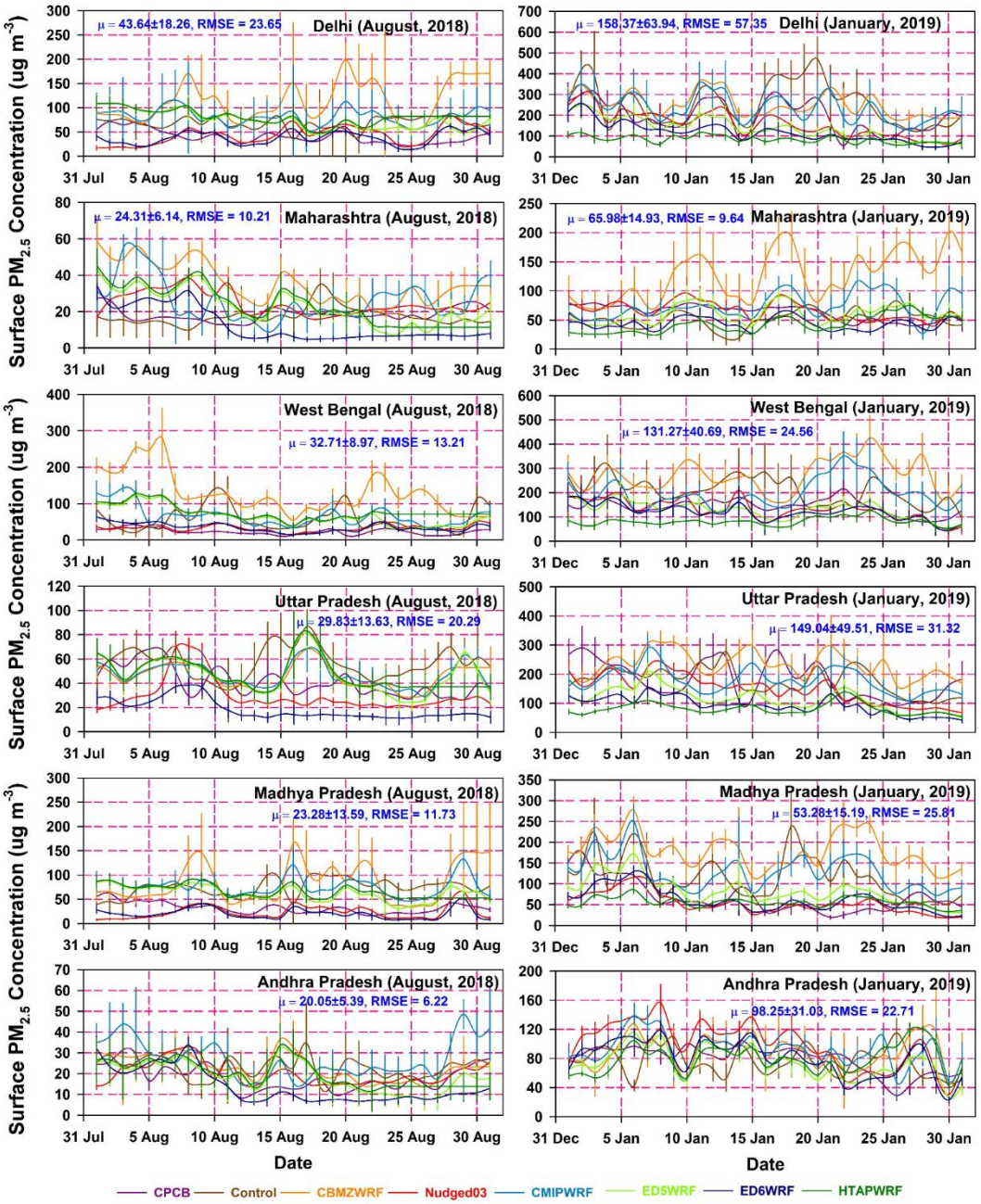


Figure 2.14: Daily mean time series comparison of surface $PM_{2.5}$ for selected Indian states from different WRF-Chem chemical mechanism and emission inventory sensitivity simulations against CPCB measurements. Temporal mean ± standard deviation (μ ± 1σ), together with RMSE of Nudged03, are indicated within each panel.

Although MOZART-MOSAIC consistently outperforms CBMZ-MOSAIC for the present configurations and evaluation periods, this result should be interpreted in a process-based context rather than as an indication of universal superiority. The improved performance of MOZART-MOSAIC during January 2019 is physically consistent with its more comprehensive treatment of ozone-NOx-VOC chemistry, heterogeneous reactions, aerosol thermodynamics, and volatility-basis-set (VBS) secondary organic aerosol formation. These processes become increasingly important under wintertime conditions characterized by weak photolysis, shallow boundary layers,

and enhanced multiphase chemistry, which are prevalent over northern India during severe pollution episodes.

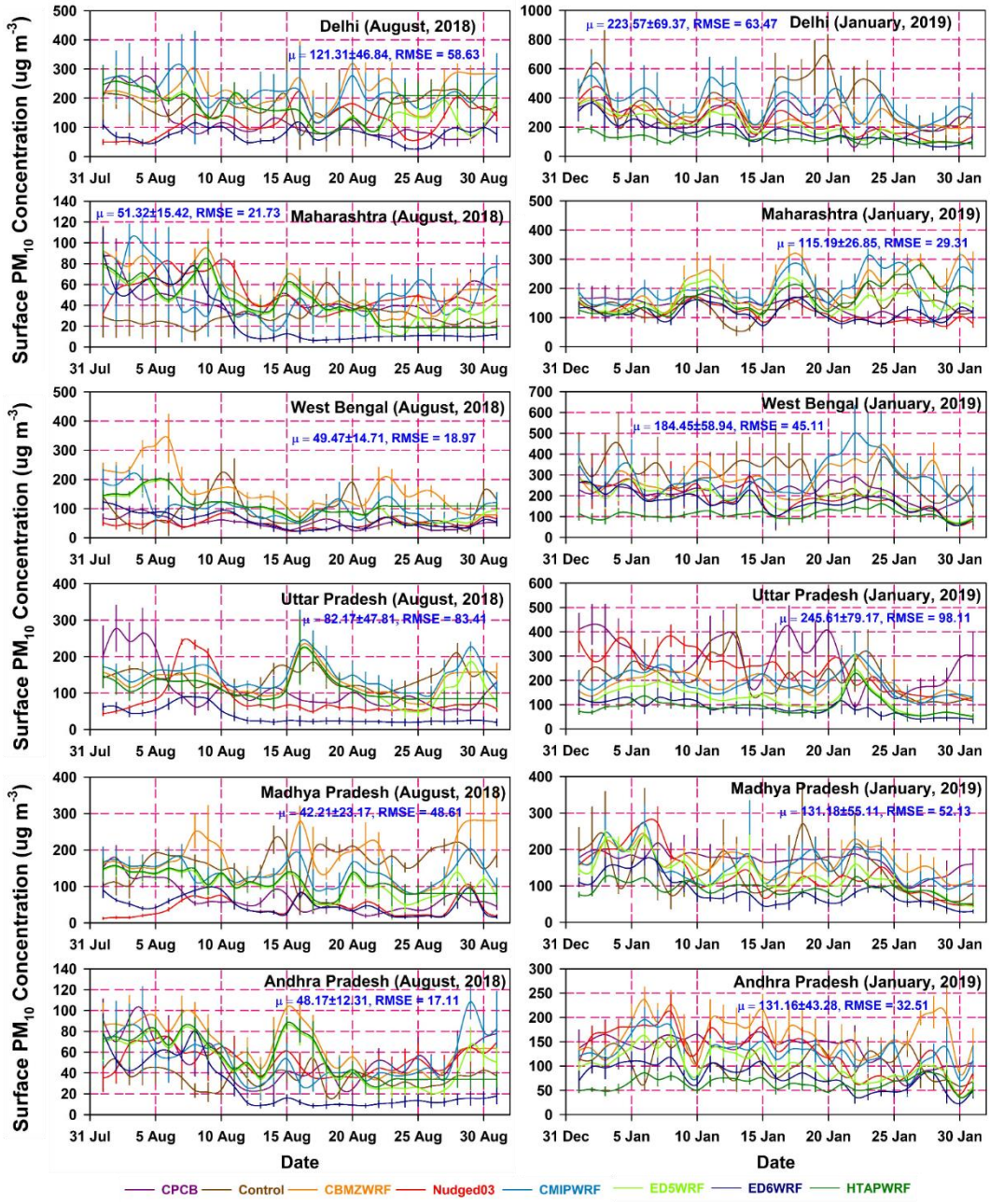


Figure 2.15: Daily mean time series comparison of surface PM_{10} for selected Indian states from different WRF-Chem chemical mechanism and emission inventory sensitivity simulations against CPCB measurements. Temporal mean ± standard deviation (μ ± 1σ), together with RMSE of Nudged03, are indicated within each panel.

At the same time, it is important to recognize that apparent improvements in model skill may partially reflect compensating errors among meteorology, emissions, and chemistry. For example, uncertainties in emission magnitudes, spatial allocation, or vertical mixing can offset biases in chemical production or loss pathways, leading to improved agreement with observations without necessarily implying optimal representation of individual processes (Fig. 2.16). Under

different regimes, such as pre-monsoon dust-dominated conditions or post-monsoon biomass-burning periods, the relative importance of mineral dust chemistry, aerosol optical properties, fire emission injection heights, and plume aging may alter the comparative performance of chemical mechanisms. Consequently, the advantages identified here for MOZART-MOSAIC should be viewed as regime-dependent, and further evaluation across additional seasons, years, and emission scenarios is required to assess broader transferability.

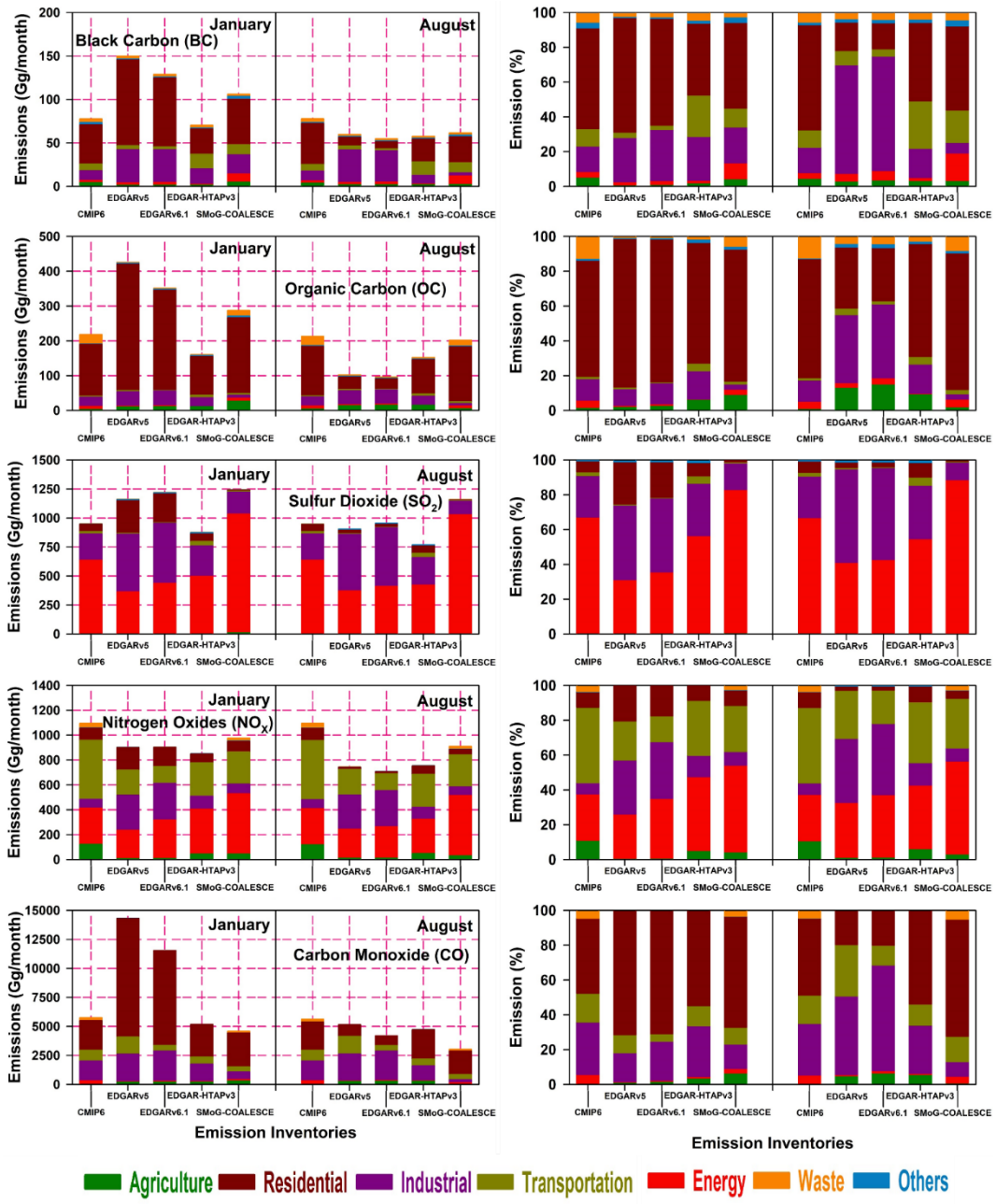


Figure 2.16: Bar charts showing the monthly total and sectoral emission comparison over India from different emission inventories used in the WRF-Chem emission inventory sensitivity simulations for various primary anthropogenic chemical species for August and January (left panel). The right panel represents the relative contribution of different emission sectors to the total emissions over the Indian region for the respective chemical species and period.

2.3.4 Grid Nudging Sensitivity

Grid nudging was applied in WRF-Chem to improve the realism of large-scale meteorological fields by gently constraining the model toward reanalysis data while preserving local variability essential for accurate representation of pollutant transport and dispersion. Fig. 2.17 & 2.18 and Table 2.5 illustrate the influence of different nudging strengths on surface meteorological and chemical variables, demonstrating that a nudging coefficient of 0.0005 s^{-1} provided the most effective balance between correcting large-scale biases and maintaining mesoscale dynamical fidelity. This optimal strength aligns with earlier recommendations for regional air-quality modelling, which emphasize that nudging should correct synoptic features without suppressing local circulations (Bowden et al., 2012; Zittis et al., 2018).

Table 2.5: Regression statistics Surface $PM_{2.5}$, PM_{10}, SO_2 and SO_4 over the Entire Indian region from different WRF-Chem chemical mechanism, grid-nudging, grid-nudging strength and approach sensitivity simulations for both study periods, evaluated against MERRA-2 observational datasets.

Regression Statistics for Surface $PM_{2.5}$ between MERRA2 and Different WRF-Chem Sensitivity Simulations Over India												
	Control			CBMZWRF			Nudged03			Nudged05		
Month	MAE (ug/m^3)	r^2	RMSE (ug/m^3)	MAE (ug/m^3)	r^2	RMSE (ug/m^3)	MAE (ug/m^3)	r^2	RMSE (ug/m^3)	MAE (ug/m^3)	r^2	RMSE (ug/m^3)
August 2018	13.62	0.33	27.48	15.47	0.35	23.32	12.43	0.37	21.67	14.61	0.31	35.83
January 2019	28.47	0.48	69.74	32.48	0.51	70.15	34.18	0.53	66.14	27.45	0.49	91.75
	Nudged01			NoNudPBL03			NoNudPBL05			NoNudPBL1		
August 2018	11.69	0.33	29.62	12.89	0.35	23.48	12.07	0.41	25.47	9.29	0.43	22.95
January 2019	17.84	0.42	86.10	35.86	0.51	46.97	23.93	0.53	64.34	25.17	0.56	48.14
Regression Statistics for Surface PM_{10} between MERRA2 and Different WRF-Chem Sensitivity Simulations Over India												
	Control			CBMZWRF			Nudged03			Nudged05		
Month	MAE (ug/m^3)	r^2	RMSE (ug/m^3)	MAE (ug/m^3)	r^2	RMSE (ug/m^3)	MAE (ug/m^3)	r^2	RMSE (ug/m^3)	MAE (ug/m^3)	r^2	RMSE (ug/m^3)
August 2018	57.48	0.40	105.74	63.47	0.40	99.48	58.49	0.41	106.81	61.95	0.35	109.61
January 2019	73.47	0.45	111.78	88.47	0.46	103.24	85.73	0.49	109.25	76.94	0.37	125.73
	Nudged01			NoNudPBL03			NoNudPBL05			NoNudPBL1		
August 2018	51.28	0.39	119.48	39.28	0.42	130.90	51.11	0.39	95.22	33.28	0.44	93.25
January 2019	71.89	0.36	116.95	49.65	0.32	66.96	63.25	0.43	87.15	65.38	0.52	95.04
Regression Statistics for Surface SO_2 between MERRA2 and Different WRF-Chem Sensitivity Simulations Over India												
	Control			CBMZWRF			Nudged03			Nudged05		
Month	MAE (ug/m^3)	r^2	RMSE (ug/m^3)	MAE (ug/m^3)	r^2	RMSE (ug/m^3)	MAE (ug/m^3)	r^2	RMSE (ug/m^3)	MAE (ug/m^3)	r^2	RMSE (ug/m^3)
August 2018	6.14	0.32	7.78	5.47	0.33	8.74	4.95	0.35	6.08	4.09	0.37	6.68
January 2019	6.89	0.39	6.93	6.73	0.38	5.88	5.51	0.41	4.74	4.38	0.31	5.22
	Nudged01			NoNudPBL03			NoNudPBL05			NoNudPBL1		
August 2018	3.06	0.43	5.03	3.69	0.41	3.97	4.53	0.38	3.45	4.53	0.49	2.33
January 2019	6.11	0.31	3.77	6.71	0.34	2.97	7.08	0.45	1.79	4.15	0.39	2.53
Regression Statistics for Surface SO_4 between MERRA2 and Different WRF-Chem Sensitivity Simulations Over India												
	Control			CBMZWRF			Nudged03			Nudged05		
Month	MAE (ug/m^3)	r^2	RMSE (ug/m^3)	MAE (ug/m^3)	r^2	RMSE (ug/m^3)	MAE (ug/m^3)	r^2	RMSE (ug/m^3)	MAE (ug/m^3)	r^2	RMSE (ug/m^3)
August 2018	3.29	0.25	9.77	2.12	0.35	7.87	1.22	0.27	9.48	1.25	0.38	8.57
January 2019	3.78	0.36	6.83	3.47	0.45	8.74	1.51	0.39	6.59	1.31	0.41	7.48
	Nudged01			NoNudPBL03			NoNudPBL05			NoNudPBL1		
August 2018	1.32	0.41	8.62	1.33	0.25	7.48	1.18	0.42	6.41	1.16	0.39	6.48
January 2019	1.34	0.39	5.48	1.43	0.43	8.94	1.41	0.44	9.17	1.42	0.47	5.52

Excessive nudging at 0.001 s^{-1} weakened boundary-layer turbulence, sea-breeze circulations, and urban heat-island effects, all of which are crucial for pollutant dispersion. Conversely, weaker nudging at 0.0003 s^{-1} was insufficient to correct synoptic-scale wind and

temperature biases, allowing errors in the reanalysis boundary conditions to propagate through the domain (Table 2.5).

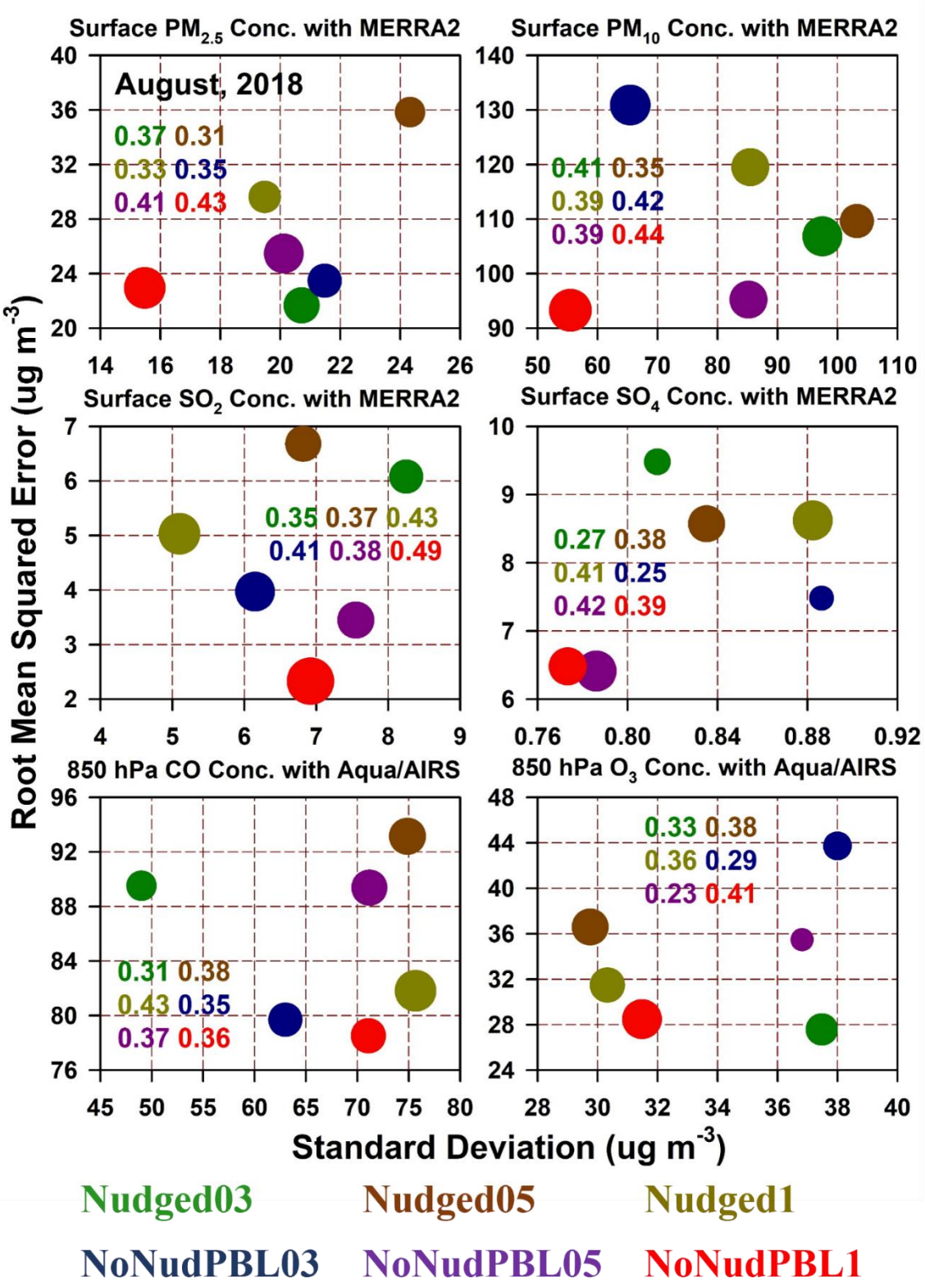


Figure 2.17: Bubble plot representation of statistical comparisons for various surface and 850 hPa pollutants over the Indian region against MERRA2 and Aqua/AIRS for different WRF-Chem nudging coefficient sensitivity simulations for August 2018. Bubble size represents RMSE, colour indicates various experiments, and inset values show Coefficients of determination (r^2).

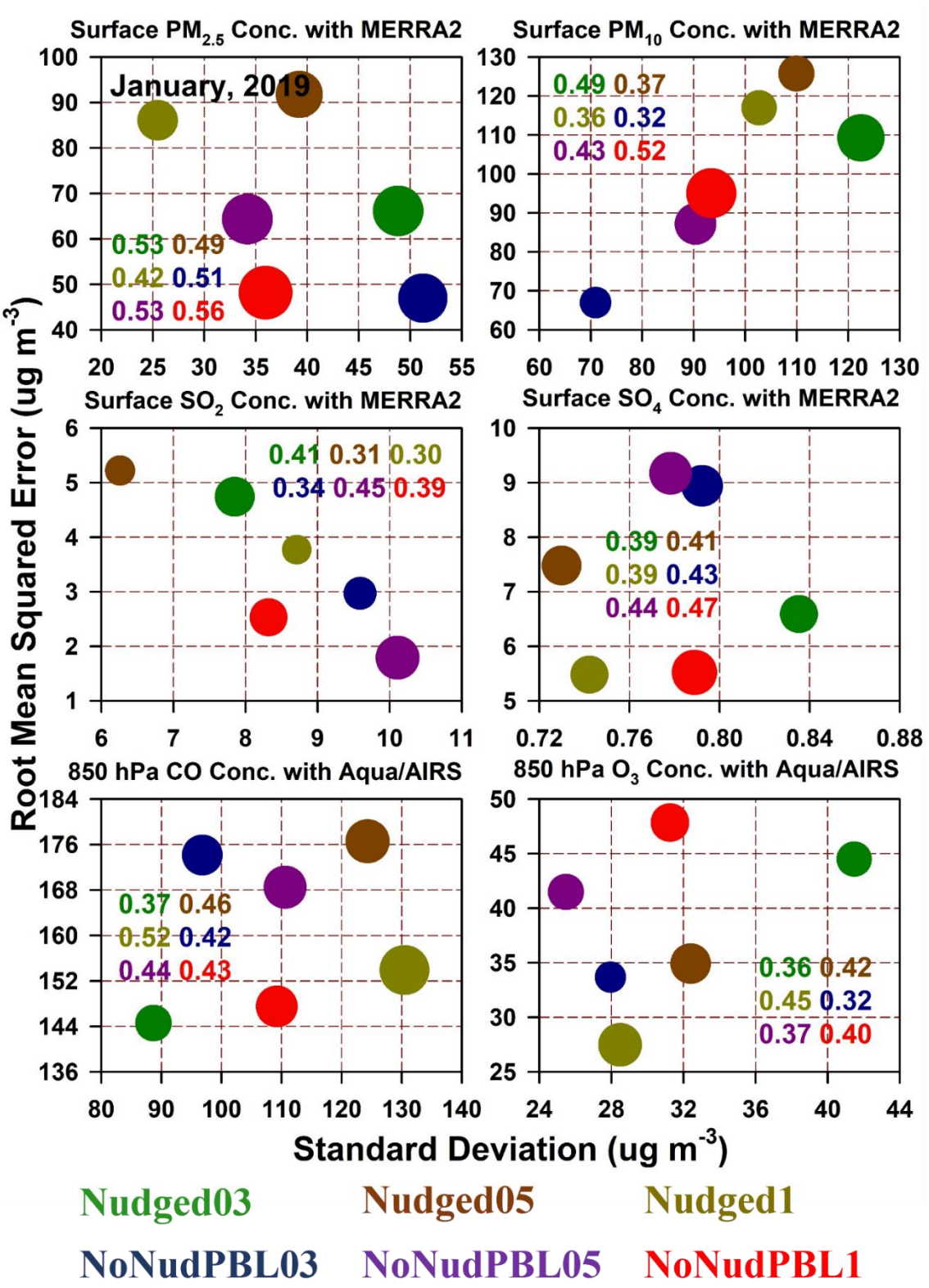


Figure 2.18: Bubble plot representation of statistical comparisons for various surface and 850 hPa pollutants over the Indian region against MERRA2 and Aqua/AIRS for different WRF-Chem nudging coefficient sensitivity simulations for January 2019. Bubble size represents RMSE, colour indicates various experiments, and inset values show Coefficients of determination (r^2).

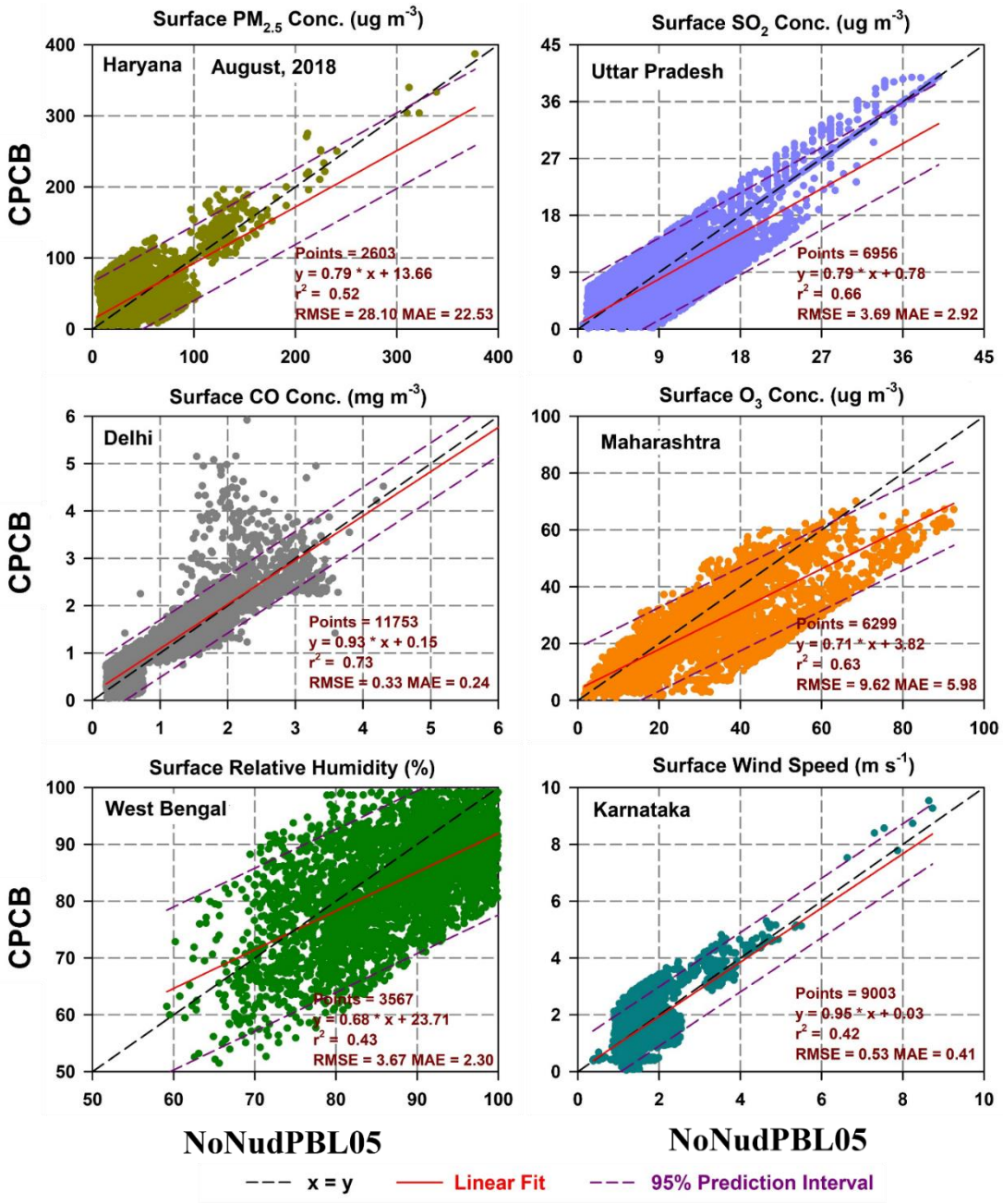


Figure 2.19: A statistical comparison of preferred WRF-Chem-simulated meteorological parameters and pollutant concentrations with CPCB measurements is shown for various Indian states with available continuous monitoring data (see Fig. 2.1) for August 2018. Panels report state-wise regression statistics (MAE, RMSE, and r^2) indicated in parentheses, enabling direct quantitative assessment of model skill across regions.

Fig. 2.2 & 2.7, reinforced by vertical structure diagnostics in Fig. 2.4 and Table 2.5, show that moderate nudging (0.0005 s^{-1}) significantly improved the representation of vertical temperature profiles during January 2019. The enhanced simulation of temperature inversions and boundary-layer stability strengthened the model's ability to capture conditions that trap pollutants near the surface over northern India. Improved inversion strength was accompanied by better reproduction of low-level wind speed and direction, which play a critical role in determining

wintertime $PM_{2.5}$ and NO_x accumulation (Table 2.5). In addition, moderate nudging improved moisture and relative humidity fields, enhancing the simulation of fog, haze, cloud microphysics, and wet deposition processes features especially important during strongly stratified winter conditions.

These meteorological improvements translated directly into enhanced pollutant simulations. Fig. 2.17 & 2.19 demonstrate that the 0.0005 s^{-1} nudging configuration produced substantially more accurate $PM_{2.5}$ and NO_x concentrations, particularly during stagnant cold-season episodes when small errors in stability and wind fields can lead to large discrepancies in pollutant predictions (Table 2.5). Thus, the analyses clearly indicate that moderate grid nudging at 0.0005 s^{-1}, applied above the PBL, provides the optimal configuration for improving both meteorological and air-quality predictions over India. It corrects large-scale biases without eroding mesoscale variability essential for pollutant dispersion. These findings further support its inclusion in the preferred WRF-Chem configuration identified in this study, alongside ERA5 initial and boundary conditions, the YSU PBL scheme, the Lin microphysics scheme, the MOZART-MOSAIC chemical mechanism, and the SMoG-COALESCE emission inventory (see Fig. 2.11 & 2.12).

Finally, when evaluated as part of the optimized model setup, this nudging configuration contributed substantially to improved agreement with CPCB ground observations across major Indian states (Fig. 2.19). Coefficients of determination ranged from 0.41 for surface $PM_{2.5}$ in Rajasthan (January 2019) to 0.73 for surface CO in Delhi (August 2018), while meteorological parameters such as wind speed and relative humidity showed r^2 values of 0.42 (Karnataka, August 2018) and 0.67 (Andhra Pradesh, January 2019), respectively (Fig. 2.20). These results highlight the importance of grid nudging in enhancing the fidelity of meteorological and chemical simulations over India's complex atmospheric environment and emphasise its value in generating reliable, policy-relevant air-quality forecasts.

Therefore, the sensitivity experiments demonstrate that differences in model configuration can lead to changes of 20-50% in key performance metrics, emphasizing that physically consistent choices of meteorological forcing, PBL and microphysics schemes, chemical mechanisms, emission inventories, and nudging strategies are essential for reliable air-quality simulations over India.

We note that the present evaluation does not explicitly include pre-monsoon dust-dominated conditions or post-monsoon biomass-burning episodes. Consequently, while the optimized configuration is robust across monsoon and winter extremes, additional uncertainties may arise in seasons where mineral dust emissions, aerosol mixing state and optical properties, and biomass-burning emission timing/injection heights play a dominant role. Extending the optimized configuration to these regimes is a logical next step to further refine season-specific aerosol and emission process representations.

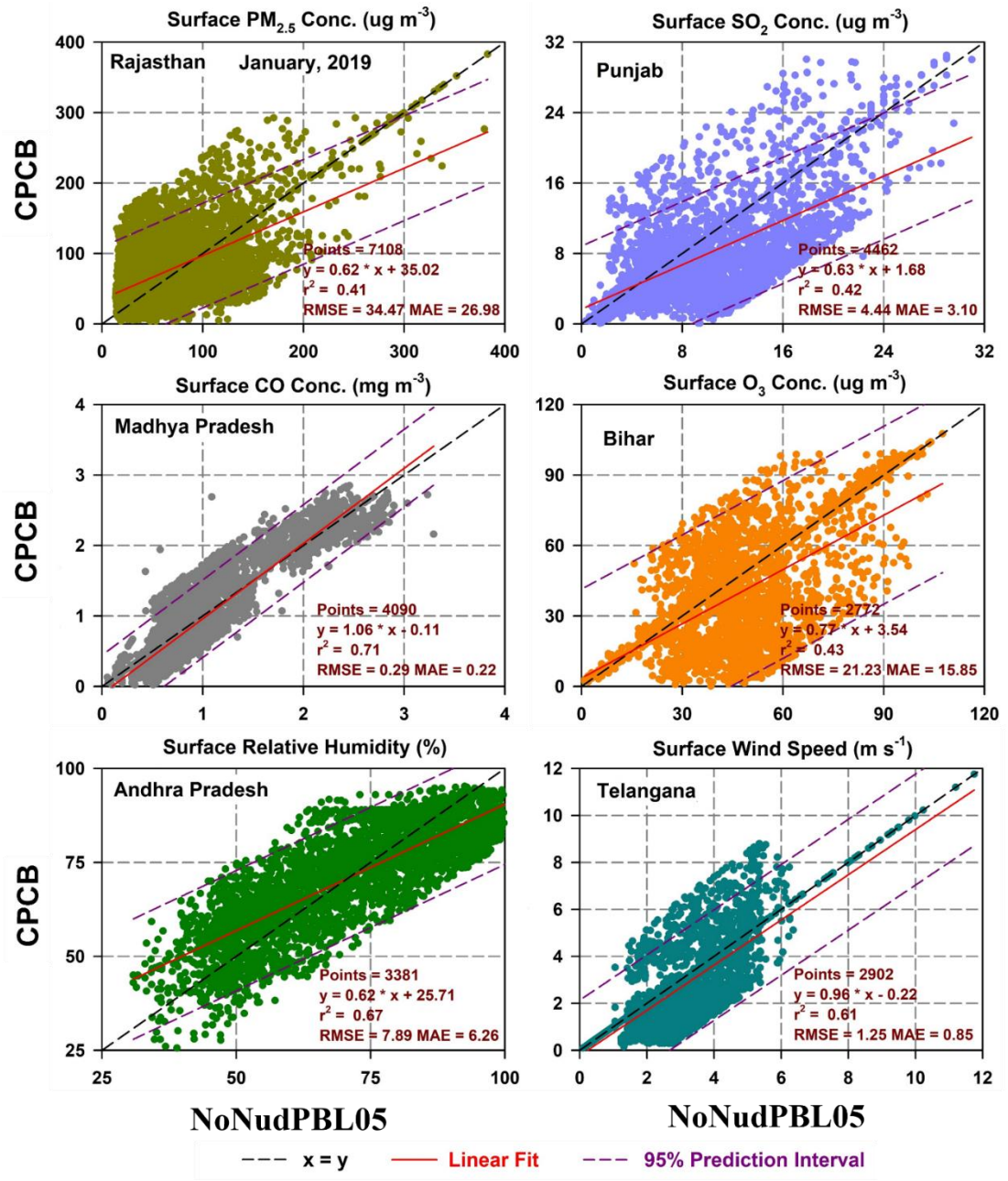


Figure 2.20: A statistical comparison of preferred WRF-Chem-simulated meteorological parameters and pollutant concentrations with CPCB measurements is shown for various Indian states with available continuous monitoring data (see Fig. 2.1) for January 2019. Panels report state-wise regression statistics (MAE, RMSE, and r^2) indicated in parentheses, enabling direct quantitative assessment of model skill across regions.

2.4 Summary and Conclusions

This study presents a comprehensive, multi-component sensitivity analysis of WRF-Chem (v4.2.2) to assess its ability to simulate meteorology and air quality over India under two sharply contrasting seasonal regimes, peak monsoon conditions (August 2018) and peak winter conditions (January 2019). By systematically perturbing meteorological initial and boundary conditions, planetary boundary layer (PBL) schemes, microphysics schemes, chemical mechanisms, anthropogenic emission inventories, and grid-nudging strengths, while holding all other settings fixed in each experiment, we identify an optimal model configuration that significantly improves the realism of both meteorological fields and pollutant distributions. The deliberate use of monsoon and winter periods provides a stringent test of WRF-Chem's coupled meteorology-chemistry behaviour across India's broad range of dynamical, thermodynamic, and removal conditions.

Across all experiments, the selection of meteorological initial and boundary conditions emerged as the dominant control on model performance, establishing the baseline realism upon which chemistry and aerosol processes operate. Simulations driven by ERA5 consistently outperformed those forced by NCEP GDAS and NCEP CFSv2 for key variables, including near surface temperature, relative humidity, wind fields, cloud characteristics, and vertical thermodynamic structure. ERA5's superior resolution and improved representation of mesoscale circulation and moisture transport enhanced the simulation of monsoonal convection and rainfall-related processes, while also better capturing wintertime stagnation, inversion strength, and shallow boundary-layer evolution. These meteorological improvements translated directly into more realistic pollutant dispersion, accumulation, and removal, underscoring that credible air-quality predictions over India require meteorological forcing that robustly represents both convective and stable-regime dynamics.

Sensitivity to boundary layer physics further demonstrated that accurate representation of vertical mixing and stability is essential for reproducing observed pollution levels. Among the tested schemes, the YSU PBL scheme provided the most realistic PBL structure in both seasons. Its ability to represent shallow nocturnal PBLs and strong inversions during winter improved the simulation of near-surface pollutant build-up over northern India, while its performance under convective conditions supported more realistic daytime mixing during the monsoon. Microphysics choices introduced additional sensitivity, particularly during August when wet scavenging is the

principal removal pathway for aerosols and soluble gases. The Lin microphysics scheme produced the most realistic rainfall distribution and cloud characteristics among the tested options, contributing to improved representation of monsoon-season wet deposition and associated pollutant variability. Together, these results highlight that physically consistent boundary-layer and cloud-precipitation processes are prerequisite for reliable air-quality simulation across India's seasonal extremes.

Chemical mechanisms and emission inventories introduced substantial additional uncertainty by controlling secondary formation pathways and the magnitude and structure of emitted precursors. Within the tested configurations, MOZART-MOSAIC performed better than CBMZ-MOSAIC for multiple pollutants, consistent with its more comprehensive treatment of ozone-NO_x-VOC chemistry, aerosol thermodynamics, and secondary pollutant formation processes that are especially relevant under wintertime stagnant conditions. Emission inventory choice exerted a similarly strong influence on simulated pollution magnitudes and spatial gradients. The SMoG-COALESCE inventory, with its India-specific sectoral detail and high spatial resolution, best captured observed urban–industrial hotspots and regional gradients, whereas coarser global inventories (e.g., EDGAR and CEDS-CMIP6) tended to smooth localized emissions and systematically underpredict concentrations over densely populated and industrial corridors, particularly across the Indo-Gangetic Plain. The combined results reinforce that both chemically appropriate mechanism complexity and regionally realistic, high-resolution emissions are necessary to reproduce India's highly heterogeneous pollution environment.

Grid nudging experiments further emphasized the need to balance synoptic-scale realism with preservation of mesoscale and boundary-layer variability. A moderate nudging coefficient of 0.0005 s^{-1} applied above the PBL provided the best overall performance, improving large-scale circulation patterns, vertical thermal structure, and winter inversion strength without excessively damping local circulations and mixing processes that govern pollutant dispersion. Stronger nudging suppressed mesoscale variability relevant to air quality, whereas weaker nudging did not adequately constrain synoptic-scale biases. These findings support the use of moderate, above-PBL nudging as a pragmatic approach for extended regional air-quality simulations over India.

Based on the combined evaluation, the preferred WRF-Chem configuration for India in this study consists of ERA5 meteorological initial and boundary conditions, the YSU PBL scheme, Lin microphysics, the MOZART-MOSAIC chemical mechanism, the SMoG-COALESCE anthropogenic emission inventory, and grid nudging (0.0005 s^{-1}) applied above the boundary layer.

This configuration improves the simulation of near-surface meteorology, pollutant concentrations, and their spatiotemporal patterns across diverse Indian regions under both monsoon and winter regimes. Agreement with CPCB observations and satellite/reanalysis products confirms that the optimized setup provides a robust foundation for applications requiring physically consistent meteorology–chemistry coupling, including air-quality forecasting, retrospective assessments, and scenario-based analyses relevant to mitigation planning.

At the same time, the conclusions of this work should be interpreted with appropriate caution. The optimized configuration demonstrates robustness within the evaluated months and tested sensitivity matrix, but it should not be interpreted as universally optimal across all seasons, years, or emission scenarios. In regional air-quality modelling, improved agreement with observations can arise partly from compensating errors among meteorological forcing, emissions, and chemistry. Accordingly, the stronger performance of MOZART-MOSAIC relative to CBMZ-MOSAIC here should be viewed as regime-dependent and linked to the specific seasonal conditions examined, rather than as unconditional superiority. A further limitation is that the sensitivity experiments were conducted for peak monsoon (August) and peak winter (January) only and therefore do not explicitly evaluate pre-monsoon dust-dominated conditions or post-monsoon biomass-burning episodes. Although these processes are represented in WRF-Chem, key uncertainties such as dust emission parameterizations, aerosol optical properties, and biomass-burning emission magnitude, temporal allocation, and plume injection height may influence model skill in those regimes and therefore warrant targeted evaluation. Extending the optimized configuration to the pre- and post-monsoon periods, as well as testing its transferability across additional years and emission scenarios, constitutes an important next step toward refining season-specific process representations and strengthening the generality of the framework developed here.

Sample namelist.input Configuration

&time_control; run_days = XX, run_hours = XX, run_minutes = XX, run_seconds = XX, interval_seconds = XX, start_year = XX, start_month = XX, start_day = XX, start_hour = XX, start_minute = XX, start_second = XX, end_year = XX, end_month = XX, end_day = XX, end_hour = XX, end_minute = XX, end_second = XX, input_from_file = .true., history_interval = 60, io_form_history = 2, debug_level = 0, **&domains;** time_step = XX, time_step_fract_num = 0, time_step_fract_den = 1, max_dom = 1, s_we = 1, e_we = XX, s_sn = 1, e_sn = XX, s_vert = 1, e_vert = XX, p_top_requested = XX, dx = XX, dy = XX, grid_id = 1, parent_id = 1, i_parent_start = 1, j_parent_start = 1, parent_grid_ratio = 1, parent_time_step_ratio = 1, **&physics;** mp_physics = 2, ra_lw_physics = 4, ra_sw_physics = 4, radt = 30, sf_sfclay_physics = 1, cu_physics = 5, ishallow = 1, bl_pbl_physics = 1, sf_surface_physics = 2, cudt = 5, sf_urban_physics = 0, surface_input_source = 3, num_soil_layers = 4, num_land_cat = 21, do_radar_ref = 1, cu_rad_feedback = .true., slope_rad = 0, topo_shading = 0, progn = 1, cu_diag = 1, **&fdda;** grid_fdda = 1, gfdda_interval_m = 360, gfdda_end_h = 1200, io_form_gfdda = 2, fgdt = 0, if_no_pbl_nudging_uv = 1, if_no_pbl_nudging_t = 1, if_no_pbl_nudging_q = 1, if_zfac_uv = 0, k_zfac_uv = 10, if_zfac_t = 0, k_zfac_t = 10, if_zfac_q = 0, k_zfac_q = 10, guv = 0.0005, gt = 0.0005, gq = 0.0005, dk_zfac_uv = 1, dk_zfac_t = 1, dk_zfac_ph = 1, **&dynamics;** w_damping = 0, diff_opt = 1,km_opt = 4, damp_opt = 0, diff_6th_opt = 0, diff_6th_factor = 0.12, base_temp = 290, zdamp = 5000., dampcoef = 0.2, non_hydrostatic = .true., moist_adv_opt = 1, scalar_adv_opt = 1, moist_adv_opt = 2, scalar_adv_opt = 2, chem_adv_opt = 2, tke_adv_opt = 2, **&chem;** kemit = 1, chem_opt = 202, bioemdt = 30, io_style_emissions = 2, emiss_inpt_opt = 102, emiss_opt = 10, chem_in_opt = 0, phot_opt = 2, gas_drydep_opt = 1, aer_drydep_opt = 1, bio_emiss_opt = 3, dust_opt = 3, dmsemis_opt = 1, seas_opt = 1, gas_bc_opt = 1, gas_ic_opt = 1, aer_bc_opt = 1, aer_ic_opt = 1, gaschem_onoff = 1, aerchem_onoff = 1, wetscav_onoff = 1, cldchem_onoff = 1, biomass_burn_opt = 2, aer_ra_feedback = 1, aer_op_opt = 1, photdt = 30, chemdt = 5,

Chapter 3: Drivers of $PM_{2.5}$ Changes over North India during the COVID-19 Period: Emissions Controls versus Meteorology

3.1 Introduction

Ambient fine particulate matter ($PM_{2.5}$) pollution represents one of the most severe environmental and public health challenges in India. Nearly the entire population is exposed to annual mean $PM_{2.5}$ concentrations exceeding the World Health Organization (WHO) guideline value of 10 μg m^{-3}, and approximately three-fourths of the population experience concentrations above the National Ambient Air Quality Standards (NAAQS) threshold of 40 μg m^{-3} (Balakrishnan et al., 2019). Such chronic exposure has profound implications for population health and productivity, and it reflects the combined influence of diverse emission sources, transport, industry, power generation, construction, residential combustion, agricultural residue burning, and episodic natural contributions such as dust, operating under highly variable meteorological conditions.

In response to this pervasive exposure and the persistence of extreme pollution episodes, the Government of India launched the National Clean Air Programme (NCAP) in 2019, aiming to achieve a 20-30% reduction in $PM_{2.5}$ levels across 131 non-attainment cities by 2024 relative to 2017 levels. While the NCAP framework represents an important national commitment, a key scientific and policy question remains: how much of an observed change in $PM_{2.5}$ can be attributed to emission reductions, and how much is simply the outcome of meteorology-driven variability? This question is particularly relevant in India, where seasonal transitions and synoptic-scale disturbances can cause large concentration fluctuations even without strong changes in emissions.

Against this policy backdrop, the COVID-19 pandemic and the unprecedented nationwide lockdown implemented from 25 March 2020 created a unique, unplanned “natural experiment” by abruptly altering anthropogenic emission patterns across the country. The lockdown imposed stringent restrictions on transportation, industrial operations, construction activities, and commercial establishments, leading to an abrupt decline in emissions from these sectors. As a result, pronounced reductions in several primary and secondary air pollutants were reported, particularly over urban areas. Importantly, however, changes in ambient $PM_{2.5}$ during the lockdown were not governed solely by emission reductions. Meteorological conditions, including boundary layer height, wind speed and direction, precipitation, temperature, and humidity, strongly modulate pollutant dispersion, accumulation, wet scavenging, and chemical transformation (Xie et al., 2024). Consequently, $PM_{2.5}$ changes during the lockdown and subsequent unlock phases reflect the combined influence of emission perturbations and meteorology, rather than emission changes alone.

Attribution is further complicated by regional transport and transboundary influences. India's air quality is shaped not only by local emissions but also by inflow from upwind regions, long-range transport of biomass-burning plumes, and episodic dust transport, which can amplify or offset local emission-driven changes (Kumar et al., 2020; Tibrewal et al., 2022). Therefore, interpreting lockdown-related changes purely as "emission reductions" risks overestimating the effectiveness of sector-specific controls if meteorological ventilation was favourable, or underestimating control potential if ventilation was unfavourable.

A growing body of literature has documented substantial improvements in air quality across India during the COVID-19 lockdown, often reporting sharp declines in $PM_{2.5}$ and gaseous pollutants over major cities (Jain et al., 2020; Zhang et al., 2021). However, many early studies focused primarily on the strict lockdown period, did not extend through the unlock phases, and relied on observations from a limited number of Central Pollution Control Board (CPCB) monitoring stations. These limitations constrain spatial representativeness and hinder robust national-scale attribution because the same emission reductions can lead to very different concentration responses depending on meteorology. Recent advances integrating satellite-derived $PM_{2.5}$ datasets with ground-based observations have substantially improved spatial coverage and consistency, enabling more comprehensive assessments of $PM_{2.5}$ changes across India (Dey et al., 2020; Katoch et al., 2023).

In this chapter, we combine satellite-derived $PM_{2.5}$ estimates with simulations from the Weather Research and Forecasting model coupled with Chemistry (WRF-Chem) to systematically evaluate $PM_{2.5}$ variability across India from the pre-lockdown period through successive lockdown and unlock phases. By explicitly separating meteorology-induced variability from activity-restricted emission reductions, we provide a more physically grounded interpretation of observed air quality changes. This approach also enables identification of persistent sources, particularly residential combustion and open burning, that remained largely unaffected or were amplified during the lockdown. Overall, the chapter provides evidence for why short-term activity restrictions did not yield sustained compliance with NAAQS and highlights the need for long-term, multi-sectoral mitigation strategies.

3.2 Datasets and Methodology

3.2.1 Model Description and Simulation Details

We employed the Weather Research and Forecasting model coupled with Chemistry (WRF-Chem, version 4.2.2) to simulate $PM_{2.5}$ concentrations over India during the pre-lockdown, lockdown, and unlock phases of the COVID-19 period. WRF-Chem has been widely applied and evaluated for air quality studies over India (Agarwal et al., 2024; Reyes-Villegas et al., 2023; Srivastava et al., 2024), largely because it treats meteorology and chemistry in a coupled framework, allowing interactions among transport, boundary-layer evolution, chemical production, and removal processes to be represented consistently.

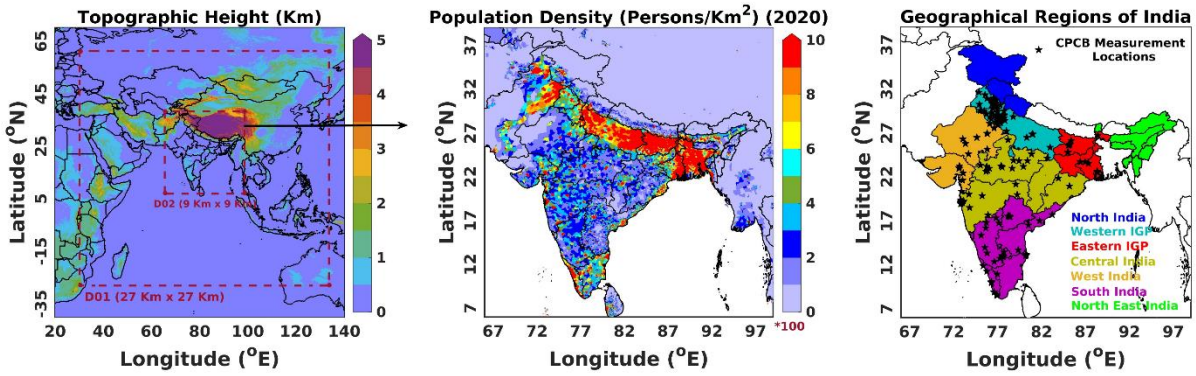


Figure 3.1: WRF-Chem simulation domain with topographic height (left) and 2020 population density from GPWv4 (centre). The right panel shows the seven Indian geographical regions North India (NI), Northeast India (NEI), Central India (CI), South India (SI), West India (WI), Eastern Indo-Gangetic Plain (EIGP), and Western Indo-Gangetic Plain (WIGP) alongside CPCB measurement sites active in 2020. This configuration was used to assess the effects of emission changes and meteorological variability during the COVID-19 lockdown across the Indian region.

Simulations were conducted for 4 February-30 June for each year from 2015 to 2020, with the first 20 days treated as spin-up and excluded from analysis. A two-domain nested configuration was adopted, with the inner domain covering the Indian landmass at 9 km x 9 km horizontal resolution, centred over Bilaspur, India (22.38°N, 82.13°E). The inner and outer domains comprised 307 × 319 and 321 × 331 grid cells, respectively (Fig. 3.1). This setup allows representation of both regional transport (outer domain) and finer-scale gradients in emissions and meteorology relevant for surface $PM_{2.5}$ variability (inner domain).

Meteorological forcing was provided by ERA5 reanalysis, with grid nudging applied to winds, temperature, and water vapour above the planetary boundary layer to constrain large-scale circulation while preserving near-surface processes essential for pollutant mixing and accumulation (Zittis et al., 2018). A nudging coefficient of 0.0005 s^{-1} and a 6-hour nudging interval were used. Anthropogenic emissions were prescribed using the EDGAR-v6.1 inventory. To disentangle meteorology-driven variability from emission-driven changes, six WRF-Chem simulations were performed to represent pre-lockdown, lockdown, and unlock phases, and a subtraction-based framework was applied for each phase (Table 3.1).

Emission details used in WRF-Chem Simulations:

Biogenic emissions were calculated online using MEGAN, while biomass burning emissions were derived from FINN-v2.5. Gas-phase chemistry was represented using MOZART-4 coupled with the MOSAIC four-bin aerosol scheme, including grid-scale aqueous chemistry and an extended Volatility Basis Set (VBS) treatment of organic aerosols. Six-hourly chemical boundary conditions were obtained from Whole Atmosphere Community Climate Model (WACCM) simulations. This configuration supports representation of both primary $PM_{2.5}$ and secondary aerosol formation pathways relevant under India's complex NO_x-VOC-oxidant conditions and seasonally varying photochemistry.

Accurate representation of emission reductions during the lockdown was achieved by applying COvid-19 adjustmeNt Factors fOR eMissions (CONFORM) (Doumbia et al., 2021) to EDGAR-v6.1 (2018) for major pollutants and to EDGAR-v5 (2015) for VOCs. These daily global adjustment factors reflect sector-specific activity changes across Industry, Power, Residential, Transport, and Public/Commercial sectors. The largest nationwide reduction in $PM_{2.5}$ emissions (~31%) occurred during Lockdown Phase 3, with Northern India, Central India, and the Eastern Indo-Gangetic Plain (IGP) experiencing declines of ~39%, ~32%, and ~31%, respectively (Fig. 3.2). These spatial contrasts are critical because they imply that a uniform national narrative of air quality improvement may not reflect regionally heterogeneous emission responses.

CONFORM Emission Adjustment Factor	**EDGAR-v5 and EDGAR-v6.1 Emission Activity**
Gridded daily Average adjustment-factor for **Power Sector**	Power industry
Gridded daily Average adjustment-factor for **Industry Sector**	Food and Paper, Combustion for manufacturing, Iron and steel production, Non-ferrous metals production, Non-metallic minerals production, Oil refineries and Transformation industry, Fuel exploitation
Gridded daily Average adjustment-factor for **Residential Sector**	Fossil Fuel Fires, Energy for buildings, Non energy use of fuels
Gridded daily Average adjustment-factor for **Public and Commercial Sector**	Agricultural waste burning, Chemical processes, Solid waste incineration, Agricultural Soils, Manure Management, Solid waste landfills, Solvents and products use, Wastewater handling
Gridded daily Average adjustment-factor for **Transport Sector**	Aviation climbing & descent, Aviation cruise, Aviation landing & take off, Aviation supersonic, Railways, pipelines, off-road transport, Shipping, Road transportation resuspension, Road transportation no resuspension

Table 3.1: WRF-Chem model simulations setup.

Sl No.	**Emissions**	**Meteorology**	**Simulation Name**
1	CONFORM Adjusted (2020)	ERA5 (2020)	LOCK20
2	EDGAR-v6.1 (2018) [CO, No_x, NH_3, SO_2, PM_{10}, $PM_{2.5}$, BC and OC] EDGAR-v5 (2015) [VOCs]	ERA5 (2015)	ANO15
3		ERA5 (2016)	ANO16
4		ERA5 (2017)	ANO17
5		ERA5 (2018)	ANO18
6		ERA5 (2019)	ANO19

A comparison of total $PM_{2.5}$ emissions during the non-COVID-19 reference period [Pre-Lockdown: 24 February-24 March 2020] with those during successive phases of restricted activity

[Lockdown Phase-1: 25 March-14 April; Phase-2: 15 April-3 May; Phase-3: 4-17 May; Phase-4: 18–31 May], as well as the subsequent transition to the new-normal [Unlock: 1-30 June], reveals a pronounced reduction in emissions associated with mobility and industrial restrictions. The largest nationwide decline in $PM_{2.5}$ emissions, approximately 31%, was observed during Lockdown Phase-3 (Fig. 3.2). Regionally, the most substantial reductions occurred over Northern India, Central India, and the Eastern Indo-Gangetic Plain (IGP), where $PM_{2.5}$ emissions decreased by about 39%, 32%, and 31%, respectively, reflecting the combined effects of stringent activity curtailment across major urban, industrial, and transport-dominated sectors.

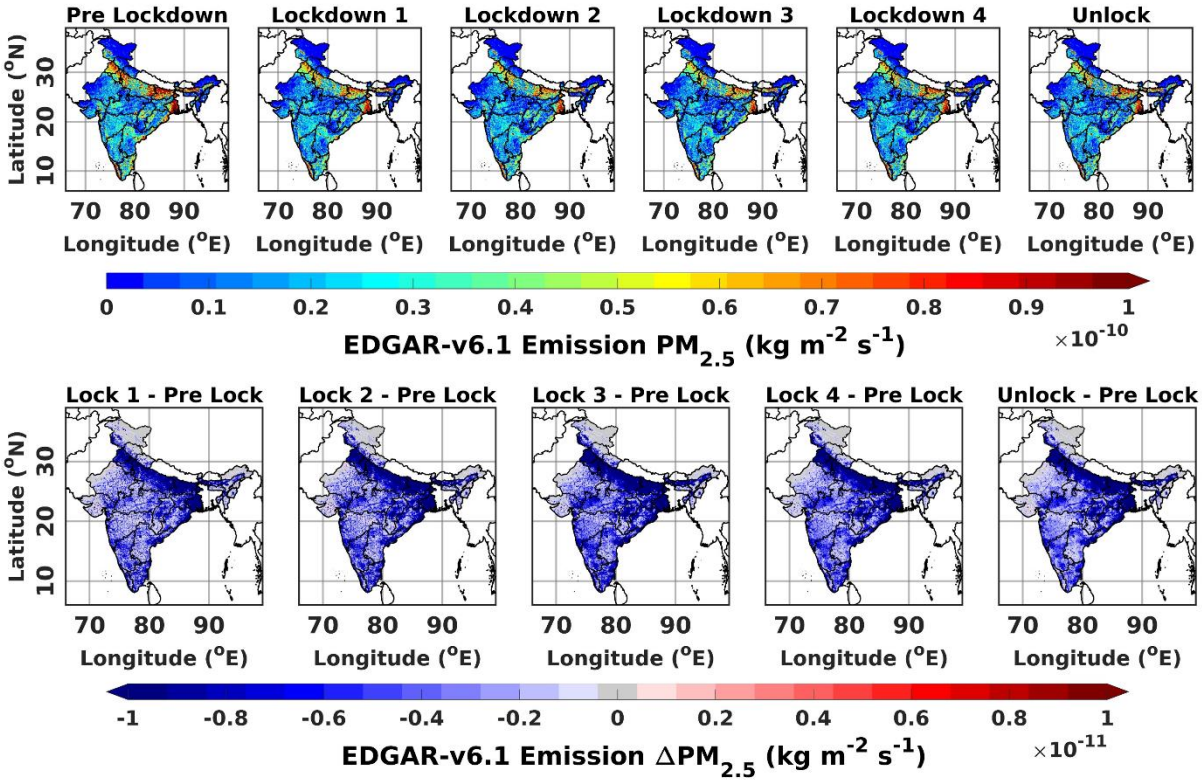


Figure 3.2: Spatial distributions of total $PM_{2.5}$ emissions in 2020 and their changes relative to the non-COVID-19 (pre-lockdown) period over the entire study timeframe.

3.2.2 Satellite-$PM_{2.5}$ database

To complement the model simulations and to ensure consistent national-scale spatial coverage, a high-resolution satellite-derived $PM_{2.5}$ dataset developed under the SAANS initiative was employed (Dey et al., 2020; Katoch et al., 2023). This product provides daily $PM_{2.5}$ estimates at a spatial resolution of 1 km × 1 km, enabling a more detailed representation of spatial gradients and regional pollution hotspots that are not fully captured by the Central Pollution Control Board (CPCB) monitoring network. Satellite-derived $PM_{2.5}$ data for the period 24 February-30 June were

extracted for the years 2015-2020 to construct a multi-year reference baseline representative of typical interannual variability during the late winter to pre-monsoon transition.

Table 3.2: Quantifying the contributions of emission reductions and meteorological variability.

Mean $PM_{2.5}$ from each Phase of Lockdown (2020) - Mean $PM_{2.5}$ from Pre Lockdown (2020)	Effect of meteorology induced change and activity restricted reduction in $PM_{2.5}$ for each Phase of Lockdown (2020)
Mean of the [Mean $PM_{2.5}$ from each Phase of Lockdown period (2015 to 2019) - Mean $PM_{2.5}$ from Pre Lockdown period (2015 to 2019)]	Effect of only meteorology induced change in $PM_{2.5}$ for each Phase of Lockdown (2020)
{Mean $PM_{2.5}$ from each Phase of Lockdown (2020) - Mean $PM_{2.5}$ from Pre Lockdown (2020)} - {Mean of the [Mean $PM_{2.5}$ from each Phase of Lockdown period (2015 to 2019) - Mean $PM_{2.5}$ from Pre Lockdown period (2015 to 2019)]}	Effect of only activity restricted reduction in $PM_{2.5}$ for each Phase of Lockdown (2020)

The contributions of emission reductions and meteorological variability to observed $PM_{2.5}$ changes were quantified using a consistent subtraction-based framework, summarized in Table 3.2. For each lockdown phase in 2020, the total change in $PM_{2.5}$ concentration was calculated as the difference between the phase-wise mean $PM_{2.5}$ concentration and the corresponding pre-lockdown mean in 2020. This total change reflects the combined influence of altered emissions and contemporaneous meteorological conditions. To isolate the effect of meteorology alone, the mean $PM_{2.5}$ difference between each lockdown phase and the pre-lockdown period was calculated for the reference years 2015-2019, and the average of these differences was taken as the meteorology-induced change. The emission-driven reduction in $PM_{2.5}$ for each lockdown phase in 2020 was then obtained as the residual, defined as the difference between the total observed change in 2020 and the estimated meteorology-induced component.

The same subtraction methodology applied to the WRF-Chem simulations (Table 3.2) was applied consistently to the satellite-derived $PM_{2.5}$ dataset to ensure methodological coherence across observational and modelling analyses. For 2020, phase-wise mean $PM_{2.5}$ concentrations were compared with the pre-lockdown reference period to estimate total changes, while meteorology-driven changes were derived from the averaged phase-wise $PM_{2.5}$ differences over

2015-2019. Emission-driven reductions were subsequently inferred as residuals. By treating the 2015-2019 period as a meteorological climatology, this framework minimizes the likelihood that anomalous meteorological conditions in any single year disproportionately influence the inferred emission signal.

A schematic overview of the methodological framework adopted in this study is outlined below. The total change in $PM_{2.5}$ concentration during Lockdown Phase-1 in 2020 was calculated as the difference between the mean $PM_{2.5}$ concentration observed during the lockdown period (25 March-14 April 2020) and the mean concentration during the corresponding pre-lockdown reference period (24 February-24 March 2020). To isolate the contribution of meteorological variability, the meteorology-induced change in $PM_{2.5}$ was estimated as the average $PM_{2.5}$ change over the same calendar period for the five preceding years (2015-2019), when no lockdown-related emission perturbations were present. The emission-driven reduction in $PM_{2.5}$ during Lockdown Phase-1 was then derived by subtracting the meteorology-induced change from the total observed $PM_{2.5}$ change in 2020.

This analytical framework was applied consistently across all subsequent lockdown phases as well as the unlock period to ensure methodological consistency. In addition, to examine day-to-day variability, daily $PM_{2.5}$ anomalies for 2020 were computed relative to the corresponding five-year climatological mean (2015-2019). These anomalies were subsequently normalized by the five-year standard deviation. A normalized anomaly value less than -1 indicates that the observed daily reduction in $PM_{2.5}$ exceeded the typical range of interannual variability, providing strong evidence that the decrease in concentrations was primarily driven by emission reductions associated with lockdown measures rather than by meteorological fluctuations alone.

Overall, the combined use of high-resolution satellite observations, multi-year climatological baselines, and a consistent subtraction-based attribution framework provides a robust and independent assessment of the relative roles of emission changes and meteorology in shaping $PM_{2.5}$ variability during the COVID-19 lockdown period over India.

3.2.3 Validation and Quantification of Contributions Process

To ensure that the inferred impacts of COVID-19 activity restrictions on $PM_{2.5}$ were physically meaningful and statistically defensible, we carried out a rigorous, multi-dataset evaluation of both (i) the WRF-Chem simulations and (ii) the satellite-derived $PM_{2.5}$ product against independent reference datasets. Ground-based observations from the Central Pollution Control Board (CPCB) were used as the primary benchmark for surface $PM_{2.5}$, while MERRA-2 reanalysis surface $PM_{2.5}$ fields were used as an additional nationally consistent reference. This multi-source validation was essential because India's monitoring network, although rapidly expanding, still exhibits uneven spatial coverage, and both model- and satellite-based $PM_{2.5}$ estimates can be sensitive to regional aerosol composition, boundary-layer structure, and the representation of dust and secondary aerosol processes.

To ensure that the evaluation was based on robust spatial sampling and did not rely on a small number of isolated stations, we restricted the analysis to states containing at least five operational CPCB monitoring sites during the lockdown analysis window (24 February-30 June 2020). This criterion yielded a geographically representative set of states spanning five major regions across India (Fig. 3.1; Table 3.3), allowing assessment of performance across contrasting emission environments, ranging from the heavily polluted Indo-Gangetic Plain (IGP) to coastal and peninsular regions where marine influence, rainfall scavenging, and boundary-layer ventilation are typically stronger.

Recognizing the known quality concerns associated with CPCB datasets reported in earlier studies (Barrero et al., 2015; Sharma et al., 2022; Vohra et al., 2025), we applied stringent quality-control procedures prior to computing daily mean $PM_{2.5}$. Specifically, we removed outliers and filtered stations exhibiting constant or repetitive values that can artificially distort daily and phase-wise averages. These steps are consistent with established practices for producing reliable daily $PM_{2.5}$ time series from regulatory datasets (Singh et al., 2020; Zhou et al., 2024) and were applied uniformly across the lockdown and unlock periods to avoid introducing phase-dependent biases. Model and satellite performance were then quantified using complementary statistical metrics: Mean Absolute Error (MAE) to evaluate absolute deviations, Pearson's correlation coefficient (r) to assess temporal co-variability, the coefficient of determination (r^2) to quantify explained variance, and Root Mean Square Error (RMSE) to penalize large discrepancies (Table 3.4).

Table 3.3: Central Pollution Control Board Sites with measurement data available from February 24 to June 30, 2020.

Madhya Pradesh: Mahakaleshwar Temple Ujjain, Suryakiran Bhawan NCL Singrauli, Sector-2 Industrial Area Pithampur, Sector-D Industrial Area Mandideep, Bhopal Chauraha Dewas, Bandhavgar Colony Satna Birla Cement, Shrivastav Colony Damoh, Shasthri Nagar Ratlam IPCA Lab, KJS Cements, T T Nagar Bhopal, Chhoti Gwaltoli Indore, Marhatal Jabalpur, Gole Bazar Katni, Deen Dayal Nagar Sagar, City Center Gwalior.

Maharashtra: Bandra Mumbai, More Chowk Waluj Aurangabad, Karve Road Pune, MIDC Khutala Chandrapur, Solapur Solapur, GPO Civil Lines Nagpur, Gangapur Road Nashik, Vasai West Mumbai, Nerul Navi Mumbai, Kurla Mumbai, Vile Parle West Mumbai, Chhatrapati Shivaji Intl. Airport (T2) Mumbai, Powai Mumbai, Borivali East Mumbai, Mahape Navi Mumbai, Worli Mumbai, Khadakpada Kalyan, Sion Mumbai, Colaba Mumbai.

New Delhi: CRRI Mathura Road, North Campus DU, IGI Airport (T3), Pusa, Aya Nagar, Lodhi Road, Shadipur, IHBAS Dilshad Garden, NSIT Dwarka, ITO Delhi, DTU Delhi, Sirifort, Mandir Marg, R K Puram, Punjabi Bagh, Anand Vihar, Ashok Vihar, Dr. Karni Singh Shooting Range, Dwarka Sector 8, Jahangirpuri, Jawaharlal Nehru Stadium, Major Dhyan Chand National Stadium, Narela, Najafgarh, Okhla Phase 2, Nehru Nagar, Rohini, Patparganj, Sonia Vihar, Wazirpur, Vivek Vihar, Bawana, Mundka, Sri Aurobindo Marg, Alipur.

Uttar Pradesh: Sector 62 Noida, Vasundhara Ghaziabad, Sector 125 Noida, Kendriya Vidyalaya Lucknow, Ardhali Bazar Varanasi, Nehru Nagar Kanpur, Lalbagh Lucknow, Talkatora District Industries Center Lucknow, Sanjay Palace Agra, Lajpat Nagar Moradabad, Knowledge Park III Greater Noida, Yamunapuram Bulandshahr, New Mandi Muzaffarnagar, Anand Vihar Hapur, Sanjay Nagar Ghaziabad, Indirapuram Ghaziabad, Loni Ghaziabad, Jai Bhim Nagar Meerut, Knowledge Park V Greater Noida, Sector 116 Noida, Sector 1 Noida, Gomti Nagar Lucknow, Pallavpuram Phase 2 Meerut, Ganga Nagar Meerut.

Odisha: Talcher Coalfields Talcher, GM Office Brajrajnagar. **Jharkhand:** Tata Stadium Jorapokhar. **Chandigarh:** Sector 25.

Bihar: IGSC Planetarium Complex Patna, Muzaffarpur Collectorate Muzaffarpur, Collectorate Gaya, Muradpur Patna, Rajbansi Nagar Patna, Samanpura Patna, Govt. High School Shikarpur Patna, DRM Office Danapur Patna, Industrial Area Hajipur, SFTI Kusdihra Gaya.

Telangana: Bollaram Industrial Area Hyderabad, ICRISAT Patancheru Hyderabad, IDA Pashamylaram Hyderabad, Sanathnagar Hyderabad.

West Bengal: Ghusuri Howrah, Rabindra Bharati University Kolkata, Victoria Kolkata, Padmapukur Howrah, Asansol Court Area Asansol, Ward 32 Bapupara Siliguri, Belur Math Howrah, Fort William Kolkata, Jadavpur Kolkata, Rabindra Sarobar Kolkata, Bidhannagar Kolkata, Ballygunge Kolkata.

Punjab: Punjab Agricultural University Ludhiana, RIMT University Mandi Gobindgarh, Golden Temple Amritsar, Model Town Patiala, Civil Line Jalandhar, Kalal Majra Khanna, Ratanpura Rupnagar Ambuja Cements, Hardev Nagar Bathinda.

Haryana: Vikas Sadan Gurugram, MD University Rohtak, Sector 6 Panchkula, Sector 16A Faridabad, NISE Gwal Pahari Gurugram, Sector 2 IMT Manesar, Murthal Sonipat, Sector 7 Kurukshetra, Municipal Corporation Office Dharuhera, Arya Nagar Bahadurgarh, Gobind Pura Yamuna Nagar, H.B. Colony Bhiwani, Sector 18 Panipat, Sector 12 Karnal, Shyam Nagar Palwal, F Block Sirsa, Patti Mehar Ambala, Shastri Nagar Narnaul, Huda Sector Fatehabad, General Hospital Mandikhera, Police Lines Jind, Urban Estate II Hisar, Nathu Colony Ballabgarh, Rishi Nagar Kaithal, Mini Secretariat Charkhi Dadri, New Industrial Town Faridabad, Sector 30 Faridabad, Sector 11 Faridabad, Teri Gram Gurugram, Sector 51 Gurugram.

Kerala: Plammoodu Thiruvananthapuram, Udyogamandal Eloor, Vyttila Kochi, Palayam Kozhikode, Kacheripady Ernakulam, Thavakkara Kannur, Kariavattom Thiruvananthapuram, Polayathode Kollam.

Andhra Pradesh: Tirumala Tirupati, Greater Visakhapatnam Municipal Corporation Visakhapatnam, Anand Kala Kshetram Rajamahendravaram, Secretariat Amaravati.

Tamil Nadu: Velachery_Res. Area Chennai, Alandur Bus Depot Chennai, Manali Chennai, Manali Village Chennai, SIDCO Kurichi Coimbatore.

Karnataka: BTM Layout Bengaluru, Peenya Bengaluru, BWSSB Kadabesanahalli Bengaluru, Deshpande Nagar Hubballi, Bapuji Nagar Bengaluru, Hebbal Bengaluru, Hombegowda Nagar Bengaluru, Jayanagar 5th Block Bengaluru, Chikkaballapur Rural Chikkaballapur, Silk Board Bengaluru, Lal Bahadur Shastri Nagar Kalaburagi, Hebbal 1st Stage Mysuru, Collector Office Yadgir, Vijay Nagar Ramanagara, Vidayagiri Bagalkot, Kalyana Nagara Chikkamagaluru, Vinoba Nagara Shivamogga, Ibrahimpur Vijayapura.

Rajasthan: Police Commissionerate Jaipur, Collectorate Jodhpur, Moti Doongri Alwar, RIICO Ind. Area III Bhiwadi, Civil Lines Ajmer, Adarsh Nagar Jaipur, Shrinath Puram Kota, Indira Colony Vistar Pali, Shastri Nagar Jaipur, Ashok Nagar Udaipur.

Gujarat: Maninagar Ahmedabad, GIDC Ankleshwar, Sector 10 Gandhinagar, Phase 4 GIDC Vatva, Phase 1 GIDC Vapi, Nandesari Industries Association.

3.2.3.1 Validation using CPCB measurements and MERRA-2 reanalysis

Across the five major geographical regions of India, the satellite-derived $PM_{2.5}$ dataset reproduced CPCB-observed variability with consistently high skill (Fig. 3.3). Region-wise Pearson correlation coefficients (r) ranged from 0.79 to 0.87, while RMSE values remained between 5.32 and 12.62 µg m^{-3}. Importantly, regression slopes were broadly comparable across regions, indicating that the satellite product captured not only temporal co-variability but also the relative magnitude of $PM_{2.5}$ variations across differing pollution regimes. When all regions were combined, the satellite-CPCB comparison yielded r = 0.86 and RMSE = 10.93 µg m^{-3}, demonstrating strong overall performance at the national scale.

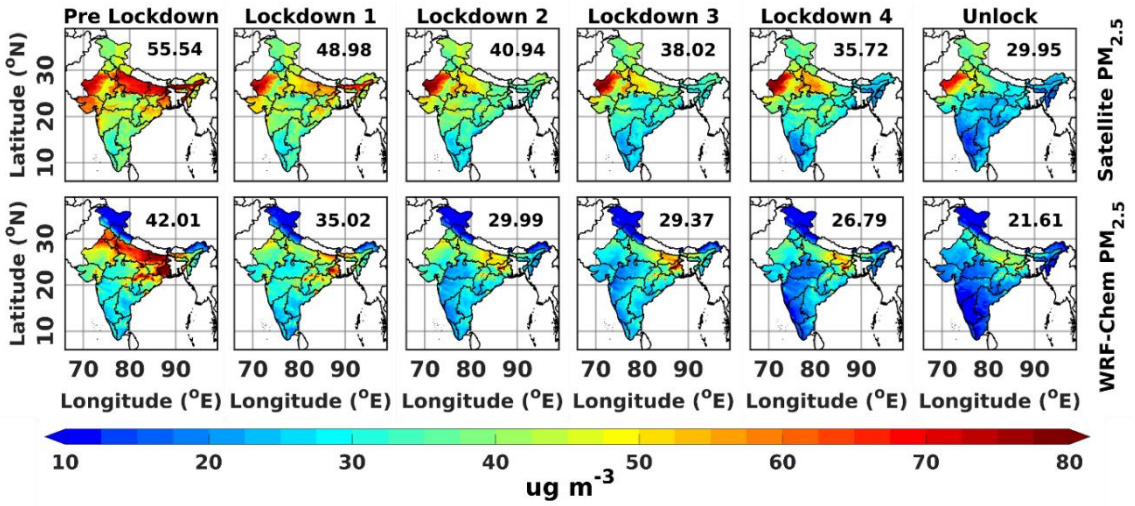


Figure 3.3: Spatial distribution of ambient $PM_{2.5}$ concentrations (µg m^{-3}) over India during the pre-lockdown, four lockdown phases, and unlock period, from satellite data (top) and WRF-Chem simulations (bottom).

When compared against MERRA-2 surface $PM_{2.5}$ for the entire country, the satellite dataset also showed robust agreement (r = 0.85; RMSE = 7.09 µg m^{-3}). The slightly lower RMSE in the satellite-MERRA-2 comparison relative to satellite-CPCB reflects the fact that both products represent spatially gridded fields and thus share smoother spatial variability than point-scale

station observations, which can capture strong hyper-local emission influences and micro-meteorological effects.

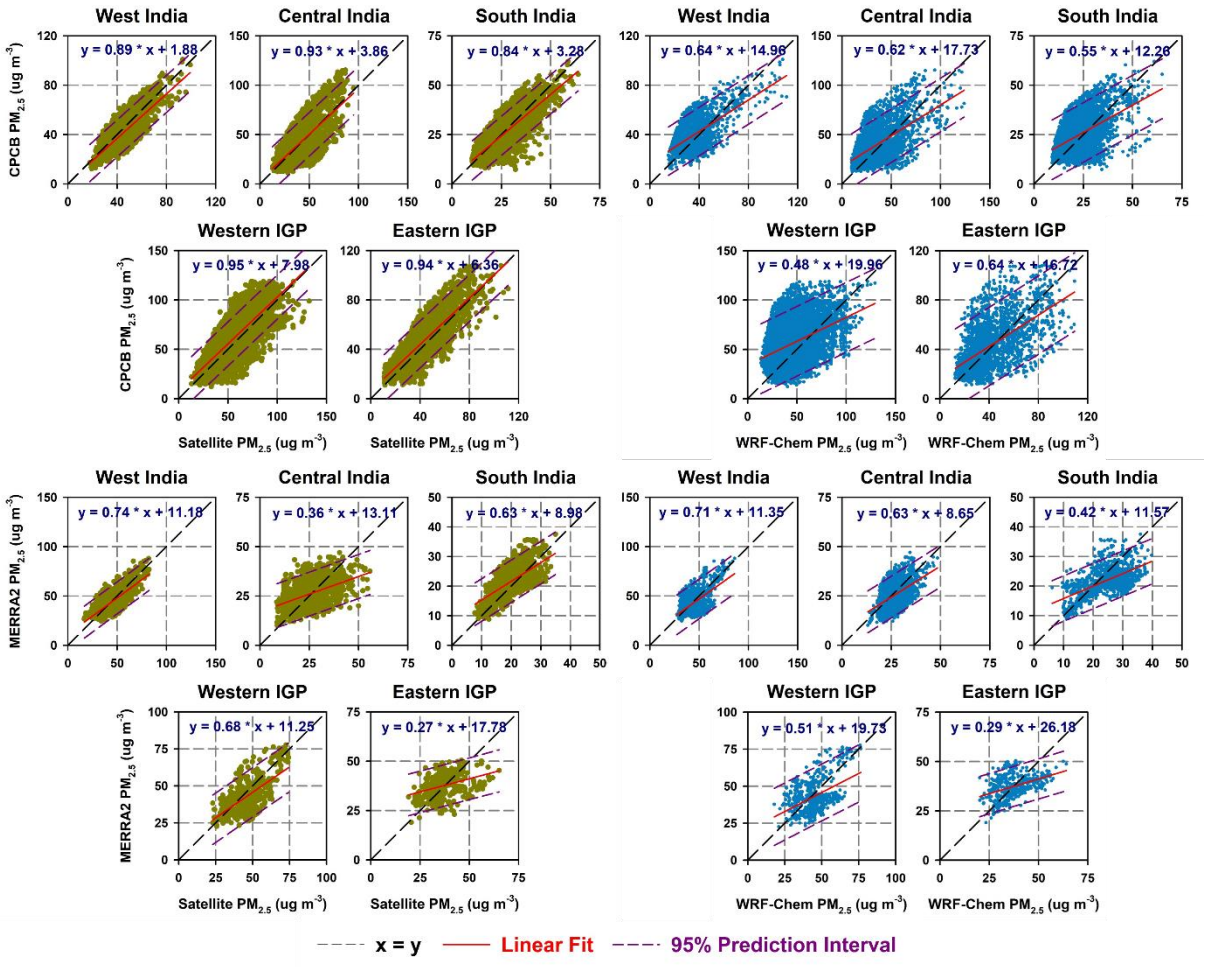


Figure 3.4: Comparison of 24-hour satellite-derived $PM_{2.5}$ and WRF-Chem simulated $PM_{2.5}$ concentrations against CPCB observations (top panel) from continuous monitoring stations and MERRA-2 surface $PM_{2.5}$ data (bottom panel) across various Indian regions (see Fig. 3.1). The regression statistics, including the slope-intercept form of the equation of a straight line, are explicitly displayed within the plot.

The WRF-Chem simulations exhibited moderate to good performance against CPCB observations across regions, with r values ranging from 0.51 to 0.73 and RMSE values between 8.58 and 17.65 µg m^{-3} (Fig. 3.4). However, agreement with MERRA-2 was comparatively weaker, particularly over the IGP region where r values were approximately 0.5 (Fig. 3.5). This reduced performance, especially toward the end of the study period, suggests that WRF-Chem had difficulty fully capturing processes that become increasingly influential during the late lockdown and unlock phases, most notably the contribution from wind-blown dust transport during the early monsoon transition.

Spatial distributions of surface $PM_{2.5}$ from satellite data, WRF-Chem simulations, and MERRA-2 reanalysis (Fig. 3.6 & 3.7) provide additional context for these performance differences by highlighting where and when the datasets diverge in their representation of regional gradients and hotspots. Detailed regression statistics quantifying these comparisons across regions and across lockdown/unlock phases are summarized in Table 3.4.

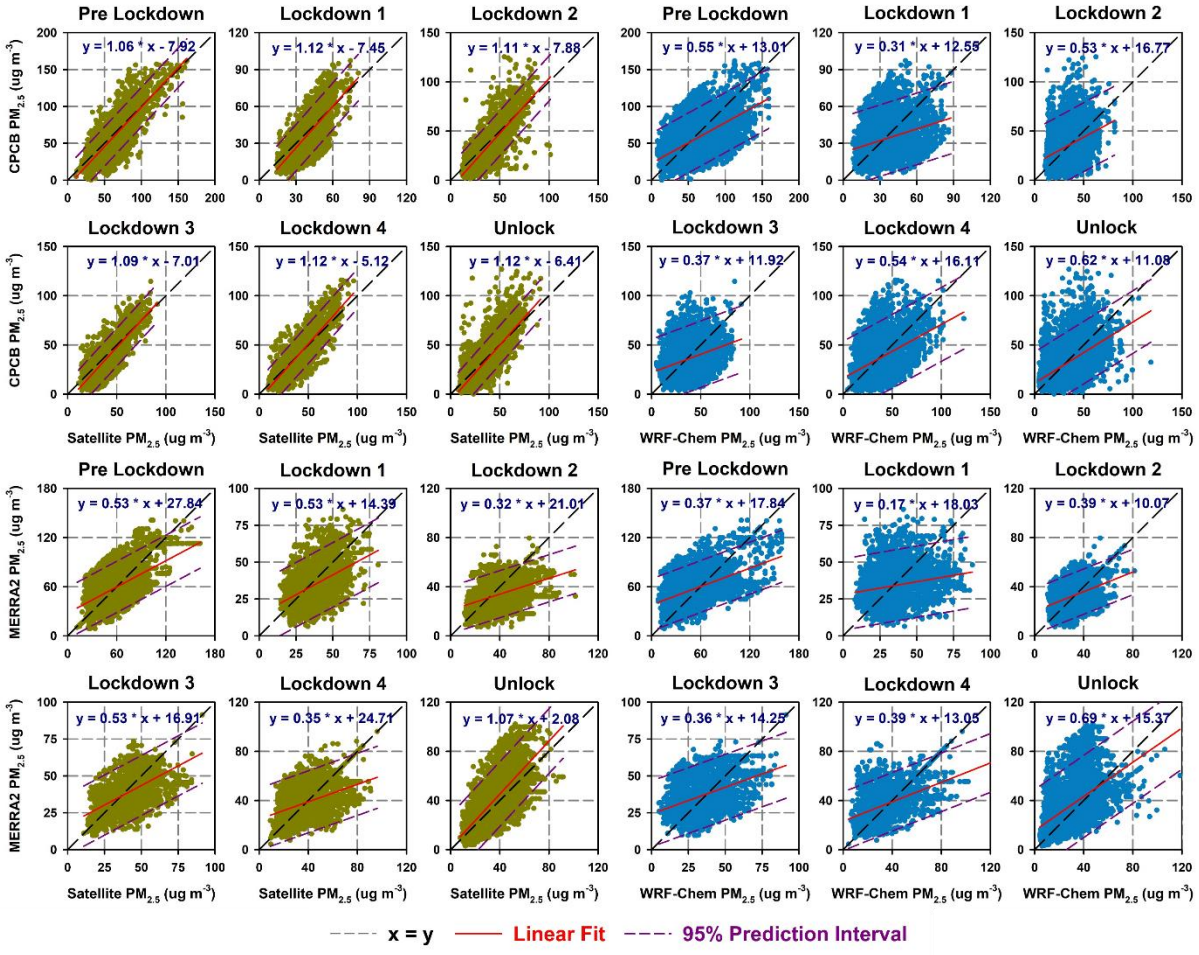


Figure 3.5: Comparison of 24-hour satellite-derived $PM_{2.5}$ and WRF-Chem simulated $PM_{2.5}$ concentrations against CPCB observations (top panel) from continuous monitoring stations and MERRA-2 surface $PM_{2.5}$ data (bottom panel) for the entire pre-lockdown to unlock period across India. The regression statistics, including the slope-intercept form of the equation of a straight line, are explicitly displayed within the plot.

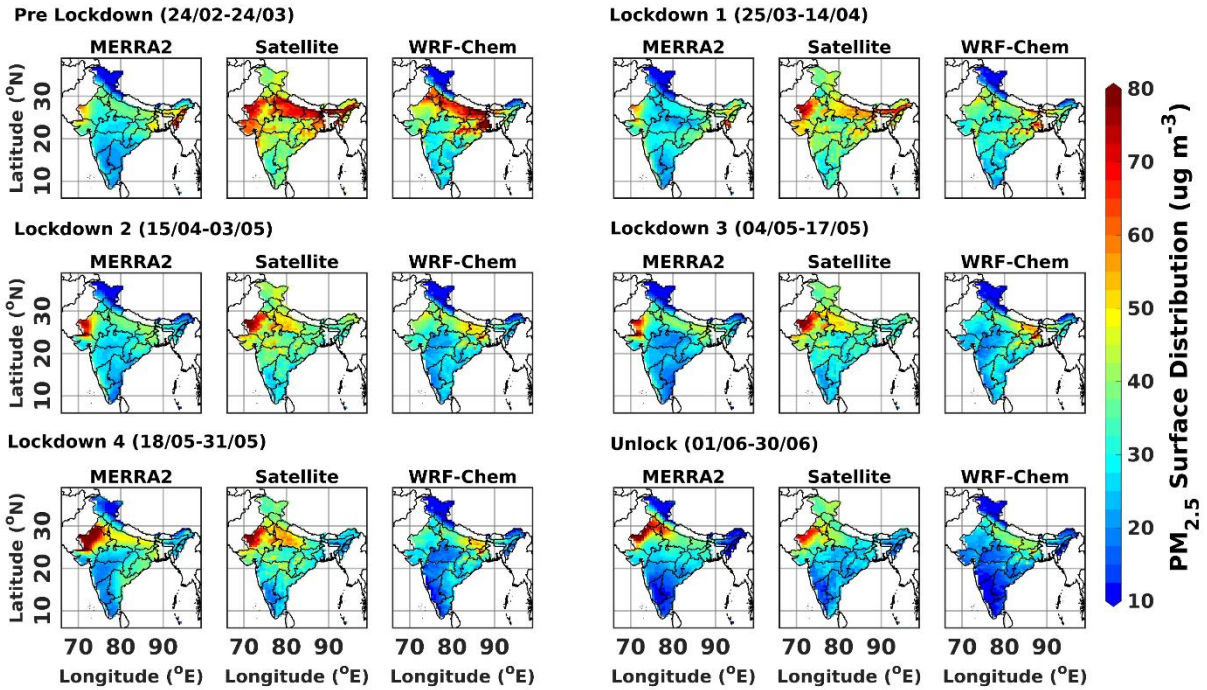


Figure 3.6: Spatial distribution of surface $PM_{2.5}$ concentrations over India during the pre-lockdown, four lockdown phases, and unlock period, based on satellite data, WRF-Chem simulations, and MERRA-2.

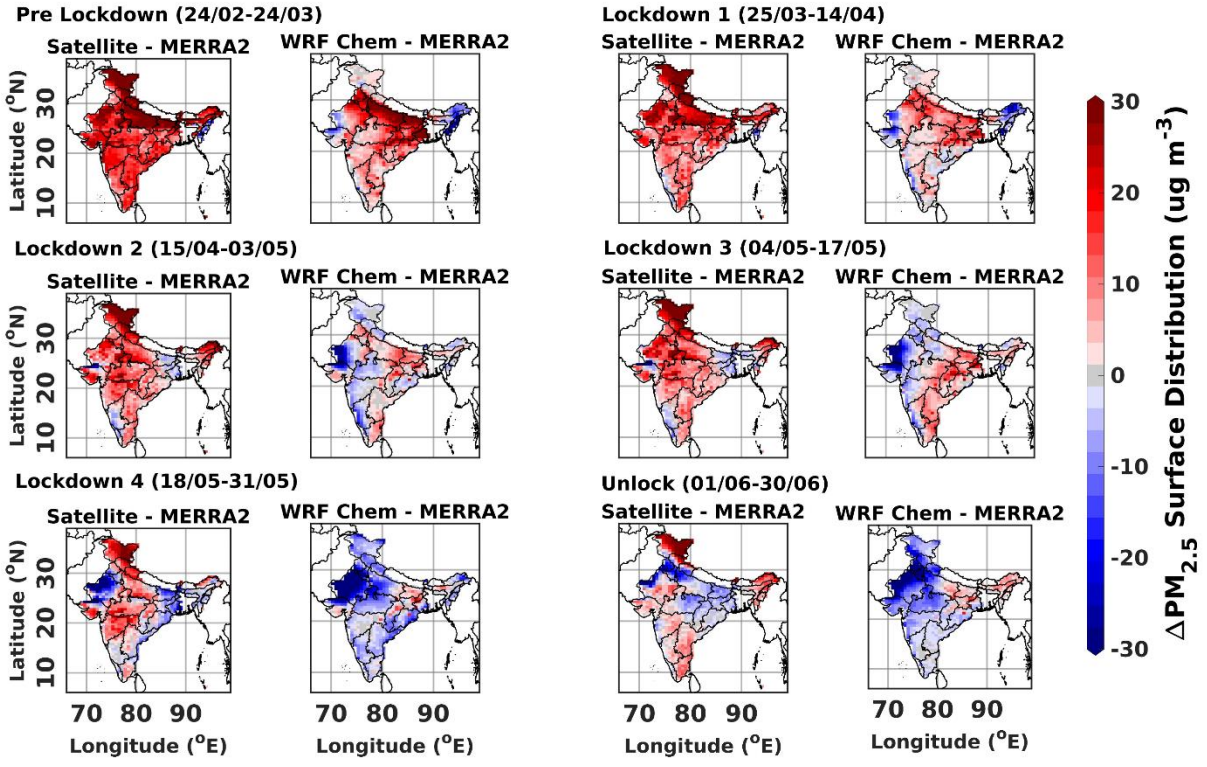


Figure 3.7: Differences in $PM_{2.5}$ concentrations across lockdown and unlock phases derived from satellite data, WRF-Chem simulations, and MERRA-2 reanalysis.

Table 3.4: Regression statistics comparing satellite-derived and WRF-Chem simulated $PM_{2.5}$ with CPCB and MERRA-2 surface $PM_{2.5}$ across the geographical regions shown in Fig. 3.1 and different phases of lockdown and unlock period.

		Satellite $PM_{2.5}$ vs CPCB $PM_{2.5}$				WRF-Chem $PM_{2.5}$ vs CPCB $PM_{2.5}$			
Region	**Count**	**MAE ($\mu g/m^3$)**	**r**	**r^2**	**RMSE ($\mu g/m^3$)**	**MAE ($\mu g/m^3$)**	**r**	**r^2**	**RMSE ($\mu g/m^3$)**
India	**25023**	**8.18**	**0.86**	**0.74**	**10.93**	**13.81**	**0.74**	**0.55**	**18.51**
WI	**1985**	**6.78**	**0.87**	**0.76**	**8.46**	**9.53**	**0.73**	**0.53**	**11.91**
CI	**4190**	**8.47**	**0.79**	**0.62**	**11.36**	**12.60**	**0.71**	**0.50**	**13.14**
SI	**4317**	**4.04**	**0.82**	**0.67**	**5.32**	**6.81**	**0.69**	**0.48**	**8.58**
WIGP	**11965**	**8.79**	**0.81**	**0.66**	**12.62**	**9.69**	**0.51**	**0.24**	**16.59**
EIGP	**2566**	**8.35**	**0.87**	**0.76**	**10.54**	**13.07**	**0.63**	**0.40**	**17.65**
		Satellite $PM_{2.5}$ vs MERRA2 $PM_{2.5}$				**WRF-Chem $PM_{2.5}$ vs MERRA2 $PM_{2.5}$**			
India	**5334**	**5.55**	**0.85**	**0.72**	**7.09**	**6.69**	**0.81**	**0.66**	**8.50**
WI	**852**	**7.52**	**0.77**	**0.59**	**8.97**	**8.65**	**0.63**	**0.40**	**9.86**
CI	**1542**	**4.73**	**0.73**	**0.53**	**5.91**	**5.81**	**0.69**	**0.48**	**7.30**
SI	**991**	**3.57**	**0.75**	**0.56**	**4.33**	**4.88**	**0.75**	**0.56**	**6.11**
WIGP	**564**	**7.82**	**0.71**	**0.50**	**8.64**	**9.49**	**0.48**	**0.34**	**9.15**
EIGP	**402**	**6.23**	**0.61**	**0.37**	**6.91**	**6.46**	**0.46**	**0.31**	**7.83**

		Satellite $PM_{2.5}$ vs CPCB $PM_{2.5}$				WRF-Chem $PM_{2.5}$ vs CPCB $PM_{2.5}$			
Period	**Count**	**MAE ($\mu g/m^3$)**	**r**	**r^2**	**RMSE ($\mu g/m^3$)**	**MAE ($\mu g/m^3$)**	**r**	**r^2**	**RMSE ($\mu g/m^3$)**
Pre Lockdown	**5957**	**9.56**	**0.85**	**0.72**	**14.26**	**11.85**	**0.66**	**0.44**	**14.53**
Lockdown 1	**3859**	**7.86**	**0.79**	**0.62**	**10.16**	**13.93**	**0.57**	**0.32**	**18.20**
Lockdown 2	**3523**	**8.90**	**0.79**	**0.62**	**12.28**	**12.10**	**0.62**	**0.38**	**16.87**
Lockdown 3	**2621**	**7.96**	**0.84**	**0.71**	**10.47**	**9.67**	**0.58**	**0.34**	**12.19**
Lockdown 4	**2664**	**7.49**	**0.88**	**0.77**	**10.43**	**12.03**	**0.61**	**0.37**	**13.92**
Unlock	**5817**	**7.48**	**0.85**	**0.72**	**10.45**	**13.19**	**0.62**	**0.38**	**14.52**
		Satellite $PM_{2.5}$ vs MERRA2 $PM_{2.5}$				**WRF-Chem $PM_{2.5}$ vs MERRA2 $PM_{2.5}$**			
Pre Lockdown	**6259**	**8.87**	**0.65**	**0.42**	**14.76**	**19.89**	**0.58**	**0.34**	**14.61**
Lockdown 1	**3948**	**9.90**	**0.58**	**0.34**	**12.50**	**14.13**	**0.53**	**0.28**	**17.69**
Lockdown 2	**3832**	**10.99**	**0.59**	**0.35**	**14.40**	**9.65**	**0.61**	**0.37**	**12.23**
Lockdown 3	**2847**	**9.24**	**0.63**	**0.40**	**13.41**	**12.18**	**0.62**	**0.38**	**15.51**
Lockdown 4	**2945**	**11.44**	**0.61**	**0.37**	**15.93**	**12.25**	**0.59**	**0.35**	**16.59**
Unlock	**6147**	**10.52**	**0.62**	**0.38**	**14.28**	**13.72**	**0.57**	**0.32**	**18.49**

Time-series evaluation at the state scale further supports these findings (Fig. 3.8). The satellite-derived $PM_{2.5}$ time series captured day-to-day and phase-wise variations observed in CPCB measurements and MERRA-2 throughout the analysis period. In contrast, WRF-Chem simulations substantially underestimated $PM_{2.5}$ during the final two lockdown phases and the

unlock period across many states, even though the model reproduced the initial concentration decline associated with the onset of lockdown restrictions. This behaviour indicates that while the model responded appropriately to imposed emission reductions, it did not fully represent the evolving background aerosol burden later in the season, consistent with underestimated dust contributions and possible biases in boundary-layer ventilation and regional transport.

A key limitation affecting anthropogenic aerosol loading in the modelling framework is the reliance on the EDGAR-v6.1 emission inventory, which is based on 2018 activity data and is therefore two years older than the 2020 study period. Given the rapid economic growth and industrial and mobility changes across South Asia during that interval, the use of an older inventory likely contributed to systematic underestimation of $PM_{2.5}$ concentrations in the regional model simulations.

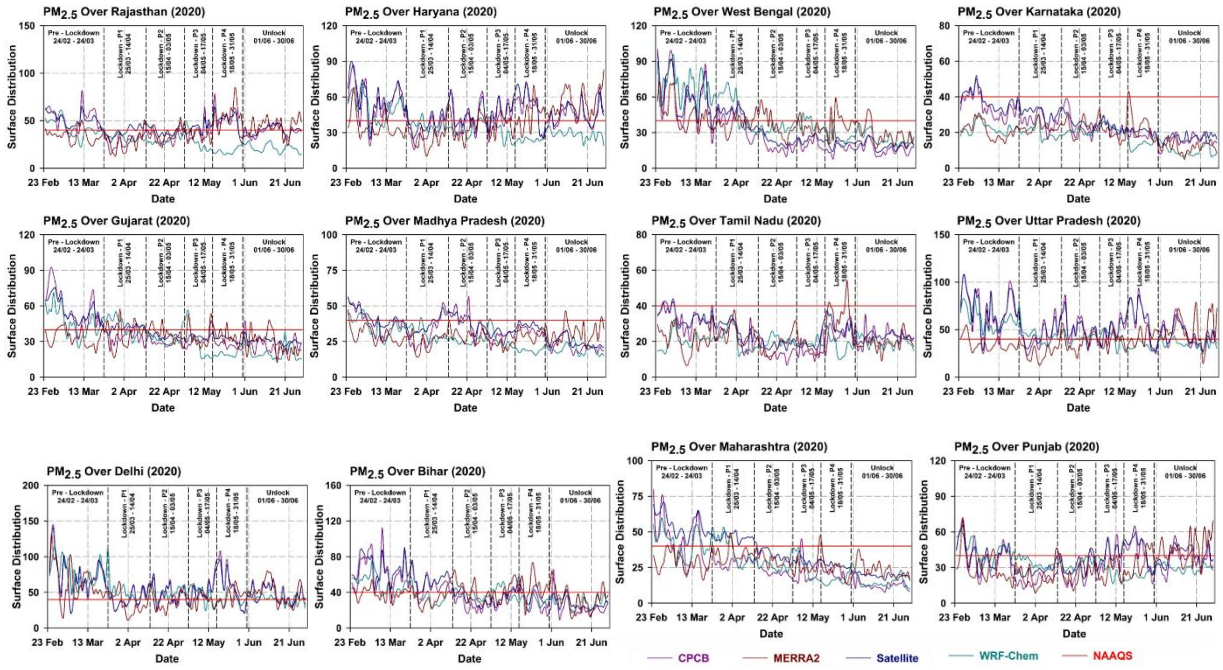


Figure 3.8: Daily mean time-series comparison of surface $PM_{2.5}$ concentrations (µg m^{-3}) from the pre-lockdown to unlock period in 2020 for Delhi, Bihar, Rajasthan, Haryana, Gujarat, Madhya Pradesh, West Bengal, Karnataka, Tamil Nadu, Uttar Pradesh, Maharashtra, and Punjab.

The analysis also indicates several additional sources of discrepancy that can influence WRF-Chem performance, including uncertainties in near-surface winds and wind direction, boundary-layer height, temperature, and humidity, each of which directly affects pollutant ventilation, mixing, and secondary aerosol formation. Likewise, uncertainties in chemical processes such as photolysis, secondary aerosol production, and wet/dry deposition can further modulate model–observation differences. Although the WRF-Chem configuration adopted here

was extensively evaluated across multiple physical and chemical parameterizations (Chapter 2), these factors remain intrinsic sources of uncertainty for regional $PM_{2.5}$ modelling over India. Finally, accurate representation of emissions, including their diurnal cycles and seasonal evolution, remains critical for reproducing both absolute $PM_{2.5}$ levels and the timing of changes during rapidly evolving conditions such as the lockdown.

To disentangle meteorology-driven $PM_{2.5}$ variability from changes induced by restricted anthropogenic activity, we adopted a dual attribution strategy based on both WRF-Chem simulations and satellite-derived $PM_{2.5}$ fields. This combined approach is particularly important over India, where emission inventory uncertainties and the seasonally varying contribution of natural aerosols, especially dust transported from arid regions, can complicate attribution (Goswami et al., 2012; Vadrevu et al., 2011). Satellite observations provide spatially continuous estimates of total particulate loading but cannot directly isolate sectoral emission changes. In contrast, model simulations explicitly represent changes in emissions and thus allow the observed variability to be attributed to activity restrictions, once the influence of meteorological conditions has been carefully accounted. By integrating model-based and satellite-based assessments, we reduce dependence on any single dataset and mitigate the limitations inherent to each. This combined framework provides a more robust and nuanced understanding of how meteorology and emission changes jointly shaped $PM_{2.5}$ concentrations during an exceptional period of enforced emission reductions. A key component of this framework is the use of the 2015-2019 average as a reference for meteorology-driven variability, which is examined and justified in the following subsection.

3.2.3.2 Analysis for using the 2015-2019 Average to Estimate Meteorology-Driven Variability in 2020

Our attribution framework quantifies the total $PM_{2.5}$ change in 2020 based on differences between lockdown (and unlock) phases and the pre-lockdown reference period and then compares this with analogous phase-wise differences averaged over 2015-2019. The objective is to isolate the portion of the 2020 change that is attributable to activity restrictions, under the assumption that meteorological conditions in 2020 were not anomalous relative to the distribution captured over the preceding five years.

To rigorously test this assumption, we conducted an extensive analysis of key meteorological drivers of $PM_{2.5}$ variability using ERA5 reanalysis, including 2-m air temperature,

surface temperature, boundary-layer height, 10-m wind speed, specific humidity, relative humidity, and total cloud cover. Across most of India and throughout the analysis window (24 February-30 June), the 2020 values for each meteorological variable remained within ±1σ of the corresponding 2015-2019 distributions, indicating that 2020 did not represent a meteorologically exceptional year that could systematically bias the inferred emission contribution. Quantitatively, differences between 2020 and the 2015-2019 mean ranged from -0.7°C to +2°C for 2-m air temperature and from approximately -1.2°C to +2°C for surface temperature. Near-surface wind speed differences were within approximately -0.8 to +1.0 m s^{-1}, while boundary-layer height differences fell within -50 to +90 m. Importantly, no abrupt shifts in circulation regimes, boundary-layer behaviour, or moisture evolution were detected during pre-lockdown, the four lockdown phases, or the unlock period that would invalidate the use of the multi-year mean as a representative meteorological reference.

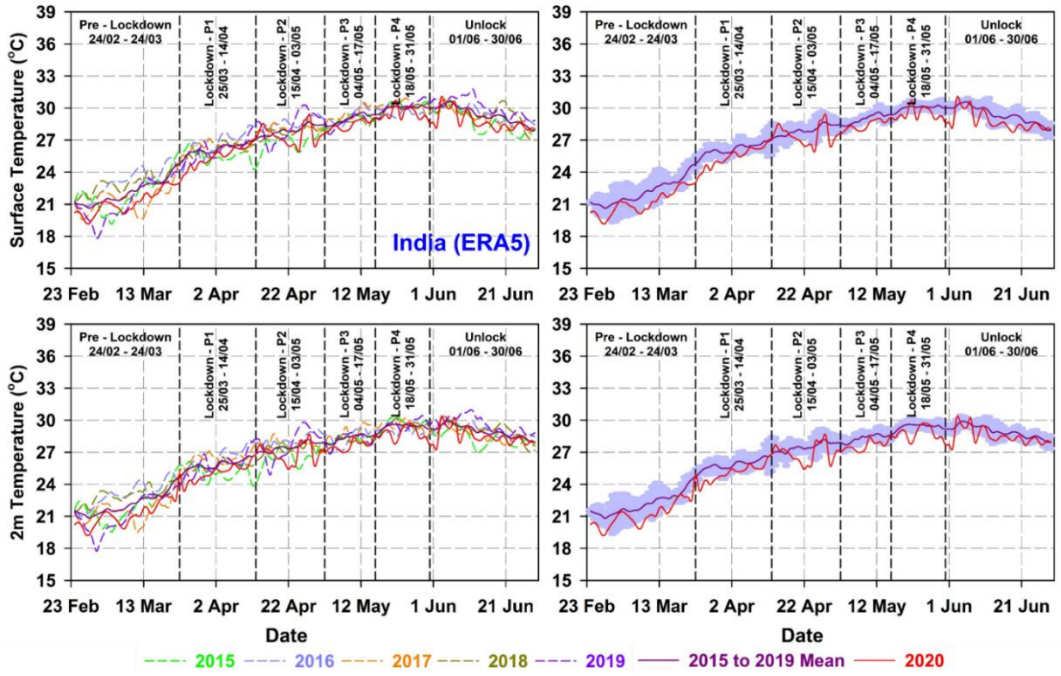


Figure 3.9: Daily mean time-series comparison of surface temperature (top) and 2-meter air temperature (bottom) from the pre-lockdown to unlock period in 2020 over the entire Indian region, based on ERA5 reanalysis data. The left panels show the comparison for individual years from 2015 to 2020 along with the 2015-2019 multi-year mean. The right panels compare the 2020 time series with the 2015-2019 mean. The shaded area represents ±1σ of the 2015-2019 multi-year mean.

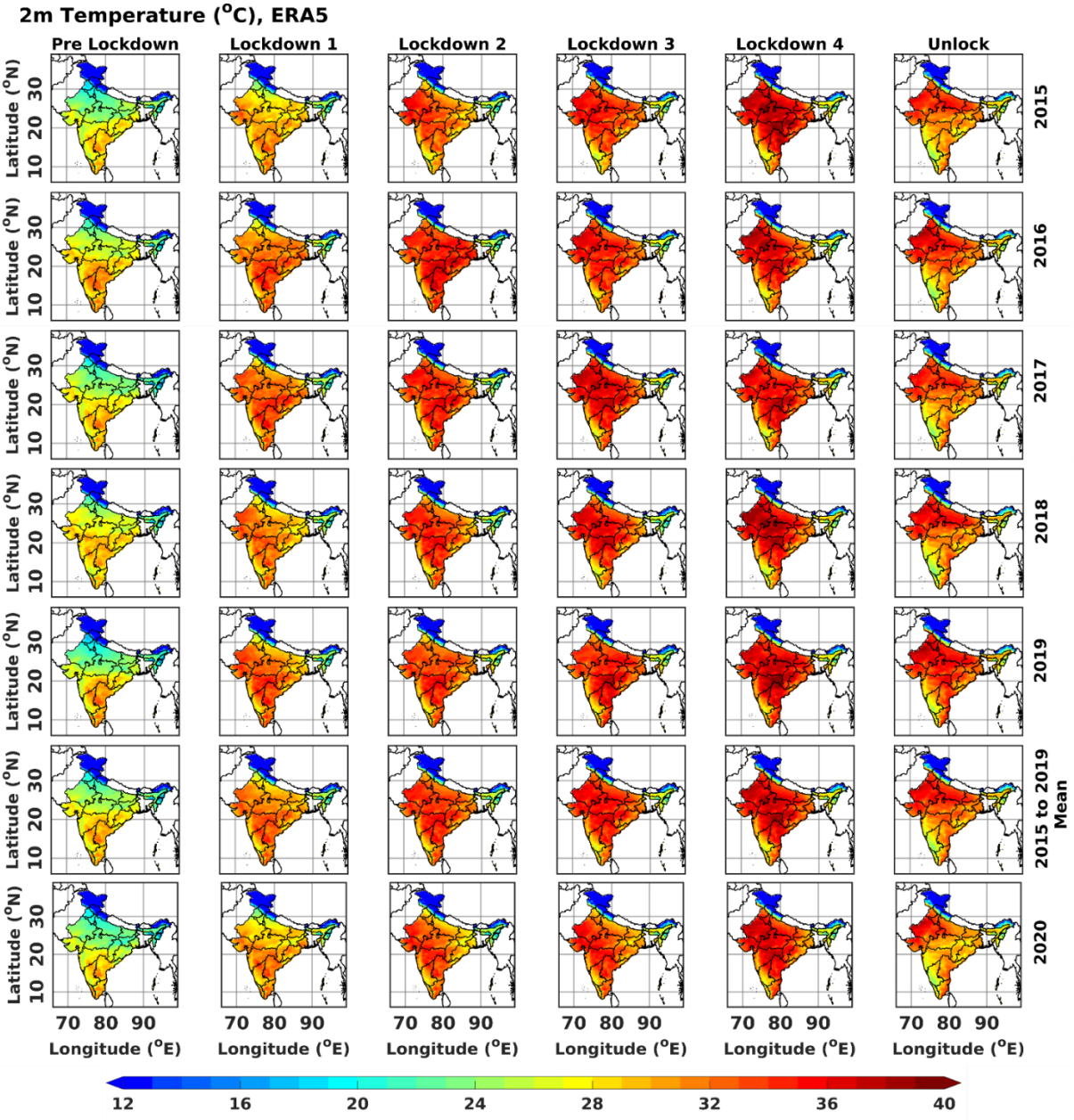


Figure 3.10: Spatial distribution of 2-meter air temperature over India during the pre-lockdown period, four lockdown phases, and the unlock period, based on individual years from 2015 to 2020, along with the 2015-2019 multi-year mean.

In addition, all WRF-Chem simulations were forced consistently using ERA5 meteorological fields and were constrained by grid nudging above the planetary boundary layer (nudging coefficient = 0.0005 s^{-1}). This ensured that large-scale circulation features remained comparable across all simulated years, further reducing the likelihood that differences between 2020 and the reference period arise from inconsistent meteorological forcing rather than genuine interannual variability.

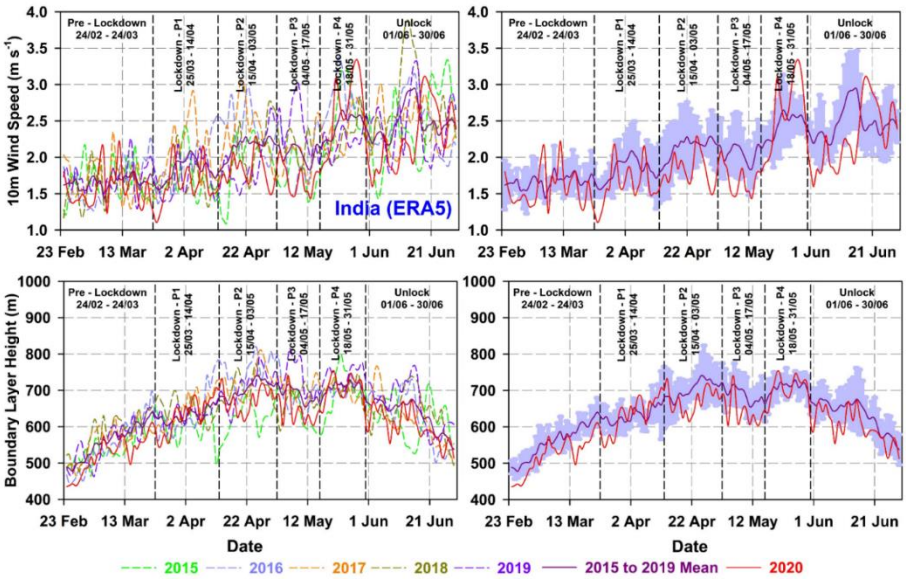


Figure 3.11: Daily mean time-series comparison of 10-meter wind speed (top) and boundary layer height (bottom) from the pre-lockdown to unlock period in 2020 over the entire Indian region, based on ERA5 reanalysis data. The left panels show the comparison for individual years from 2015 to 2020 along with the 2015-2019 multi-year mean. The right panels compare the 2020 time series with the 2015-2019 mean. The shaded area represents ±1σ of the 2015-2019 multi-year mean.

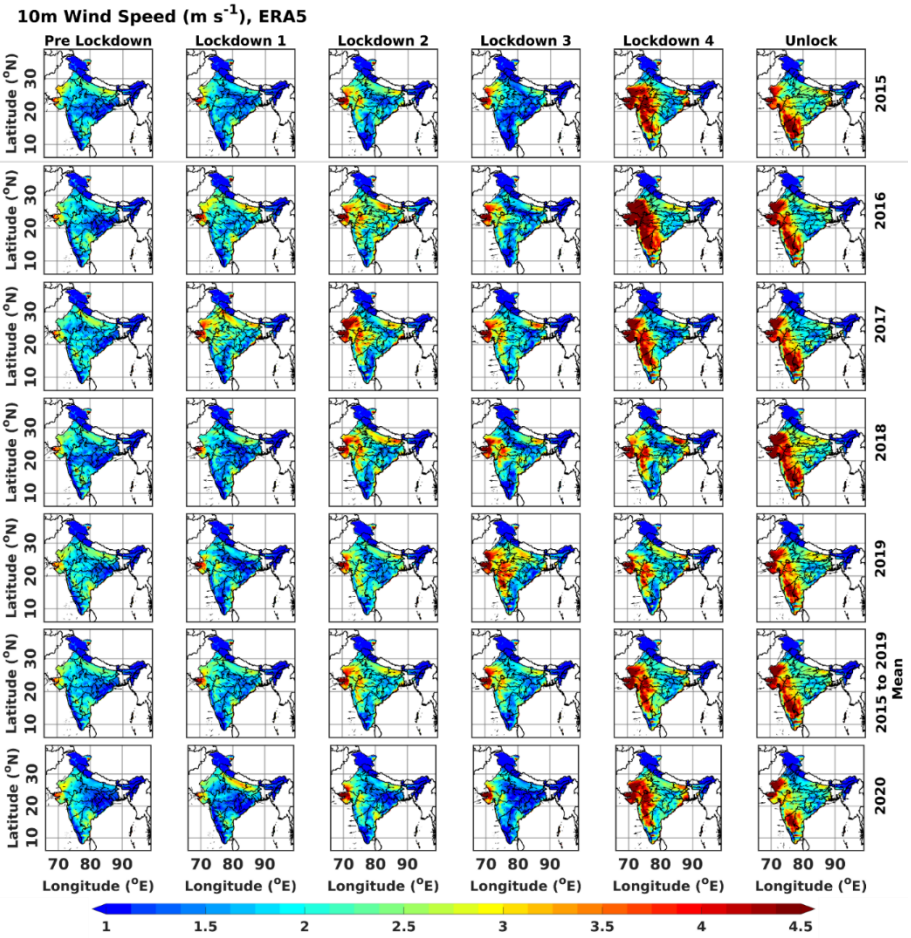


Figure 3.12: Spatial distribution of 10-meter wind speed over India during the pre-lockdown period, four lockdown phases, and the unlock period, based on individual years from 2015 to 2020, along with the 2015-2019 multi-year mean.

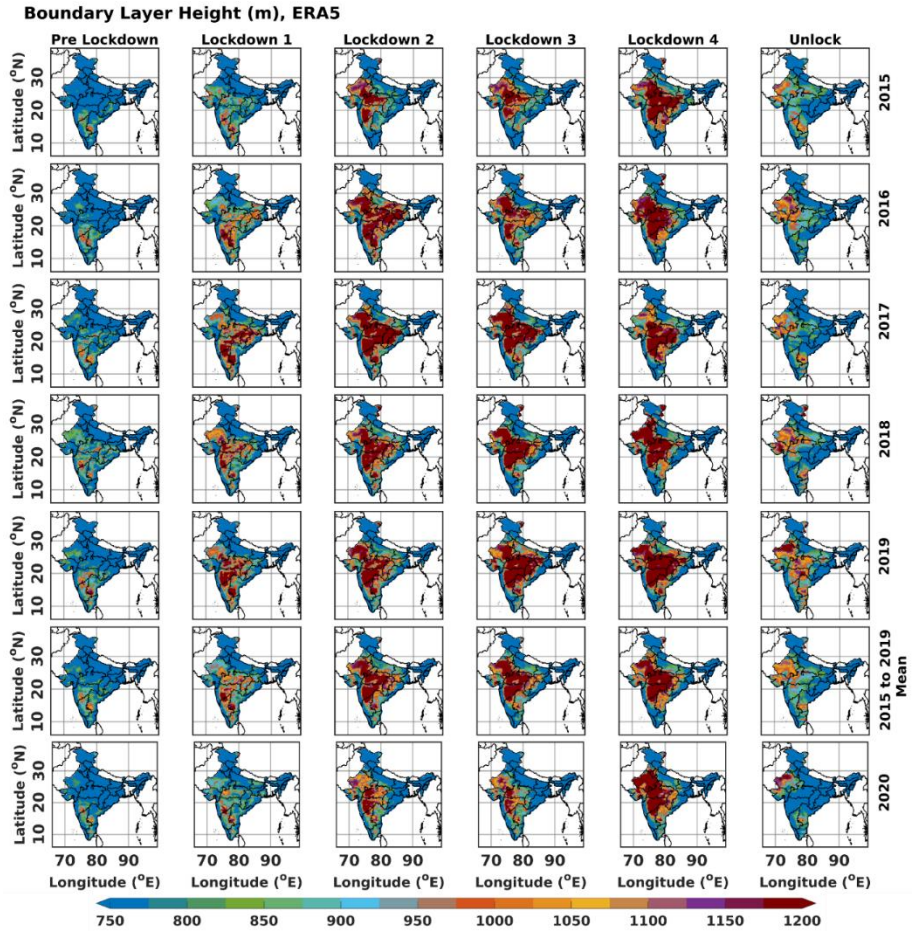


Figure 3.13: Spatial distribution of boundary layer height over India during the pre-lockdown period, four lockdown phases, and the unlock period, based on individual years from 2015 to 2020, along with the 2015-2019 multi-year mean.

Time-series and spatial comparison plots for temperature (Fig. 3.9 & 3.10), wind speed and boundary-layer height (Fig. 3.11 to 3.13), and humidity and cloud cover (Fig. 3.14 & 3.15) collectively demonstrate that 2020 meteorology remained broadly consistent with the 2015-2019 climatological envelope. Since boundary-layer height and near-surface winds strongly regulate ventilation and stagnation, particularly over the IGP, this consistency is especially important for ensuring that the attribution of $PM_{2.5}$ changes to activity restrictions is not confounded by unusual meteorological anomalies.

Overall, the ERA5-based assessment provides strong, independent support for the central assumption of the attribution framework: meteorological conditions during 2020 were well within the range of interannual variability represented by 2015-2019. This strengthens confidence in using the multi-year mean differences as a robust estimate of meteorology-driven variability and thereby supports the credibility of the emission-attribution results presented in this chapter.

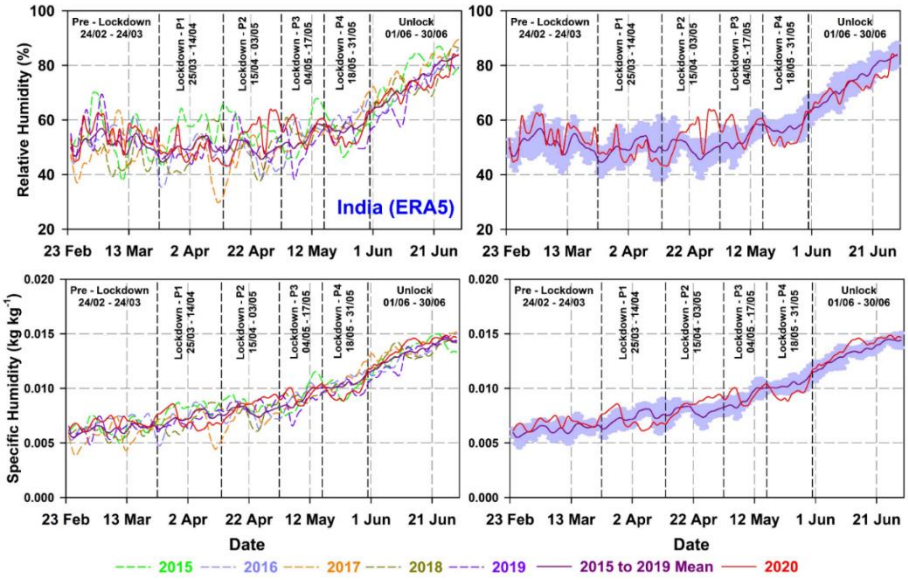


Figure 3.14: Daily mean time-series comparison of relative humidity (top) and specific humidity (bottom) from the pre-lockdown to unlock period in 2020 over the entire Indian region, based on ERA5 reanalysis data. The left panels show the comparison for individual years from 2015 to 2020 along with the 2015-2019 multi-year mean. The right panels compare the 2020 time series with the 2015-2019 mean. The shaded area represents ±1σ of the 2015-2019 multi-year mean.

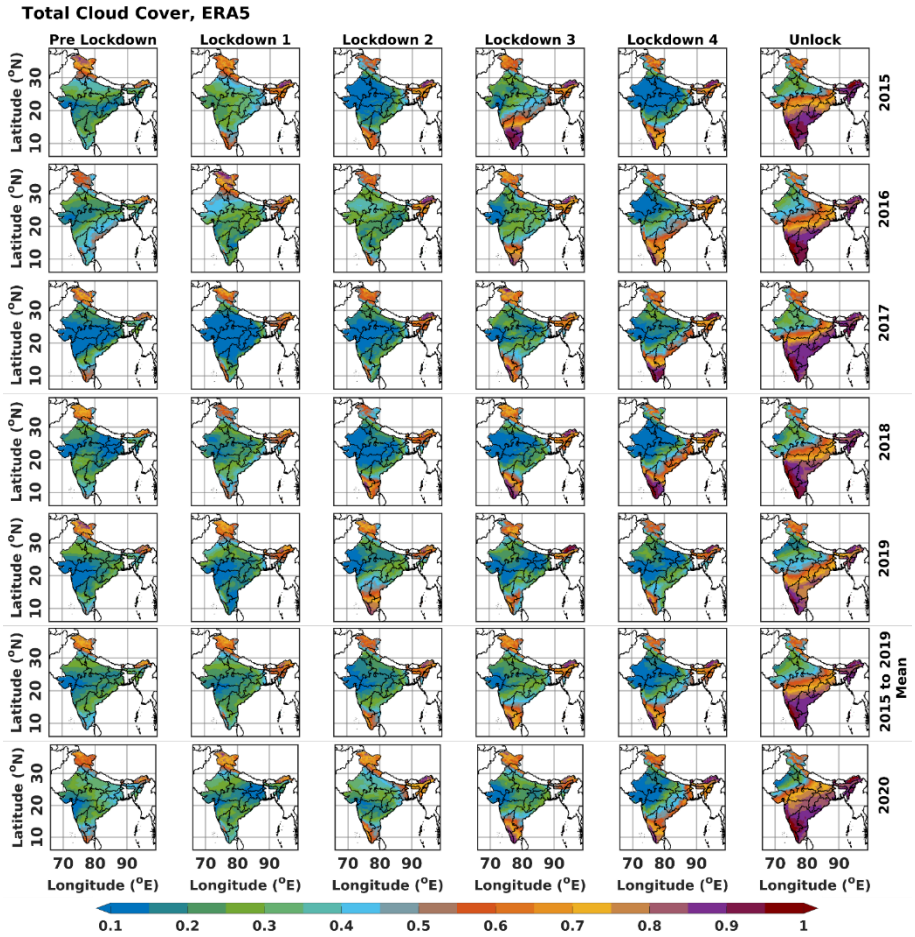


Figure 3.15: Spatial distribution of total cloud cover over India during the pre-lockdown period, four lockdown phases, and the unlock period, based on individual years from 2015 to 2020, along with the 2015-2019 multi-year mean.

The time series and spatial comparison analysis of specific humidity, relative humidity, and total cloud cover over the Indian region further support our assumption that the multi-year average can be used as a representative reference for the meteorological conditions of 2020. These results provide strong evidence supporting the robustness of our original assumption.

3.3 Results and Discussion

3.3.1 Pre-Lockdown Conditions and Initial Lockdown-Driven Changes

Prior to the COVID-19 lockdown, ambient $PM_{2.5}$ exposure across India remained persistently high, with regional mean concentrations frequently exceeding the National Ambient Air Quality Standards (NAAQS) annual threshold of 40 μg m^{-3} (Balakrishnan et al., 2019). During the pre-lockdown window (24 February-24 March 2020), satellite-derived $PM_{2.5}$ indicates that exceedances were widespread across most of the country, with lower values largely confined to high-altitude and complex-terrain regions where reduced local emissions, enhanced ventilation, and lower boundary-layer aerosol loading typically suppress near-surface $PM_{2.5}$ (Fig. 3.3). The Indo-Gangetic Plain (IGP) stands out as the most severely impacted region, consistent with its long-recognized status as one of the most polluted and population-dense corridors in the Indian subcontinent. The satellite-derived pre-lockdown mean $PM_{2.5}$ reached 63.14 μg m^{-3} over the Eastern IGP (EIGP) and 61.52 μg m^{-3} over the Western IGP (WIGP). WRF-Chem simulated comparable magnitudes, 66.77 μg m^{-3} over EIGP and 63.10 μg m^{-3} over WIGP, suggesting that the model captured the broad spatial contrast between the IGP and other regions during late-winter to early pre-monsoon transition conditions (Table 3.5).

Table 3.5: Population-weighted ambient $PM_{2.5}$ concentrations (μg m^{-3}) across India and its seven geographical regions during the entire study period in 2020 (μ±1σ) (Values are pixel means).

Satellite $PM_{2.5}$ WRF-Chem $PM_{2.5}$						
Region	**Pre Lockdown (μ±1σ)**	**Lockdown 1**	**Lockdown 2**	**Lockdown 3**	**Lockdown 4**	**Unlock**
India	55.54±5.27 42.01±10.33	48.98±4.98 35.02±6.82	40.94±4.98 29.99±6.40	38.02±4.77 29.37±6.34	35.72±5.81 26.80±6.50	29.95±5.18 21.61±5.50
NI	43.33±3.15 12.07±5.80	41.34±2.84 12.20±3.94	42.29±3.18 8.76±3.85	39.40±2.74 6.55±3.29	37.97±2.59 8.26±3.07	38.12±2.67 6.94±4.77
NEI	55.82±9.48 30.21±7.29	50.67±7.26 29.78±5.60	36.83±2.95 20.29±4.37	33.14±3.43 24.21±5.32	26.35±2.43 19.53±4.01	24.32±3.00 15.94±3.08
CI	47.46±4.84 41.46±7.54	42.17±4.17 36.56±4.95	38.09±3.92 28.14±4.56	33.01±3.72 27.48±4.89	34.17±4.08 23.35±4.88	24.93±2.46 20.57±4.08
SI	39.74±3.13 31.33±4.92	35.13±3.22 30.02±4.20	29.70±3.08 24.92±3.51	26.73±2.71 25.59±3.73	27.70±3.93 21.93±4.54	20.78±3.75 15.28±2.65
WI	59.66±6.27 45.92±4.83	52.64±7.33 36.71±4.12	53.51±7.48 37.34±2.88	51.85±7.37 28.38±2.56	51.96±7.20 31.56±2.85	44.40±5.49 23.74±2.46
EIGP	63.14±5.55 66.77±14.21	52.55±5.13 47.97±9.52	36.79±2.86 43.02±8.08	35.69±3.15 45.74±9.13	31.90±3.75 41.42±8.32	26.87±2.36 35.14±5.98
WIGP	61.52±4.24 63.10±9.00	46.63±4.45 40.94±5.87	45.14±3.37 41.86±5.36	46.44±4.48 36.59±5.56	48.92±4.06 28.87±6.08	38.04±3.41 36.31±5.75

Outside the IGP, satellite data show the lowest pre-lockdown exposure over South India (39.74 μg m^{-3}), while WRF-Chem suggests the lowest values over North India (12.07 μg m^{-3}). At the all-India scale, satellite $PM_{2.5}$ averages 55.54 μg m^{-3}, whereas WRF-Chem yields 42.01 μg m^{-3}. This offset is informative in itself: the lower modelled national mean likely reflects (i) limitations in representing wind-blown dust contributions during the pre-monsoon period and/or (ii) biases associated with baseline anthropogenic emissions used for the simulations, which may under-represent rapidly evolving activity patterns in parts of India. Importantly, however, both datasets identify the same first-order structure: a high-$PM_{2.5}$ IGP core and relatively lower burdens over peninsular India (Fig. 3.3; Table 3.5).

Table 3.5 summarizes the phase-wise evolution of population-weighted $PM_{2.5}$ over India and its seven geographical regions. The pre-lockdown spatial pattern and the subsequent phase-wise changes must be interpreted as the combined outcome of (a) strong regional contrasts in emissions (industry, transport, residential fuel combustion, and open burning), (b) seasonal evolution in meteorology and boundary-layer mixing during February-June, and (c) variations in episodic sources such as biomass burning and dust transport. Even before any lockdown restrictions, the persistence of high $PM_{2.5}$ over the IGP indicates that the baseline is anchored not only by urban-industrial activity but also by diffuse and hard-to-control sources such as household solid-fuel combustion and agricultural residue burning, which have broad spatial footprints and can sustain elevated regional background concentrations. The nationwide lockdown that began on 25 March 2020 abruptly altered this baseline state. Stringent restrictions on transportation, industrial activity, construction, and public gatherings were implemented to curb virus transmission (Kumar et al., 2020; Sharma et al., 2020; Zhang et al., 2021). This created an unprecedented, rapid emission perturbation that, unlike planned interventions, occurred nearly simultaneously across multiple sectors, offering a rare opportunity to evaluate the sensitivity of $PM_{2.5}$ to sudden emission changes against the backdrop of evolving pre-monsoon meteorology.

Early assessments, many based on city-focused CPCB networks, reported striking improvements in air quality during the strict lockdown period (Jain et al., 2020; Mahato et al., 2020; Singh et al., 2020). These studies captured large reductions in urban $PM_{2.5}$ and co-emitted gases such as NO_2 and CO, consistent with reduced road traffic and curtailed industrial activity. However, city-scale analyses can over-emphasize the response of locally dominated emission sectors and may not represent the regional background that is influenced by household emissions, open burning, and transported aerosols. Moreover, many early studies did not extend through the unlock period, and they often did not explicitly isolate meteorological influences (e.g., ventilation changes, boundary-layer height evolution, synoptic wind shifts) from emission-driven responses.

By integrating satellite-derived $PM_{2.5}$ with WRF-Chem simulations and explicitly considering both lockdown and unlock phases, this work provides a more spatially comprehensive and temporally continuous view of how $PM_{2.5}$ evolved across India under an extraordinary, multi-sector emission disruption.

3.3.2 Quantifying the Relative Contributions of Emission Reductions and Meteorological Variations

To quantify the drivers of $PM_{2.5}$ changes during 2020, we compared each lockdown phase (25 March-31 May 2020) and the unlock period (1-30 June 2020) against pre-lockdown conditions and separated the contributions of activity-restricted emission reductions from meteorology-induced variability using the subtraction framework (Table 3.2). The emission inventory analysis indicates that reductions were strongly sector dependent. The largest decreases occurred in transport and public activity sectors, reaching up to 61.25% during Lockdown Phase 1 (Fig. 3.16), consistent with suppressed mobility and curtailed commercial operations. Industrial emissions also declined substantially, though the magnitude of reduction diminished as restrictions were progressively relaxed. In contrast, residential emissions increased by 20.67% during Phase 1 and remained elevated (10.25%) even during the unlock phase (Fig. 3.16), plausibly reflecting increased household energy demand and altered daily activity patterns during prolonged indoor stays.

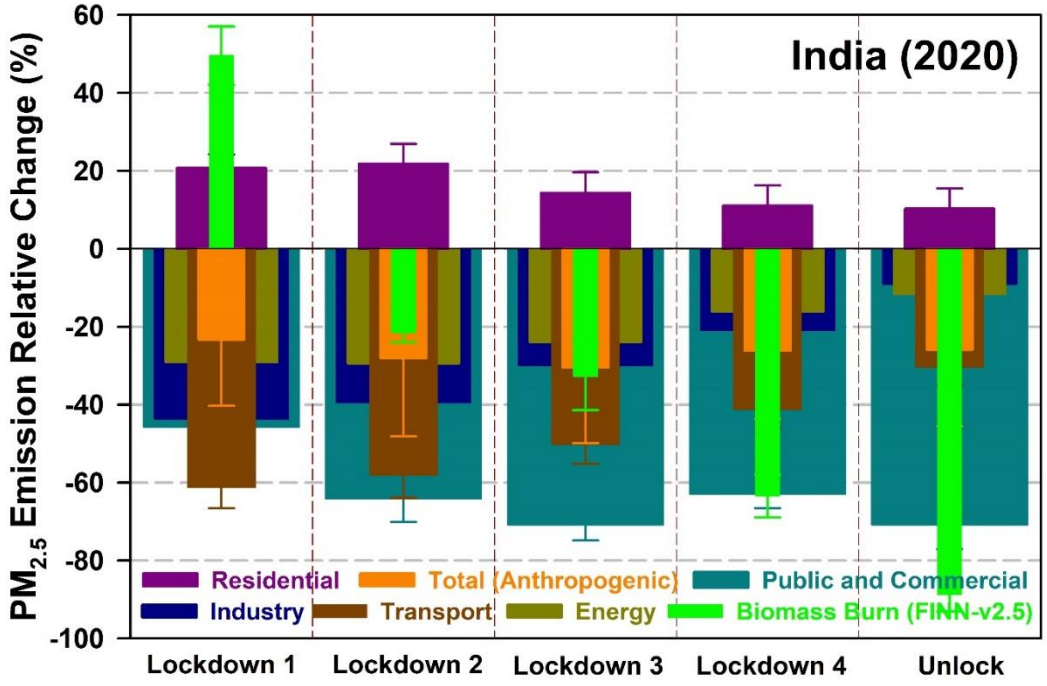


Figure 3.16: Bar chart illustrating the relative changes in $PM_{2.5}$ emissions from various sectors, as well as the total anthropogenic and biomass burning (FINN-v2.5) emissions, across different lockdown and unlock phases compared to the pre-lockdown baseline for all of India.

At the national scale, total $PM_{2.5}$ emissions across India reached a maximum reduction of ~30.53% during Lockdown Phase 3 (Fig. 3.2), before rebounding as activity resumed. Nevertheless, observed $PM_{2.5}$ concentrations did not decline uniformly in space or in proportion to emission reductions. This nonlinearity is expected because ambient $PM_{2.5}$ responds not only to primary emissions but also to atmospheric processing (secondary aerosol formation), boundary-layer dilution, wet/dry deposition, and regional transport, processes that can amplify or dampen the impact of emission changes depending on prevailing meteorology.

In terms of regional responses, satellite-derived estimates indicate pronounced $PM_{2.5}$ decreases over the WIGP (~24%) and EIGP (~17%) when averaged over the post-25 March period, consistent with the strong reduction in transport/industrial activity over dense urban and industrial corridors. WRF-Chem similarly indicates larger declines, ~35% over WIGP and ~27% over EIGP, reflecting the model's sensitivity to emission perturbations within the IGP hotspot. However, in North and Northeast India, both datasets show smaller declines and, in some cases, local increases: satellite indicates reductions of only ~5% (North) and ~8% (Northeast), while WRF-Chem indicates ~11% (North) and ~5% (Northeast). These muted responses point to persistent and/or episodic sources that were not strongly curtailed by lockdown measures, including biomass burning and forest fires (Goswami et al., 2012), agricultural residue burning (Vadrevu et al., 2011), and enhanced contributions from natural aerosols such as dust during the pre-monsoon period.

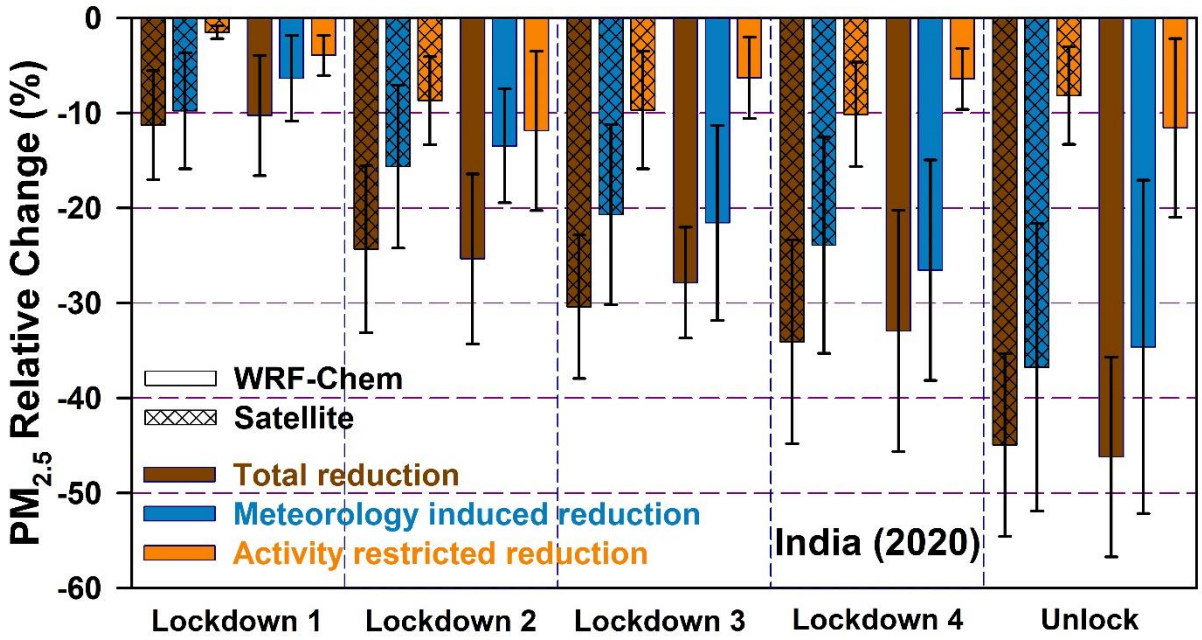


Figure 3.17: Grouped bar chart showing the total relative changes in ambient $PM_{2.5}$ concentrations across India during each lockdown and unlock phase, compared to the pre-lockdown baseline. Each bar distinguishes the contributions of meteorology-induced variations from those resulting from activity-restricted emission reductions.

Table 3.6: Population-weighted total relative changes in ambient $PM_{2.5}$ concentrations (%) across India and its seven geographical regions during each lockdown and unlock phase, compared to the pre-lockdown baseline, along with the contributions of meteorology-induced variations and activity-restricted emission reductions. The reported values represent pixel-level means.

	Satellite $PM_{2.5}$ Relative Change (%)					WRF-Chem $PM_{2.5}$ Relative Change (%)				
	Total Reduction (Meteorology induced reduction; Activity restricted reduction) (Average)									
Region	**Lock 1**	**Lock 2**	**Lock 3**	**Lock 4**	**Unlock**	**Lock 1**	**Lock 2**	**Lock 3**	**Lock 4**	**Unlock**
India	-11 (-9; -2)	-24 (-15; -9)	-30 (-20; -10)	-34 (-24; -10)	-45 (-37; -8)	-10 (-6; -4)	-25 (-13; -12)	-28 (-22; -6)	-33 (-26; -7)	-46 (-34; -12)
NI	-4 (1; -5)	-3 (-1; -2)	-9 (-2; -7)	-12 (-1; -11)	-12 (-4; -8)	11 (26; -15)	-26 (21; -47)	-46 (-20; -26)	-28 (-24; -4)	-50 (-39; -11)
NEI	-8 (-17; 9)	-30 (-29; -1)	-37 (-35; -2)	-50 (-41; -9)	-53 (-48; -5)	6 (-8; 14)	-31 (-25; -6)	-20 (-9; -11)	-30 (-29; -1)	-38 (-31; -7)
CI	-11 (-6; -5)	-19 (-13; -6)	-30 (-19; -11)	-27 (-21; -6)	-47 (-41; -6)	-9 (-14; 5)	-30 (-42; 12)	-32 (-51; 19)	-42 (-37; -5)	-50 (-46; -4)
SI	-11 (-10; -1)	-25 (-17; -8)	-33 (-23; -10)	-30 (-23; -7)	-48 (-44; -4)	-3 (-11; 8)	-18 (-15; -3)	-16 (-13; -3)	-29 (-23; -6)	-51 (-39; -12)
WI	-12 (5; -17)	-11 (7; -18)	-14 (4; -18)	-13 (2; -15)	-26 (-12; -14)	-19 (-6; -13)	-17 (5; -22)	-37 (-51; 14)	-30 (-24; -6)	-48 (-37; -11)
EIGP	-17 (-21; 4)	-40 (-27; -13)	-42 (-32; -10)	-48 (-37; -11)	-56 (-48; -8)	-27 (-1; -26)	-34 (-8; -26)	-30 (3; -33)	-37 (-21; -16)	-46 (-23; -23)
WIGP	-24 (-5; -19)	-25 (-1; -24)	-22 (2; -24)	-19 (-3; -16)	-35 (-14; -21)	-35 (3; -38)	-33 (-12; -21)	-42 (-18; -24)	-43 (-25; -18)	-42 (-23; -19)

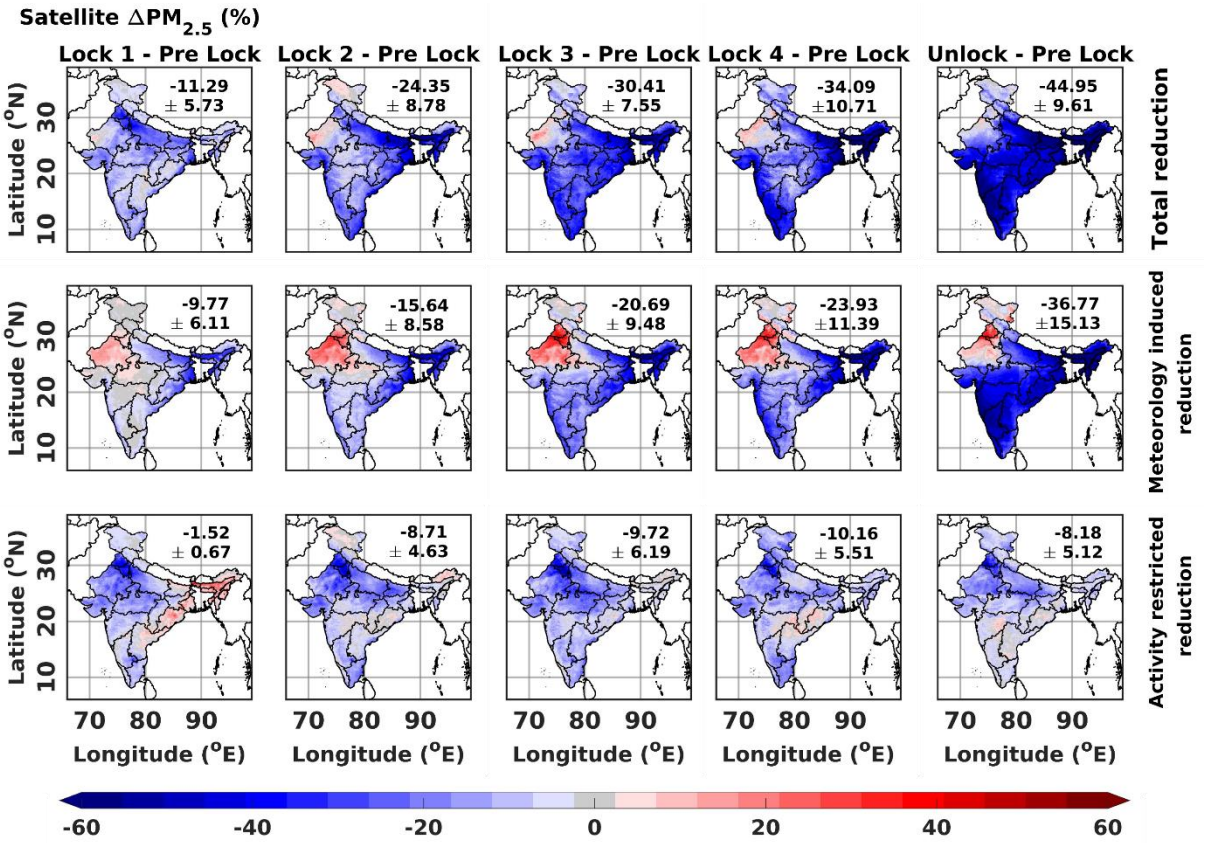


Figure 3.18: Spatial distribution of total relative changes in ambient $PM_{2.5}$ (top), and the separate contributions from meteorology (middle) and activity restrictions (bottom) during each lockdown and unlock phase, compared to pre-lockdown conditions. Results are based on satellite-derived $PM_{2.5}$ data. Mean values are explicitly displayed within the plot.

The subtraction-based attribution clarifies that meteorology dominated the early-phase response. After Lockdown Phase 1, population-weighted satellite $PM_{2.5}$ over India decreased by 11% relative to pre-lockdown, but 9% of this reduction was meteorology-driven and only 2% was attributable to activity restrictions (Fig. 3.17; Table 3.5). WRF-Chem yields a comparable total reduction (10%), with meteorology contributing 6% and emission cuts contributing 4% (Table 3.6). The stronger meteorological contribution is consistent with the seasonal transition from late winter to pre-monsoon, when rising temperatures and strengthening boundary-layer mixing generally enhance ventilation and reduce near-surface accumulation even without emission reductions.

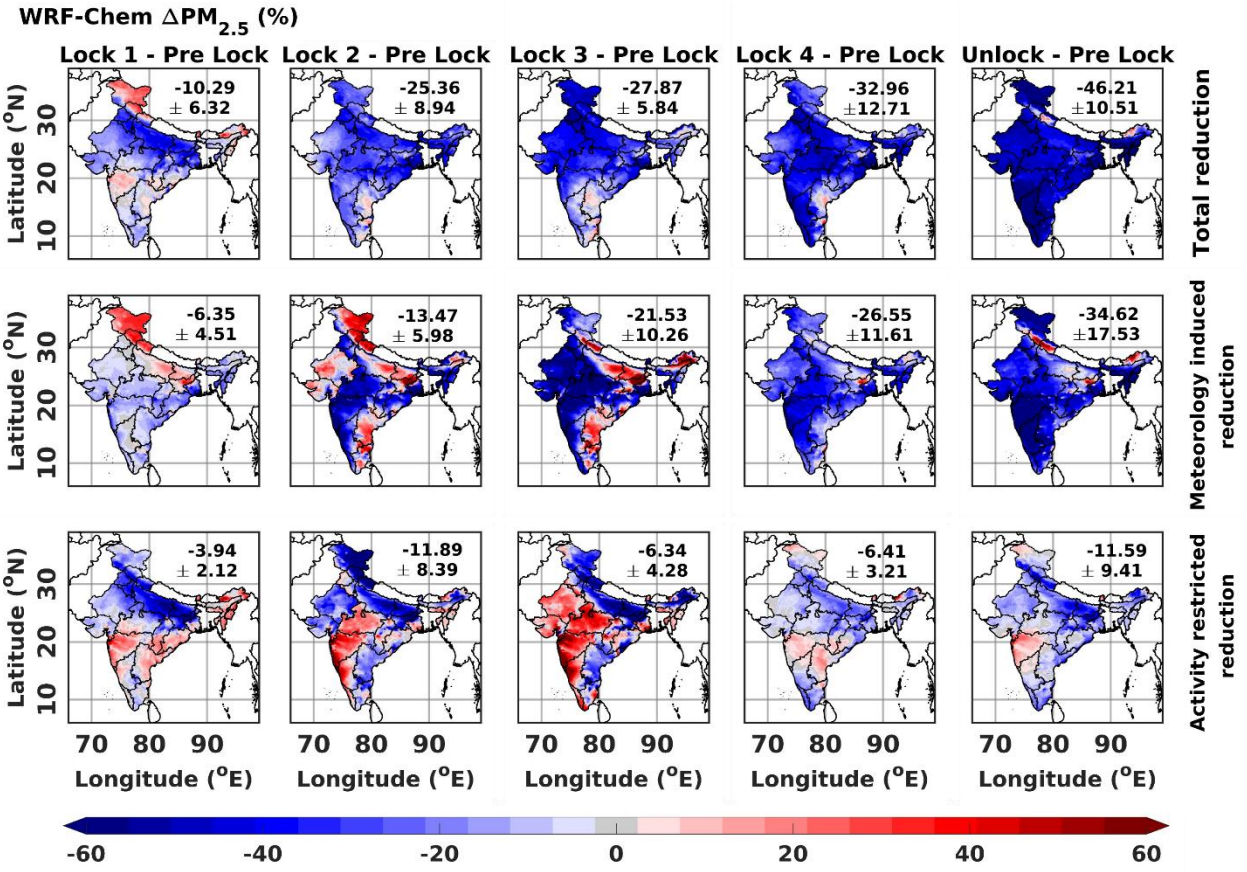


Figure 3.19: Spatial distributions of total relative changes in ambient $PM_{2.5}$ (top), and the separate contributions from meteorology (middle) and activity restrictions (bottom) during each lockdown and unlock phase, relative to pre-lockdown conditions, based on WRF-Chem simulations. Mean values are explicitly displayed within the plot.

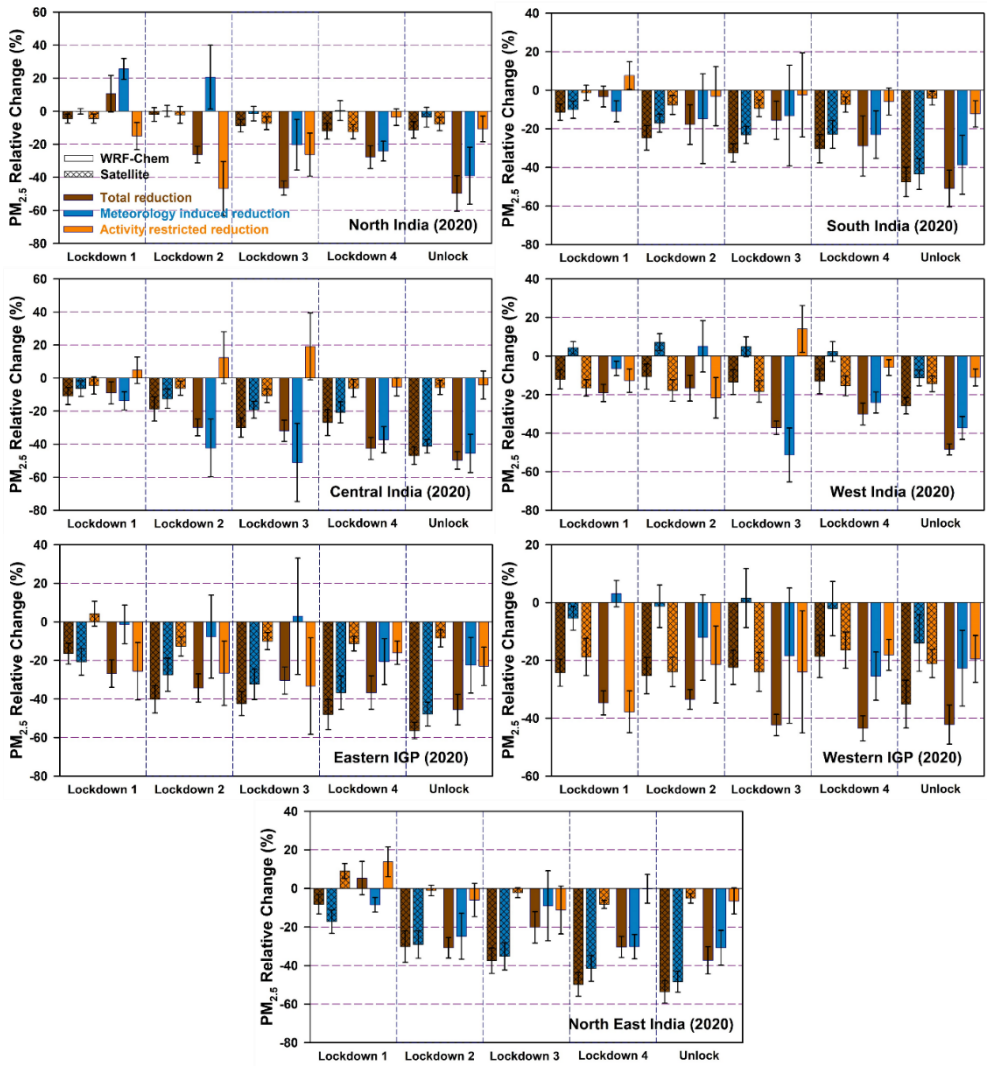


Figure 3.20: Grouped bar chart showing total relative changes in ambient $PM_{2.5}$ concentrations and the contributions from meteorology and activity restrictions during each lockdown and unlock phase, compared to the pre-lockdown baseline, across seven Indian regions.

During Lockdown Phase 2, both datasets show larger total reductions (24% from satellite and 25% from WRF-Chem). In this phase, emission reductions contributed more substantially (9–12%), but meteorology remained the larger share (13-15%) (Fig. 3.18; Table 3.6). For subsequent phases and the unlock period, WRF-Chem indicates emission-related reductions of 6%, 7%, and 12%, respectively (Fig. 3.19), while meteorology continues to explain a dominant fraction of the total change (Fig. 3.20). This persistent dominance of meteorology implies that the net $PM_{2.5}$ burden during March–June is highly sensitive to boundary-layer evolution and synoptic transport, such that even large sectoral emission cuts may yield only modest national-scale concentration declines when dispersion conditions are favourable.

Meteorological dominance is particularly evident during the unlock phase: although several anthropogenic activities resumed, $PM_{2.5}$ did not rebound to pre-lockdown levels in many

regions. This indicates that atmospheric dispersion and ventilation remained favourable, temporarily suppressing the concentration response to rising emissions. Yet $PM_{2.5}$ still exceeded the NAAQS over key regions, especially the IGP (Table 3.5), highlighting that short-lived emission shocks, however large, are insufficient for sustained compliance when baseline concentrations are high and persistent sources remain active. Finally, a comparison with city-level studies reinforces the importance of scale. Sharma et al. (2020) reported a 43% $PM_{2.5}$ reduction during the first lockdown phase based on CPCB observations from 22 cities, whereas our national-scale assessment yields more modest reductions (~10-11%) for the same phase. City networks are more sensitive to reductions in local traffic and industrial activity, while national/regional averages incorporate continued emissions from households and open burning and include influences from transported pollution and dust. The persistence of household contributions is particularly critical: household air pollution is estimated to contribute 25-30% of ambient $PM_{2.5}$ in India (Rao et al., 2021), and such emissions were not only sustained but may have increased during lockdown (Fig. 3.16). In addition, post-harvest residue burning continued after the wheat harvest, enhancing regional $PM_{2.5}$ through direct emissions and secondary aerosol formation downwind.

3.3.3 Normalized Anomaly and Ventilation Coefficient Analysis: Seasonal and Spatial Heterogeneity

India exhibits strong seasonal variability in $PM_{2.5}$ (Katoch et al., 2023), with maxima typically occurring in post-monsoon and winter due to stagnation, shallow boundary layers, and enhanced emissions from heating and burning, and minima during the monsoon due to efficient wet scavenging and stronger ventilation. The lockdown coincided with the pre-monsoon season (March-May), a period when rising surface temperatures and increasing boundary-layer depth generally enhance the Ventilation Coefficient (VC), favouring dilution of near-surface pollutants. However, this "seasonal cleaning tendency" does not guarantee uniform reductions because pre-monsoon also brings enhanced dust transport, frequent biomass burning after the wheat harvest, and strong photochemistry that can promote secondary aerosol formation under certain precursor regimes (Bhandari et al., 2020). Consequently, $PM_{2.5}$ responses during the lockdown are expected to be spatially heterogeneous and tightly coupled to synoptic variability. The normalized anomaly analysis provides a rigorous way to judge whether $PM_{2.5}$ reductions during 2020 exceeded what would typically be expected from interannual variability. The time series of normalized anomalies from satellite and WRF-Chem (Fig. 3.21) shows pronounced regional contrasts, with some regions exhibiting sustained negative anomalies (reductions beyond typical variability) and others remaining largely within ±1, implying that observed changes were not exceptional relative to

recent years. Spatial patterns of normalized anomalies (Fig. 3.22) further demonstrate that the lockdown signal was not uniform across India.

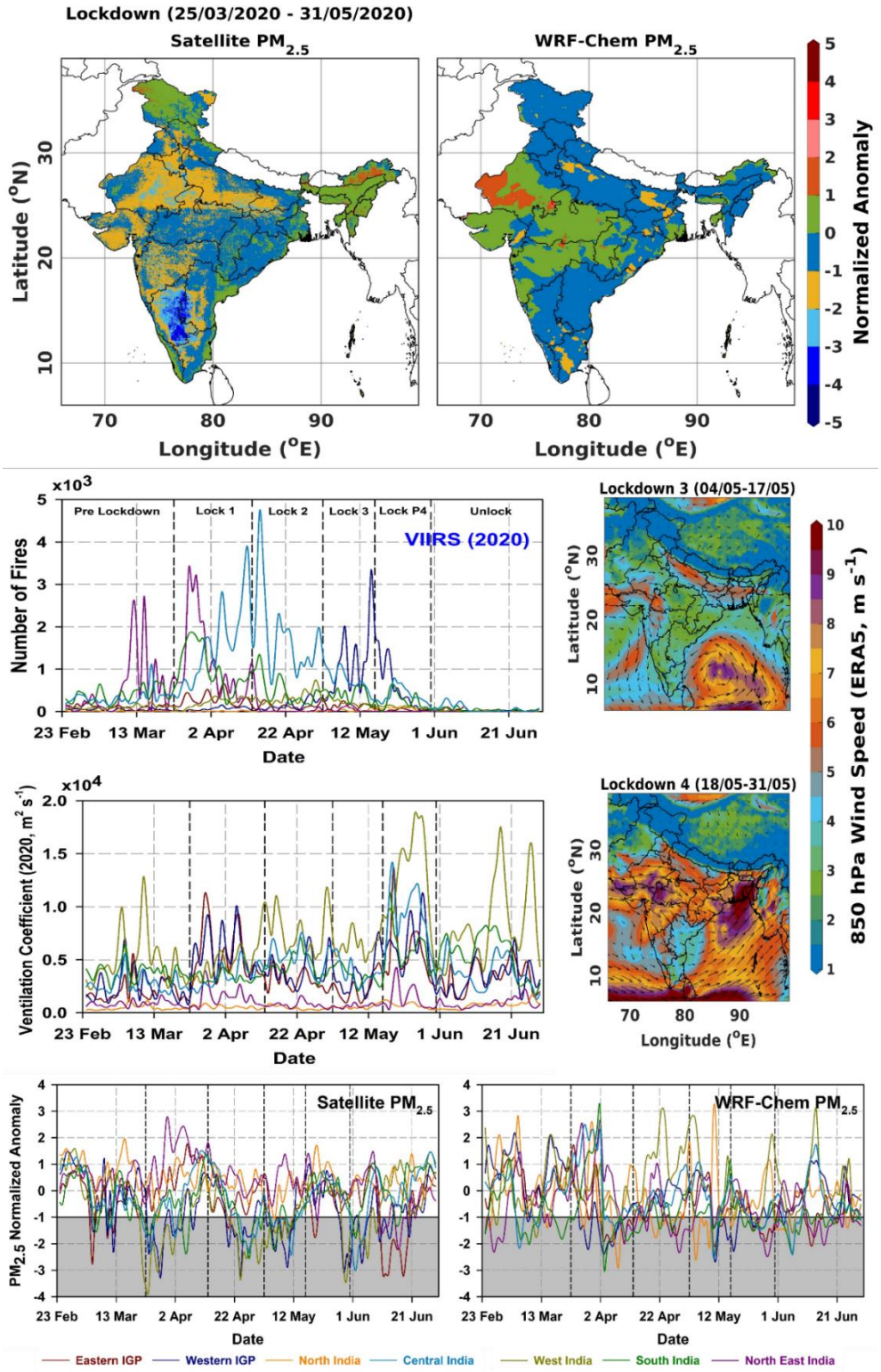


Figure 3.21: Spatial distribution of normalized $PM_{2.5}$ anomalies (top), time series of zone-wise normalized $PM_{2.5}$ anomalies from satellite data (bottom left) and WRF-Chem simulations (bottom right) for the entire lockdown period (March 25-May 31, 2020). The ventilation coefficient (VC) and VIIRS fire counts are shown (middle left) for pre-lockdown, each lockdown phase, and the unlock period across seven regions. ERA5 850 hPa wind speeds for the last two lockdown phases are presented (middle right) for all of India.

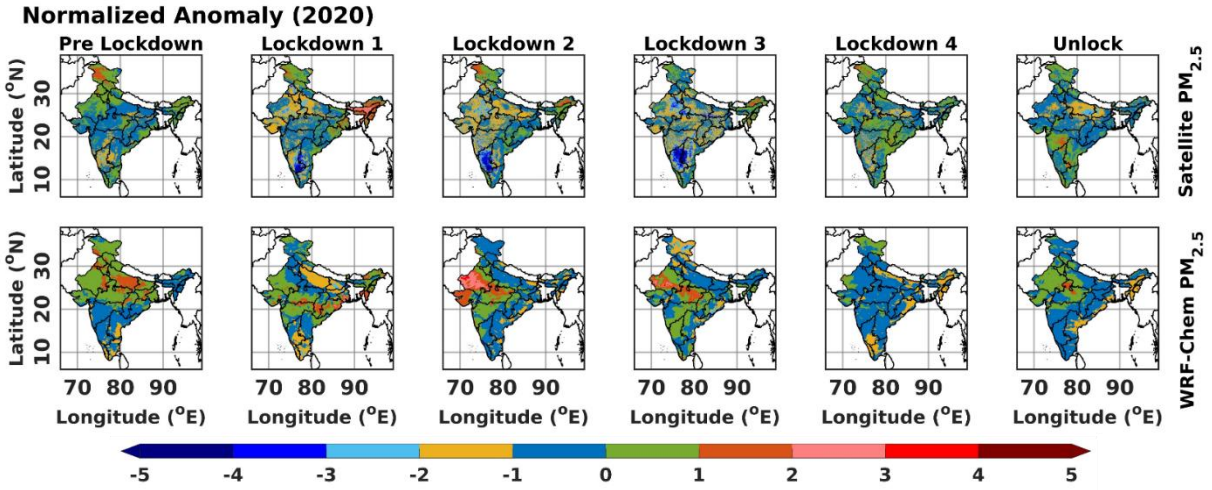


Figure 3.22: Normalized $PM_{2.5}$ anomalies from satellite data and WRF-Chem simulations for different lockdown phases over India.

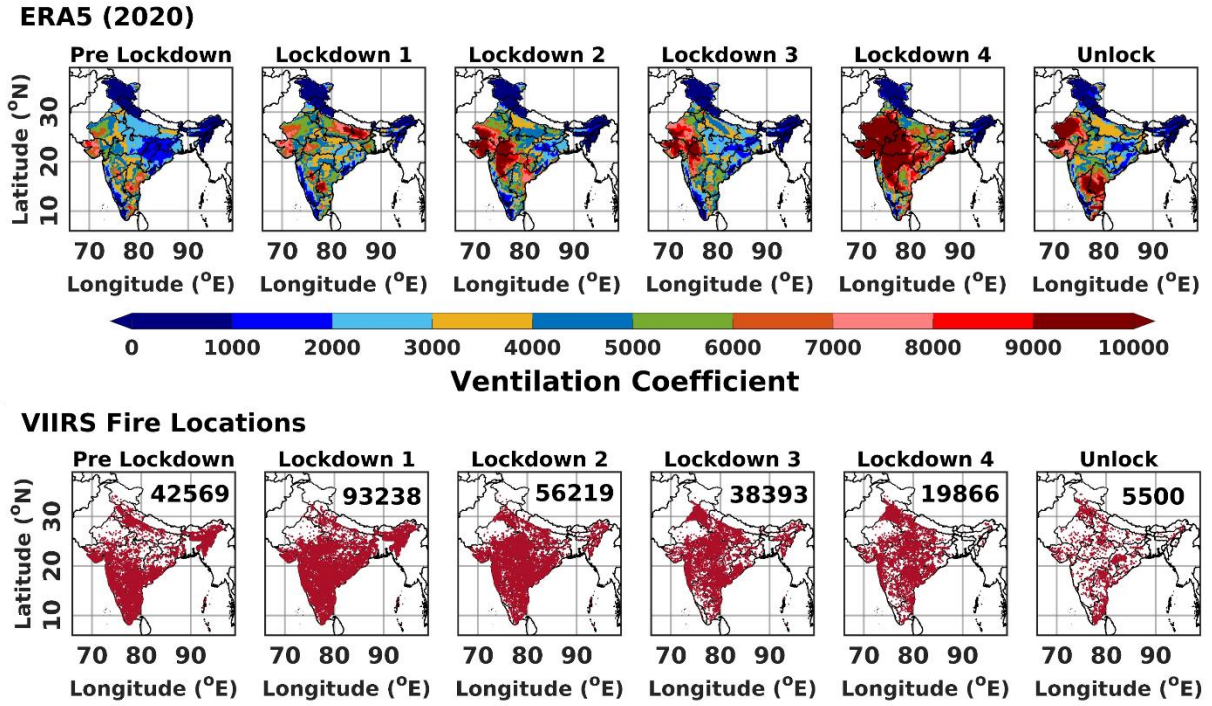


Figure 3.23: Spatial distribution of the Ventilation Coefficient (VC) from ERA5 (top) (m^2 s^{-1}) and VIIRS fire counts (bottom) over India during the pre-lockdown, phased lockdown, and unlock periods.

Several features stand out. First, the Western IGP shows consistently strong reductions, with normalized anomalies often below -1 during the lockdown period (Fig. 3.21), indicating that concentration declines exceeded the typical interannual variability and therefore likely contain a robust emission-reduction signal. Second, in contrast, North India and Northeast India generally show anomaly reductions that remain within ±1 (Fig. 3.22), suggesting that meteorology and background/episodic sources dominated variability and muted the detectable lockdown signal. Third, Central, Northeast, and South India show $PM_{2.5}$ increases during Lockdown Phases 1 and

2 in both datasets, reflecting that emission reductions in transport/industry were not sufficient to offset contributions from biomass burning, local sources, or transported pollution under prevailing winds.

The combined VC and VIIRS fire-count diagnostics (Fig. 3.21 & Fig. 3.23) help interpret these patterns mechanistically. Regions that experienced higher VC tended to show larger $PM_{2.5}$ reductions because stronger mixing and ventilation reduced near-surface accumulation. This appears particularly relevant during Lockdown Phase 1, when significant reductions were observed in West India, Central India, and both IGP subregions (Fig. 3.21 & Fig. 3.23). However, high VC can also "dilute" the apparent impact of emission reductions in an attribution sense: when ventilation is strong, concentrations fall even without emission cuts, thereby increasing the meteorology-driven fraction of the total reduction (consistent with Table 3.6).

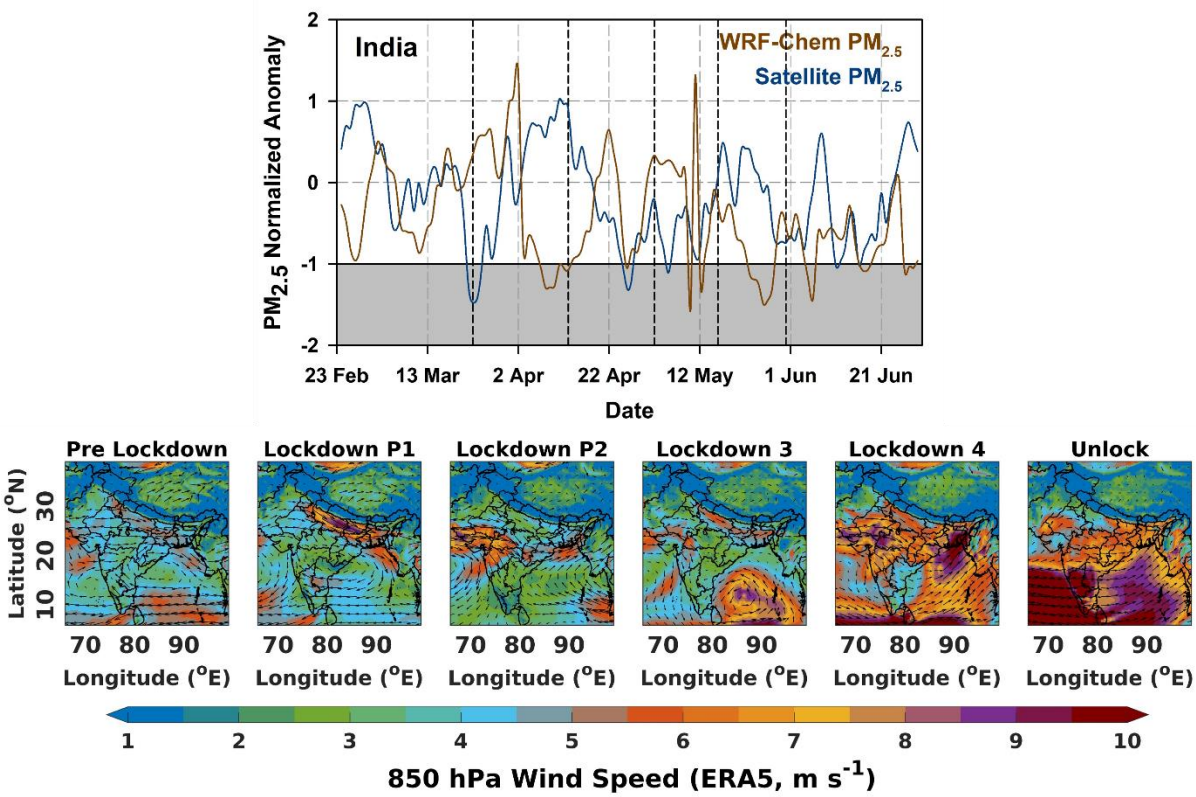


Figure 3.24: Time-series comparison of normalized $PM_{2.5}$ anomalies (top) from satellite data and WRF-Chem simulations, and 850 hPa ERA5 wind speed (bottom) over the study period across India.

Later phases show additional complexity. During Lockdown Phases 3 and 4, regional circulation changes associated with Cyclone Amphan, together with enhanced dust transport from neighbouring desert regions, altered $PM_{2.5}$ distributions over the IGP, West India, and Central India (Fig. 3.24). Dust events can elevate $PM_{2.5}$ even during strong emission reductions, particularly when synoptic winds favour transport into densely populated regions. Biomass burning also

influenced spatial patterns: for example, the Western IGP experienced elevated $PM_{2.5}$ during Phase 4 due to extensive biomass burning (Fig. 3.23). Likewise, the transport pathways inferred from the wind fields suggest that open burning in South India during Phase 1 could influence Central India under anticyclonic flow (Fig. 3.24), while westerly winds could advent emissions towards the Eastern IGP during Phase 2. During the unlock phase, $PM_{2.5}$ in the IGP and West India once again exceeded 40 $\mu g\ m^{-3}$ (Table 3.5), re-crossing the annual NAAQS threshold despite continued meteorological ventilation. This indicates that as emissions began to recover, the concentration response re-emerged in the most polluted regions, but the persistence of burning and dust-related contributions continued to modulate the magnitude and timing of rebound.

3.4 Summary and Conclusions

The nationwide COVID-19 lockdown in India constituted an unprecedented, quasi-experimental perturbation to anthropogenic activity and therefore offered a rare opportunity to disentangle the relative roles of emission changes and meteorology in governing ambient $PM_{2.5}$ variability. By integrating a high-resolution regional chemical transport modelling framework (WRF-Chem) with a nationwide, high-resolution satellite-derived $PM_{2.5}$ database and analysing the full sequence of pre-lockdown, phased-lockdown, and unlock periods (24 February-30 June 2020), this study provides a comprehensive and policy-relevant assessment of the processes that controlled $PM_{2.5}$ during an extraordinary period of forced emission reductions.

A central finding is that the observed decline in $PM_{2.5}$ after the onset of lockdown about 29% at the national scale, was driven predominantly by meteorology, while activity-restricted emission reductions explained a smaller fraction (only ~8-9% on average). The emission inventory analysis confirms that restrictions strongly reduced emissions from transport and public activity sectors (up to 61.25% during Lockdown Phase 1), but these gains were partly offset by an increase in residential emissions (~20.67% during Phase 1) associated with intensified household energy use during prolonged indoor stays (Fig. 3.16). This sectoral asymmetry is crucial for interpretation: even an extreme reduction in mobility and industrial activity does not translate linearly into $PM_{2.5}$ reductions when persistent and spatially diffuse sources, especially residential combustion and open burning, remain active or intensify. Moreover, the strong influence of meteorology demonstrates that dispersion, mixing, and removal processes can amplify or suppress the concentration response to emission controls, consistent with the role of ventilation and wet/dry deposition in shaping near-surface pollutant burdens (Xie et al., 2024).

The pre-lockdown baseline across India was already severely elevated, particularly over the Indo-Gangetic Plain (IGP), where satellite-derived $PM_{2.5}$ reached 63.14 μg m^{-3} in the Eastern IGP and 61.52 μg m^{-3} in the Western IGP (Table 3.5). As a result, even substantial short-term emission cuts did not yield widespread compliance with the NAAQS annual threshold of 40 μg m^{-3}, especially over the IGP. The subtraction-based attribution further shows that early-phase reductions, such as the ~11% decrease during Lockdown Phase 1, were largely meteorology-driven, with only a small emission-driven component (Fig. 3.17; Table 3.5). This finding highlights an important interpretation: during the February–June seasonal transition, meteorology can account for a large portion of the observed "improvement," and therefore apparent air-quality gains cannot be attributed to emission reductions alone without explicit meteorological normalization.

The regional response to lockdown was strongly heterogeneous, reflecting differences in baseline emissions, atmospheric processing, and transport. The IGP exhibited the most pronounced reductions, and at times $PM_{2.5}$ decreased by more than 50% during specific phases and sub-regions (e.g., Eastern IGP during the unlock phase in the satellite-derived product, and Western IGP during Lockdown Phase 4 in the model simulations). Yet, even in this most responsive region, concentrations often remained above the NAAQS because of the high baseline and the continued influence of household emissions, biomass burning, and dust transport. Normalized anomaly diagnostics provide additional evidence that the lockdown signal was not spatially uniform: the Western IGP frequently exhibited anomalies below -1, indicating reductions exceeding typical interannual variability, whereas several other regions largely remained within the historical variability envelope (Fig. 3.21-3.24). These patterns emphasize that regional transport and episodic influences, such as dust incursions and biomass-burning plumes, can dominate $PM_{2.5}$ variability and obscure the signal of local emission changes (Kumar et al., 2020; Tibrewal et al., 2022).

The study also clarifies why some earlier reports, often focused on a limited number of cities and the strict lockdown window, found substantially larger $PM_{2.5}$ declines. City-based monitoring networks are highly sensitive to reductions in local traffic and industrial activity, whereas national-scale assessment must account for persistent, spatially widespread sources (e.g., residential combustion, agricultural residue burning) and for regional and transboundary contributions that can sustain background $PM_{2.5}$ even when urban emissions decline. By extending the analysis through the unlock phase and applying a consistent subtraction-based framework to distinguish meteorology-driven variability from activity-restricted reductions, this chapter

demonstrates that a broader spatial and temporal lens is essential to avoid overestimating the effectiveness of short-term sectoral controls.

Collectively, these results have three key implications for air-quality management in India. First, severe but short-lived emission shocks, even when nationwide, do not guarantee sustained $PM_{2.5}$ improvements because concentration outcomes are strongly regulated by meteorological ventilation and removal processes (Xie et al., 2024). Second, persistent sources such as residential combustion and open burning can substantially limit the gains achieved by controlling transport and industrial sectors; therefore, mitigation strategies must explicitly target these sources to achieve durable reductions. Third, the strong regional heterogeneity in responses indicates that effective policy must be regionally tailored and aligned with seasonal meteorological context, rather than relying on uniform, one-size-fits-all interventions.

From a policy perspective, these findings reinforce the need to strengthen long-term, multi-sectoral strategies under programmes such as the NCAP, with particular emphasis on household energy transitions and reductions in open burning. Scaling up clean-fuel adoption initiatives (e.g., Pradhan Mantri Ujjwala Yojana, PMUY), improving waste management, and implementing effective alternatives to agricultural residue burning (including incentives and viable residue-utilization pathways) are likely to yield larger and more sustained $PM_{2.5}$ benefits than controls focused primarily on mobility restrictions. Finally, robust evaluation and adaptive policymaking require an expanded monitoring and assessment framework that integrates satellite observations, model simulations, and improved ground-based measurements, including rural and background sites, to enable meteorologically normalized trend analysis, better source attribution, and more reliable evaluation of interventions over time and space.

In conclusion, the COVID-19 lockdown demonstrated that dramatic reductions in selected anthropogenic activities can produce visible, but often transient, improvements in air quality. At the same time, it exposed the limitations of relying on narrow sectoral controls without addressing persistent household and open-burning sources, and without accounting for the dominant modulation by meteorology and regional transport. Sustainable compliance with the NAAQS and long-term reductions in $PM_{2.5}$ across India will therefore require a comprehensive, regionally tailored, and meteorology-aware mitigation strategy that targets the full spectrum of emission sources and is evaluated using integrated observational-modelling approaches.

Chapter 4: Disentangling Sectoral and Species Drivers of Surface $PM_{2.5}$ in the NCT Delhi Airshed

4.1 Introduction

Particulate matter (PM) is among the most harmful air pollutants affecting human health and is strongly associated with both acute and chronic morbidity and mortality (Manisalidis et al., 2020). Epidemiological evidence links PM exposure to cardiovascular and cerebrovascular disease, ischemic heart disease, stroke, lung cancer, and a spectrum of respiratory outcomes ranging from aggravated asthma to chronic obstructive pulmonary disease. The health burden is particularly severe for particles with aerodynamic diameters smaller than 2.5 μm ($PM_{2.5}$), which can penetrate deeply into the alveolar region and enter systemic circulation. Because a substantial fraction of anthropogenic particle mass is concentrated in this fine mode, $PM_{2.5}$ serves as a policy-relevant indicator of combustion-related pollution and secondary aerosol formation.

Recent global burden estimates indicate that exposure to PM contributes to more than 10.2 million premature deaths annually, including over 3.9 million in China and more than 2.5 million in India (Vohra et al., 2021). Within India, Delhi routinely experiences some of the highest $PM_{2.5}$ concentrations worldwide (Apte et al., 2015). Yet, despite substantial attention, the relative roles of sources, atmospheric processing, and regional transport that together sustain Delhi's PM burden remain incompletely constrained. A particularly important gap for air-quality management is understanding how within-city emissions interact with regional emissions and chemistry over the broader Indo-Gangetic Plain (IGP), thereby shaping surface $PM_{2.5}$ in the megacity's airshed (Apte et al., 2019; Pant et al., 2016).

Delhi's primary PM sources include on-road and non-road transport, biomass combustion for cooking and heating, open waste burning, construction and road dust resuspension, and emissions from formal and informal industries (including brick kilns) as well as electric power generation (Guttikunda et al., 2012; Pant et al., 2012). Measurements indicate that sub-micrometre particulate matter (PM_1) represents a relatively large fraction (30-40%) of Delhi's aerosol burden compared with other megacities (Bhandari et al., 2020), highlighting the importance of combustion sources and secondary aerosol processes. However, a large component of $PM_{2.5}$ in northern India is not emitted directly as particles; instead, it forms secondarily via atmospheric oxidation of gaseous precursors. This distinction is crucial because control strategies that focus only on primary PM emissions can underperform when secondary formation pathways dominate mass, especially during stagnation episodes and in chemically reactive environments.

Ambient PM is therefore best understood as a mixture of primary and secondary components. Primary particles are emitted directly and include black carbon, mineral dust, trace metals, and primary organic carbon (Kroll et al., 2008). Secondary inorganic aerosol forms from gas-to-particle conversion involving sulfur dioxide, nitrogen oxides, and ammonia (Singh et al., 2021), while secondary organic aerosol (SOA) forms from oxidation of volatile organic compounds (VOCs) and subsequent partitioning into the particle phase (Kota et al., 2018; Kroll & Seinfeld, 2008).

Across India, anthropogenic sources associated with rapid economic development, transport, industries, and power plants, coexist with emissions from traditional energy use (firewood and dung combustion), open waste burning, and agricultural residue burning (Guo et al., 2017). Modelling studies have evaluated PM drivers in selected regions and seasons (Ghude et al., 2016). For example, Guo et al. (2017) report dominant contributions from the residential sector (~80 $\mu g\ m^{-3}$) and industry (~70 $\mu g\ m^{-3}$); however, a persistent limitation in parts of the literature is insufficient quantification of SOA formation and sector-resolved influences on primary organic aerosol (POA), secondary inorganic aerosol (SIA), and SOA across India (Kota et al., 2018; Kroll et al., 2008). These limitations matter because policy choices differ substantially depending on whether $PM_{2.5}$ mass is dominated by (i) directly emitted carbonaceous particles, (ii) nitrate-ammonium systems sensitive to NH_3 and NO_x, or (iii) sulfate systems sensitive to SO_2 and oxidant fields, or (iv) SOA sensitive to VOC mixtures and oxidation regimes.

Major knowledge gaps thus remain in quantifying the source apportionment of total, primary, and secondary $PM_{2.5}$ during the post-monsoon and winter periods across northern India. Several studies document the importance of regional pollution over the IGP, but are constrained by spatial coverage, limited seasonality, or city-centric interpretations. Monitoring-based analyses suggest that biomass burning, followed by transport, can be a major contributor over the IGP (Villalobos et al., 2015). Wintertime $PM_{2.5}$ is amplified by shallow boundary layers, suppressed turbulence, and enhanced long-range transport from western regions (Nair et al., 2007).

Many studies rely primarily on observations in individual cities rather than an integrated regional assessment (Ojha et al., 2020; Schnell et al., 2018), while others target selected seasons. Dispersion-modelling analyses over the IGP (Bran et al., 2017; Venkataraman et al., 2018) help address parts of the problem but also point to unresolved scientific questions about how meteorology, chemistry, and emissions interact. For instance, a six-month evaluation indicates that meteorology can exert a stronger influence than chemistry over northern India (Ojha et al., 2020),

and wintertime $PM_{2.5}$ increases sharply because the ventilation coefficient (VC) decreases by roughly a factor of four relative to post-monsoon conditions (Villalobos et al., 2015). While some work reports seasonal source contributions for selected IGP cities (Sahu et al., 2011), a cohesive airshed-scale perspective remains limited.

Long-range transport further complicates Delhi's air-quality management because emissions from rural and peri-urban regions can substantially affect downwind urban receptors over hundreds to thousands of kilometres (Gupta et al., 2013). In addition, notable discrepancies persist between published estimates of black carbon and dust emissions and the magnitudes required to reproduce observed concentrations in regional models (David et al., 2019; Verma et al., 2017). Only a limited number of studies explicitly quantify both primary and secondary contributions to $PM_{2.5}$ across the wider northern India region that includes the NCT-Delhi airshed. Importantly, $PM_{2.5}$ in NCT-Delhi is not controlled by crop residue burning (CRB) alone; multiple emission sectors contribute both to the baseline and to episodic extremes.

Agricultural emissions, for example, have increased with rising crop productivity and expansion of diesel-powered machinery such as tractors and irrigation pumps (Pandey et al., 2014). In the residential sector, a substantial fraction of households still relies on solid fuels burned in inefficient stoves, driving both ambient and indoor pollution (Mahato et al., 2020; Singh et al., 2020; Venkataraman et al., 2024). Similar combustion technologies persist in informal industries such as brick kilns and agro-processing units. Household air pollution remains the second-largest risk factor for India's disease burden, and residential biomass combustion contributes substantially to net-positive radiative forcing at the global scale (Seay et al., 2021; Unger et al., 2010; Venkataraman et al., 2010).

The National Capital Region (NCR) hosts numerous large point and area sources, including thermal power plants, cement factories, smelters, brick kilns, rice mills, and mineral-processing facilities, many of which employ outdated technologies and emit substantial $PM_{2.5}$ and precursor gases (Chatterjee et al., 2023; Guttikunda et al., 2023; Venkataraman et al., 2018). For example, rice mills frequently burn husk and residues in inefficient furnaces, and jaggery production units burn sugarcane waste, both of which contribute meaningfully to local PM emissions (Conibear et al., 2020). Fugitive emissions from stone crushers and mineral grinding units further degrade air quality in NCAP-designated cities (Ganguly et al., 2020; Guttikunda et al., 2025). During the post-monsoon and winter months, festive activities starting with Diwali and extending through Dev Deepawali, Christmas, and New Year can elevate PM and trace gas concentrations (Patowary et

al., 2024; Saha et al., 2021). Firecracker emissions combined with low ventilation and stable boundary layers can generate severe, persistent pollution episodes (Dwivedi et al., 2025; Ravindra et al., 2022).

In parallel, micro, small, and medium enterprises (MSMEs) across northern India often rely on coal and heavy oils, producing elevated $PM_{2.5}$ and SO_2 emissions (Lal et al., 2025; Pandey et al., 2014). Transition pathways, such as cleaner fuels (natural gas, electricity, solar thermal), electrified smelting, alternative fuels, and waste-heat recovery, could reduce industrial emissions by 30-40% while generating economic co-benefits (Seay et al., 2021; Singh et al., 2021). Poorly blended fuels used in commercial vehicles and outdated agricultural machinery further compound the regional emissions problem.

The analysis presented in the preceding chapter demonstrates that, despite temporary declines in primary anthropogenic emissions during the COVID-19 lockdown, the observed reduction in $PM_{2.5}$ was governed primarily by favourable meteorological conditions rather than emission reductions alone (Nandi et al., 2025). This result highlights the need for sustained, long-term mitigation and motivates an airshed perspective that integrates sources, chemistry, and transport. In this chapter, we use a high-resolution, online-coupled atmospheric chemistry-transport modelling framework with updated anthropogenic emissions and near-real-time biomass burning inputs to conduct a comprehensive sectoral and chemical-composition analysis of surface $PM_{2.5}$ across northern India, with a specific focus on Delhi-NCR and the NCT-Delhi airshed.

The framework enables us to (i) isolate contributions from major emission sectors and upwind source regions and (ii) examine the seasonal evolution of $PM_{2.5}$ chemical composition. By integrating sectoral attribution, chemical characterization, and meteorological sensitivity, our overarching objective is to demonstrate that Delhi cannot achieve sustained air-quality improvement through local controls alone and that durable reductions require a coordinated, multi-sector, airshed-scale strategy for NCT-Delhi and the broader northern India region. The results are intended to support a scientifically grounded, regionally integrated air-quality management approach that is aligned with dominant sources and their spatiotemporal behaviour, thereby enabling more effective mitigation of $PM_{2.5}$ over the NCT-Delhi airshed.

4.2 Methodology

4.2.1 Model Description

We employ the Weather Research and Forecasting model coupled with Chemistry (WRF-Chem, v4.2.2) (Grell et al., 2005) to simulate surface $PM_{2.5}$ and co-emitted/chemically coupled species over northern India, with a particular focus on Delhi-NCR and the NCT-Delhi airshed region encompassing Punjab and Haryana. WRF-Chem provides an online-coupled representation of meteorology and chemistry and has been widely used and evaluated for air-quality applications over India, enabling process attribution and policy-relevant sensitivity experiments (Lal et al., 2025; Mogno et al., 2021; Nandi et al., 2025; Venkataraman et al., 2024). Simulations cover 17 August 2019 to 31 January 2020, thereby including the late monsoon transition, post-monsoon, and winter pollution season. The first 15 days are treated as model spin-up to minimize the influence of initial chemical conditions.

A two-way nested configuration is adopted: an outer domain (15 km x 15 km, 140 x 150 grid cells) covering the Indian subcontinent and an inner high-resolution domain (5 km x 5 km, 126 x 138 grid cells) centred over NCT-Delhi (28.61° N, 77.21° E) and encompassing the principal northern Indian states (Fig. 4.1). This configuration is designed to better resolve urban–rural gradients, capture key emission hotspots, and represent mesoscale transport pathways that connect upwind agricultural regions to downwind urban receptors.

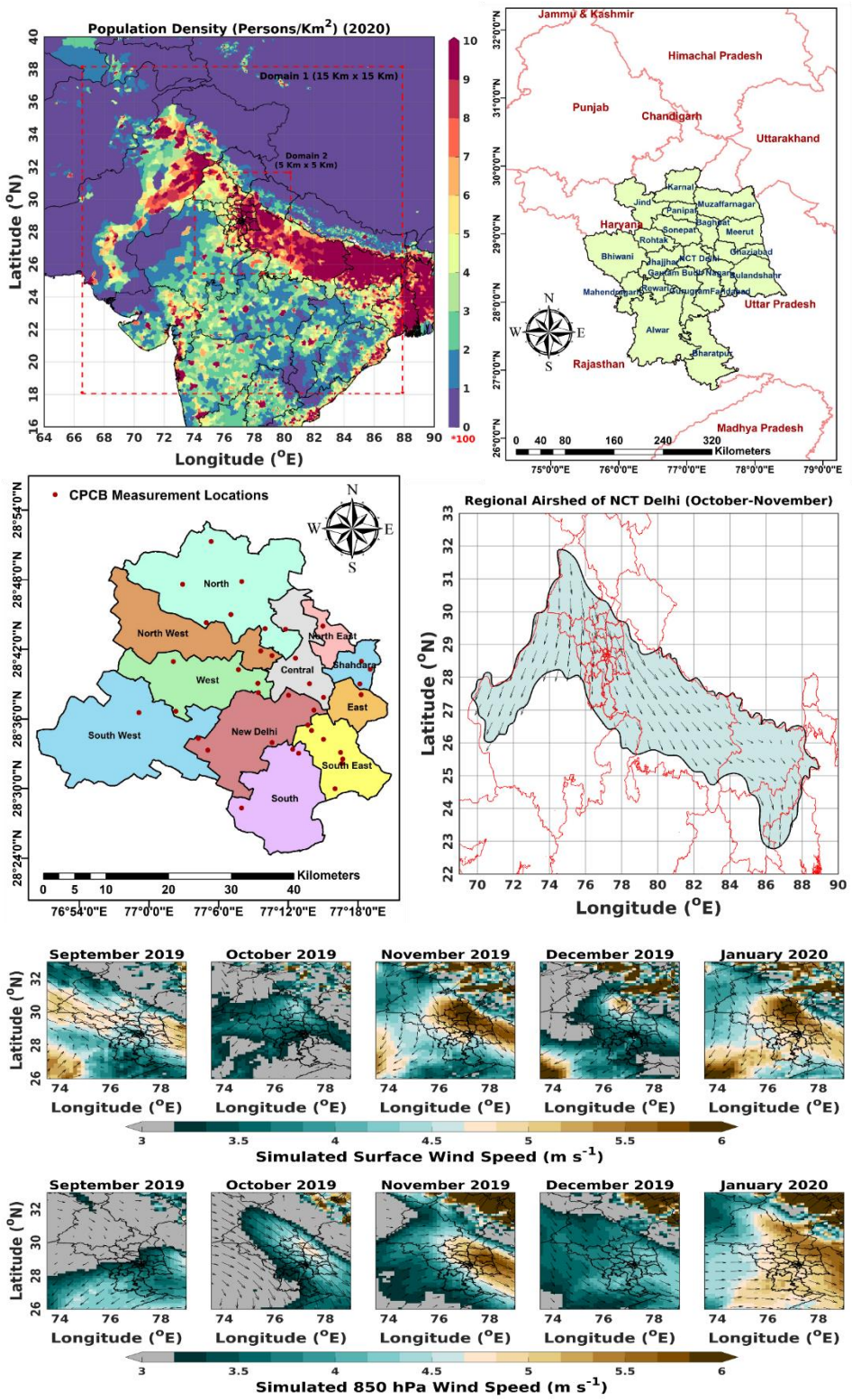


Figure 4.1: Model domains and regional context: The top-left panel shows the WRF-Chem outer and inner simulation domains overlaid with 2020 population density from GPWv4. The top-right panel provides a zoomed-in view of the high-resolution inner domain with highlighted Delhi-NCR region. The middle-left panel maps NCT-Delhi, its administrative districts, and CPCB monitoring stations active during 2019-2020. The middle-right panel depicts the NCT-Delhi airshed for October-November (Kumar et al., 2025) ***(Punjab, Haryana, and Delhi-NCR), overlaid with simulated WRF-Chem wind flow patterns. The bottom panel presents monthly simulated surface and 850-hPa wind speeds and flow directions across North India, highlighting seasonal changes in regional transport.***

Meteorological initial and boundary conditions are derived from ERA5 at 6-hourly resolution and are assimilated into WRF using grid nudging of winds, temperature, and water vapour above the planetary boundary layer to keep large-scale circulation consistent with reanalysis while allowing near-surface and mesoscale structures to evolve (Zittis et al., 2018). A nudging coefficient of 0.0005 s^{-1} is applied.

Anthropogenic emissions of $PM_{2.5}$ and major precursors are prescribed using the India-specific Speciated Multi-Pollutant Generator inventory (SMoG-COALESCE, 2019, 5 km) (Venkataraman et al., 2024), which provides sector-resolved emissions for residential, transport, industry, energy, agriculture, waste burning, and additional categories. This sectoral detail is essential for controlled perturbation experiments. Volatile organic compound emissions are supplemented using EDGAR-v5 (2015) (Crippa et al., 2020). Biogenic emissions are computed online using MEGAN (Guenther et al., 2006). Biomass burning emissions, including CRB, are taken from FINN-v2.5 (Wiedinmyer et al., 2023).

Gas-phase chemistry is represented using MOZART-4 (Emmons et al., 2010) coupled with MOSAIC (Zaveri et al., 2008) in a four-bin size framework. Grid-scale aqueous chemistry is included, and organic aerosols are treated using a Volatility Basis Set (VBS) approach (Knote et al., 2014), allowing the model to represent both POA and SOA evolution in a chemically consistent manner. Chemical boundary conditions are updated every 6 hours from global WACCM simulations (Gettelman et al., 2019). Photolysis is treated using FTUV (Tie et al., 2003). A detailed discussion of SMoG-COALESCE sectoral $PM_{2.5}$ emissions and the full WRF-Chem configuration is provided (Fig. 4.2 & 4.3 and Table 4.1).

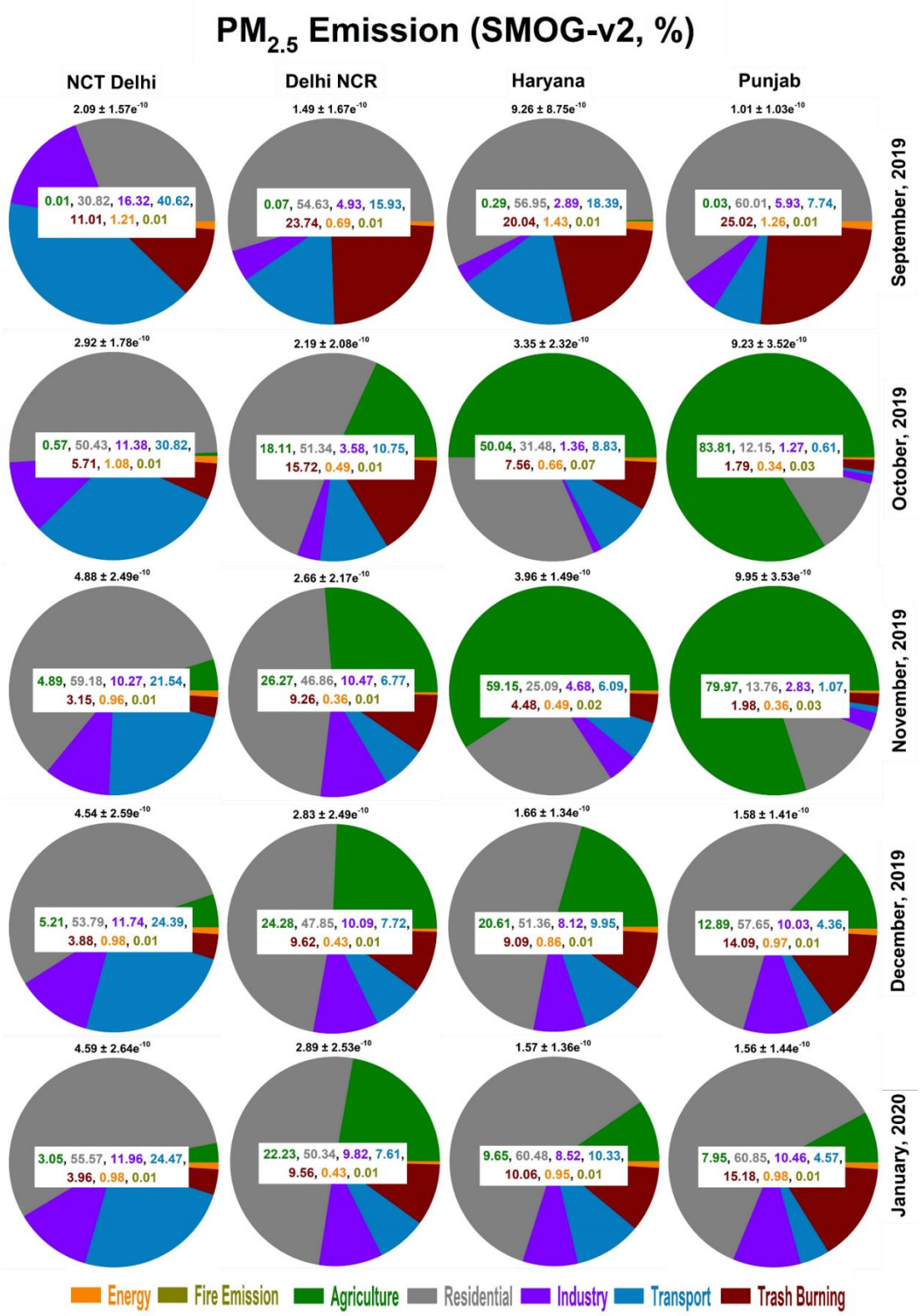


Figure 4.2: Sectoral contributions to $PM_{2.5}$ emissions from the SMoG-COALESCE inventory. The pie chart displays the mean percentage contribution from each sector, illustrating the relative importance of major emission sources across the study region.

Sectoral analysis using SMoG-COALESCE indicates that transport emissions dominate surface $PM_{2.5}$ over NCT-Delhi during September, whereas the residential sector becomes increasingly dominant toward winter, consistent with seasonal shifts in fuel use for

heating/cooking and changes in atmospheric dispersion. Within SMoG-COALESCE, the agricultural sector aggregates emissions from agricultural machinery, tractors, irrigation pumps, and locally manufactured low-cost commercial vehicles using poorly blended fuels, together with agricultural waste burning (AWB), commonly termed crop residue burning (CRB).

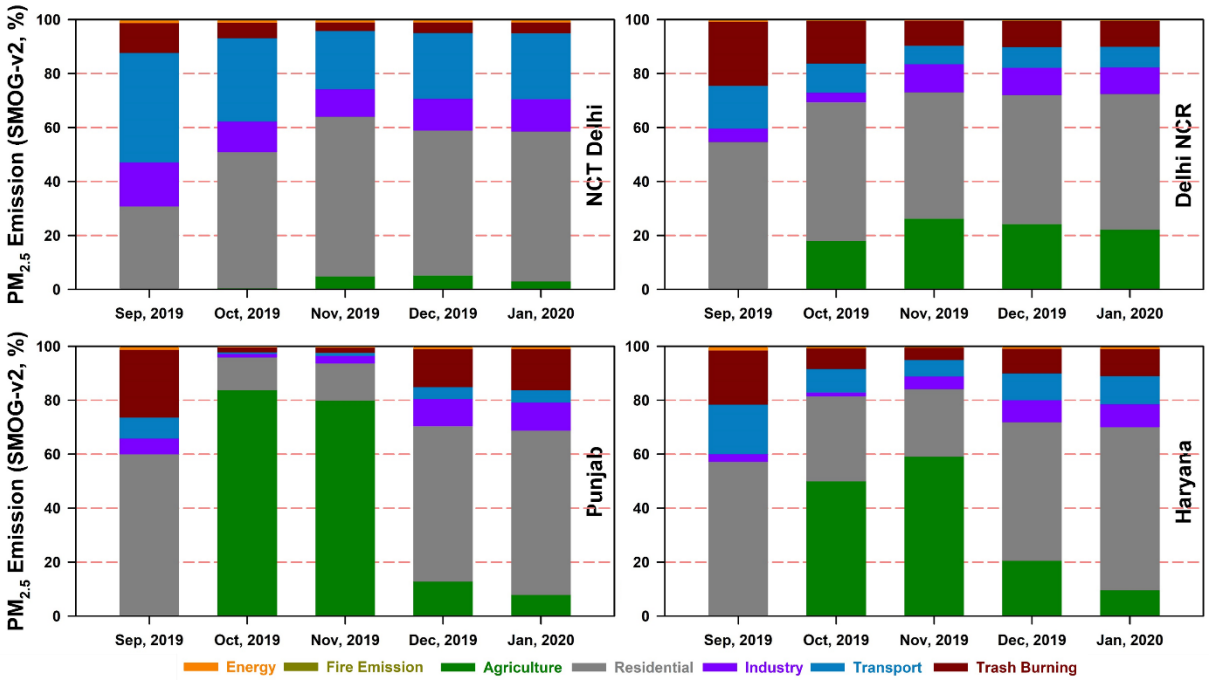


Figure 4.3: Stacked bar chart showing the sectoral contributions to $PM_{2.5}$ emissions derived from the SMoG-COALESCE inventory, highlighting the relative magnitude and variability of emissions from major source sectors.

This categorization explains the strong increase in "agriculture" emissions over Punjab and Haryana during October-November when CRB peaks. Across northern India, the residential sector remains the largest contributor through the study period, reflecting widespread use of inefficient biomass and waste-burning technologies. To prevent double counting of CRB, only 8.6% of agricultural-sector $PM_{2.5}$ emissions in SMoG-COALESCE are retained as non-CRB agricultural activities during preprocessing (Lal et al., 2025). The stacked-bar diagnostics further indicate that industrial emissions remain relatively steady over NCT-Delhi during the study period, implying a persistent baseline industrial contribution to ambient $PM_{2.5}$.

4.2.2 Simulation Details

The primary focus of this study is not only to examine the policy relevance of existing interventions, but more fundamentally to quantify the influence of major emission sectors on surface $PM_{2.5}$ and to characterize how $PM_{2.5}$ chemical composition evolves from late monsoon to

winter. Sectoral contributions identify the emission categories that dominate the burden and therefore offer the highest mitigation leverage, whereas chemical composition constrains the importance of secondary formation, informs exposure/toxicity interpretation, and provides a basis for evaluating the need to control gaseous precursors in addition to primary PM. Together, sectoral attribution and composition analysis provide a mechanistic foundation for airshed-scale mitigation planning in northern India.

We adopt a sensitivity-based source apportionment framework that accounts for non-linear atmospheric chemistry. Rather than relying solely on a decomposition that assumes linear additivity, we interpret the sensitivity of $PM_{2.5}$ to perturbations in sectoral emissions as an effective indicator of source influence. In addition to the control simulation, we conduct seven emission perturbed simulations in which emissions from each major sector agriculture, biomass burning, transport, waste burning, energy, industry, and residential, are individually set to zero across the study domain (Pandey et al., 2014; Venkataraman et al., 2024). The difference between the control and each zero-out simulation approximates the influence of that sector on $PM_{2.5}$, while the residual between total $PM_{2.5}$ and the sum of sectoral contributions is attributed to other sources, including biogenic emissions, liquid-water in aerosols, natural dust, forest fires, and grassland fires (Lal et al., 2025). Recognizing the non-linearity of atmospheric chemistry, these contributions should be interpreted as indicative source influences rather than exact "shares," and are best viewed as representative source profiles.

Furthermore, due to the non-linear nature of atmospheric chemical processes and interactions among precursor species, the $PM_{2.5}$ response to emission reductions from individual sectors is not strictly additive (Lal et al., 2025; Venkataraman et al., 2024). As a result, the contribution estimated from a given zero-out simulation reflects the system's sensitivity to the removal of that sector under the prevailing atmospheric conditions and the emission inventory used in this study, rather than its exact standalone fractional attribution (Pandey et al., 2014; Venkataraman et al., 2024). Consequently, the sum of individual sectoral contributions may differ from the total $PM_{2.5}$ burden, and these values should be interpreted as indicative measures of relative sectoral influence rather than precise quantitative shares (Singh et al., 2021). These estimates are therefore best viewed as representative sensitivity-based indicators, consistent with the inherent limitations of numerical modelling, including uncertainties associated with initial and boundary conditions, emission inputs, and process parameterizations. In this work, we have used the best available high-resolution, India-specific emission inventory, SMoG-COALESCE (Venkataraman et al., 2024), to minimize such uncertainties; however, residual limitations remain

(Lal et al., 2025; Pandey et al., 2014). These constraints are intrinsic to sensitivity-based modelling approaches and should be considered when interpreting the results, particularly in the context of designing multi-sector mitigation strategies.

We represent $PM_{2.5}$ composition using the dominant mass components: BC, organic aerosols (OA), nitrate (NO_3^-), sulfate (SO_4^{2-}), and ammonium (NH_4^+) (Bhattu et al., 2024; Mogno et al., 2021). The difference between total $PM_{2.5}$ and the sum of these components is grouped as "Others," which includes remaining inorganic species, aerosol water, and natural dust (Rathore et al., 2025). Primary $PM_{2.5}$ is defined as mass directly emitted (including BC, primary organic carbon, Na^+, Cl^-, other primary inorganic compounds, liquid water associated with primary particles, and natural dust), whereas secondary $PM_{2.5}$ comprises NO_3^-, SO_4^{2-}, NH_4^+, and SOA produced through atmospheric transformation and partitioning (Kumar et al., 2025).

Given the complexity of $PM_{2.5}$ formation in highly polluted environments and unavoidable uncertainties in emission inventories and chemical parameterizations, the source apportionment results are best interpreted as approximate but policy-informative diagnostics. Despite these limitations, the resulting sectoral fingerprints and composition patterns provide quantitative evidence that can directly inform city- and state-level action plans and help prioritize mitigation pathways. The WRF-Chem configuration and the complete set of source-apportionment simulations are summarized in Table 4.1.

Table 4.1: WRF-Chem model setup for source apportionment of $PM_{2.5}$.

Sl No.	Emissions	Simulation Name
0	SMoG-COALESCE (v2) (BC, OC, SO_2, NH_3, CO, NO_x, $PM_{2.5}$, PM_{10}), EDGAR-v5 (VOCs) & BB Emission	Control
1	Over Domain All Sector Emission 100% & Over Domain BB Emission 0%	0BB DOM
2	Over Domain Residential Sector Emission 0% & Over Domain BB Emission 100%	0RES DOM
3	Over Domain Transport Sector Emission 0% & Over Domain BB Emission 100%	0TRA DOM
4	Over Domain Industry Sector Emission 0% & Over Domain BB Emission 100%	0IND DOM
5	Over Domain Energy Sector Emission 0% & Over Domain BB Emission 100%	0ENE DOM
6	Over Domain Agriculture Sector Emission 0% & Over Domain BB Emission 100%	0AGR DOM
7	Over Domain Trash Sector Emission 0% & Over Domain BB Emission 100%	0TRASH DOM

4.2.3 Validation of WRF-Chem simulated $PM_{2.5}$ concentrations

We first evaluate the WRF-Chem control simulation against multiple observational products to establish confidence in the simulated magnitude, spatial distribution, and temporal evolution of $PM_{2.5}$. Model surface $PM_{2.5}$ is compared with (i) a satellite-derived $PM_{2.5}$ product (Katoch et al., 2023), (ii) CPCB monitoring observations, and (iii) MERRA-2 reanalysis. For CPCB, only sites with at least 140 valid daily $PM_{2.5}$ values out of 153 days (September 2019-January 2020) are retained to ensure statistical robustness. Given known issues in CPCB data quality and continuity (Barrero et al., 2015; Sharma et al., 2022; Vohra et al., 2025), we apply rigorous QC procedures, removing statistical outliers and excluding periods with constant or obviously erroneous values (Singh et al. 2020; Zhou et al. 2024). Model performance is quantified using MAE, Pearson's r, and RMSE (Sharma et al., 2023). In addition to total $PM_{2.5}$, we evaluate key constituents (BC, OA, and $SO4^{2-}$) to diagnose whether the model captures both primary emissions variability and the seasonal evolution of secondary aerosol formation.

4.3 Results and Discussion

4.3.1 Validation using satellite-derived $PM_{2.5}$, CPCB measurements and MERRA-2 reanalysis

A scientifically robust sectoral attribution and chemical interpretation hinges on whether the control simulation reproduces the observed $PM_{2.5}$ behaviour across the NCT-Delhi airshed specifically (i) the spatial gradients from upwind agricultural states to downwind urban receptors, (ii) the seasonal transition from monsoon-influenced conditions into post-monsoon accumulation and winter stagnation, and (iii) the day-to-day variability driven by changing ventilation and episodic emissions such as crop-residue burning (CRB). We therefore evaluate WRF-Chem $PM_{2.5}$ using three complementary observational constraints: satellite-derived $PM_{2.5}$ (spatial completeness and regional gradients), CPCB monitoring (in situ temporal fidelity in populated and urban environments), and MERRA-2 reanalysis (a consistent reanalysis framework that also enables speciated comparisons for selected aerosol constituents).

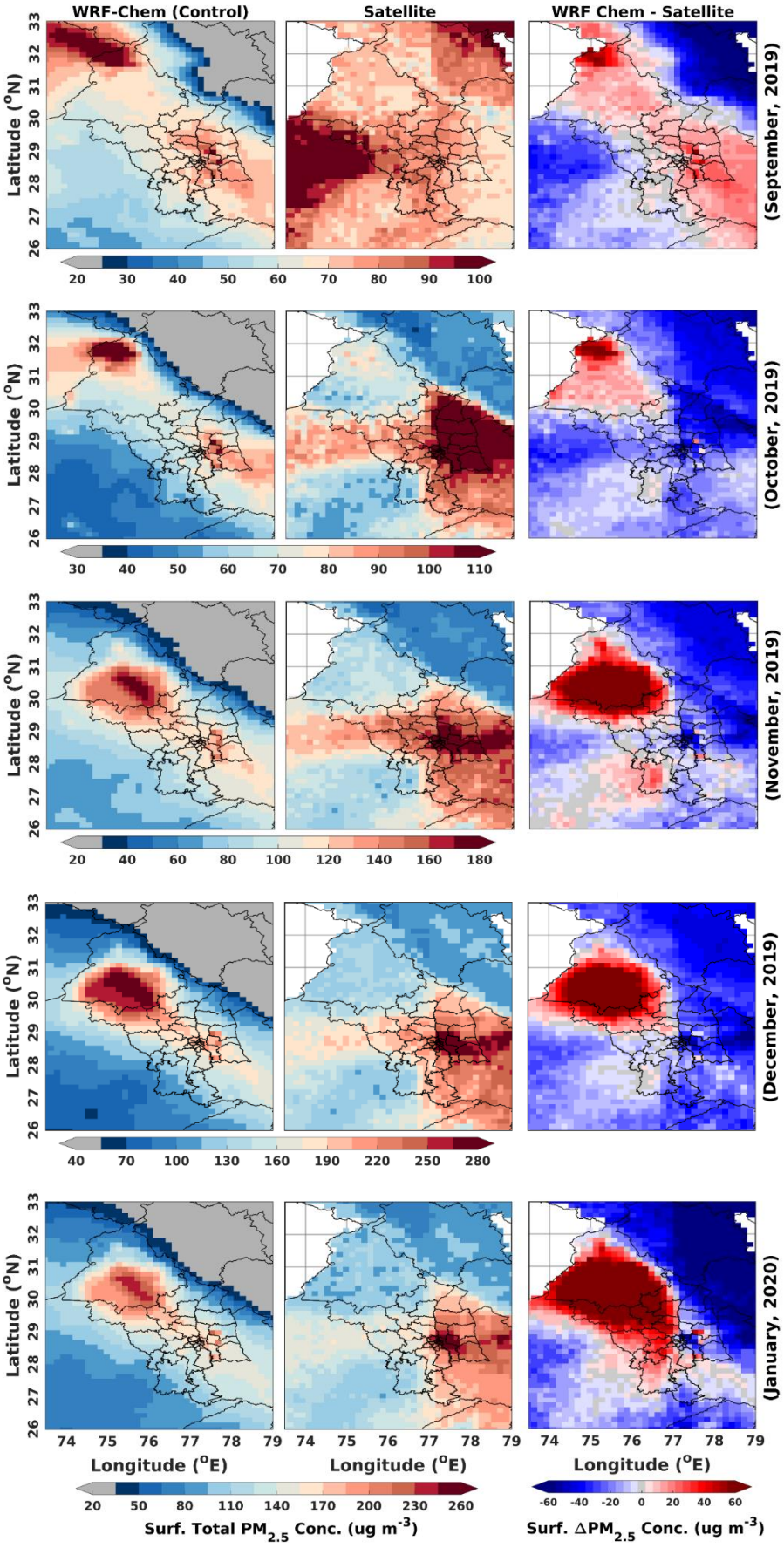


Figure 4.4: Monthly spatial distributions of surface $PM_{2.5}$ over North India from satellite-derived estimates and the WRF-Chem control simulation, along with the corresponding spatial bias fields illustrating areas of model underestimation and overestimation.

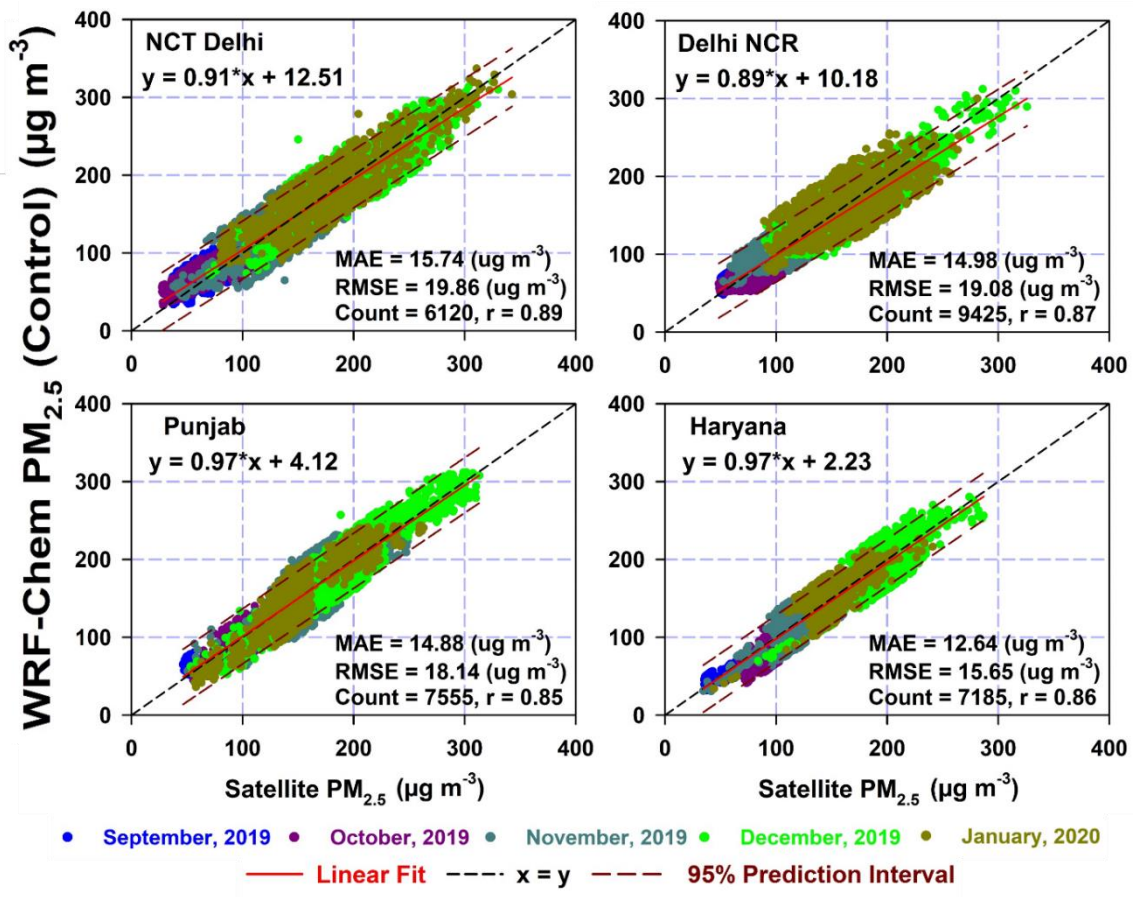


Figure 4.5: Comparison of 24-hour satellite-derived $PM_{2.5}$ concentrations with corresponding values from the WRF-Chem control simulation across NCT-Delhi, Delhi-NCR, Haryana, and Punjab for the entire study period. The slope-intercept form of the linear regression fit and associated statistical metrics are shown within each panel.

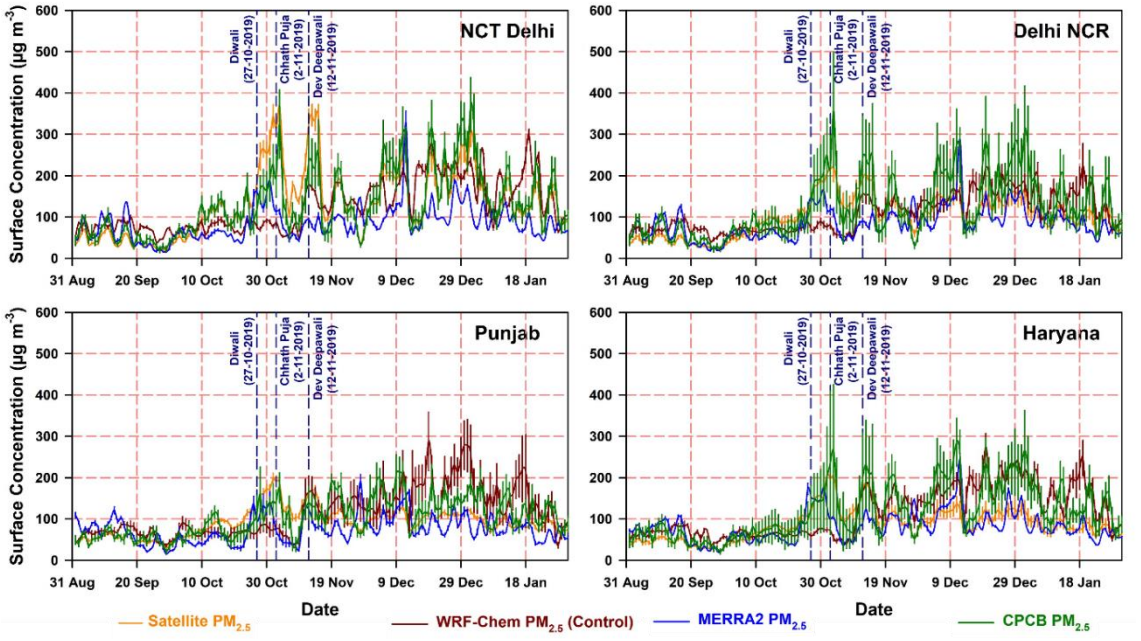


Figure 4.6: Daily mean time-series of surface $PM_{2.5}$ concentrations (µg m^{-3}) over the study period, comparing CPCB observations, satellite-derived estimates, the WRF-Chem control simulation, and MERRA-2 reanalysis for NCT-Delhi, Delhi-NCR, Haryana, and Punjab.

Across the four agriculturally intensive regions emphasized in this chapter, the WRF-Chem control simulation exhibits strong agreement with satellite-derived $PM_{2.5}$ (Fig. 4.4), with Pearson correlation coefficients ranging from 0.85 to 0.89 and RMSE values of 15.65-19.86 μg m^{-3}. The near consistency of regression slopes across regions (Fig. 4.5) provides evidence that the model captures not only co-variability but also a broadly coherent sensitivity of $PM_{2.5}$ to seasonal meteorology and regional emission patterns. Mechanistically, this indicates that (a) the ERA5-driven meteorological forcing and grid-nudging strategy are sufficiently constraining synoptic-to-mesoscale transport pathways relevant for the Indo-Gangetic Plain and the NCT-Delhi airshed, and (b) the adopted emissions and chemistry representation reproduce the large-scale spatial contrast between the agricultural burning corridor (Punjab-Haryana) and the downwind urban receptor region (Delhi-NCR). The implication is that the control simulation provides an adequate process-realistic baseline for interpreting the sectoral perturbation experiments and the inferred chemical composition changes later in Section 4.3.2.

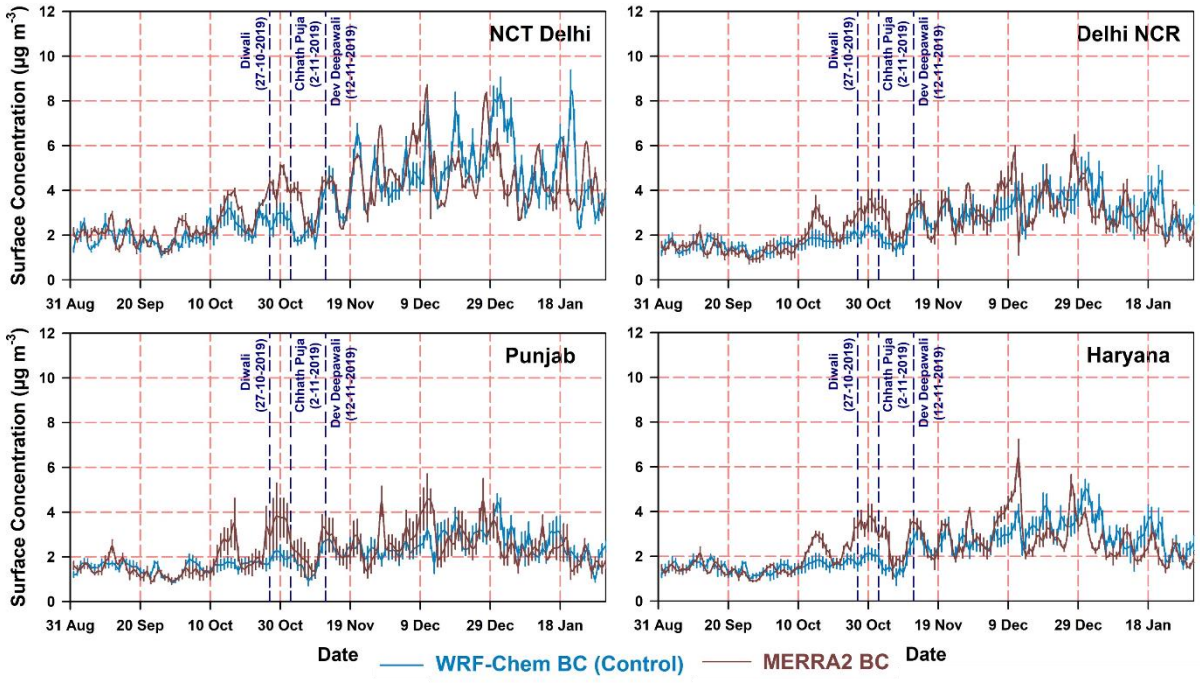


Figure 4.7: Daily mean time-series comparison of surface Black Carbon (BC) concentrations (μg m^{-3}) from the WRF-Chem control simulation and MERRA-2 reanalysis for NCT-Delhi, Delhi-NCR, Haryana, and Punjab over the full study period.

Comparisons with CPCB observations indicate moderate-to-good agreement (Fig. 4.6), supporting the model's ability to capture the observed temporal evolution of surface $PM_{2.5}$. Skill, however, degrades when evaluated against MERRA-2, especially during the peak CRB months (October–November) and in winter (December-January), when atmospheric stability is strongest and boundary-layer mixing is most suppressed (Fig. 4.6). Such seasonally varying performance is expected over northern India because wintertime $PM_{2.5}$ is highly sensitive to small biases in

boundary-layer height, near-surface winds, and stability: even modest underestimation of mixing height or wind speed can yield large concentration overestimates, while excessive mixing or overly strong scavenging can lead to underestimation. The mechanism–evidence link is reflected in the seasonal cycle itself: agreement weakens for NCT-Delhi and Punjab in winter but improves during post-monsoon conditions (Fig. 4.6), consistent with the shift from relatively ventilated conditions toward stagnation-dominated accumulation. The implication is that wintertime absolute concentrations should be interpreted cautiously, but the model can still provide credible relative sensitivities, particularly when the timing of stagnation and CRB episodes is well captured.

On average, WRF-Chem shows a systematic tendency to overestimate $PM_{2.5}$, and this bias manifests spatially as overprediction over Punjab and underprediction over Delhi-NCR and Haryana (Fig. 4.4). Several plausible and not mutually exclusive mechanisms can generate this spatial dipole. Overprediction in Punjab may reflect (i) overestimation of CRB emissions magnitude or duration, (ii) insufficient removal via wet scavenging or dry deposition during burning days, and/or (iii) overly efficient secondary aerosol formation in smoke-influenced plumes. Conversely, underprediction over Delhi-NCR and Haryana can arise from (i) unresolved sub-grid urban heterogeneity and near-road hotspots within a 5 km grid cell, (ii) underrepresentation of local resuspension/fugitive dust and other coarse-to-fine contributions, and/or (iii) biases in nocturnal stability and urban canopy effects that affect near-surface mixing and pollutant trapping. In parallel, satellite-derived $PM_{2.5}$ products represent spatially averaged conditions and are sensitive to aerosol vertical distribution and humidity, while CPCB observations, despite rigorous quality control, may still reflect site-specific artefacts and representativeness issues. Thus, perfect closure among satellite, CPCB, and MERRA-2 should not be expected. Instead, model performance should be judged primarily on whether the control run reproduces the month-to-month rise into winter and the timing and relative magnitude of regional enhancements during CRB and stagnation events (Fig. 4.4-4.6), which are the key dynamical regimes governing the airshed's high-$PM_{2.5}$ season.

The model captures the overall seasonal evolution of $PM_{2.5}$ reasonably well and performs best during the monsoon-influenced part of the period, whereas reduced winter skill likely reflects compounded challenges that are widely recognized for regional models over India, including topographic influences on boundary-layer structure, surface moisture and soil temperature biases that control stability, and errors in low-level moisture transport (Rakesh et al., 2009; Ratnam at al., 2005). Mechanistically, winter in the Indo-Gangetic Plain is characterized by shallow nocturnal boundary layers and persistent inversions; under such conditions, land-atmosphere coupling and turbulence closure become decisive for surface $PM_{2.5}$. The implication for this chapter is that

sectoral attribution should be interpreted as an *effective influence* under realistic meteorology, rather than as an exact deterministic partitioning that would be invariant to model structural uncertainty.

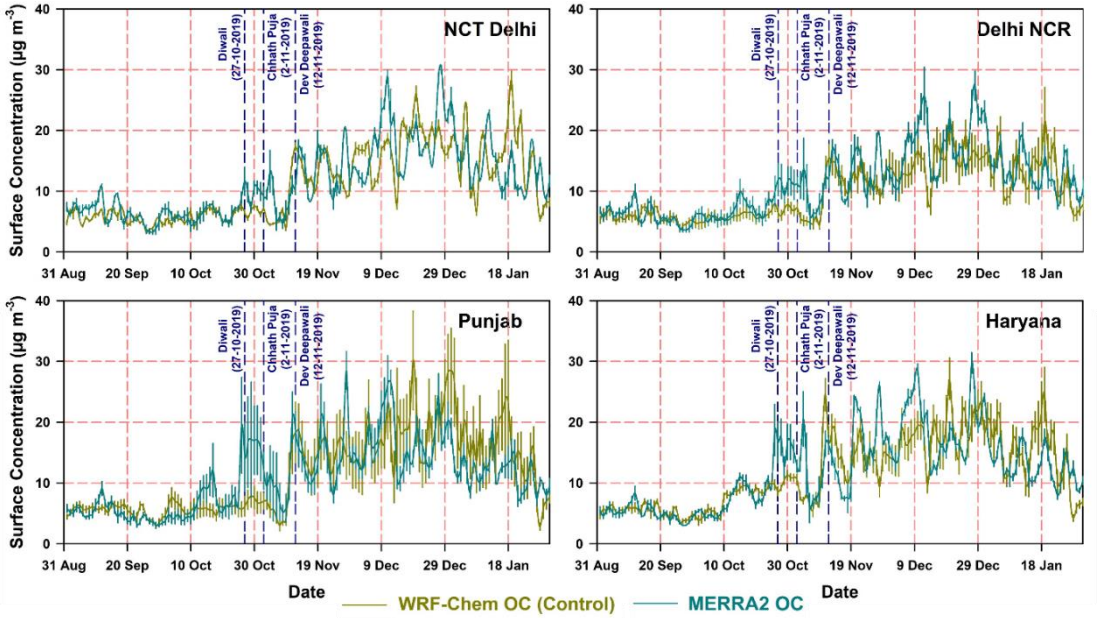


Figure 4.8: Daily mean time-series comparison of surface Organic Carbon (OC) concentrations (µg m^{-3}) from the WRF-Chem control simulation and MERRA-2 reanalysis for NCT-Delhi, Delhi-NCR, Haryana, and Punjab over the full study period.

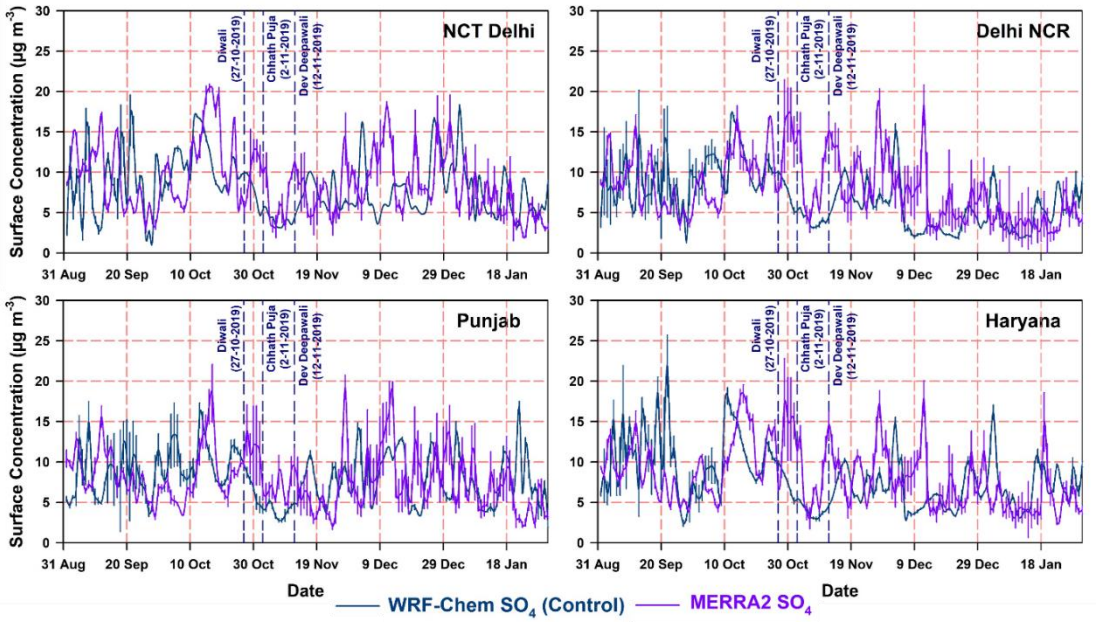


Figure 4.9: Daily mean time-series comparison of surface sulfate (SO_4^{2-}) concentrations (µg m^{-3}) from the WRF-Chem control simulation and MERRA-2 reanalysis for NCT-Delhi, Delhi-NCR, Haryana, and Punjab across the entire study period.

Beyond total $PM_{2.5}$, consistency in key aerosol constituents provides a stronger test of whether emissions and chemistry are behaving plausibly in the control simulation. The daily mean time series indicates that WRF-Chem reproduces the temporal variability of black carbon (BC)

(Fig. 4.7), organic carbon (OC) (Fig. 4.8), and sulfate (SO_4^{2-}) (Fig. 4.9) reasonably well relative to MERRA-2. The mechanism–evidence link is that BC and OC variability closely tracks combustion emissions and transport, whereas sulfate additionally reflects oxidation pathways and regional precursor availability; capturing these simultaneously suggests that both primary emissions and secondary processing are represented with reasonable fidelity. Nevertheless, residual discrepancies likely reflect uncertainties in meteorological fields (wind speed/direction, boundary-layer height, temperature, humidity) and limitations in atmospheric chemistry (secondary formation pathways, photolysis rates, and deposition processes). Although multiple combinations of physics and chemistry parameterizations were tested (Chapter 2), some structural biases remain difficult to remove completely. Accurate representation of emissions, particularly diurnal and seasonal variability, is therefore critical for skill, and the use of the SMoG-COALESCE 2019 inventory, closely aligned with the simulation period and provided at high spatial resolution, likely contributes to the improved representation of primary pollutants in this modelling framework.

4.3.2 Sectoral Contributions and Chemical Composition of $PM_{2.5}$ in the NCT-Delhi Airshed

To interpret the mitigation scenarios in a process-based and policy-relevant framework, we use the source-apportionment simulations (Table 4.1) to quantify sectoral influences and compositional contributions to surface $PM_{2.5}$ over the NCT-Delhi airshed and the broader northern India region. Having established that the control simulation reproduces the dominant spatiotemporal behaviour of $PM_{2.5}$ (Section 4.3.1), we now link mechanism, evidence, and implication: (i) how emissions, transport, and chemistry create the observed seasonal and spatial patterns; (ii) how these mechanisms are reflected in the sectoral and species diagnostics (Fig. 4.10-4.14; Tables 4.2-4.5); and (iii) what the results imply for prioritizing mitigation strategies that can meaningfully reduce both baseline and episodic $PM_{2.5}$ in NCT-Delhi.

4.3.2.1 Sectoral Influences and Seasonal Structure of the Airshed Burden

Over NCT-Delhi, the residential sector emerges as the dominant contributor, accounting for ~53% of total $PM_{2.5}$ over the study period (Fig. 4.10), consistent with previous analyses for the NCT-Delhi airshed (Kumar et al., 2025). Mechanistically, this dominance reflects three reinforcing features of residential emissions in northern India: they are spatially extensive (distributed across rural-urban gradients), temporally persistent (daily and seasonal rather than confined to short episodes), and particularly impactful during winter when low ventilation prolongs pollutant residence times. The implication is that even strong controls on traffic or industry may yield limited

sustained gains if residential combustion emissions across the airshed remain high, because they maintain the baseline burden onto which episodic contributions (e.g., CRB) are superimposed.

Organic aerosols (OA) account for ~55% of $PM_{2.5}$ mass over NCT-Delhi (Table 4.2), with smaller contributions from BC, sulfate, nitrate, ammonium, and a residual "Other" category. Across northern India more broadly, OA contributes over 50% of surface $PM_{2.5}$, consistent with earlier reports (Rathore et al., 2025) (Fig. 4.11). Mechanistically, OA dominance indicates the combined importance of primary organic emissions from combustion and secondary organic aerosol (SOA) formation via VOC oxidation. The implication is that effective mitigation must treat OA as both a primary and secondary problem: controlling direct combustion emissions reduces primary OA and BC, while reducing VOCs targets the secondary fraction that persists even when primary PM is partially curtailed.

In September 2019, when monsoon dynamics still exert influence, "Other sources" contribute up to ~15% of surface $PM_{2.5}$ over NCT-Delhi (Fig. 4.12; Table 4.2). This is mechanistically consistent with a larger role of aerosol water and transported dust under transitional meteorology, both of which can increase mass that is not straightforwardly attributable to a single anthropogenic sector. The implication is that early-season $PM_{2.5}$ can be comparatively less responsive to direct anthropogenic controls, reinforcing the need for seasonally informed expectations when evaluating mitigation performance.

Contributions from transport (~13%), industry (~6%), and energy (~5%) remain comparatively stable across seasons (Fig. 4.12; Table 4.2), indicating that mitigation in these sectors yields year-round benefits rather than improvements limited to the high-pollution months. Mechanistically, these sectors are tied to persistent urban and peri-urban activity patterns, and their emissions contribute to both primary PM and the precursor pool for secondary formation. The implication is that sustained controls in these sectors are essential for long-term exposure reduction, even if they do not fully eliminate the extreme episodes driven by regional burning and stagnation.

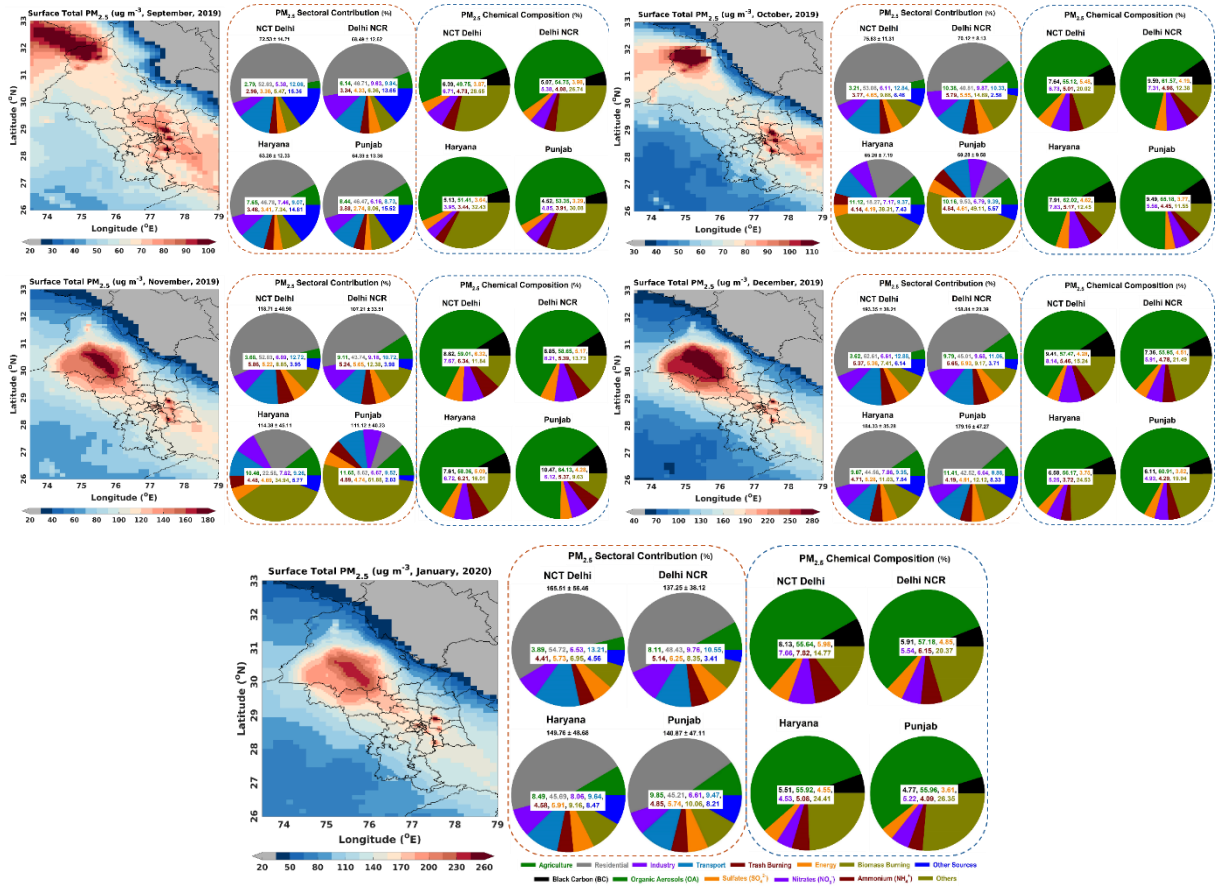


Figure 4.10: Monthly spatial distribution of surface $PM_{2.5}$ concentrations over northern India from the WRF-Chem control simulation (left panel). The middle panel shows monthly pie charts of sectoral contributions to surface $PM_{2.5}$ across four agriculturally and economically significant northern Indian states, derived from the emission-perturbed WRF-Chem simulations. The right panel presents corresponding monthly pie charts of $PM_{2.5}$ chemical composition from the control simulation. Mean percentage contributions for each sector or chemical species are indicated within the respective charts.

Table 4.2: Monthly sectoral contributions and chemical composition of surface $PM_{2.5}$ derived from the WRF-Chem control simulation over NCT-Delhi.

NCT-Delhi								
Surface $PM_{2.5}$ Sectoral Contribution (%) ($\mu \pm 1\sigma$)								
Sectors	**Agriculture**	**Residential**	**Industry**	**Transport**	**Trash Burning**	**Energy**	**Biomass Burning**	**Other Sources**
Sep, 2019	2.79 ± 0.76	52.63 ± 7.84	5.38 ± 0.97	12.06 ± 1.33	2.96 ± 1.21	3.36 ± 1.92	5.47 ± 2.77	15.35 ± 9.84
Oct, 2019	3.21 ± 1.36	53.08 ± 6.99	6.11 ± 2.58	12.84 ± 2.61	3.77 ± 2.57	4.65 ± 2.75	9.88 ± 3.93	6.46 ± 3.09
Nov, 2019	3.68 ± 2.66	52.83 ± 10.45	6.89 ± 2.33	12.72 ± 2.21	5.86 ± 2.14	5.22 ± 1.62	8.85 ± 4.83	3.95 ± 2.86
Dec, 2019	3.62 ± 1.62	52.61 ± 8.83	6.61 ± 2.17	12.88 ± 1.52	5.37 ± 2.62	5.36 ± 1.31	7.41 ± 3.97	6.14 ± 3.33
Jan, 2020	3.89 ± 2.16	54.72 ± 9.91	6.53 ± 3.28	13.21 ± 2.06	4.41 ± 2.86	5.73 ± 1.23	6.95 ± 3.01	4.56 ± 2.77
Surface $PM_{2.5}$ Chemical Composition (%) ($\mu \pm 1\sigma$)								
Species	**BC**	**OA**	**SO_4^{2-}**	**NO_3^-**	**NH_4^+**	**Other**		
Sep, 2019	6.39 ± 0.69	49.75 ± 6.03	3.87 ± 2.52	6.71 ± 4.34	4.73 ± 3.64	28.55 ± 10.08		
Oct, 2019	7.64 ± 0.71	55.12 ± 3.86	5.48 ± 2.36	6.73 ± 4.05	5.01 ± 2.58	20.02 ± 10.53		
Nov, 2019	8.82 ± 1.53	59.01 ± 5.59	6.32 ± 2.26	7.67 ± 4.28	6.34 ± 4.79	11.84 ± 9.37		
Dec, 2019	9.41 ± 1.89	57.47 ± 5.53	4.28 ± 3.34	8.14 ± 5.21	5.46 ± 2.72	15.24 ± 11.84		
Jan, 2020	8.13 ± 1.87	55.64 ± 6.82	5.98 ± 3.80	7.66 ± 3.73	7.82 ± 3.18	14.77 ± 11.98		

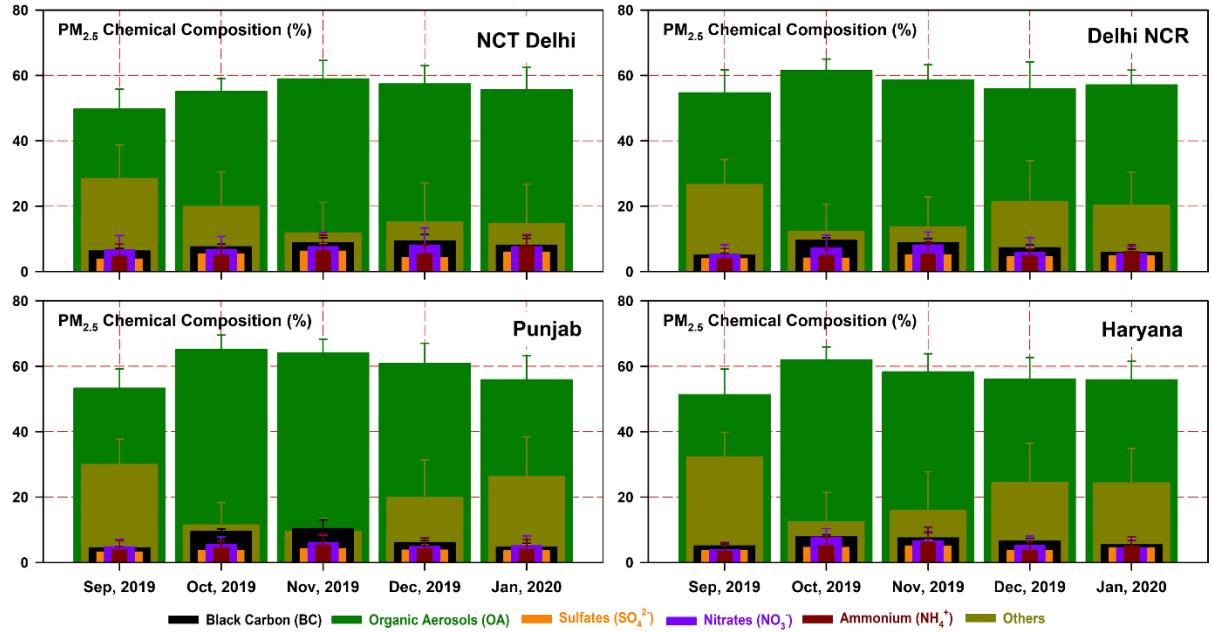


Figure 4.11: Monthly chemical composition of surface $PM_{2.5}$ across the selected northern Indian states, presented as bar charts and derived from the WRF-Chem control simulation.

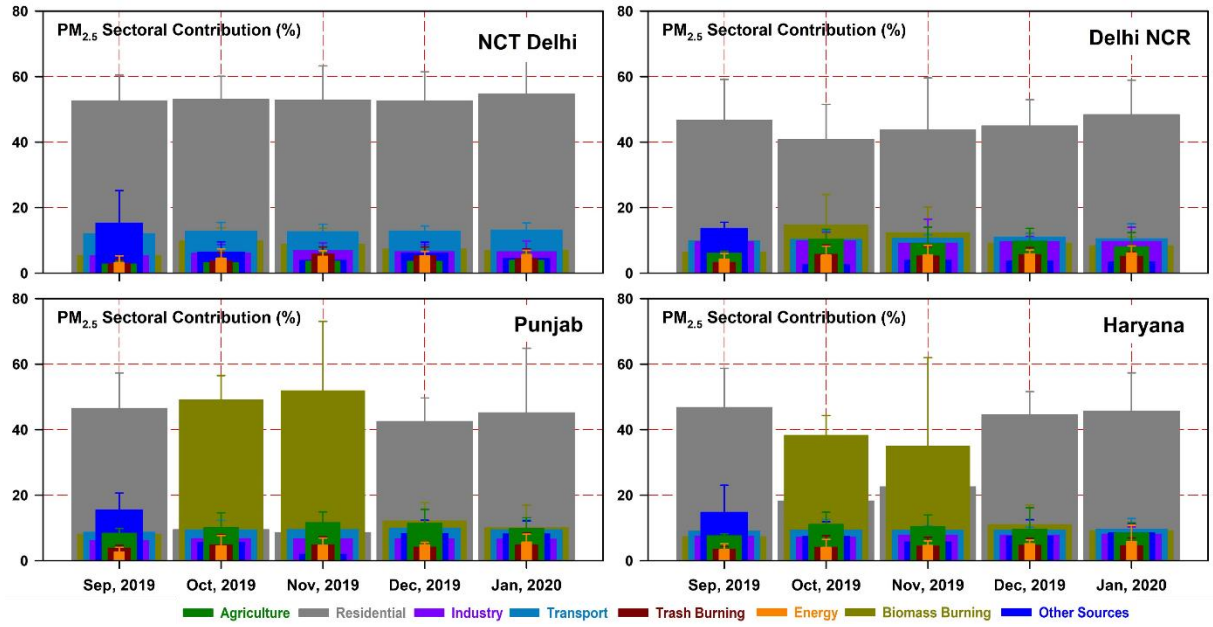


Figure 4.12: Monthly sectoral contributions to surface $PM_{2.5}$ concentrations across four agriculturally and economically significant states in northern India, illustrated through bar charts and derived from the suite of WRF-Chem emission-perturbed simulations.

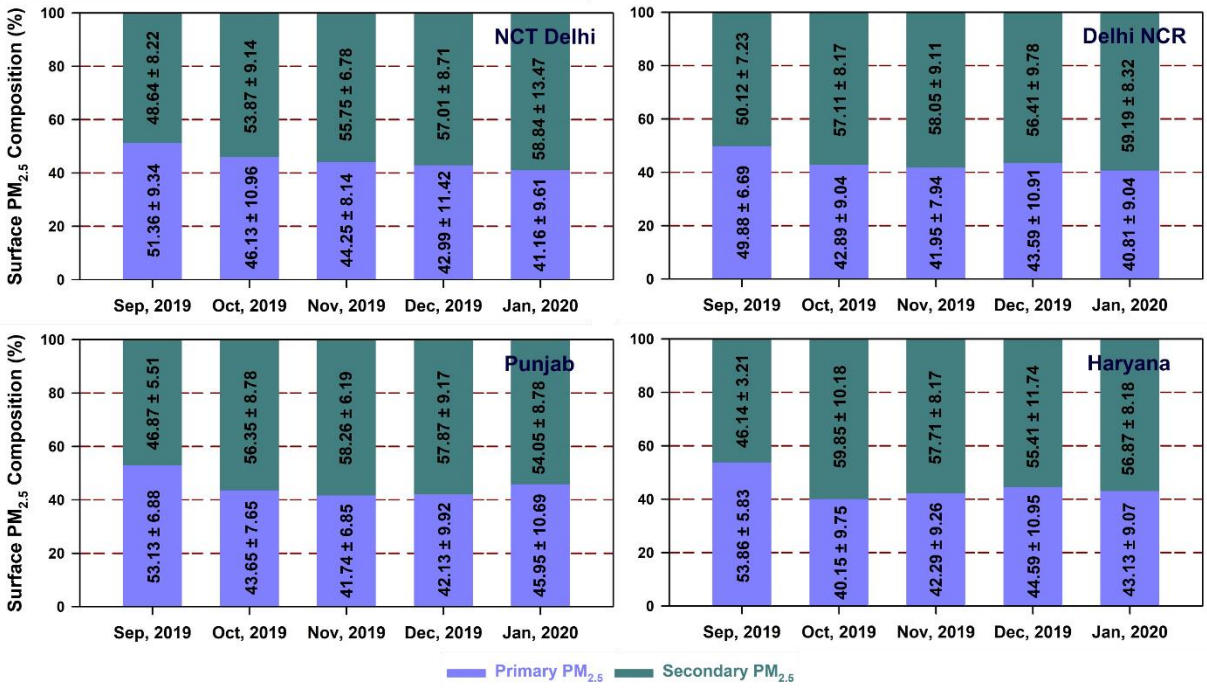


Figure 4.13: Monthly stacked bar charts showing the relative contributions of primary and secondary $PM_{2.5}$ to surface $PM_{2.5}$ concentrations over NCT-Delhi, Delhi-NCR, Punjab, and Haryana, based on the WRF-Chem control simulation. Mean contributions ($\mu \pm 1\sigma$) for each component are indicated within the bars.

4.3.2.2 Primary versus Secondary $PM_{2.5}$: Dominance of Secondary Formation in Winter

A central compositional result is the dominance of secondary aerosols across the high-pollution season. During winter (December 2019-January 2020), secondary $PM_{2.5}$ dominates over primary $PM_{2.5}$ across northern India, with ~57% of surface $PM_{2.5}$ (and ~58% over NCT-Delhi) attributed to secondary aerosol formation (Fig. 4.13). During the post-monsoon months (October–November 2019), secondary $PM_{2.5}$ again predominates over NCT-Delhi, contributing ~55% of total mass. In contrast, during September, primary $PM_{2.5}$ accounts for ~53% of the total across the region, consistent with stronger dust influence from arid western deserts (Dey et al., 2010; Singh et al. 2021). Mechanistically, winter stagnation enhances gas-to-particle conversion by increasing atmospheric residence time and aerosol surface area, while the regional abundance of NO_x, SO_2, and NH_3 supports sustained formation of nitrate–ammonium and sulfate. The implication is that wintertime mitigation cannot be achieved by primary PM controls alone; it also requires precursor controls (NO_x, SO_2, NH_3, and VOCs) that directly target secondary formation pathways.

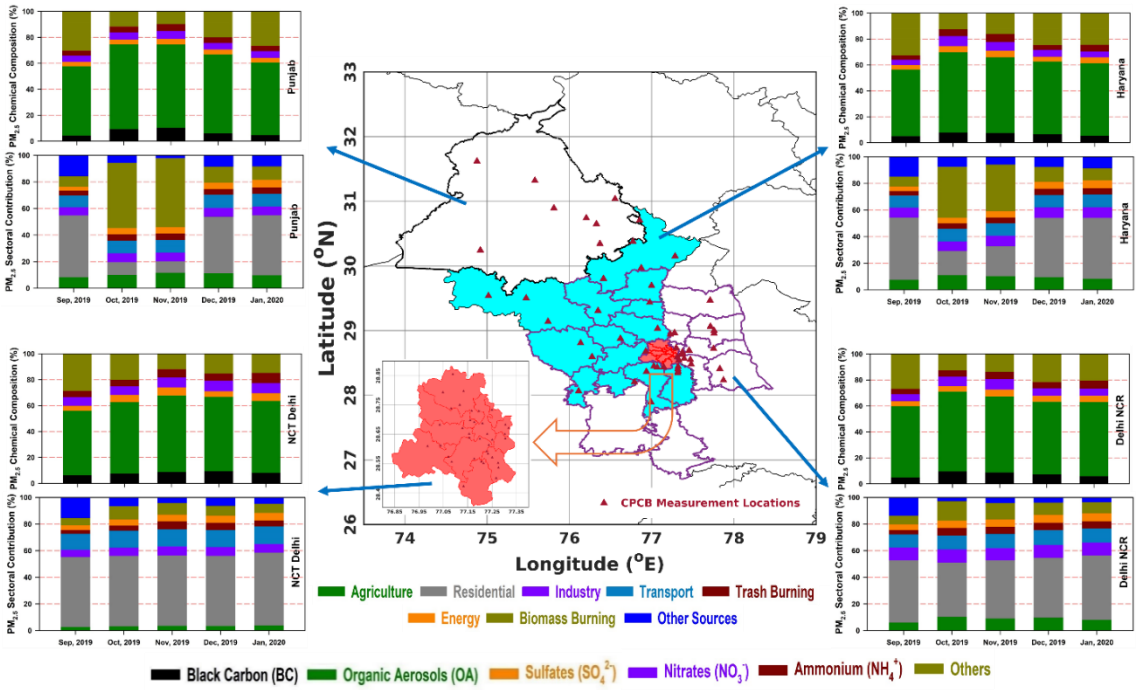


Figure 4.14: Monthly stacked bar charts showing sectoral contributions and chemical composition of surface $PM_{2.5}$ from WRF-Chem control and emission-perturbed simulations for the period September 2019-January 2020.

The limited seasonal variability in the fractional contributions of secondary inorganic aerosol (SIA) components, SO_4^{2-} (~5%), NO_3^- (~7%), and NH_4^+ (~6%), (Fig. 4.13; Table 4.2) suggests that while absolute $PM_{2.5}$ levels rise markedly into winter, the chemical mixture retains a broadly similar balance among secondary components. Mechanistically, this indicates that wintertime concentration increases are driven more by enhanced accumulation and efficient partitioning under stagnant conditions than by a fundamentally different chemical regime. The implication is that interventions that lower the regional precursor pool are likely to reduce $PM_{2.5}$ across multiple months, but their visible benefits will be largest during periods when meteorology amplifies accumulation.

4.3.2.3 Regional heterogeneity and the role of CRB in extreme episodes

BC concentrations over NCT-Delhi show a modest but distinct enhancement during peak CRB episodes (Fig. 4.11), reflecting advection of biomass-burning plumes from Punjab and Haryana. Mechanistically, CRB emits OA-rich and BC-containing smoke that is efficiently transported downwind under prevailing north-westerly flows, elevating receptor-region concentrations even when local emissions remain unchanged. The implication is that reducing CRB yields dual benefits: lowering $PM_{2.5}$ mass and reducing the light-absorbing BC fraction during the most polluted season, which is relevant for both health impacts and radiative forcing considerations.

Table 4.3: Monthly sectoral contributions and chemical composition of surface $PM_{2.5}$ derived from the WRF-Chem control simulation over Haryana.

Haryana								
Surface $PM_{2.5}$ Sectoral Contribution (%) (μ ± 1σ)								
Sectors	**Agriculture**	**Residential**	**Industry**	**Transport**	**Trash Burning**	**Energy**	**Biomass Burning**	**Other Sources**
Sep, 2019	7.65 ± 0.56	46.78 ± 11.92	7.46 ± 0.65	9.07 ± 0.59	3.48 ± 0.76	3.41 ± 1.76	7.34 ± 2.99	14.81 ± 2.20
Oct, 2019	11.12 ± 3.65	18.27 ± 12.51	7.17 ± 3.22	9.37 ± 3.23	4.14 ± 3.42	4.19 ± 3.30	38.31 ± 5.97	7.43 ± 4.44
Nov, 2019	10.46 ± 4.47	22.58 ± 5.09	7.82 ± 2.27	9.26 ± 1.34	4.48 ± 2.67	4.69 ± 1.36	34.94 ± 7.01	5.77 ± 3.28
Dec, 2019	9.67 ± 2.46	44.56 ± 6.99	7.86 ± 1.28	9.35 ± 0.86	4.71 ± 2.04	5.28 ± 0.98	11.03 ± 6.88	7.54 ± 4.98
Jan, 2020	8.49 ± 3.09	45.69 ± 11.64	8.06 ± 2.24	9.64 ± 2.22	4.58 ± 2.33	5.91 ± 2.88	9.16 ± 2.23	8.47 ± 2.59

Surface $PM_{2.5}$ Chemical Composition (%) (μ ± 1σ)						
Species	**BC**	**OA**	**SO_4^{2-}**	**NO_3^-**	**NH_4^+**	**Other**
Sep, 2019	5.13 ± 0.52	51.41 ± 7.73	3.64 ± 2.30	3.95 ± 5.21	3.44 ± 2.58	32.43 ± 7.38
Oct, 2019	7.91 ± 0.56	62.02 ± 3.86	4.62 ± 1.95	7.83 ± 7.52	5.17 ± 2.54	12.45 ± 8.98
Nov, 2019	7.61 ± 1.62	58.36 ± 5.50	5.09 ± 1.85	6.72 ± 6.74	6.21 ± 4.54	16.01 ± 11.71
Dec, 2019	6.58 ± 0.82	56.17 ± 6.46	3.75 ± 3.39	5.25 ± 6.82	3.72 ± 5.77	24.53 ± 11.91
Jan, 2020	5.51 ± 1.28	55.92 ± 5.65	4.55 ± 3.82	4.53 ± 4.41	5.08 ± 4.72	24.41 ± 10.48

The sectoral and composition diagnostics reveal strong spatial heterogeneity across Punjab-Haryana-Delhi-NCR. During the peak CRB season, biomass burning contributes ~50% of $PM_{2.5}$ in Punjab, ~36% in Haryana, and ~13% in Delhi-NCR (Fig. 4.14; Tables 4.3-4.5). In Punjab, approximately 65% of the biomass-burning-related $PM_{2.5}$ mass is OA (Fig. 4.14), while in Haryana ~60% is OA (Table 4.3); over Delhi-NCR, the CRB contribution is smaller in fractional terms but remains OA-dominated. Mechanistically, this pattern indicates that CRB is the dominant episodic driver in upwind agricultural states, while Delhi-NCR experiences a superposition of transported episodic smoke on a large locally sustained baseline dominated by residential and other anthropogenic sectors. The implication is that eliminating CRB would substantially reduce the frequency and intensity of extreme episodes, but sustained compliance and large reductions in annual exposure in NCT-Delhi also require deep reductions in residential combustion and persistent urban-sector emissions.

Across Delhi-NCR, Haryana, and Punjab, residential emissions contribute more than 40% of surface $PM_{2.5}$ (Fig. 4.14), but this contribution exhibits pronounced seasonal variability in Punjab and Haryana, where the residential share drops to ~15% during peak CRB months as biomass burning becomes the dominant source (Fig. 4.14). Mechanistically, this "share shift" occurs because episodic CRB adds a large additional aerosol burden that changes the fractional composition even if residential emissions do not decrease. The implication is that source contributions should be interpreted in both fractional and absolute terms: policies targeting residential emissions are critical for reducing the baseline year-round, while CRB interventions are essential for preventing seasonal spikes.

Table 4.4: Monthly sectoral contributions and chemical composition of surface $PM_{2.5}$ derived from the WRF-Chem control simulation over Delhi-NCR.

Delhi-NCR								
Surface $PM_{2.5}$ Sectoral Contribution (%) (μ ± 1σ)								
Sectors	**Agriculture**	**Residential**	**Industry**	**Transport**	**Trash Burning**	**Energy**	**Biomass Burning**	**Other Sources**
Sep, 2019	6.14 ± 0.52	46.71 ± 12.41	9.63 ± 3.68	9.84 ± 0.56	3.34 ± 0.73	4.33 ± 1.64	6.36 ± 3.13	13.65 ± 1.87
Oct, 2019	10.38 ± 3.01	40.81 ± 10.68	9.87 ± 2.60	10.33 ± 2.60	5.79 ± 2.77	5.55 ± 2.66	14.69 ± 9.35	2.58 ± 1.20
Nov, 2019	9.11 ± 4.88	43.74 ± 15.82	9.18 ± 7.31	10.72 ± 1.03	5.24 ± 2.80	5.65 ± 2.83	12.38 ± 7.80	3.98 ± 2.20
Dec, 2019	9.79 ± 3.82	45.01 ± 7.93	9.68 ± 1.54	11.06 ± 1.01	5.65 ± 2.15	5.93 ± 1.10	9.17 ± 3.21	3.71 ± 1.67
Jan, 2020	8.11 ± 4.32	48.43 ± 10.46	9.76 ± 4.21	10.55 ± 4.53	5.14 ± 1.32	6.25 ± 2.04	8.35 ± 2.65	3.41 ± 2.45
Surface $PM_{2.5}$ Chemical Composition (%) (μ ± 1σ)								
Species	**BC**	**OA**	**SO_4^{2-}**	**NO_3^-**	**NH_4^+**	**Other**		
Sep, 2019	5.07 ± 0.52	54.75 ± 6.95	3.98 ± 2.43	5.38 ± 2.80	4.08 ± 2.93	26.74 ± 7.53		
Oct, 2019	9.59 ± 0.73	61.57 ± 3.42	4.19 ± 1.80	7.31 ± 3.83	4.96 ± 2.44	12.38 ± 8.20		
Nov, 2019	8.85 ± 1.19	58.65 ± 4.57	5.17 ± 1.50	8.21 ± 3.87	5.39 ± 3.68	13.73 ± 9.14		
Dec, 2019	7.36 ± 0.82	55.95 ± 8.18	4.51 ± 2.78	5.91 ± 4.38	4.78 ± 2.20	21.49 ± 12.40		
Jan, 2020	5.91 ± 0.96	57.18 ± 4.50	4.85 ± 3.06	5.54 ± 2.14	6.15 ± 2.07	20.37 ± 9.98		

Table 4.5: Monthly sectoral contributions and chemical composition of surface $PM_{2.5}$ derived from the WRF-Chem control simulation over Punjab.

Punjab								
Surface $PM_{2.5}$ Sectoral Contribution (%) (μ ± 1σ)								
Sectors	**Agriculture**	**Residential**	**Industry**	**Transport**	**Trash Burning**	**Energy**	**Biomass Burning**	**Other Sources**
Sep, 2019	8.44 ± 1.42	46.47 ± 10.83	6.16 ± 0.51	8.73 ± 0.48	3.88 ± 0.85	2.74 ± 1.32	8.06 ± 1.79	15.52 ± 3.13
Oct, 2019	10.16 ± 4.45	9.53 ± 3.34	6.79 ± 3.07	9.39 ± 2.91	4.84 ± 3.12	4.61 ± 3.05	49.11 ± 7.42	5.57 ± 2.35
Nov, 2019	11.65 ± 3.23	8.62 ± 4.15	6.67 ± 2.66	9.52 ± 0.82	4.89 ± 3.41	4.74 ± 3.13	51.88 ± 21.17	2.03 ± 2.85
Dec, 2019	11.41 ± 2.26	42.52 ± 7.17	6.64 ± 0.68	9.88 ± 0.72	4.19 ± 1.56	4.91 ± 0.69	12.12 ± 5.56	8.33 ± 2.99
Jan, 2020	9.85 ± 4.25	45.21 ± 19.61	6.61 ± 2.28	9.47 ± 2.93	4.85 ± 3.55	5.74 ± 2.31	10.06 ± 6.86	8.21 ± 3.91
Surface $PM_{2.5}$ Chemical Composition (%) (μ ± 1σ)								
Species	**BC**	**OA**	**SO_4^{2-}**	**NO_3^-**	**NH_4^+**	**Other**		
Sep, 2019	4.52 ± 0.45	53.35 ± 5.84	3.29 ± 1.97	4.85 ± 2.27	3.91 ± 2.79	30.08 ± 7.61		
Oct, 2019	9.49 ± 0.74	65.18 ± 4.40	3.77 ± 1.46	5.56 ± 2.29	4.45 ± 2.03	11.55 ± 6.75		
Nov, 2019	10.47 ± 2.57	64.13 ± 4.12	4.28 ± 1.39	6.12 ± 2.21	5.37 ± 3.31	9.63 ± 8.90		
Dec, 2019	6.11 ± 0.58	60.91 ± 6.12	3.82 ± 1.64	4.93 ± 2.68	4.29 ± 3.14	19.94 ± 11.48		
Jan, 2020	4.77 ± 1.09	55.96 ± 7.29	3.61 ± 1.96	5.22 ± 2.90	4.09 ± 2.90	26.35 ± 12.12		

4.3.2.4 Comparison of Results with earlier literature and interpretation of residual mass

The agreement of sectoral and compositional shares with prior work strengthens confidence in the inferred source influences. Our estimated biomass-burning contribution (~34%) over NCR, Punjab, and Haryana during the CRB season is consistent with earlier modelling estimates (~32%) (Lal et al., 2025) (Fig. 4.12). Likewise, the ~5% shares from energy and waste burning and the ~10-12% shares from transport and industry over northern India align with

previous source-apportionment assessments (Kumar et al., 2025; Venkataraman et al., 2024) (Table 4.4 & 4.5). The estimated contributions of BC (~7%) and SO_4^{2-} (~6%) also closely match earlier estimates (Gani et al., 2019) (Tables 4.3 & 4.4), while NH_4^+ (~8%) and NO_3^- (~9%) are broadly consistent with prior findings (Lalchandani et al., 2021) (Fig. 4.14). Where discrepancies arise, they plausibly reflect differences in study period, meteorology, and emissions assumptions, but also the relatively higher "Other" fraction (~20%) in our simulations, which includes inorganic compounds, aerosol water, and natural dust and represents a substantial residual $PM_{2.5}$ mass (Mogno et al., 2021). Mechanistically, aerosol water and dust can vary strongly with humidity, wind speed, and surface conditions, and they may be represented differently across models and datasets. The implication is that while absolute values contain uncertainty, the hierarchy of dominant sources (residential baseline, CRB episodic dominance in Punjab–Haryana, and strong secondary formation in winter) is robust enough for policy-relevant interpretation.

Finally, the strong dominance of OA during the high-pollution season, together with the prevalence of secondary $PM_{2.5}$ (Fig. 4.13-4.14), highlights the importance of precursor control, especially VOCs, alongside primary PM emission reductions. Fig. 4.15 provides a precursor-emissions context that helps interpret this behaviour: the co-occurrence of high VOC emissions from EDGAR-v5 (2015) and strong NO_x, SO_2, and NH_3 emissions from SMoG-COALESCE (2019) creates a chemically favourable environment for both secondary organic aerosol (SOA) and secondary inorganic aerosol (SIA) formation. Mechanistically, this explains why secondary fractions remain large even when some primary-emitting sectors are mitigated. The implication is that effective airshed management requires coordinated strategies that jointly reduce primary PM and the precursor pool (VOC controls and NO_x/SO_2/NH_3 reductions), rather than treating $PM_{2.5}$ as primarily a direct-emission problem.

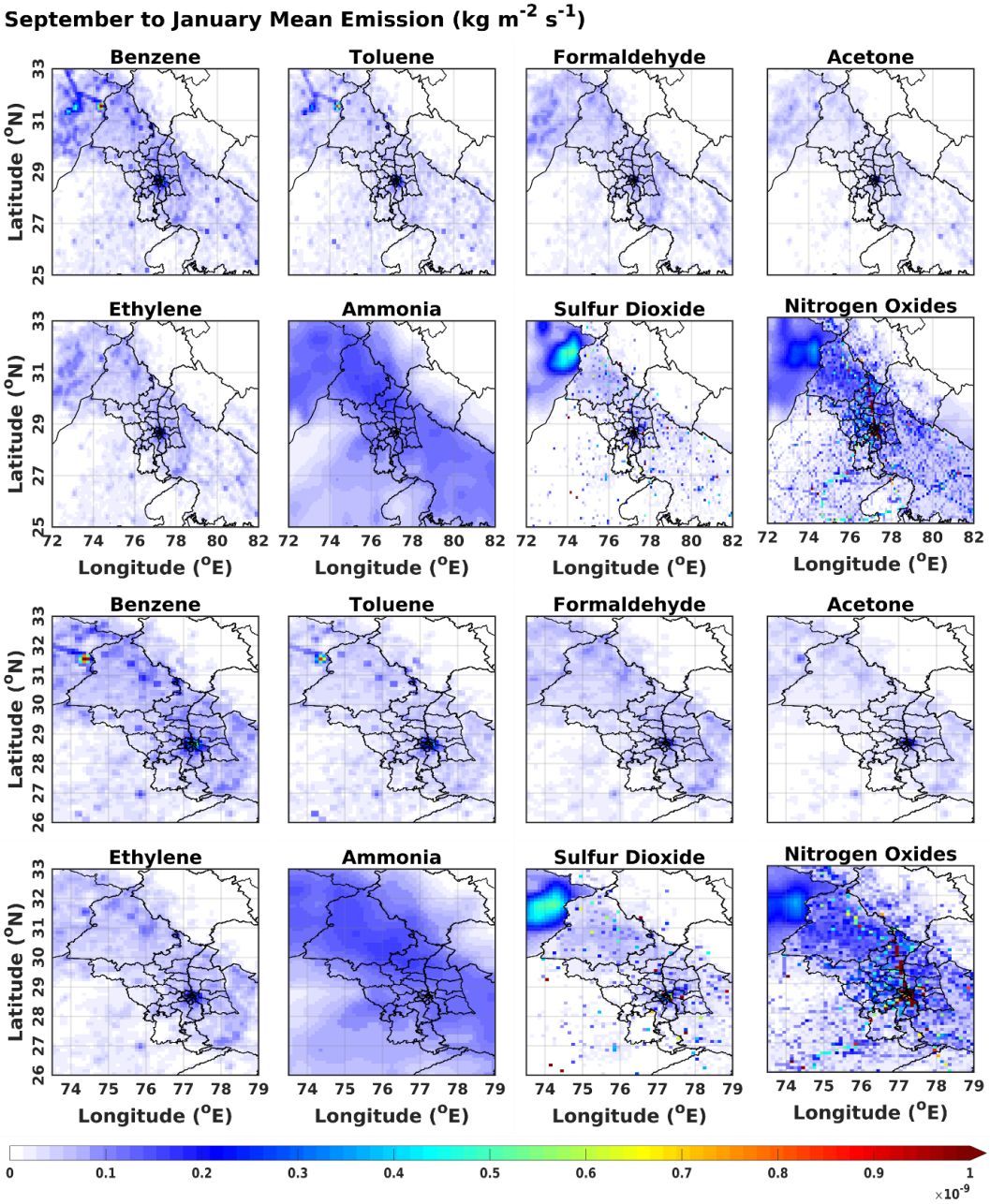


Figure 4.15: Spatial comparison of September-January mean emissions of major VOCs, Benzene, Toluene, Formaldehyde, Acetone, and Ethylene, from EDGAR-v5 (2015), alongside key gaseous precursors, NO_x, SO_2, and NH_3, from SMoG-COALESCE (2019). The top panels show the emission distributions across the broader North India domain, while the bottom panels present a zoomed-in view over the inner study region.

4.4 Summary and Conclusions

Improving ambient air quality has become a central priority of environmental policy in India. Under the National Clean Air Programme (NCAP), participating cities developed action plans that primarily emphasise within-city (in-boundary) emission controls. A key conclusion from

this chapter is that such an approach is intrinsically limited for northern India because transboundary transport from outside administrative boundaries can dominate or strongly modulate urban $PM_{2.5}$. In other words, the airshed, not the city boundary, is the scientifically appropriate unit for management. This motivates the core objective of this study: to identify the chemical and physical drivers responsible for persistently high $PM_{2.5}$ across northern India's agriculturally productive states and the NCT-Delhi airshed.

Using WRF-Chem simulations at high resolution (5 km) driven by a national, sector-resolved emission inventory and validated against both ground-based and satellite-derived $PM_{2.5}$ observations, we provide an integrated assessment of regional aerosol sources and composition. Residential biomass combustion for cooking and heating emerges as the dominant and most persistent contributor, responsible for approximately one-third of total $PM_{2.5}$ emissions across the broader domain and accounting for ~40-50% of surface $PM_{2.5}$ over key northern Indian states during much of the period. This result is especially consequential because residential emissions are spatially diffuse, occur year-round, and intensify in winter when ventilation is weakest. The implication is that large-scale transitions in household energy use can yield outsized benefits: transitioning the nearly 500 million biomass-dependent people to clean energy access and accelerating the shift from fossil fuels to renewable energy could collectively remove up to 62% of primary PM sources.

A second central conclusion is that secondary aerosol formation is a dominant driver of the $PM_{2.5}$ burden, especially for major urban receptors. Over NCT-Delhi, gas-to-particle conversion associated with SO_2, NO_x, NH_3, and VOC emissions yields a large secondary fraction; in winter, secondary $PM_{2.5}$ accounts for ~57% of total $PM_{2.5}$ over northern India and ~58% over NCT-Delhi (Fig. 4.15). This finding explains why Delhi can remain among the most polluted cities globally even when local primary emission controls are strengthened: a large fraction of $PM_{2.5}$ mass is produced regionally and depends on precursor emissions and atmospheric processing. Effective mitigation therefore requires coordinated regional action and cannot rely on local, city-only strategies.

The source-apportionment experiments further contextualize episodic extremes. During the October-November CRB period, biomass burning contributes ~50% of $PM_{2.5}$ in Punjab, ~36% in Haryana, and ~13% in Delhi-NCR, with OA dominating the biomass-burning-related mass. Water-associated aerosol mass and desert dust form a substantial part of the residual "Other" category, and BC increases sharply over Punjab and Haryana during peak CRB activity. Prevailing north-westerly winds efficiently transport these plumes toward NCT-Delhi, elevating both $PM_{2.5}$

and BC during the most polluted weeks of the year. These mechanisms collectively indicate that while eliminating CRB would substantially reduce the frequency and intensity of the worst episodes, it would not eliminate the baseline pollution problem in NCT-Delhi unless residential combustion and other sustained anthropogenic sources are addressed simultaneously.

From a policy standpoint, these results strengthen the case for combined control packages that target (i) primary emissions from residential combustion, transport, and industry, and (ii) precursor gases that drive secondary $PM_{2.5}$, including VOCs, NO_x, SO_2, and NH_3. They also highlight the importance of enforcement and real-world evaluation. While programs such as Pradhan Mantri Ujjwala Yojana (PMUY), Unnat Chulha Abhiyan, and NCAP aim to reduce household emissions, the quantitative impacts of these measures on ambient $PM_{2.5}$ and CO require rigorous assessment under real implementation conditions. Such evaluation is essential for translating program scale-up into verified air-quality benefits, particularly over the NCT-Delhi airshed.

The chapter also highlights a practical airshed implication: achieving clean air over the National Capital Region during post-monsoon and winter may be feasible only if CRB is eliminated across all major contributing states within the NCT-Delhi airshed, alongside strengthened implementation of sectoral controls on transport, residential, and industrial emissions. A sustained 50% reduction in emissions from these three sectors could plausibly yield substantial improvements in NCT-Delhi air quality, but only if measures are coordinated regionally and coupled to precursor controls that limit secondary formation. Although recent reports suggest CRB has declined during 2023-2024 over Punjab and Haryana, uncertainties in detection and reporting imply that updated, comprehensive assessment of CRB emissions and transboundary impacts remains a critical future research direction.

As with all regional chemical transport modelling studies, our results are subject to structural and parametric uncertainties. Despite the overall robust model performance, the results of this study remain subject to several sources of uncertainty inherent to regional air-quality modelling. These include uncertainties in anthropogenic emissions, particularly their magnitude, spatial and temporal allocation, and sectoral representation, as well as limitations in the detection and quantification of CRB, including fire counts, burned area estimation, and plume injection heights. Additional uncertainties arise from the representation of secondary aerosol formation and multiphase chemistry, especially under wintertime conditions characterized by weak photochemistry, shallow boundary layers, and enhanced heterogeneous processing.

Meteorological initial and lateral boundary conditions, along with model physical and chemical parameterizations, also influence pollutant transport, dispersion, and chemical transformation. Although we have used the high-resolution, India-specific SMoG-COALESCE inventory and a thoroughly evaluated WRF-Chem configuration with the MOZART-MOSAIC chemical mechanism to minimize these uncertainties, residual errors and potential compensating biases among emissions, meteorology, and chemistry may still affect model performance. Importantly, while these uncertainties may affect the precise magnitude of simulated $PM_{2.5}$ reductions, they are unlikely to alter the central comparative conclusion that airshed-scale, multi-sector interventions consistently outperform city-confined measures under winter conditions. The results should therefore be interpreted in a process-based and relative sense, with emphasis on the comparative effectiveness and structural implications of mitigation strategies rather than on exact quantitative predictions of absolute $PM_{2.5}$ reductions.

Finally, the results emphasise that northern India requires explicitly seasonal and region-specific airshed management. Strong spatiotemporal variability, especially the sharp wintertime deterioration over the IGP, means that interventions must be aligned with meteorological regimes and transport pathways. Given the pronounced role of regional transport during high-pollution seasons, cooperative, science-driven, multi-scale management across states will be indispensable for achieving durable $PM_{2.5}$ reductions over NCT-Delhi and northern India.

Chapter 5: Toward Improving Regional $PM_{2.5}$ in the NCT Delhi Airshed: A Comparative Evaluation of Control Strategies

5.1 Introduction

The National Capital Territory of Delhi (NCT-Delhi), located in the north-western Indo-Gangetic Plain (IGP) and effectively landlocked by the broader Delhi-NCR, Punjab, and Haryana region, experiences some of the most severe and persistent air-pollution episodes in South Asia, particularly during the post-monsoon (October-November) and winter (December-January) seasons (Lalchandani et al., 2022; Rathore et al., 2025) . These episodes arise from the concurrence of intense anthropogenic emissions and meteorological conditions that are highly unfavourable for pollutant dispersion, including weak near-surface winds, frequent temperature inversions, shallow planetary boundary layers, and prolonged stagnation (Bikkina et al., 2019; Kanawade et al., 2020; Mangaraj et al., 2025; Sawlani et al., 2019).

As a rapidly expanding megacity, NCT-Delhi records annual mean $PM_{2.5}$ concentrations of the order of ~140 $\mu g\ m^{-3}$, exceeding the 2021 WHO Air Quality Guideline by nearly a factor of 30 (Bhattu et al., 2024; Gani et al., 2019). Chronic exposure to such extreme pollution levels imposes severe burdens on public health, regional ecosystems, agricultural productivity, transportation systems, and regional climate (Conibear et al., 2020; David et al., 2019; Lal et al., 2022; McDuffie et al., 2021). In the years immediately preceding the COVID-19 lockdown, air pollution was responsible for approximately 1.7 million premature deaths annually in India, corresponding to ~18% of total mortality, with ambient PM exposure alone accounting for nearly one million deaths (Pandey et al., 2021). Without substantive and sustained intervention, this mortality burden is projected to increase by ~50% by 2030 (Apte et al., 2018). The severity of Delhi's air-quality crisis was starkly illustrated during the November 2016 haze episode, when emergency measures, including school closures affecting more than 6000 children and restrictions on heavy-duty truck entry, were enforced (Health, 2017). In response to such recurring crises, the Government of India launched the National Clean Air Programme (NCAP), targeting a 20-30% reduction in $PM_{2.5}$ concentrations by 2024 across 131 non-attainment cities (Ganguly et al., 2020).

Air quality over NCT-Delhi is governed not only by local emissions but also by substantial regional transport within and beyond the Delhi-NCR, particularly during the post-monsoon and winter months (Ambulkar et al., 2025; Mangaraj et al., 2025; Rathore et al., 2025). The Kharif rice harvest in October-November coincides with a seasonal transition in large-scale circulation, marked by a shift from south-easterly to north-westerly winds and the onset of winter-time stagnation over the western IGP (Singh et al., 2020; Kulkarni et al., 2020; Liu et al., 2020;

Venkataraman et al., 2006). These meteorological conditions promote regional accumulation and long-range advection of pollutants across northern India, including into NCT-Delhi (Lalchandani et al., 2022; Mangaraj et al., 2025). A key episodic source during this period is the open burning of post-harvest agricultural residues in north-western India, particularly in Punjab and Haryana (Beig et al., 2020; Nagar et al., 2017).

Reported contributions of crop-residue burning (CRB) to $PM_{2.5}$ over Delhi-NCR during October-November vary widely, ranging from ~14% in recent observation-constrained analyses to 20-40% in earlier modelling studies that lacked direct measurements in source regions (Bhattu et al., 2024; Kulkarni et al., 2020; Liu et al., 2020; Mangaraj et al., 2025; Mukherjee et al., 2020; Sembhi et al., 2020). Regional emission inventories estimate annual CRB-related $PM_{2.5}$ emissions of ~137 Gg in Punjab and ~57 Gg in Haryana, while India as a whole burns ~116 Tg s^{-1} of agricultural residues, contributing approximately 9-13% of national $PM_{2.5}$ emissions (Kaiser et al., 2012; Singh et al., 2020; Venkataraman et al., 2006; Yin et al., 2019).

Satellite-based analyses using NASA's A-Train constellation indicate a 21% increase in vegetation indices, a ~60% rise in fire activity, and a 43-60% increase in aerosol loading over the IGP and Delhi in recent decades (Ambulkar et al., 2025; Beig et al., 2020; Jethva et al., 2019). Dual-carbon isotope measurements attribute ~42 ± 17% of Delhi's air pollution to regional biomass burning (Bikkina et al., 2019), while night-time particle growth events associated with biomass-burning plumes can contribute up to 70% of total particle number concentrations (Fang et al., 2023; Mishra et al., 2023). Despite this growing evidence base, substantial uncertainty persists regarding the precise contribution of CRB to NCT-Delhi's air quality.

These uncertainties stem from limitations in emission inventories, incomplete detection of small fires, strong spatial and temporal variability in burning practices, and complex meteorological controls on plume transport and dilution (Fang et al., 2023; Singh et al., 2020; Yin et al., 2019). Satellite retrievals may be biased under heavy smoke or cloud cover, while ground-based monitoring remains concentrated in urban centres, leaving large gaps over rural source regions (Singh et al., 2023). Post-burn observations at downwind sites show increases exceeding 120% in reactive gases such as VOCs (Kumar et al., 2018). Prevailing October-November winds, directed from Punjab toward the Bay of Bengal, place Haryana and parts of western Uttar Pradesh within the effective airshed of NCT-Delhi, whereas Rajasthan is frequently outside it (Kumar et al., 2025). These transport pathways strongly influence $PM_{2.5}$ over NCT-Delhi and the frequency of "Very Poor" to "Severe" Air Quality Index (AQI) days, highlighting the need for an explicitly

airshed-based perspective that integrates source contributions, chemical composition, and regional transport dynamics during the high-pollution season. Recent analyses of regional $PM_{2.5}$ climatology across Indian airsheds further reinforce that Delhi's pollution cannot be understood or managed in isolation from the surrounding IGP.

Crop-residue burning, however, represents only one component of a broader, multi-sectoral emissions landscape. Agricultural emissions have intensified with rising productivity and widespread use of diesel-powered tractors, combine harvesters, and irrigation pumps (Pandey et al., 2014). In the residential sector, a substantial fraction of households continues to rely on solid biomass fuels burned in inefficient stoves and traditional combustion technologies, which are also prevalent in informal industries such as brick kilns and small food- and agro-processing units (Mahato et al., 2020; Singh et al., 2020; Venkataraman et al., 2024). Household air pollution remains the second leading risk factor for India's disease burden, and residential biomass combustion is a significant contributor to global net-positive radiative forcing (Seay et al., 2021; Unger et al., 2010; Venkataraman et al., 2010).

The Delhi-NCR also hosts numerous large-scale industrial sources, including thermal power plants, cement factories, metal smelters, brick kilns, rice mills, mineral grinding units, and stone crushers, many of which operate with outdated technologies and highly polluting fuels (Chatterjee et al., 2023; Kumar et al., 2017). A large fraction of these units is located in peri-urban and rural areas, beyond the routine oversight of urban local bodies, complicating regulatory enforcement (Guttikunda et al., 2023; Venkataraman et al., 2018). Fugitive emissions from mineral-processing units and stone crushers further intensify local pollution hotspots, particularly in NCAP-designated cities (Ganguly et al., 2020; Guttikunda et al., 2025). Festive activities add another episodic stressor, as widespread firecracker use during Diwali and subsequent festivals produces sharp, short-lived spikes in particulate matter and trace gases that, under stagnant conditions, can push AQI into the "Severe" category for several days (Dwivedi et al., 2025; Patowary et al., 2024; Ravindra et al., 2022; Saha et al., 2021).

Micro, small, and medium enterprises (MSMEs) across northern India remain heavily dependent on coal, heavy oils, and other high-emission fuels, leading to elevated $PM_{2.5}$ and SO_2 emissions (Lal et al., 2025; Pandey et al., 2014). Transitions to cleaner fuels, electrification, alternative fuels, and waste-heat recovery technologies could reduce industrial emissions by 30-40% while delivering economic co-benefits (Seay et al., 2021; Singh et al., 2021). In parallel, locally manufactured low-cost vehicles operating on poorly blended fuels and low-quality

lubricants contribute substantially to $PM_{2.5}$ emissions in both the transport and agricultural sectors, while outdated irrigation pumps and agricultural machinery further compound the emissions burden across the IGP (Kumar et al., 2017; Pandey et al., 2014).

Our earlier analysis of the COVID-19 lockdown demonstrated that although primary anthropogenic emissions declined temporarily, observed reductions in surface $PM_{2.5}$ were dominated by favourable meteorological conditions rather than emission reductions alone (Nandi et al., 2025). This finding highlights that sustainable improvements in air quality require structural, long-term emission reductions implemented in concert with an explicit understanding of meteorological controls. Collectively, the evidence points to the necessity of a multi-sectoral, regionally integrated mitigation strategy involving city authorities, state pollution control boards, industrial stakeholders, and national regulators.

Against this backdrop, the present chapter systematically evaluates the effectiveness of controlling emissions from four key sectors, residential, transport, industry, and crop-residue burning, across both Delhi-NCR and the broader NCT-Delhi airshed encompassing Punjab and Haryana (Kumar et al., 2025). Focusing on the most severe air-pollution period from September 2019 to January 2020, when population exposure and health risks peak, we employ a high-resolution, online-coupled atmospheric chemistry-transport model configured with the latest anthropogenic and near-real-time biomass-burning emissions. This framework enables us to quantify how surface $PM_{2.5}$ concentrations and AQI categories respond to realistic and strengthened implementations of existing policies under varying meteorological regimes, including episodes of extreme winter stagnation. The overarching objective is to demonstrate, quantitatively and mechanistically, that Delhi cannot clean its air through local actions alone, and that meaningful and sustained improvements in air quality require a coordinated, multi-sector, airshed-scale mitigation strategy for NCT-Delhi and northern India.

5.2 Datasets and Methodology

5.2.1 Model Description and Simulation Details

We use the Weather Research and Forecasting model coupled with Chemistry (WRF-Chem, v4.2.2) (Grell et al., 2005) to simulate surface $PM_{2.5}$ and co-emitted gaseous and particulate species over northern India, with a specific focus on Delhi-NCR and the wider NCT-Delhi airshed encompassing Punjab and Haryana. WRF-Chem is well suited for this purpose because it represents meteorology and chemistry within a single, online-coupled framework, allowing emissions, transport, chemical transformation, deposition, and aerosol-radiation-meteorology feedback to evolve consistently. This capability has supported its extensive application and evaluation for air-quality studies over India, particularly for source attribution and policy-relevant sensitivity experiments (Lal et al., 2025; Mogno et al., 2021; Nandi et al., 2025; Venkataraman et al., 2024).

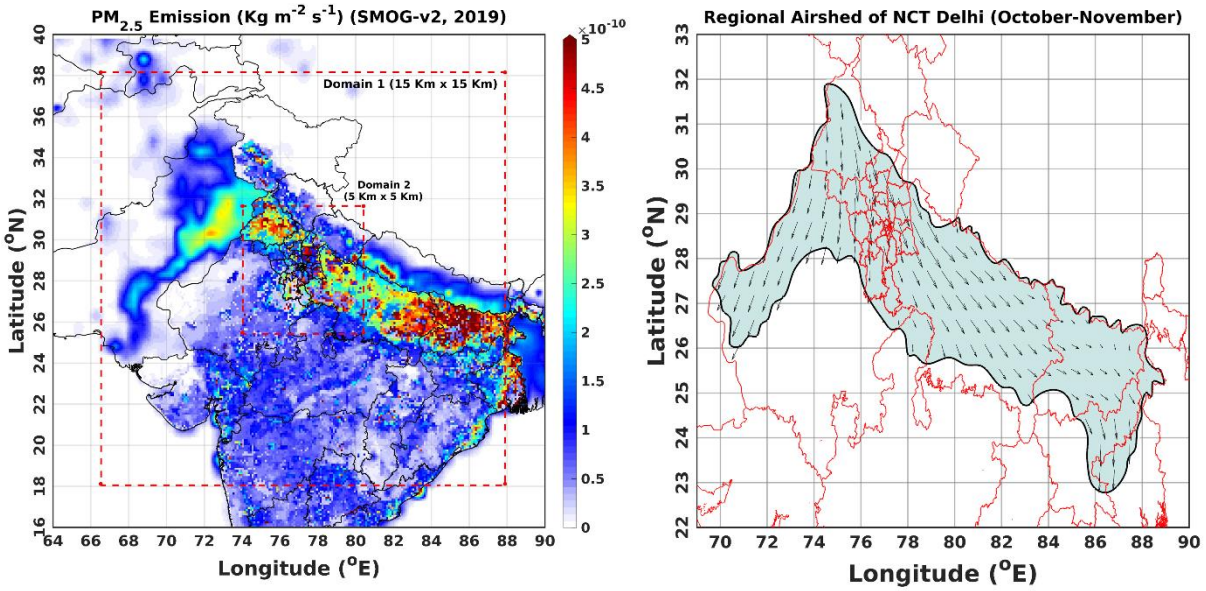


Figure 5.1: WRF-Chem simulation domain overlaid with 2019 $PM_{2.5}$ mean emission from SMoG-COALESCE emission inventory (left). The right panel illustrates the NCT-Delhi airshed region for October-November (Kumar et al., 2025), overlaid with WRF-Chem simulated wind flow directions.

The simulations span 17 August 2019 to 31 January 2020, capturing the transition from the retreating monsoon through the post-monsoon burning season and into the winter stagnation period, when the most hazardous $PM_{2.5}$ conditions typically occur over northern India. The first 15 days are treated as spin-up to reduce the influence of initial conditions on both aerosols and reactive gases. The model uses a two-way nested domain configuration designed to resolve both regional transport and fine-scale gradients near the Delhi megacity: an outer domain at 15 km x 15 km resolution (140 x 150 grid cells) covering the Indian subcontinent, and an inner domain at

5 km x 5 km resolution (126 x 138 grid cells) centred over NCT-Delhi (28.61° N, 77.21° E), encompassing the major emission regions and transport corridors of northern India (Fig. 5.1). This setup is intended to capture (i) sharp urban-rural contrasts in emissions and concentrations, (ii) the advection of pollution plumes from Punjab and Haryana into Delhi during the post-monsoon and winter months, and (iii) local hotspots associated with dense road networks, residential combustion clusters, and industrial activity within the airshed.

Table 5.1: WRF-Chem model setup for analysing emission control strategies.

Sl No.	Emissions	Simulation Name
Baseline Scenario		
0	SMoG-COALESCE (BC, OC, SO_2, NH_3, CO, NO_x, $PM_{2.5}$, PM_{10}), EDGAR-v5 (VOCs) & Biomass Burning Emission (BB) (FINN-v2.5) (Over Domain All Sector Emission and BB Emission 100%)	Control
City-Centric Policy Paradigm		
1	Over Domain All Sector Emission 100% & Over NCR BB Emission 0%	0BB NCR
2	Over NCR Transport Sector Emission 50% & Over NCR BB Emission 0%	50T NCR
3	Over NCR Residential Sector Emission 50% & Over NCR BB Emission 0%	50R NCR
4	Over NCR Industry Sector Emission 50% & Over NCR BB Emission 0%	50I NCR
5	Over NCR Transport, Residential and Industry Sector Emission 50% & Over NCR BB Emission 0%	50TRI NCR
Airshed-Scale Interventions		
6	Over Domain All Sector Emission 100% & Over NCT-Delhi Airshed BB Emission 0%	0BB NPH
7	Over NCT-Delhi Airshed Transport Sector Emission 50% & Over NCT-Delhi Airshed BB Emission 0%	50T NPH
8	Over NCT-Delhi Airshed Residential Sector Emission 50% & Over NCT-Delhi Airshed BB Emission 0%	50R NPH
9	Over NCT-Delhi Airshed Industry Sector Emission 50% & Over NCT-Delhi Airshed BB Emission 0%	50I NPH
10	Over NCT-Delhi Airshed Transport, Residential and Industry Sector Emission 50% & Over NCT-Delhi Airshed BB Emission 0%	50TRI NPH
Nationwide Regulatory Architecture		
11	Over Domain Transport, Residential and Industry Sector Emission 50% & Over Domain BB Emission 0%	50TRI DOM

To quantify the air-quality benefits of sectoral mitigation strategies at different spatial governance scales, we perform a total of 12 WRF-Chem simulations (Table 5.1). One simulation serves as the baseline (Control), representing nominal 2019 emissions from all sectors. Five simulations impose sector-specific emission reductions within the Delhi-NCR administrative boundary, targeting residential, transport, and industrial sectors, together with crop-residue

burning (CRB). Another five simulations implement the same mitigation logic across the broader NCT-Delhi airshed (Punjab, Haryana, and Delhi-NCR), explicitly reflecting the fact that the dominant transport pathways influencing NCT-Delhi pollution during October-January extend well beyond Delhi's administrative limits, especially during the post-monsoon period when regional inflow is often strongest. Finally, one simulation explores a domain-wide mitigation case, in which the same level of sectoral reductions is applied uniformly across the entire model domain, providing an upper bound on potential regional gains under fully coordinated action.

The 0BB NCR simulation isolates the effect of eliminating CRB emissions only within Delhi-NCR, while keeping all other sectoral emissions unchanged relative to the Control simulation. The 50T NCR, 50R NCR, and 50I NCR simulations represent strong but sector-focused mitigation within NCR: each applies a 50% reduction in the transport, residential, or industrial sector, respectively, while simultaneously enforcing a complete CRB ban within NCR. The 50TRI NCR simulation represents a combined local-control package, in which transport, residential, and industrial emissions are all reduced by 50% within NCR alongside full elimination of NCR CRB emissions. Together, these NCR-focused experiments quantify the extent to which aggressive but city-centric mitigation, broadly consistent with the operational logic of episodic interventions such as GRAP, can reduce $PM_{2.5}$ within NCT-Delhi, where exposure and health risks are greatest.

A parallel suite, 0BB NPH, 50T NPH, 50R NPH, 50I NPH, and 50TRI NPH, implements the same mitigation strategies across the broader NCT-Delhi airshed (Punjab, Haryana, and Delhi-NCR). These airshed-scale experiments are explicitly designed to evaluate the incremental benefits of controlling emissions in upwind regions that (i) host high seasonal biomass-burning activity, (ii) contain large residential and industrial emission sources, and (iii) frequently lie along dominant transport pathways into NCT-Delhi during the high-pollution season. The final experiment, 50TRI DOM, applies 50% reductions in transport, residential, and industrial emissions uniformly across the full model domain, while eliminating biomass-burning (BB) emissions throughout the domain, thereby providing an upper bound on improvements achievable under coordinated regional mitigation beyond the immediate airshed.

Meteorological initial and boundary conditions are obtained from the ERA5 reanalysis at 6-hourly resolution and are incorporated into WRF using grid nudging for winds, temperature, and water vapour above the planetary boundary layer (Zittis et al., 2018). A nudging coefficient of 0.0005 s^{-1} is applied to maintain consistency with large-scale circulation while preserving the

model's ability to develop mesoscale structure relevant for boundary-layer evolution and pollutant transport. Anthropogenic emissions of $PM_{2.5}$ and its precursors are taken primarily from the India-specific Speciated Multi-Pollutant Generator (SMoG-COALESCE, 2019; 5 km) (Venkataraman et al., 2024), which provides sector-resolved emissions for residential, transport, industry, energy, agriculture, waste burning, and additional source categories.

This sectoral structure is critical for the present perturbation framework, as it allows the imposed reductions to be applied consistently and transparently by sector and region. Volatile organic compound (VOC) emissions are supplemented using EDGAR-v5 (2015) (Crippa et al., 2020), while biogenic emissions are computed online using the Model of Emissions of Gases and Aerosols from Nature (MEGAN) (Guenther et al., 2006). Biomass-burning emissions, including CRB, are prescribed from FINN-v2.5 (Wiedinmyer et al., 2023), providing near-real-time spatiotemporal variability that is essential to represent episodic fire emissions during October-November.

Gas-phase chemistry is represented using the updated MOZART-4 mechanism (Emmons et al., 2010), coupled with the MOSAIC aerosol module (Zaveri et al., 2008) using a four-bin aerosol size distribution. The configuration includes grid-scale aqueous chemistry and an extended treatment of organic aerosol evolution via the Volatility Basis Set (VBS) approach (Knote et al., 2014), which improves representation of secondary organic aerosol formation and partitioning under varying oxidant and meteorological conditions. Chemical boundary conditions are updated every 6 hours using global simulations from the Whole Atmosphere Community Climate Model (WACCM) (Gettelman et al., 2019), ensuring a time-varying large-scale chemical environment. Photolysis rates are calculated using the Fast Tropospheric Ultraviolet-Visible (FTUV) scheme (Tie et al., 2003). A comprehensive overview of the model configuration, including the spatial distribution of SMoG-COALESCE $PM_{2.5}$ emissions and the distribution of active fires detected by MODIS and VIIRS during the study period, is provided in Fig. 5.2.

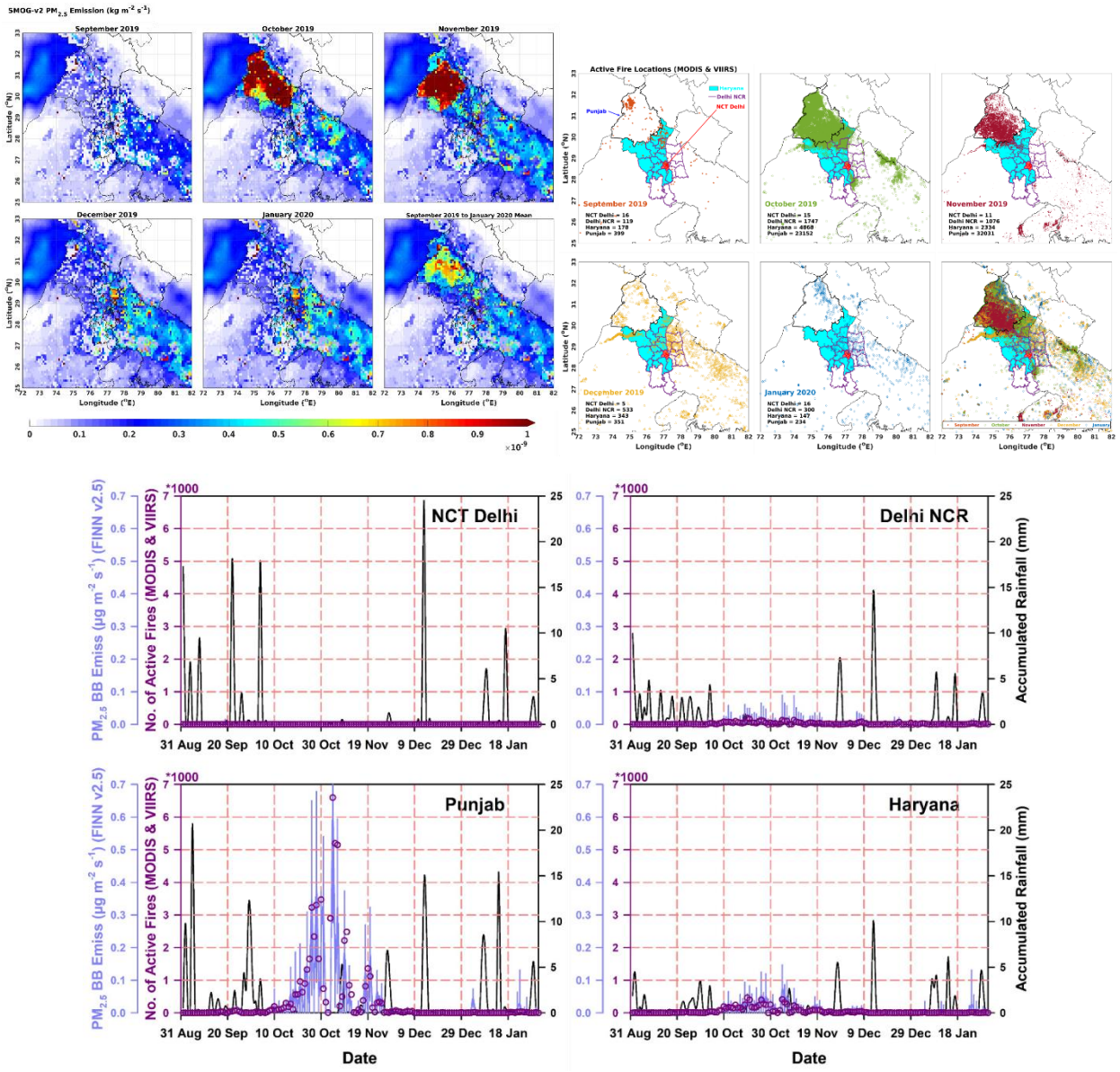


Figure 5.2: Monthly spatial distribution of SMoG-COALESCE $PM_{2.5}$ emissions (top panel) and active fire locations detected by MODIS and VIIRS (middle panel) across the study region, together with their cumulative distribution over the full analysis period. The bottom panel shows daily time series of surface $PM_{2.5}$ emissions from FINN-v2.5, MODIS and VIIRS fire counts, and IMD accumulated rainfall (mm day^{-1}) for NCT-Delhi, Delhi-NCR, Punjab, and Haryana throughout the study period.

5.2.2 Policy Context and Design of Mitigation Scenarios

The mitigation scenarios in this chapter are designed to represent policy-plausible strengthening of measures that already exist, rather than idealized interventions with unclear feasibility. Accordingly, we focus on national and regional policy frameworks that target the residential, transport, and industrial sectors, together with measures aimed at reducing agricultural biomass burning. The model experiments are constructed to approximate an ambitious but

interpretable benchmark, at least a 50% emission reduction in each targeted sector, allowing us to test how far vigorous implementation of current programmes and regulations could lower surface $PM_{2.5}$ over NCT-Delhi. In particular, we link sectoral reductions conceptually to enhanced effectiveness and enforcement of measures under PMUY, NCAP, Unnat Chulha Abhiyan, Saubhagya, the Graded Response Action Plan (GRAP), and relevant sector-specific regulations.

5.2.2.1 Indian Government Policies to Reduce Residential Sector Air Pollutant Emissions

Residential emissions remain a dominant contributor to $PM_{2.5}$ exposure in many parts of northern India, primarily through solid-fuel combustion for cooking and heating, and through associated practices such as household waste burning. The Government of India has implemented several key initiatives intended to accelerate transitions toward cleaner household energy and lower-emitting combustion technologies. These include: (i) the Pradhan Mantri Ujjwala Yojana (PMUY, 2016), which expands access to clean cooking fuels (LPG) among below-poverty-line households; (ii) the Unnat Chulha Abhiyan (2014), which promotes improved biomass cookstoves with higher combustion efficiency; (iii) the Saubhagya Scheme (2017), which expands rural electrification and enables greater reliance on electricity for household energy needs; and (iv) the National Clean Air Programme (NCAP, 2019), which supports state and city action plans that include residential-sector interventions. Complementary regulatory instruments include the Solid Waste Management Rules (2016) and state-level bans on firewood/coal use in selected urban areas, including measures implemented under GRAP in Delhi-NCR.

I. Pradhan Mantri Ujjwala Yojana (PMUY): Provides LPG connections to women from below-poverty-line (BPL) households, aiming to reduce indoor air pollution and lower household $PM_{2.5}$ emissions.
II. Unnat Chulha Abhiyan: Promotes improved biomass cookstoves (ICS) with higher combustion efficiency, resulting in a 30-50% reduction in particulate matter (PM) emissions.
III. National Clean Air Programme (NCAP): Encourages state-level action plans to restrict open burning, promote adoption of clean cooking fuels, and strengthen waste-management practices in residential settings.
IV. Pradhan Mantri Sahaj Bijli Har Ghar Yojana (Saubhagya Scheme): Expands last-mile electricity connectivity, encouraging electric lighting, heating, and potentially cooking, thereby reducing dependence on kerosene and biomass and lowering $PM_{2.5}$, CO, and black carbon emissions.

V. Solid Waste Management Rules (2016): Prohibit open burning of household waste, including leaves, plastics, and biomass, to mitigate emissions at source.

VI. State-Level Firewood/Coal Ban Notifications: Implemented in several non-attainment cities and under GRAP for Delhi-NCR, discouraging or banning coal, wood, and kerosene use and mandating transitions to cleaner fuels such as LPG, PNG, or electricity.

Policy / Programme	Target Sector	Key Pollutant Reduced	Estimated Reduction	Mechanism
Pradhan Mantri Ujjwala Yojana (PMUY)	Residential Cooking	$PM_{2.5}$, BC, CO	40-60% reduction in household $PM_{2.5}$ emissions	Replacement of biomass with LPG
Unnat Chulha Abhiyan	Residential Cooking	$PM_{2.5}$, CO, OC	30-50% reduction in PM emissions	Improved combustion efficiency cookstoves
National Clean Air Programme (NCAP)	Residential & Waste Burning	$PM_{2.5}$, PM_{10}	20-30% reduction target in $PM_{2.5}$ (city-level overall target by 2024-2026)	Clean fuel adoption and biomass burning control
Saubhagya Scheme	Residential Energy	$PM_{2.5}$, CO, BC	15-25% reduction in household combustion emissions	Electrification reduces kerosene and biomass use
Solid Waste Management Rules (2016)	Waste Burning	$PM_{2.5}$, PM_{10}, Toxic pollutants	Up to 80-100% reduction (where open burning eliminated)	Ban on open waste burning
GRAP / State-Level Fuel Ban	Residential Fuel Use	$PM_{2.5}$, SO_2, BC	20-40% reduction in local residential $PM_{2.5}$	Shift from coal/wood to LPG, PNG, electricity

5.2.2.2 Indian Government Policies to Reduce Transport Sector Air Pollutant Emissions

Transport emissions are addressed through progressively stringent vehicle and fuel standards, fleet modernization, and technology transitions. A central pillar is the phased implementation of Bharat Stage (BS) emission norms, BS-I (2000), BS-II (2005), BS-III (2010), BS-IV (2017), and BS-VI (2020), which tighten limits on particulate matter (PM), nitrogen oxides (NO_x), and hydrocarbons (HC) from on-road vehicles. These standards are complemented by policies that incentivize cleaner vehicle technologies and reduce emissions from legacy fleets, including the FAME programme (FAME-I from 2015; FAME-II from 2019–2024), the Vehicle Scrappage Policy (2021), and the National Hydrogen Mission (2021). Fuel-quality upgrades (nationwide BS-VI fuels) and adoption of alternative fuels (CNG, LNG, biofuels, ethanol blending) further support reductions in transport-sector $PM_{2.5}$ and precursor emissions. In Delhi-NCR, the GRAP framework (revised in 2023) provides an episodic escalation mechanism that includes vehicle and freight restrictions triggered by real-time AQI.

I. Bharat Stage (BS) Emission Norms: BS-VI enforces stringent limits on PM, NO_x, and HC for two-wheelers, passenger vehicles, commercial fleets, and heavy-duty trucks.

II. Faster Adoption and Manufacturing of Hybrid and Electric Vehicles (FAME): FAME-I (2015) and FAME-II (2019-2024) promote electric mobility via subsidies and EV infrastructure development.

III. Vehicle Scrappage Policy (2021): Targets retirement of older, high-emitting vehicles (commercial >15 years; private >20 years) and incentivizes replacement with cleaner alternatives, reducing emissions from legacy fleets.

IV. Fuel Quality Improvement: Nationwide transition to BS-VI fuels (ultra-low sulfur petrol and diesel) reduces SO_2 and PM emissions, including from older vehicles.

V. Promotion of Cleaner Fuels: Expanded use of CNG/LNG and biofuels, and the Ethanol Blending Policy targeting E20 by 2025, intended to reduce CO and HC emissions.

VI. National Hydrogen Mission (2021): Supports green hydrogen deployment, particularly for long-distance and heavy-duty transport.

VII. GRAP Delhi-NCR: Includes transport measures such as restrictions on older diesel vehicles (particularly BS-IV and below), odd-even road rationing during severe episodes, and constraints on construction trucks and inter-state diesel freight vehicles during Stage III/IV alerts.

Policy / Programme	Target Segment	Key Pollutant Reduced	Estimated Reduction	Mechanism
Bharat Stage VI (BS-VI) Emission Norms	All on-road vehicles	$PM_{2.5}$, NO_x, HC	PM: 60-90% reduction; NO_x: 70-90% reduction (vs BS-IV diesel)	Advanced engine standards, diesel particulate filters (DPF)
FAME I & II (Electric Vehicle Promotion)	Two-wheelers, Cars, Buses	$PM_{2.5}$, NO_x, CO	100% tailpipe emission reduction (EVs)	Replacement of ICE vehicles with electric vehicles
Vehicle Scrappage Policy (2021)	Old vehicles (>15-20 yrs)	$PM_{2.5}$, NO_x, CO	15-25% reduction in fleet emissions (regional scale)	Removal of high-emitting legacy vehicles
BS-VI Fuel Introduction (Ultra-Low Sulfur Fuel)	Petrol and Diesel vehicles	$PM_{2.5}$, SO_2	PM: 10-20% reduction, SO_2: ~80% reduction	Sulfur reduced from 50 ppm to 10 ppm
CNG / LNG / Biofuel Promotion	Public transport, commercial fleet	$PM_{2.5}$, NO_x, CO	$PM_{2.5}$: 20-40% reduction	Cleaner combustion fuels
Ethanol Blending Programme (E20 target)	Petrol Vehicles	CO, HC, PM	CO: 20-30% reduction, PM: 10-15% reduction	Cleaner fuel combustion
National Hydrogen Mission	Heavy Transport (future)	$PM_{2.5}$, NO_x, CO_2	Up to 100% tailpipe PM reduction	Zero-emission hydrogen fuel
GRAP Transport Restrictions (Delhi-NCR)	Old Diesel vehicles, Freight	$PM_{2.5}$, NO_x,	15-30% episodic $PM_{2.5}$ reduction	Traffic restriction and vehicle bans

5.2.2.3 Indian Government Policies to Reduce Industrial Sector Air Pollutant Emissions

Industrial emissions are regulated through sector-specific standards under the Environment (Protection) Act, 1986, technology mandates, and monitoring requirements. Key measures include installation of Flue Gas Desulfurization (FGD) systems in coal-fired thermal power plants to control SO_2, and mandatory deployment of Continuous Emission Monitoring Systems (CEMS) for real-time reporting of major pollutants across large industrial facilities. Under severe pollution conditions, GRAP provides mechanisms for temporary shutdowns of high-emitting units and mandates the use of approved clean fuels. Fuel substitution policies encourage replacement of coal, pet-coke, and furnace oil with cleaner fuels such as Piped Natural Gas (PNG) and biomass-based alternatives. In parallel, renewable-energy deployment can reduce demand for diesel generator sets and fossil electricity; the Central Financial Assistance (CFA) scheme for rooftop solar (RTS, 2019) under MNRE's Grid-Connected Rooftop Solar Programme Phase II explicitly supports this transition.

I. National Clean Air Programme (NCAP): Industrial actions include strengthening enforcement, promoting cleaner technologies, and implementing cluster-specific emission-reduction plans.
II. Emission Standards (Environment Protection Act, 1986):
    a. Thermal Power Plants (TPPs): Required to install FGD units to control SO_2 emissions.
    b. Brick Kilns: Required to adopt zig-zag firing technology to reduce PM emissions.
III. Continuous Emission Monitoring Systems (CEMS): Mandatory monitoring of PM, SO_2, NO_x, CO, and NH_3 in major industrial sectors.
IV. GRAP Delhi-NCR: Industrial measures include temporary shutdowns of highly polluting units during severe episodes, mandatory use of approved clean fuels, and bans on diesel generator sets and hot-mix plants during Stage III/IV conditions.
V. Fuel Substitution Policy: Promotes phasing out coal, pet-coke, and furnace oil in favour of PNG and biomass-based fuels, particularly in Delhi-NCR and non-attainment cities.
VI. CFA for Rooftop Solar (RTS): MNRE support for rooftop solar across sectors; in industry, this can reduce diesel generator dependence and directly lower $PM_{2.5}$ emissions from fossil-fuel combustion.

Policy / Programme	Target Industry / Source	Key Pollutant Reduced	Estimated Reduction	Mechanism
National Clean Air Programme (NCAP)	Industrial clusters	$PM_{2.5}$, SO_2, NO_x	20-30% reduction (city-scale target)	Cleaner technologies and stricter enforcement
FGD Mandate for Thermal Power Plants	Coal-based power plants	SO_2, Secondary $PM_{2.5}$	SO_2: 80-95% reduction, $PM_{2.5}$: 20-30% indirect reduction	Flue Gas Desulfurization systems
Zig-Zag Technology for Brick Kilns	Brick manufacturing	$PM_{2.5}$, Black Carbon	PM: 40-70% reduction	Improved combustion efficiency
Continuous Emission Monitoring Systems (CEMS)	Major industries	$PM_{2.5}$, SO_2, NO_x	10-20% reduction (through compliance improvement)	Real-time monitoring and enforcement
GRAP Industrial Restrictions (Delhi-NCR)	Polluting industries, DG sets	$PM_{2.5}$, NO_x, SO_2	20-40% episodic reduction	Temporary shutdowns and fuel restrictions
Fuel Substitution Policy (Coal/Pet-coke → PNG)	Industrial boilers and furnaces	$PM_{2.5}$, SO_2, NO_x	$PM_{2.5}$: 30-60% reduction, SO_2: 50-80% reduction	Cleaner fuel transition
Rooftop Solar Programme (MNRE-CFA)	Industrial energy use	$PM_{2.5}$, CO_2	15-25% reduction in combustion emissions	Reduced diesel generator dependence

To address agricultural biomass burning, the Central Pollution Control Board (CPCB) provides guidelines for one-time financial support to paddy-straw-based palletization and torrefaction plants, aiming to integrate crop residues into energy and industrial supply chains and thereby reduce open-field burning. In addition, the Commission for Air Quality Management (CAQM) has mandated co-firing of 5-10% biomass with coal in thermal power plants located within 300 km of Delhi, as well as in captive power plants of industrial units in Delhi-NCR. In the modelling framework, these instruments collectively motivate airshed-scale scenarios that reduce CRB emissions in a way that is consistent with the direction of current policy, while still allowing us to quantify the magnitude of air-quality benefits that could accrue from stronger enforcement and accelerated implementation.

5.3 Results and Discussion

5.3.1 Impact of Delhi-NCR Only Mitigation on Air Quality in NCT-Delhi

In operational terms, the management of severe pollution episodes over NCT-Delhi is still dominated by measures implemented within the administrative boundary of Delhi-NCR, most notably through the Graded Response Action Plan (GRAP) and other short-duration emergency interventions. These actions are often triggered by observed AQI deterioration, and they implicitly

assume that curtailing emissions locally (or semi-locally within NCR) can rapidly translate into meaningful air-quality improvements over NCT-Delhi. Our first set of emission-perturbation simulations directly tests this assumption by evaluating how far a regionally extended, but still city-centric mitigation strategy can reduce $PM_{2.5}$ over NCT-Delhi when controls are confined to Delhi-NCR.

A clear result emerges immediately: eliminating crop-residue burning (CRB) emissions only within Delhi-NCR produces a small response in NCT-Delhi $PM_{2.5}$. In the 0BB NCR experiment, mean $PM_{2.5}$ over NCT-Delhi decreases by only 2.32 ± 1.15% for the full September 2019-January 2020 period, and by 2.79 ± 1.21% during October-November, the peak CRB season (Table 5.2). The mechanism underlying this limited sensitivity is straightforward: CRB emissions that affect NCT-Delhi during autumn are dominated by burning in upwind agricultural regions, primarily outside NCR. Thus, even a complete local ban within NCR removes only a small fraction of the burning-related aerosol mass and precursor gases that ultimately enter NCT-Delhi. The evidence is the weak modelled concentration response in Table 5.2, and the implication is policy-relevant: CRB-focused restrictions implemented only within NCR cannot materially alter NCT-Delhi's regional inflow burden, particularly under the prevailing post-monsoon transport pathways.

When sectoral emission reductions are added within NCR (while maintaining a complete NCR CRB ban), the response becomes stronger but remains highly sector dependent, reflecting differences in baseline emissions, spatial distribution of sources, and the extent to which each sector contributes to both primary $PM_{2.5}$ and secondary aerosol formation. A 50% reduction in NCR transport emissions reduces NCT-Delhi $PM_{2.5}$ by 3.18%, whereas an equivalent reduction in NCR residential emissions produces a substantially larger improvement of 13.29% (Fig. 5.3, Table 5.2). In contrast, cutting NCR industrial emissions by 50% yields a smaller but still detectable reduction of 1.57% (Fig. 5.3, Table 5.2). These contrasts can be interpreted mechanistically. Residential emissions in northern India, and within NCR, are spatially widespread and temporally persistent, contributing strongly to near-surface primary $PM_{2.5}$ as well as to precursor-driven secondary aerosol formation. Transport emissions, while important along road corridors and in dense urban cores, constitute a smaller fraction of total $PM_{2.5}$ mass at the regional scale, particularly during winter when secondary aerosol and regional inflow often dominate. Industrial emissions are frequently more spatially clustered, and their influence on NCT-Delhi averages can be diluted by plume dispersion and by the fact that a substantial fraction of industrial activity lies outside the immediate NCR core. The evidence for this hierarchy is the relative magnitude of

reductions in Table 5.2, and the implication is that uniform emission-reduction targets do not translate into uniform air-quality gains; instead, mitigation effectiveness depends strongly on how emissions map onto the dominant mass budget and chemistry of $PM_{2.5}$ in the receptor region.

Table 5.2: Monthly reduction in surface $PM_{2.5}$ from emission-perturbed WRF-Chem simulations, relative to the control simulation.

NCT-Delhi											
% (μ ± 1σ)	**0BB NCR**	**50T NCR**	**50R NCR**	**50I NCR**	**50TRI NCR**	**50TRI DOM**	**0BB NPH**	**50T NPH**	**50R NPH**	**50I NPH**	**50TRI NPH**
Sep, 2019	-1.63 ± 0.57	-4.63 ± 1.05	-14.81 ± 2.45	-2.96 ± 1.68	-22.67 ± 2.77	-46.94 ± 5.57	-4.63 ± 2.56	-10.09 ± 3.38	-28.34 ± 4.96	-7.06 ± 2.23	-39.71 ± 5.35
Oct, 2019	-2.96 ± 0.63	-6.19 ± 1.87	-16.27 ± 2.27	-4.51 ± 1.65	-24.60 ± 8.90	-52.12 ± 7.85	-8.40 ± 3.78	-14.16 ± 4.17	-32.27 ± 5.58	-11.16 ± 3.19	-44.43 ± 6.57
Nov, 2019	-2.63 ± 1.78	-5.88 ± 1.12	-15.84 ± 3.24	-4.37 ± 1.64	-24.40 ± 9.47	-51.44 ± 9.43	-7.52 ± 3.61	-13.27 ± 3.52	-31.32 ± 4.57	-10.62 ± 2.17	-43.75 ± 4.37
Dec, 2019	-2.26 ± 1.52	-5.41 ± 2.72	-15.38 ± 3.87	-3.86 ± 1.58	-23.85 ± 5.57	-49.91 ± 8.47	-6.28 ± 2.29	-12.09 ± 2.49	-29.97 ± 3.12	-9.24 ± 4.27	-42.34 ± 4.85
Jan, 2020	-2.13 ± 1.26	-5.40 ± 1.82	-15.76 ± 2.85	-3.73 ± 1.77	-24.41 ± 7.58	-50.94 ± 10.5	-5.94 ± 2.47	-11.87 ± 5.76	-30.51 ± 7.09	-8.87 ± 4.03	-43.13 ± 4.39
Delhi-NCR											
Sep, 2019	-5.10 ± 1.18	-9.56 ± 2.31	-26.10 ± 4.31	-9.46 ± 2.21	-38.17 ± 4.28	-48.71 ± 7.34	-6.04 ± 1.18	-11.47 ± 3.28	-31.72 ± 5.54	-11.34 ± 2.24	-42.47 ± 7.51
Oct, 2019	-11.75 ± 2.11	-16.44 ± 3.24	-30.14 ± 3.78	-16.19 ± 3.47	-42.28 ± 5.38	-52.85 ± 9.48	-13.95 ± 5.77	-19.68 ± 3.26	-36.43 ± 6.31	-19.37 ± 2.23	-47.52 ± 8.09
Nov, 2019	-9.89 ± 2.14	-14.72 ± 4.37	-29.55 ± 6.57	-14.04 ± 2.09	-41.71 ± 6.13	-52.51 ± 11.9	-11.77 ± 4.96	-17.64 ± 4.24	-35.79 ± 7.85	-16.79 ± 3.37	-46.75 ± 11.3
Dec, 2019	-7.37 ± 2.04	-12.30 ± 2.27	-27.56 ± 4.79	-11.70 ± 2.87	-40.22 ± 5.98	-51.01 ± 8.47	-8.71 ± 2.92	-14.79 ± 3.47	-33.44 ± 5.51	-14.08 ± 2.31	-44.90 ± 9.74
Jan, 2020	-6.67 ± 1.13	-11.43 ± 3.48	-28.44 ± 6.96	-11.10 ± 2.69	-41.09 ± 4.22	-52.19 ± 12.8	-7.92 ± 2.74	-13.73 ± 4.09	-34.61 ± 4.28	-13.33 ± 1.87	-45.77 ± 10.8
Punjab											
Sep, 2019	-1.63 ± 0.57	-3.34 ± 1.27	-10.90 ± 2.01	-2.81 ± 1.22	-16.98 ± 4.17	-44.03 ± 5.43	-7.23 ± 2.19	-11.15 ± 2.31	-28.18 ± 3.94	-10.03 ± 2.32	-37.91 ± 8.02
Oct, 2019	-9.81 ± 2.06	-11.72 ± 3.17	-11.78 ± 3.78	-11.17 ± 3.07	-16.22 ± 6.96	-59.62 ± 6.58	-44.21 ± 10.5	-48.42 ± 7.42	-48.45 ± 11.5	-47.26 ± 8.99	-57.08 ± 14.8
Nov, 2019	-10.35 ± 3.14	-12.32 ± 4.92	-12.08 ± 3.01	-11.73 ± 3.03	-16.58 ± 5.37	-61.56 ± 7.48	-46.66 ± 8.94	-50.98 ± 11.5	-50.59 ± 14.6	-49.67 ± 11.5	-59.06 ± 17.6
Dec, 2019	-2.46 ± 1.24	-4.45 ± 1.27	-10.91 ± 3.45	-3.72 ± 1.42	-17.18 ± 4.28	-46.34 ± 5.72	-10.95 ± 4.66	-15.34 ± 3.78	-30.07 ± 8.56	-13.94 ± 3.28	-40.41 ± 9.54
Jan, 2020	-2.04 ± 1.87	-3.94 ± 2.04	-11.04 ± 2.73	-3.32 ± 2.75	-17.35 ± 6.78	-45.83 ± 11.5	-9.08 ± 3.78	-13.35 ± 4.36	-29.41 ± 9.48	-12.00 ± 4.39	-39.71 ± 8.95
Haryana											
Sep, 2019	-5.17 ± 1.29	-8.31 ± 2.32	-21.49 ± 3.31	-7.74 ± 2.24	-30.43 ± 6.18	-41.43 ± 11.3	-6.99 ± 2.37	-11.96 ± 2.44	-32.72 ± 4.42	-11.09 ± 2.28	-35.44 ± 6.69
Oct, 2019	-26.84 ± 8.47	-30.12 ± 8.23	-33.25 ± 5.85	-29.33 ± 6.14	-40.73 ± 9.41	-53.65 ± 8.65	-36.38 ± 8.16	-41.56 ± 12.5	-46.47 ± 8.31	-40.31 ± 9.07	-52.04 ± 7.87
Nov, 2019	-24.43 ± 9.09	-27.71 ± 3.66	-32.34 ± 7.87	-27.24 ± 13.5	-40.34 ± 6.28	-53.29 ± 10.7	-33.20 ± 11.7	-38.30 ± 9.32	-45.60 ± 17.5	-37.50 ± 11.8	-51.02 ± 16.2
Dec, 2019	-7.75 ± 3.91	-11.01 ± 4.26	-23.31 ± 6.57	-10.49 ± 3.72	-32.44 ± 8.79	-43.94 ± 8.35	-10.46 ± 4.87	-15.64 ± 4.26	-35.02 ± 11.3	-14.78 ± 4.36	-38.28 ± 8.62
Jan, 2020	-6.40 ± 3.74	-9.80 ± 2.88	-22.40 ± 4.48	-9.25 ± 4.18	-31.77 ± 9.58	-43.11 ± 9.51	-8.74 ± 5.65	-14.03 ± 8.27	-33.87 ± 14.6	-13.15 ± 5.58	-38.24 ± 9.38

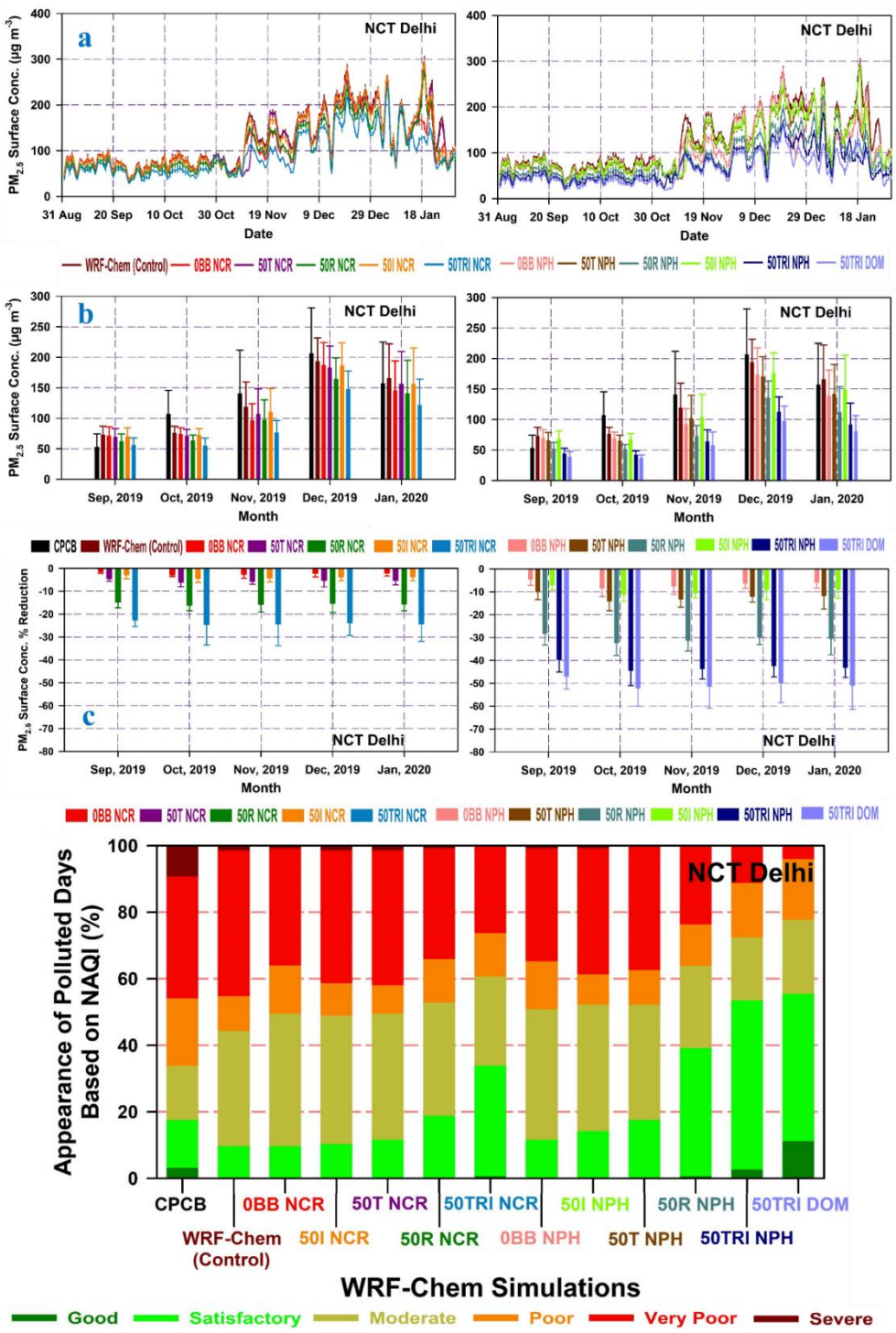


Figure 5.3: Multi-panel summary of surface $PM_{2.5}$ responses over NCT-Delhi from emission-perturbed WRF-Chem simulations for the full study period. Panel (a) shows the daily time series of $PM_{2.5}$ concentrations, panel (b) presents the corresponding monthly mean $PM_{2.5}$ concentrations as bar plots, and panel (c) illustrates the relative reductions under sector-specific emission-perturbation scenarios. In panels (a-c), the left sub-panels represent mitigation limited to Delhi-NCR (city-centric scenario), while the right sub-panels show responses under the broader NCT-Delhi airshed mitigation strategy (Punjab, Haryana, and Delhi-NCR), together with the nationwide regulatory scenario with emission controls implemented across India. The baseline simulation is included for reference, and observations from Central Pollution Control Board monitoring sites are shown in panel (b) for comparison. The bottom panel presents the overall change in the relative frequency of NAQI-defined polluted days across all scenarios.

The combined NCR mitigation package (50TRI NCR), in which transport, residential, and industrial emissions are all reduced by 50% and CRB is eliminated within NCR, produces a markedly larger response: $PM_{2.5}$ over NCT-Delhi declines by 23.98 ± 6.86% over the full study period and by 24.50 ± 9.19% during October-November (Fig. 5.3; Table 5.2). This multi-sector improvement is consistent with additive (though not strictly linear) reductions across multiple sources of both primary $PM_{2.5}$ and its gaseous precursors. Importantly, however, even this relatively ambitious NCR-only mitigation does not "solve" the winter problem: substantial $PM_{2.5}$ persists under the most stagnant conditions. The implication is central to the airshed argument developed in this chapter: local action can reduce the baseline and damp peak events, but it cannot eliminate high wintertime concentrations when transboundary inflow and meteorological suppression of dispersion remain dominant.

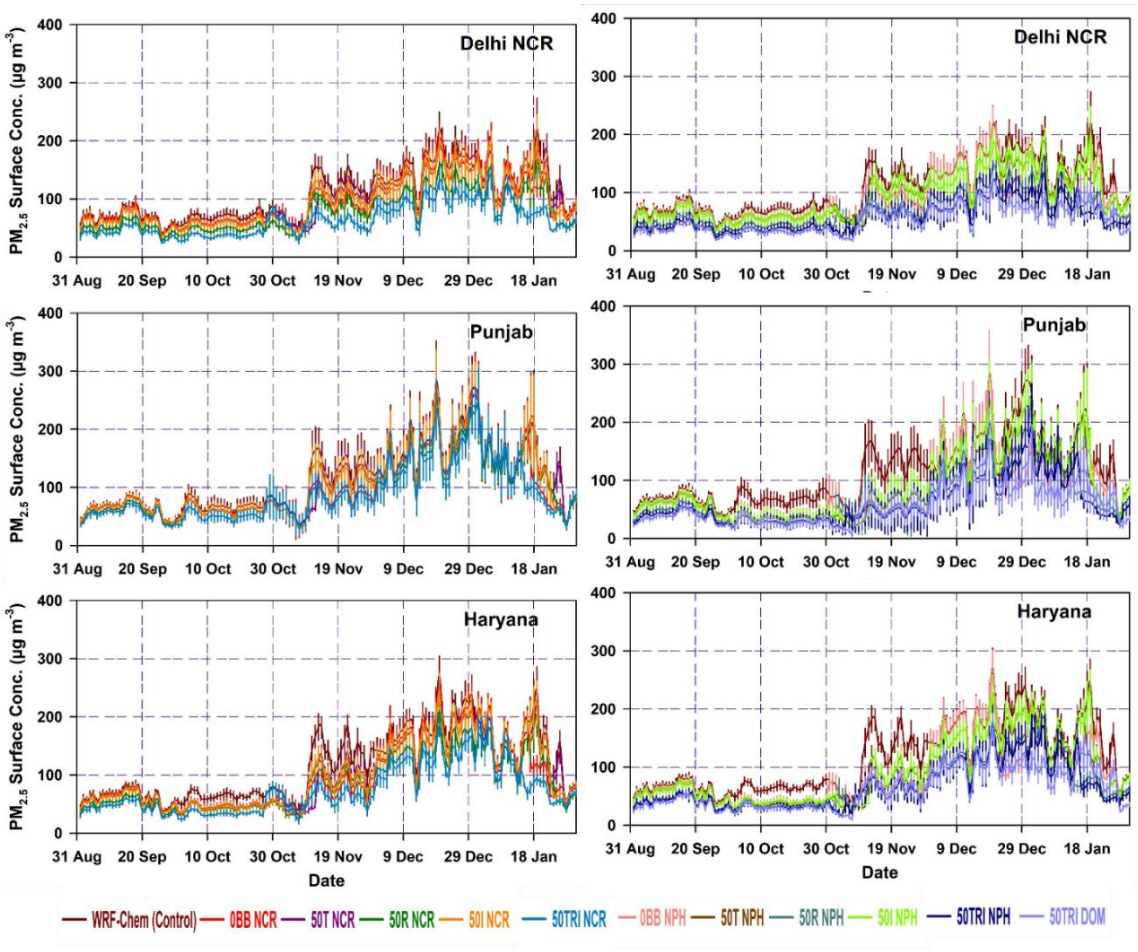


Figure 5.4: Daily time series of surface $PM_{2.5}$ concentrations over Delhi-NCR, Punjab, and Haryana for the full study period, derived from emission-perturbed WRF-Chem simulations. The left panel shows $PM_{2.5}$ responses under mitigation applied only within Delhi-NCR (city-centric scenario), while the right panel shows responses under the broader NCT-Delhi airshed mitigation strategy (Punjab, Haryana, and Delhi-NCR), along with the nationwide regulatory scenario with emission controls applied across India. The baseline scenario is included in both panels for reference.

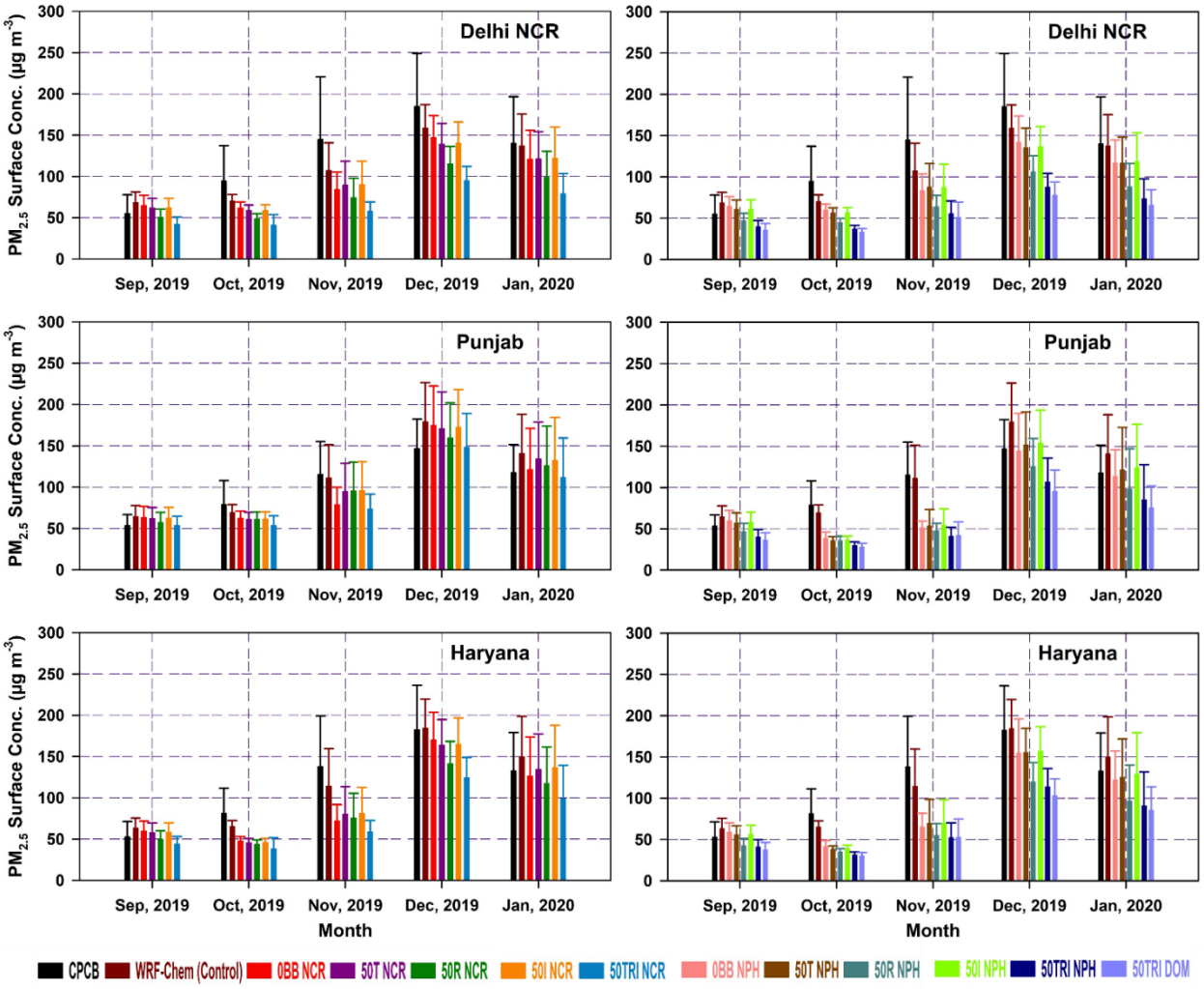


Figure 5.5: Bar plot of monthly mean surface $PM_{2.5}$ concentrations over Delhi-NCR, Punjab, and Haryana for the full study period, derived from emission-perturbed WRF-Chem simulations. The left panel presents $PM_{2.5}$ responses under mitigation limited to Delhi-NCR (city-centric scenario), whereas the right panel shows responses under the broader NCT-Delhi airshed mitigation strategy (Punjab, Haryana, and Delhi-NCR), together with the nationwide regulatory scenario with emission controls implemented across India. The baseline simulation and observed $PM_{2.5}$ concentrations from CPCB monitoring sites are included in both panels for comparison.

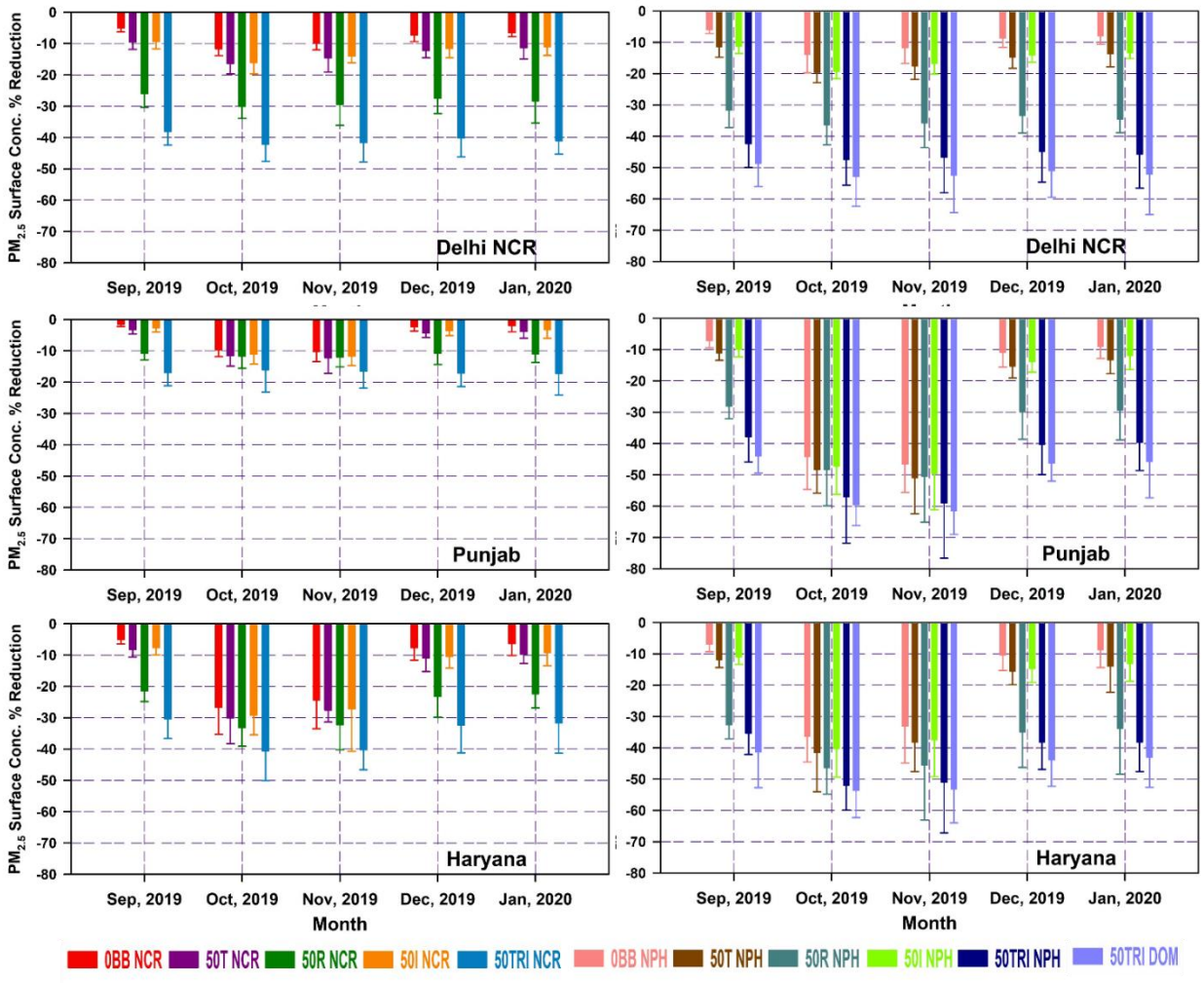


Figure 5.6: Bar charts illustrating the relative reductions in surface $PM_{2.5}$ over Delhi-NCR, Punjab, and Haryana under sector-specific emission-perturbation scenarios derived from WRF-Chem simulations. The left panel shows reductions resulting from mitigation confined to Delhi-NCR (city-centric scenario), while the right panel presents the corresponding reductions under the broader NCT-Delhi airshed mitigation strategy (Punjab, Haryana, and Delhi-NCR), as well as the nationwide regulatory scenario with emission controls implemented across India.

As Delhi-NCR is geographically contiguous with Haryana and lies near key regional transport corridors, NCR-only mitigation also produces spillover benefits beyond its administrative boundary. During October–November, restricting CRB only within NCR reduces $PM_{2.5}$ by $10.82 \pm 2.13\%$ over Delhi-NCR itself (Table 5.2), a much larger response than over NCT-Delhi because the intervention is co-located with the receptor region in this case. Adding 50% reductions in transport, residential, and industrial emissions within NCR lowers $PM_{2.5}$ by up to 32.54% over Delhi-NCR for the full period (Fig. 5.4 & Fig. 5.5). These results reinforce a key mechanism: near-field emission reductions are most effective when they directly target the

emission footprint within the receptor region, reducing local primary $PM_{2.5}$ and near-source secondary formation.

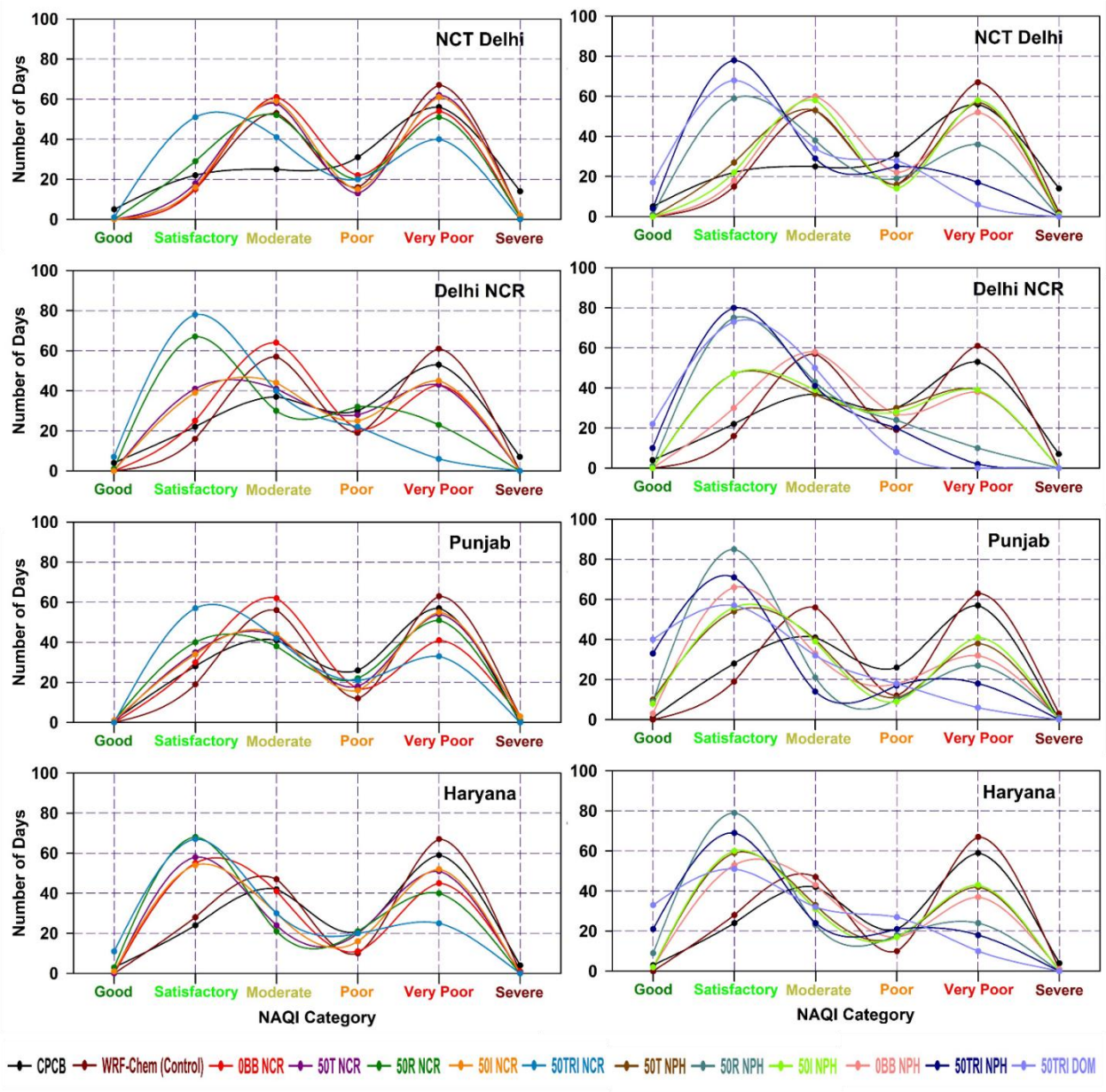


Figure 5.7: Frequency of polluted-day occurrences over NCT-Delhi, Delhi-NCR, Punjab, and Haryana, classified according to the National Air Quality Index (NAQI) and derived from emission-perturbed WRF-Chem simulations. The left panel shows occurrences under mitigation restricted to Delhi-NCR (city-centric scenario), while the right panel presents corresponding changes under the broader NCT-Delhi airshed mitigation strategy (Punjab, Haryana, and Delhi-NCR), along with the nationwide regulatory scenario with emission controls implemented across India. The baseline simulation and observed frequencies from CPCB monitoring stations are included in both panels for comparison.

Table 5.3: Frequency of polluted-day categories, as defined by the National Air Quality Index (NAQI), over the 153-day study period for each emission-perturbed simulation.

NCT-Delhi													
NAQI Category	**CPCB**	**Control**	**0BB NCR**	**50T NCR**	**50R NCR**	**50I NCR**	**50TRI NCR**	**50TRI DOM**	**0BB NPH**	**50T NPH**	**50R NPH**	**50I NPH**	**50TRI NPH**
Good	5	0	0	0	0	0	1	17	0	0	1	0	4
Satisfactory	22	15	15	18	29	16	51	68	18	27	59	22	78
Moderate	25	53	61	58	52	59	41	34	60	53	38	58	29
Poor	31	16	22	13	20	15	20	28	22	16	19	14	25
Very Poor	56	67	54	62	51	61	40	6	52	57	36	58	17
Severe	14	2	1	2	1	2	0	0	1	0	0	1	0
Delhi-NCR													
Good	4	0	0	0	1	0	7	22	0	0	1	0	10
Satisfactory	22	16	25	41	67	39	78	73	30	47	75	47	80
Moderate	37	57	64	41	30	44	40	50	58	37	43	39	41
Poor	30	19	21	28	32	25	22	8	27	30	24	28	20
Very Poor	53	61	43	43	23	45	6	0	38	39	10	39	2
Severe	7	0	0	0	0	0	0	0	0	0	0	0	0
Punjab													
Good	1	0	0	0	1	1	0	40	3	10	9	8	33
Satisfactory	28	19	30	35	40	34	57	57	66	54	85	56	71
Moderate	41	56	62	43	38	44	42	32	33	40	21	39	14
Poor	26	12	17	18	22	16	21	18	18	11	10	9	17
Very Poor	57	63	41	54	51	55	33	6	32	38	27	41	18
Severe	0	3	3	3	1	3	0	0	1	0	1	0	0
Haryana													
Good	3	0	0	0	3	1	11	33	2	2	9	2	21
Satisfactory	24	28	55	58	68	54	67	51	53	59	79	60	69
Moderate	42	47	41	24	21	30	30	32	43	33	23	31	24
Poor	21	10	11	20	21	16	20	27	17	17	18	17	21
Very Poor	59	67	45	51	40	52	25	10	37	42	24	43	18
Severe	4	1	1	0	0	0	0	0	1	0	0	0	0

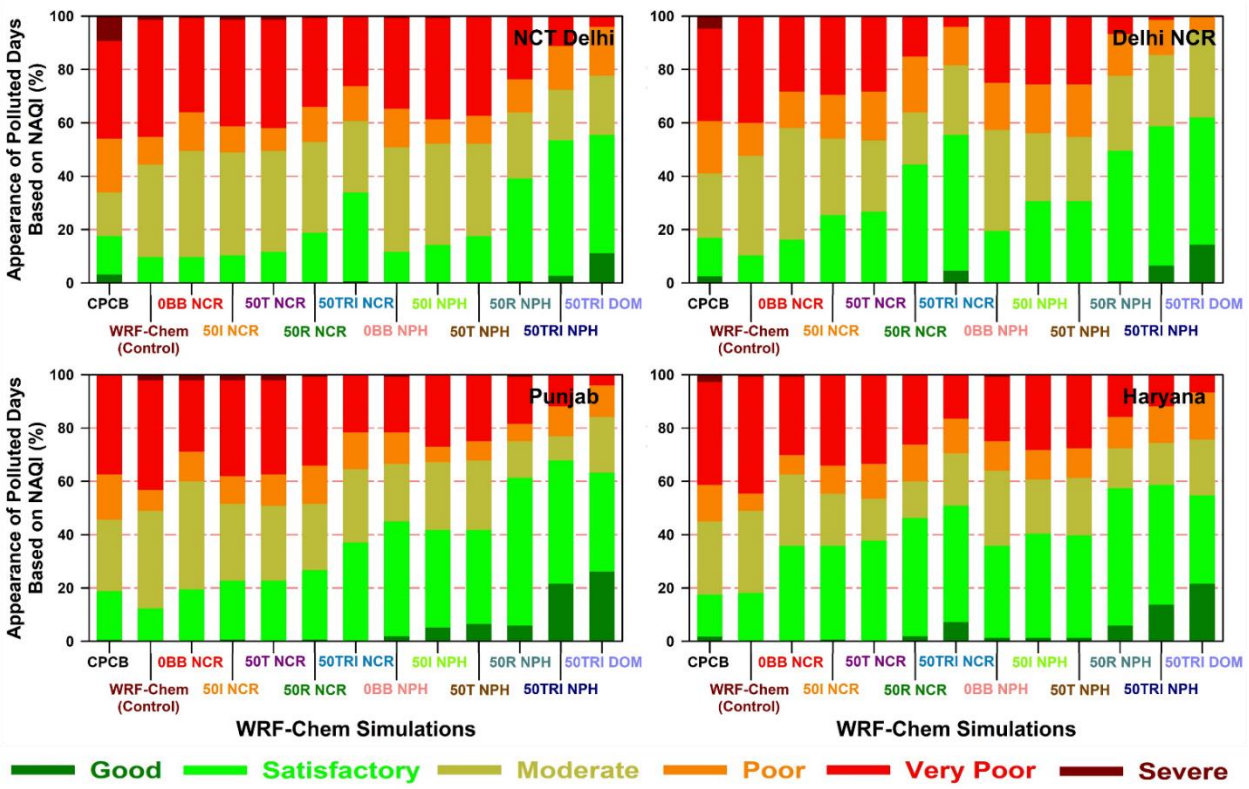


Figure 5.8: Stacked bar charts showing changes in the relative frequency of polluted-day categories, based on the National Air Quality Index (NAQI), across NCT-Delhi, Delhi-NCR, Punjab, and Haryana for all emission-perturbed WRF-Chem simulations.

Interestingly, NCR-focused actions also yield measurable reductions in the neighbouring states during peak burning months. NCR-only CRB restrictions reduce $PM_{2.5}$ by 25.63 ± 8.78% in Haryana and 10.08 ± 2.60% in Punjab during October–November (Fig. 5.6). When 50% reductions are applied across NCR transport, residential, and industry sectors (50TRI NCR), $PM_{2.5}$ decreases by 21.02% in Haryana and 11.61% in Punjab over the full period (Table 5.2). The evidence for this spillover is contained in Table 5.2 and illustrated in Fig. 5.4-5.6, and the implication is that subregional mitigation can generate multi-state co-benefits. However, the asymmetric response, especially the limited improvement over NCT-Delhi compared with the larger reductions within Delhi-NCR itself, also shows why spillover alone cannot substitute for a genuine airshed approach.

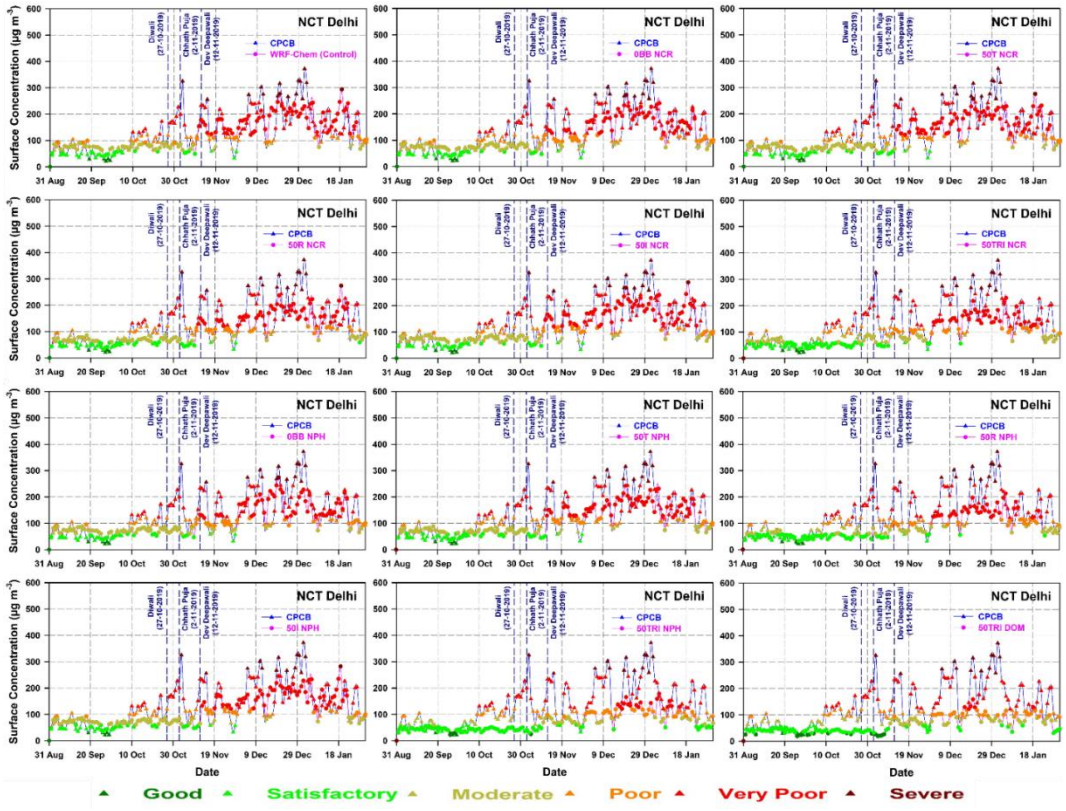


Figure 5.9: Daily time series of surface $PM_{2.5}$ over NCT-Delhi showing the occurrence of polluted-day categories (National Air Quality Index, NAQI) across all emission-perturbed simulations for the full study period.

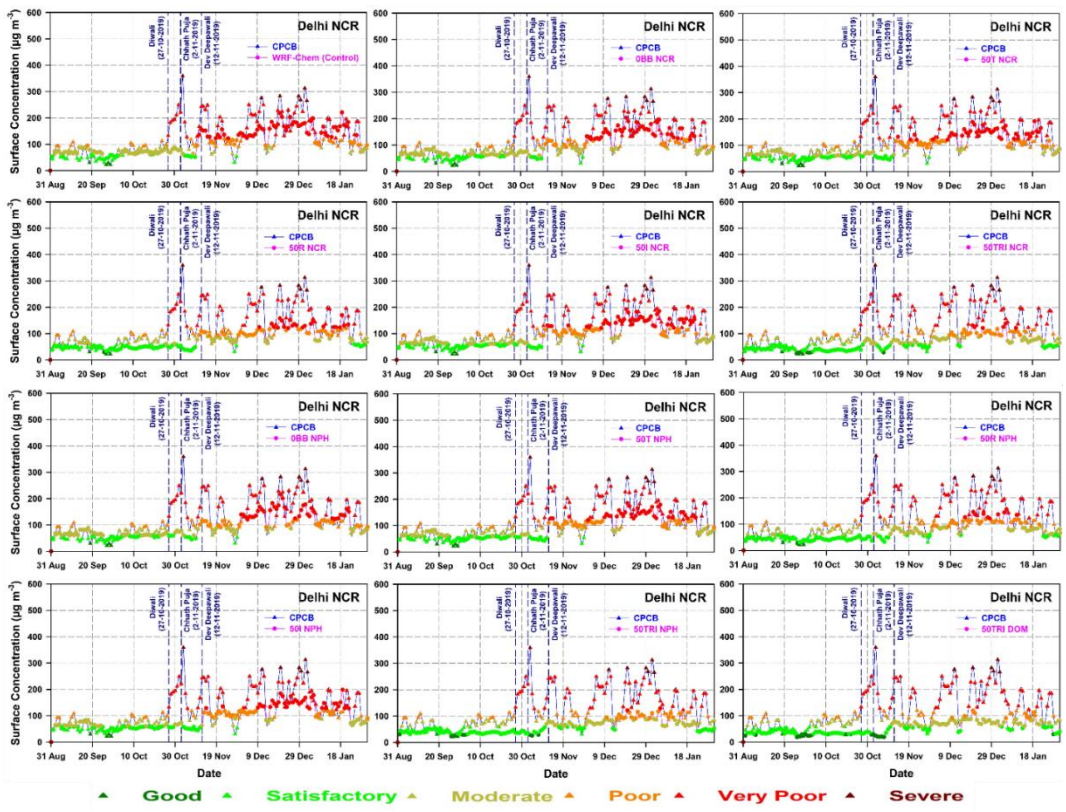


Figure 5.10: Daily time series of surface $PM_{2.5}$ over Delhi-NCR, showing the occurrence of polluted-day categories (National Air Quality Index, NAQI) across all emission-perturbed simulations for the full study period.

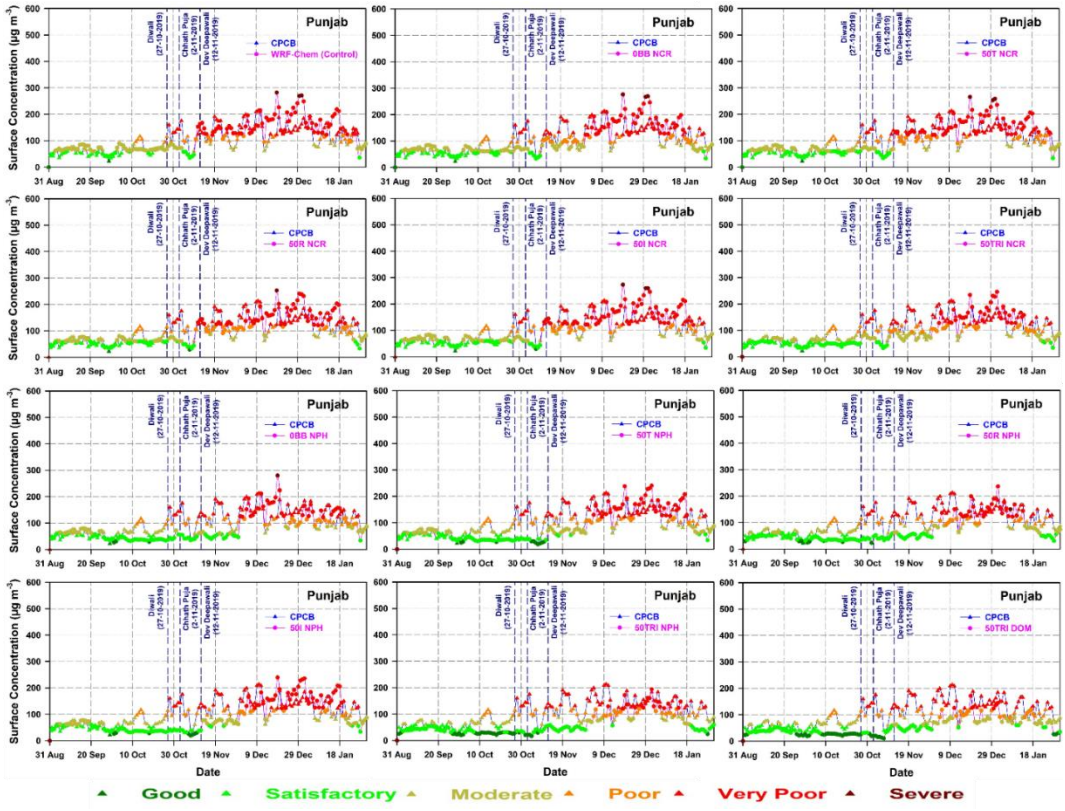


Figure 5.11: Daily time series of surface $PM_{2.5}$ over Punjab, showing the occurrence of polluted-day categories (National Air Quality Index, NAQI) across all emission-perturbed simulations for the full study period.

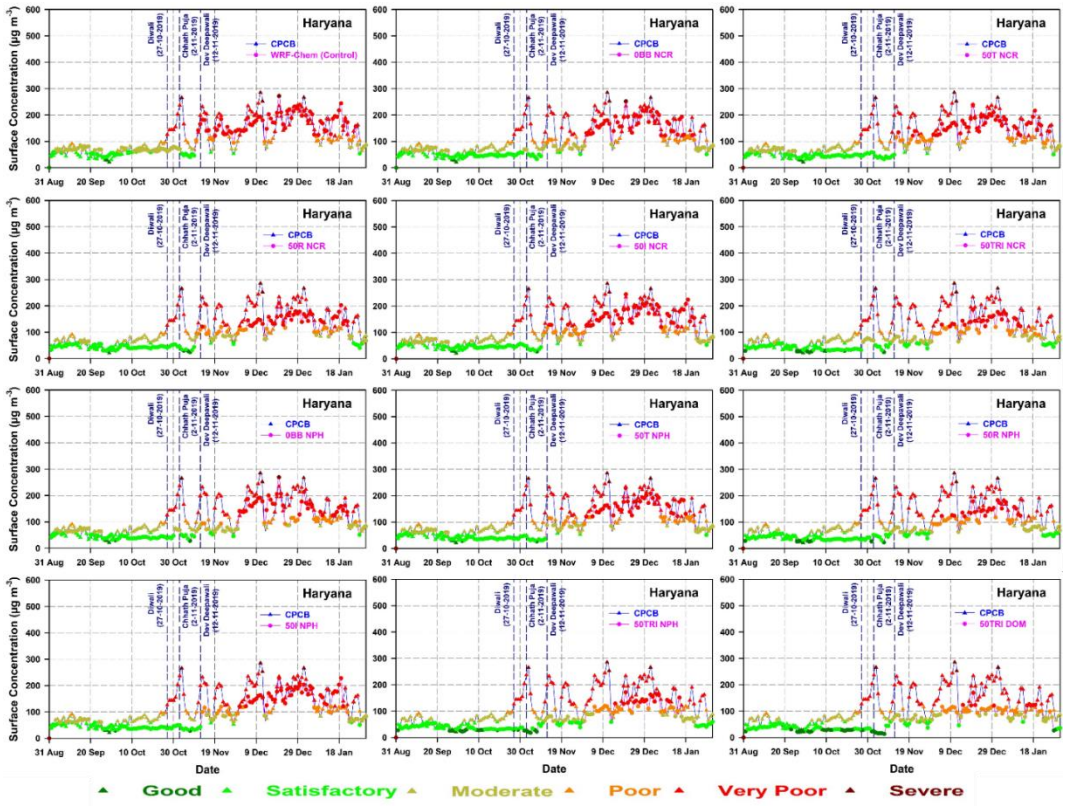


Figure 5.12: Daily time series of surface $PM_{2.5}$ over Haryana, showing the occurrence of polluted-day categories (National Air Quality Index, NAQI) across all emission-perturbed simulations for the full study period.

To convert concentration changes into exposure-relevant outcomes, we also evaluate changes in the National Air Quality Index (NAQI), which classifies daily air quality into health-based categories (Gupta et al., 2023; Radhadevi et al., 2025). This step is important because similar percentage reductions in $PM_{2.5}$ can yield very different public-health benefits depending on whether they shift days across NAQI thresholds. Under the 50R NCR scenario (50% residential reduction plus NCR CRB ban), the number of "Satisfactory" days over NCT-Delhi increases by 9%, while "Very Poor" days decrease by 10.5% (from 67 to 51 out of 153 days; Fig. 5.7). Mechanistically, this indicates that residential-sector mitigation reduces the baseline sufficiently often to move a non-trivial fraction of days below the "Very Poor" threshold. When residential, transport, and industrial reductions are applied together with a CRB ban (50TRI NCR), the distribution shifts further: "Satisfactory" and "Moderate" days reach 33% and 27% of the total, respectively (Fig. 5.8). This shift in frequency is the key evidence that multi-sector controls influence not only mean $PM_{2.5}$ but also the "tail" of high-pollution days.

Extending the combined strategy across the entire NCR further increases the number of "Satisfactory" days over NCT-Delhi to 78, while Punjab and Haryana register 57 and 67 "Satisfactory" days, respectively (Table 5.3). These statistics demonstrate that, even within a primarily NCR-framed policy lens, coordinated multi-sector measures can yield meaningful improvements in exposure categories, but they also foreshadow the larger gains achievable when the same actions are extended across the full airshed.

A notable seasonal feature is that the largest NAQI improvements occur during December–January, when $PM_{2.5}$ concentrations and exposure risks are typically highest (Fig. 5.9). This indicates that, even though post-monsoon CRB is a key episodic driver, wintertime stagnation makes the system especially sensitive to sustained reductions in baseline emissions (particularly residential combustion and persistent urban sources). Practically, the implication is that NCR-focused measures are likely to be most effective when implemented early and continuously, before the onset of the deepest winter boundary-layer suppression, rather than being deployed only as reactive emergency restrictions after AQI has already deteriorated. The day-resolved NAQI evolution across regions (Fig. 5.10-5.12) further illustrates that, while NCR-only packages reduce the frequency and severity of extreme days, they cannot consistently deliver attainment under the most adverse winter meteorological regimes, providing a quantitative basis for moving beyond city-centric control.

5.3.2 Benefits of Airshed-Scale Mitigation for NCT-Delhi Air Quality

Achieving sustained $PM_{2.5}$ reductions over NCT-Delhi that approach the National Ambient Air Quality Standards (NAAQS) for a meaningful fraction of the year requires mitigation that extends beyond Delhi-NCR and explicitly targets the broader NCT-Delhi airshed (Kumar et al., 2025). This requirement follows directly from the dominant winter-time mechanism: under synoptic conditions common to the post-monsoon and winter seasons, NCT-Delhi receives persistent inflow of $PM_{2.5}$ and precursor gases from Punjab, Haryana, and other upwind regions, and local controls alone cannot fully counteract this advected background (Kumar et al., 2025; Lal et al., 2025; Rathore et al., 2025). In other words, the receptor is embedded within a larger coupled system in which regional emissions and meteorology jointly determine local air quality.

The airshed-scale simulations provide strong evidence that mitigation applied across Punjab-Haryana-Delhi-NCR is substantially more effective than NCR-only strategies (Fig. 5.13). When CRB is eliminated across the full airshed (0BB NPH), $PM_{2.5}$ over NCT-Delhi declines by 6.55 ± 2.94% over the full study period and by 7.96 ± 3.70% during October-November (Table 5.2). The larger response relative to 0BB NCR reflects a simple mass-balance mechanism: removing burning emissions in the primary source regions eliminates a much larger fraction of fire-related primary aerosol and precursor gases before they can be transported into the Delhi receptor region. The implication is unambiguous: effective CRB mitigation for Delhi requires action in the upwind agricultural states that dominate the fire emissions entering the airshed.

When 50% reductions in transport, residential, and industrial emissions are implemented across the entire airshed in addition to eliminating CRB (50TRI NPH), mean $PM_{2.5}$ over NCT-Delhi decreases by approximately ~36% (Table 5.2; Fig. 5.3). This magnitude is qualitatively different from the NCR-only response because it reduces both (i) local emissions within the receptor region and (ii) the transported background that establishes the baseline upon which winter stagnation amplifies concentrations. Importantly, the reductions are not confined to NCT-Delhi; they are shared across the airshed, reflecting the spatial coherence of the emissions–transport system captured in Fig. 5.13.

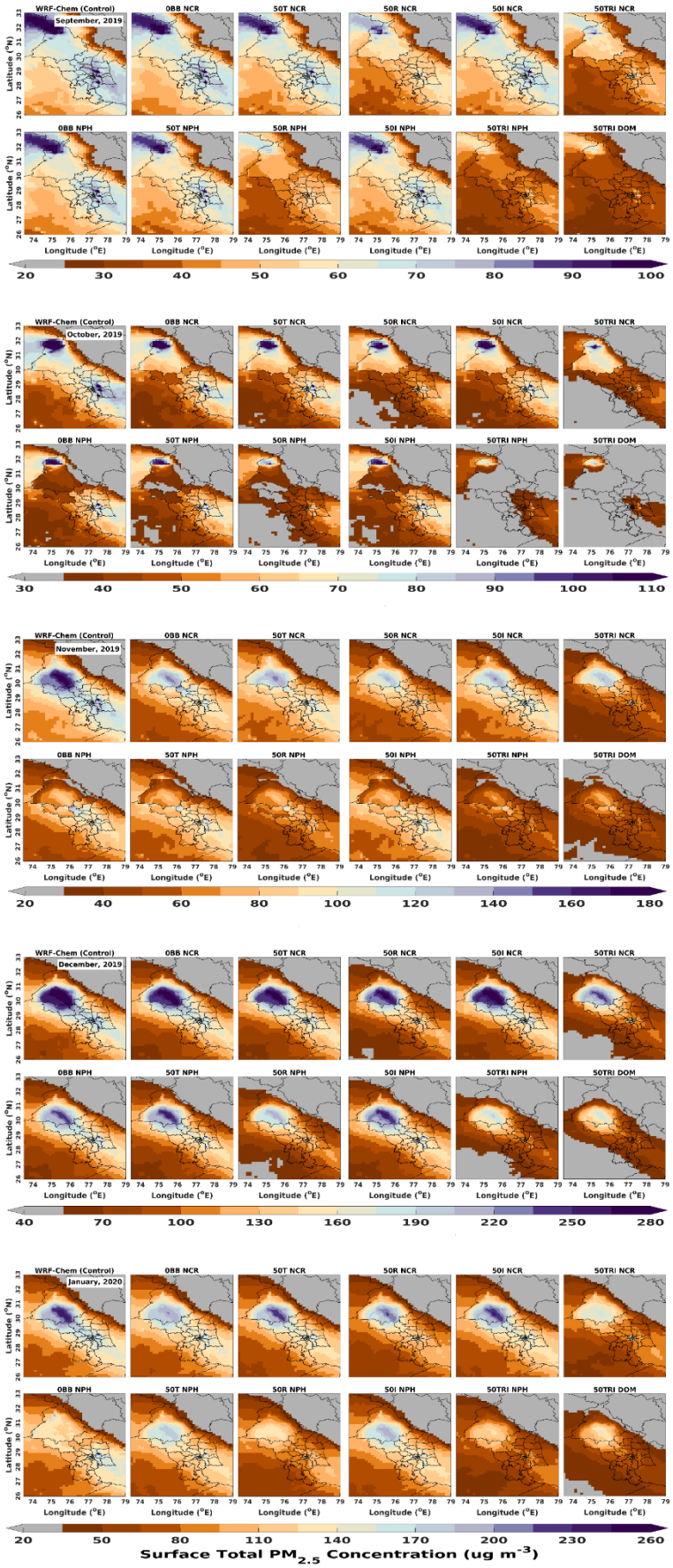


Figure 5.13: Monthly spatial distribution of surface $PM_{2.5}$ concentrations over northern India from the WRF-Chem emission-perturbed simulations for the full study period, illustrating the regional impacts of sector-specific and CRB-related mitigation scenarios.

Extending these sectoral reductions with a CRB ban across the entire model domain further amplifies the response: reductions in NCT-Delhi approach ~50% during the post-monsoon and winter months (Fig. 5.3; Table 5.2). While this domain-wide case (50TRI DOM) is intentionally idealized and exceeds near-term administrative feasibility, it is scientifically useful because it sets an upper bound on what coordinated regional action could achieve, given the same meteorological conditions.

During the peak burning period, the airshed CRB restriction demonstrates the spatial fingerprint of fire emissions particularly clearly. Eliminating CRB across the NCT-Delhi airshed reduces $PM_{2.5}$ by 12.86 ± 5.37% in Delhi-NCR, but by 45.44 ± 9.71% in Punjab and 34.79 ± 9.90% in Haryana (Table 5.2). The mechanism is that Punjab and Haryana experience the strongest direct influence of burning because they are the principal emitting regions, whereas Delhi-NCR is mainly a downwind receptor where CRB contributes as an episodic enhancement superimposed on substantial local and regional non-fire emissions. The implication is that CRB mitigation delivers the largest near-field benefits in the source states, while still providing meaningful, but secondary, improvements for Delhi.

The strongest regional improvements arise under the comprehensive mitigation scenario that couples stringent sectoral reductions with a nationwide CRB ban (Fig. 5.4 & Fig. 5.5). Although this configuration lies beyond the primary near-term policy scope of the present work, it provides a critical scientific benchmark: under this case, $PM_{2.5}$ reductions reach up to ~60% in Punjab and Haryana (Fig. 5.6), demonstrating how strongly upwind emissions control the broader background that ultimately affects NCT-Delhi. The implication is that Delhi's air-quality ceiling is set by regional emissions as much as by local emissions, particularly during the months when transport and stagnation reinforce each other.

The NAQI analysis confirms that airshed-scale mitigation does not merely lower mean $PM_{2.5}$; it substantially reshapes exposure categories. With airshed-wide CRB elimination, "Very Poor" days in NCT-Delhi decline by approximately ~10% (from 67 to 52 days) and adding a 50% reduction in residential emissions lowers "Very Poor" days further to 36 (Fig. 5.8). Under the combined 50TRI NPH scenario (50% reductions in residential, transport, and industrial emissions plus complete airshed CRB elimination), the system shifts decisively: 51% of all study days (78 of 153) fall in the "Satisfactory" category for NCT-Delhi (Table 5.3). This is the strongest evidence in the chapter that airshed-scale action can transform the seasonal exposure regime, converting a large fraction of chronically polluted days into health-relevant improvements.

A complementary, explicitly aspirational case, 50% reductions in all major anthropogenic sectors combined with a nationwide CRB ban, demonstrates even larger improvements during winter: “Good” days increase by about 22% in Punjab and 14% in Haryana, and by 11% and 14% in NCT-Delhi and Delhi-NCR, respectively, while “Satisfactory” days rise by 26% in Punjab and 22% in Haryana (Fig. 5.3 & Fig. 5.8). The implication is not that such a scenario is immediately implementable, but rather that the air-quality system responds strongly and coherently when emissions are reduced at the same scale as the meteorological transport pathways that govern pollution accumulation. This reinforces the central conclusion: city-centric, short-range interventions cannot deliver sustained improvements in Delhi’s winter air quality; only multi-sector, multi-state mitigation aligned with airshed transport dynamics can do so.

5.3.3 Role of Meteorology in Modulating $PM_{2.5}$ and Mitigation Effectiveness

Meteorology exerts first-order control on both the accumulation and dispersion of pollutants, and therefore on the apparent effectiveness of emission controls (Xie et al., 2024). For the NCT-Delhi airshed, the relevant meteorological drivers include (i) near-surface temperature (as a proxy for wintertime stability and inversion strength), (ii) precipitation (wet scavenging and ventilation associated with synoptic disturbances), (iii) boundary-layer height (BLH; the effective mixing volume available for pollutants), and (iv) the ventilation coefficient, defined here as BLH multiplied by mean horizontal wind speed, which provides an integrated measure of the atmosphere’s capacity to dilute and export pollutants.

One of the most intense pollution episodes in our study period occurs during the last week of December 2019, when very high $PM_{2.5}$ over NCT-Delhi coincides with low temperatures, very shallow BLHs (only a few hundred metres), and negligible rainfall (Fig. 5.14 & Fig. 5.15). Mechanistically, these conditions suppress vertical mixing and limit horizontal export, producing low ventilation coefficients and enabling rapid pollutant accumulation even when emissions remain steady. As winter progresses, similarly stagnant regimes recur more frequently, sustaining “Very Poor” to “Severe” air quality across the airshed and raising the baseline level upon which episodic enhancements (including remaining burning, local spikes, or regional transport) act (Fig. 5.16 & Fig. 5.17).

Importantly, however, the emission-perturbation simulations show that meaningful reductions remain achievable even under adverse meteorology, although the absolute concentrations during the most stagnant periods may still remain elevated. When CRB is restricted

within NCR and emissions from transport, residential, and industrial sectors are each reduced by 50%, $PM_{2.5}$ decreases by ~25% over NCT-Delhi on average and by ~30% across the broader airshed (Fig. 5.14-5.17). This indicates that, even when dilution is weak, reducing the source strength lowers the accumulated mass in a near-proportional manner, thereby reducing both the intensity and duration of extreme events.

Under the more expansive case where CRB is controlled across all northern Indian states and 50% reductions are applied across the three major sectors, $PM_{2.5}$ reductions over NCT-Delhi remain robust across meteorological regimes (Fig. 5.14). Specifically, $PM_{2.5}$ decreases by 38% under dry conditions (0-2 mm day^{-1} rainfall), 42% under low ventilation coefficients (0-500 m^2 s^{-1}), 40% under high temperature conditions (≥ 30 °C), and 41% under shallow BLHs (0-200 m). The evidence here is the stratified reduction statistics in Fig. 5.14, and the implication is critical for policy: structural emission reductions do not rely on "good weather" to be effective. They reduce baseline concentrations even during the worst dispersion regimes, precisely when public-health risks are greatest, although meteorology still determines whether standards are exceeded on a given day.

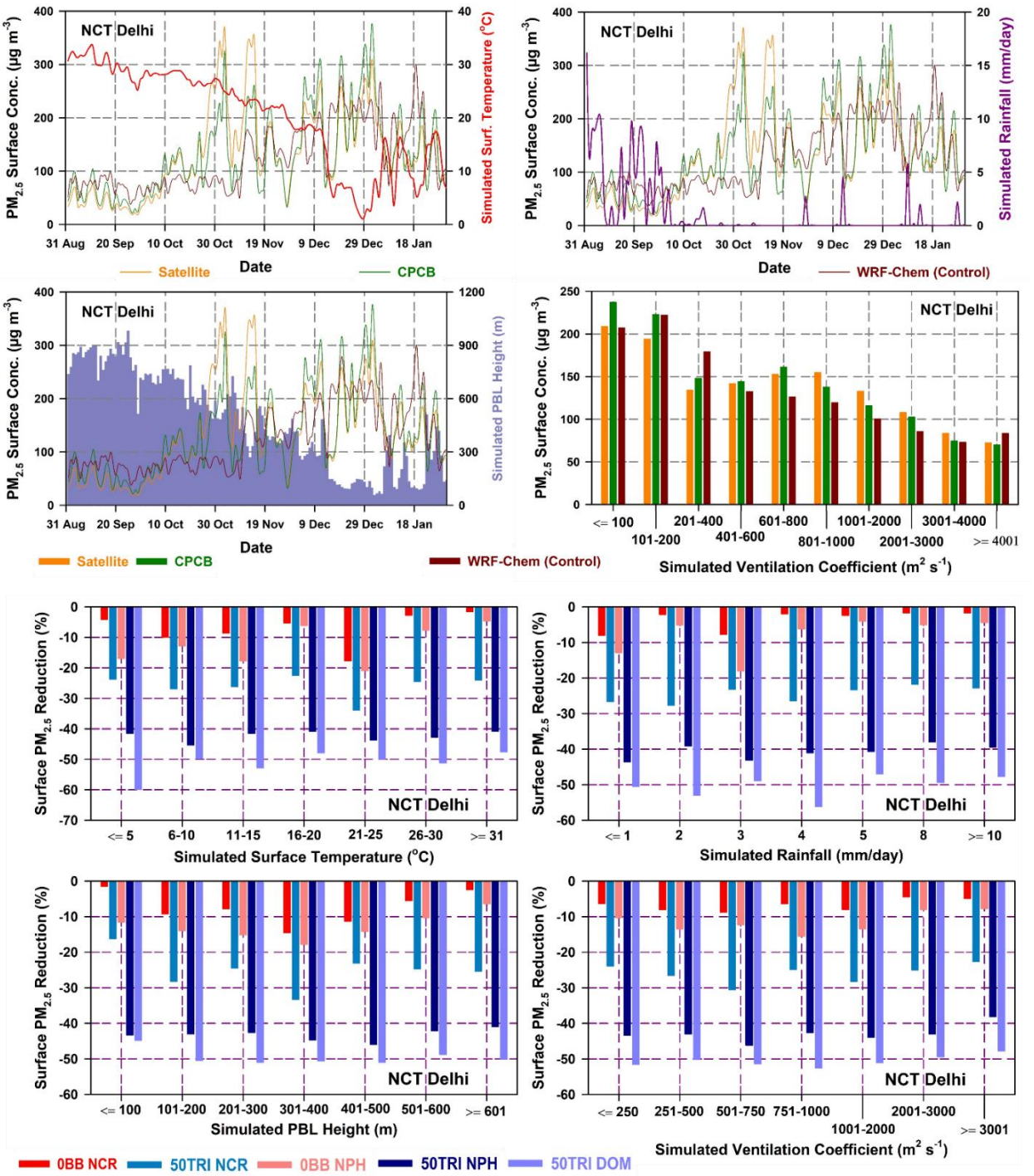


Figure 5.14: Daily time series of surface $PM_{2.5}$ from WRF-Chem, satellite retrievals, and CPCB observations, along with major meteorological variables over NCT-Delhi (top panels). The lower panels depict reductions in $PM_{2.5}$ under five emission-perturbation scenarios, grouped by meteorological-variable ranges for the study period.

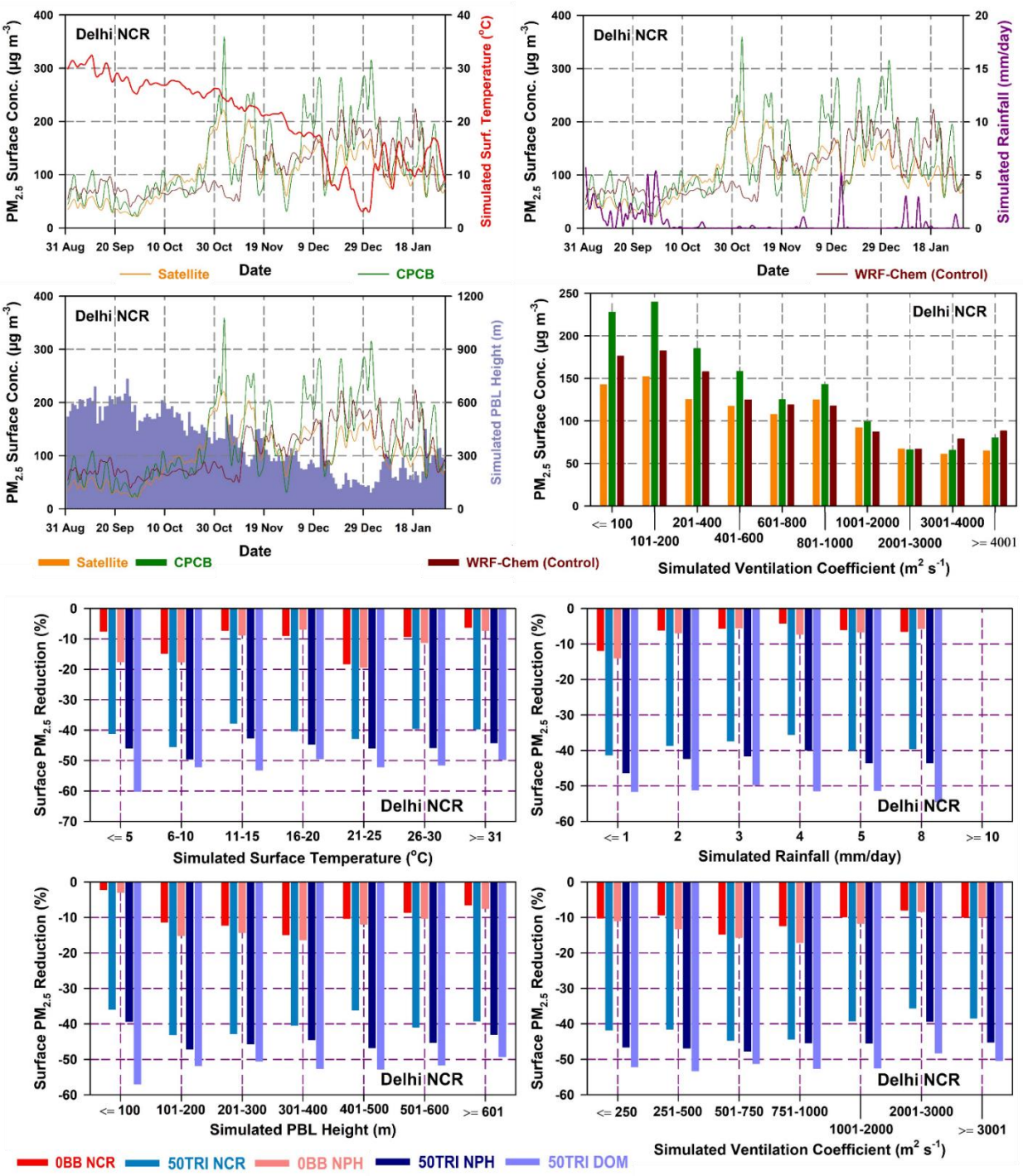


Figure 5.15: Daily time series of surface $PM_{2.5}$ over Delhi-NCR from the WRF-Chem control simulation, satellite-derived estimates, and CPCB observations, shown alongside key meteorological variables for the full study period (top two panels). The bottom two panels present the relative reductions in surface $PM_{2.5}$ achieved under five targeted emission-perturbation scenarios, stratified by ranges of selected meteorological conditions over the same period.

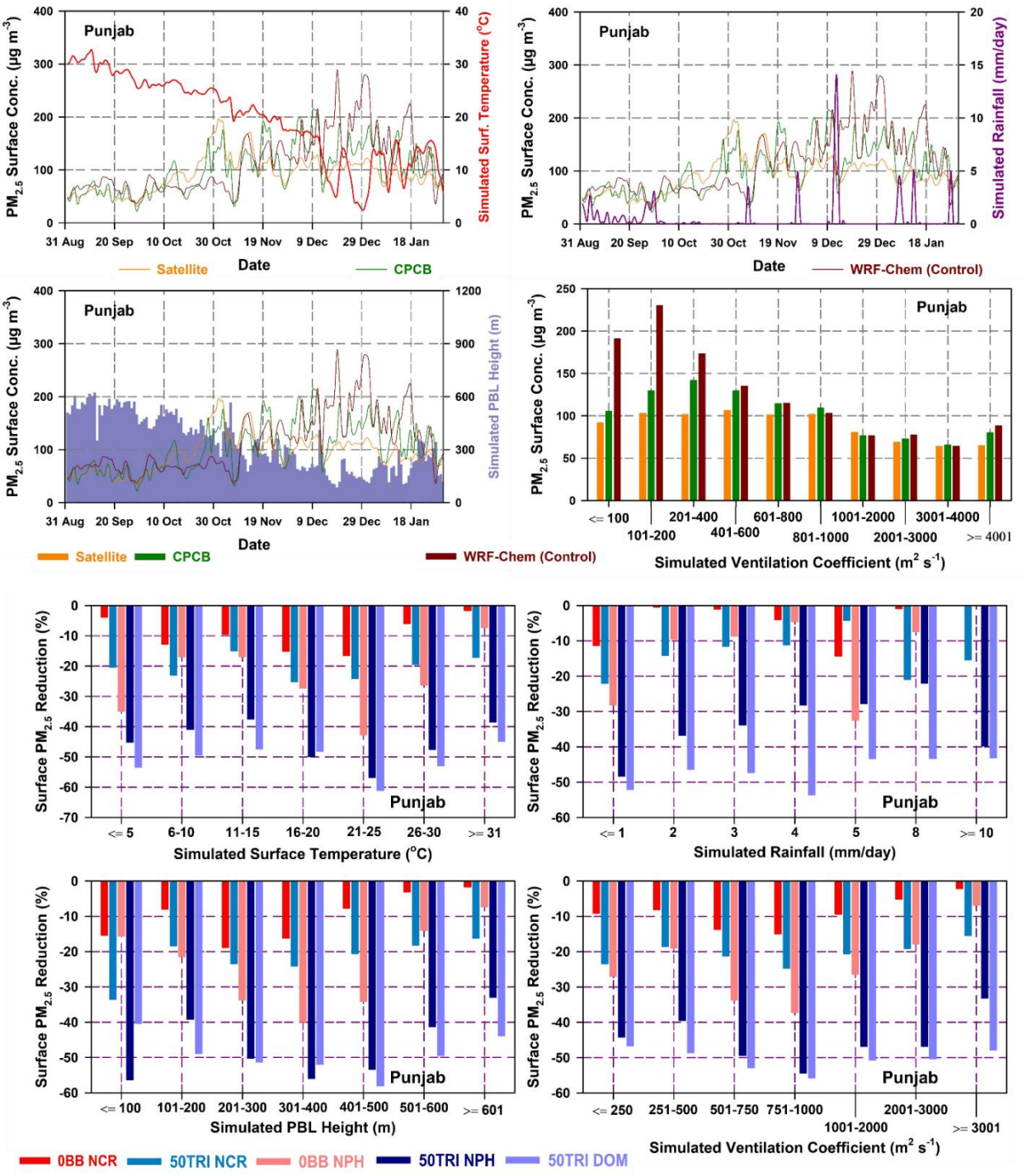


Figure 5.16: Daily time series of surface $PM_{2.5}$ over Punjab from the WRF-Chem control simulation, satellite-derived estimates, and CPCB observations, shown together with key meteorological variables for the full study period (top two panels). The bottom two panels depict the relative reductions in surface $PM_{2.5}$ under five targeted emission-perturbation scenarios, stratified by ranges of selected meteorological conditions over Punjab during the same period.

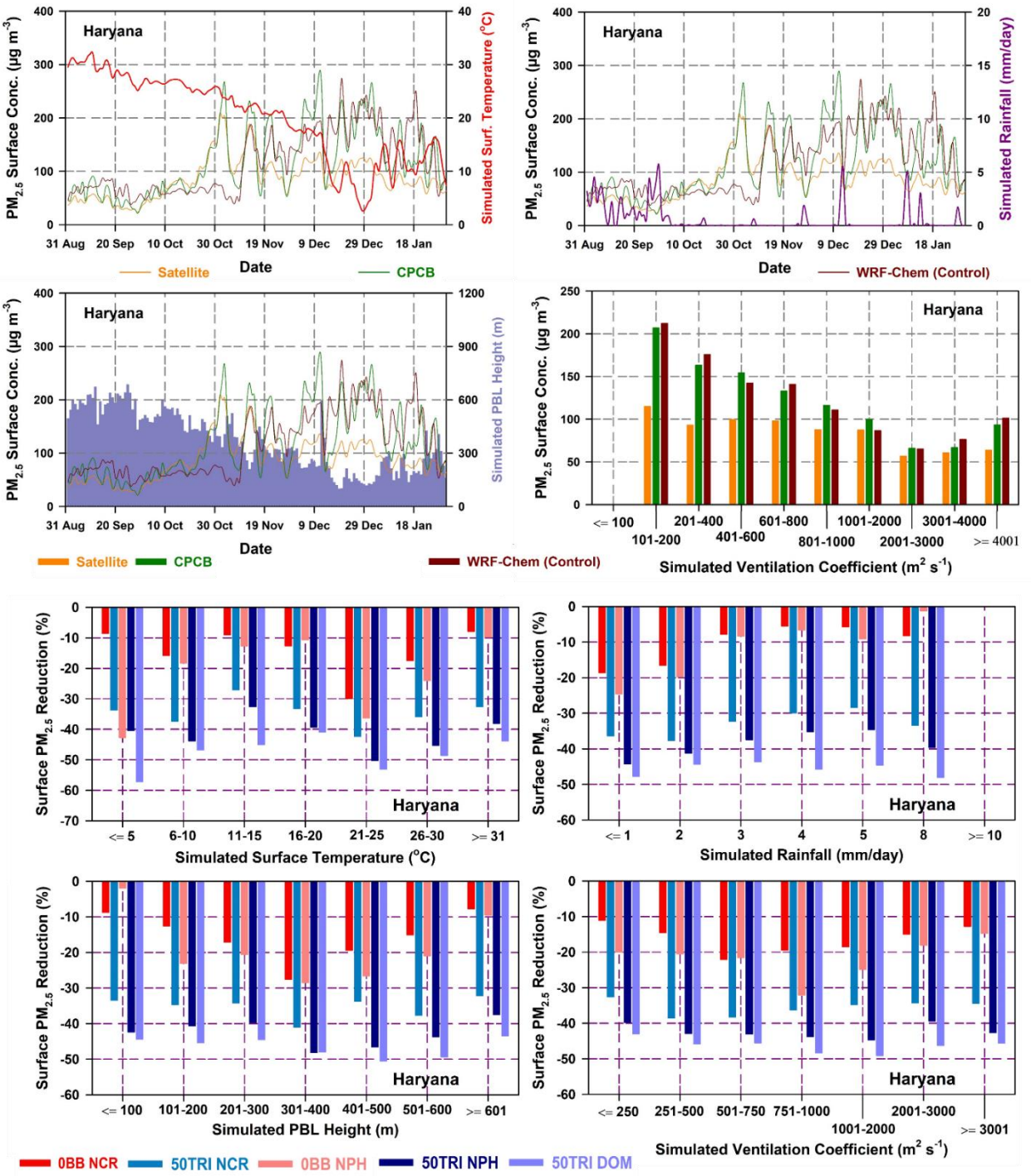


Figure 5.17: Daily time series of surface $PM_{2.5}$ over Haryana from the WRF-Chem control simulation, satellite-derived estimates, and CPCB observations, shown alongside key meteorological variables for the full study period (top two panels). The bottom two panels present the relative reductions in surface $PM_{2.5}$ achieved under five targeted emission-perturbation scenarios, stratified by different ranges of meteorological conditions over Haryana during the same period.

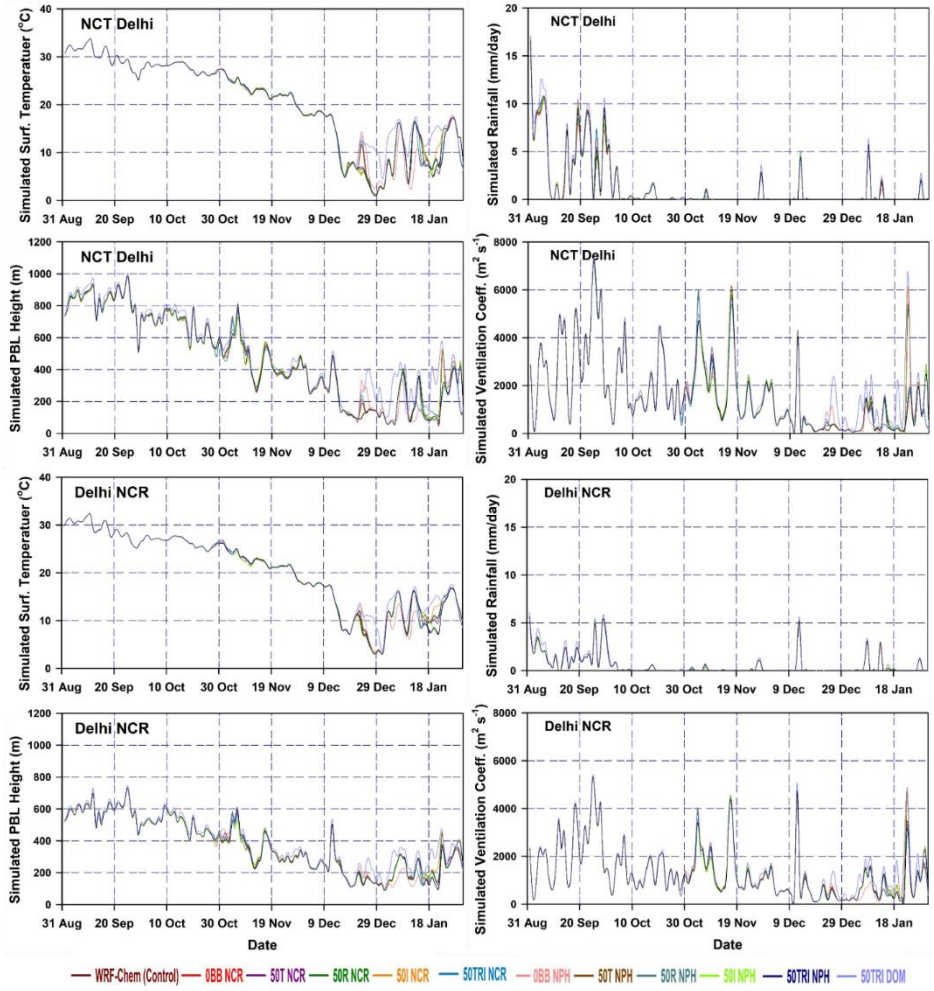


Figure 5.18: Daily time-series analysis of key meteorological variables over NCT-Delhi and Delhi-NCR for the full study period, comparing the responses simulated under the different emission-perturbed WRF-Chem scenarios.

Beyond pure dispersion effects, aerosol–meteorology feedback can further modulate both pollutant levels and meteorological state. During the late-December episode, emission reductions decrease aerosol loading and thus modify radiative fluxes, which can feed back onto near-surface temperature and BLH (Fig. 5.18 and Fig. 5.20). Conceptually, lower aerosol optical depth reduces shortwave attenuation and can alter stability and boundary-layer development; the net sign and magnitude depend on season, surface properties, and aerosol composition. In our simulations, these coupled responses are captured by the time-series comparison of meteorological variables across scenarios (Fig. 5.18 and Fig. 5.20). Consistent with the reduced aerosol burden, simulated aerosol optical depth (AOD), a column-integrated measure of aerosol extinction, declines substantially under scenarios with strong CRB controls and combined sectoral reductions (Fig. 5.19). The evidence is the coherent AOD decrease across NCT-Delhi, Delhi-NCR, Punjab, and Haryana in Fig. 5.19, and the implications extend beyond mass concentration alone: reduced AOD corresponds to improved visibility and indicates potential co-benefits in radiative forcing and solar resource availability, alongside health benefits.

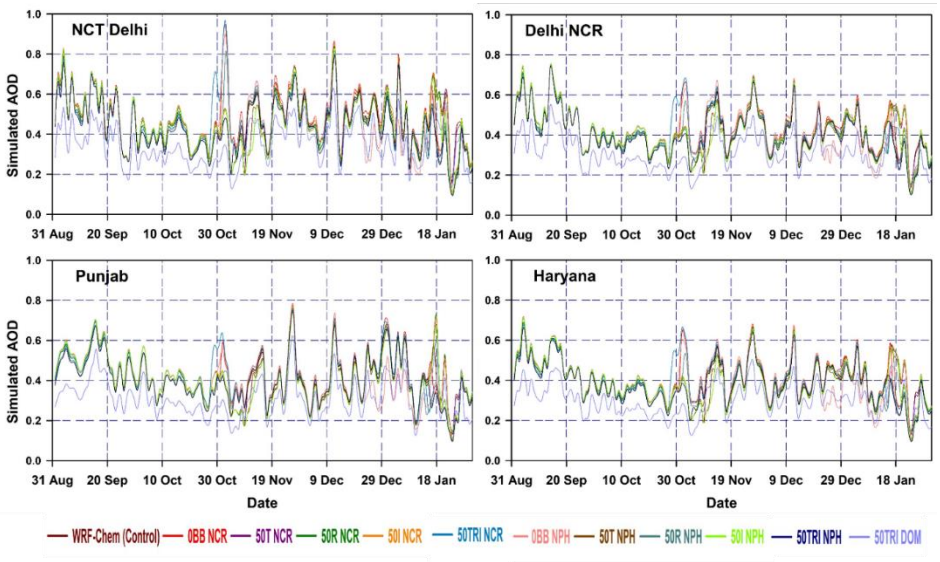


Figure 5.19: Daily time-series analysis of Aerosol Optical Depth (AOD) over NCT-Delhi, Delhi-NCR, Punjab, and Haryana for the entire study period, comparing the response across the different emission-perturbed WRF-Chem simulations.

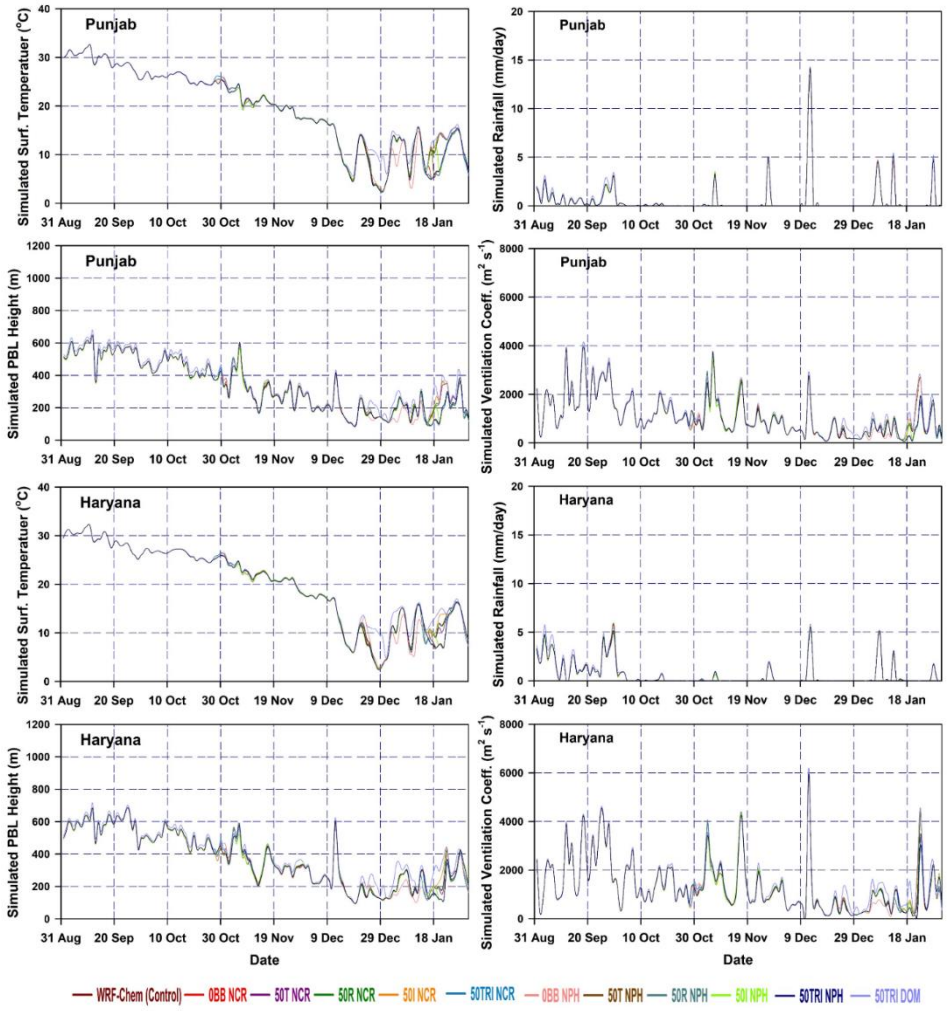


Figure 5.20: Daily time-series analysis of key meteorological variables over Punjab and Haryana for the full study period, comparing their evolution across the different emission-perturbed WRF-Chem simulations.

Overall, this chapter demonstrates that meteorology governs day-to-day variability, setting the conditions for accumulation or dilution, but emissions govern the baseline and the attainable floor of $PM_{2.5}$ during the high-pollution season. The strongest reductions occur when mitigation is implemented at the same spatial scale as the transport pathways that supply the airshed, and the benefits remain substantial even during the most stagnant episodes. This combined evidence provides a mechanistic justification for shifting from episodic, city-centric responses toward persistent, coordinated, airshed-scale emission reductions across major sectors, particularly residential combustion and CRB, complemented by transport and industrial measures.

5.4 Summary and Conclusions

Drawing on insights from the preceding chapter, which showed that the lockdown-period decline in surface $PM_{2.5}$ was driven largely by meteorological variability rather than emission reductions alone (Nandi et al., 2025), this chapter employs a high-resolution WRF-Chem modelling framework to quantify how much air quality over NCT-Delhi can improve under realistically strengthened emission-control policies applied (i) within Delhi-NCR only and (ii) across the broader airshed. The analysis focuses on September 2019-January 2020, spanning the post-monsoon and winter seasons when the region experiences its most persistent and hazardous pollution episodes, driven by the combined effects of regional biomass burning, large residential-sector emissions, and recurring meteorological stagnation.

A central conclusion is that policy action confined to Delhi-NCR produces only limited improvements in NCT-Delhi during the peak crop-residue burning (CRB) season. A complete CRB ban applied only within Delhi-NCR reduces $PM_{2.5}$ over NCT-Delhi by merely ~2-3% during October-November 2019, indicating that most of the burning-related aerosol burden affecting NCT-Delhi originates from upwind agricultural regions outside the NCR boundary. When the same CRB restriction is extended across the full NCT-Delhi airshed (Punjab, Haryana, and Delhi-NCR), the $PM_{2.5}$ reduction rises to ~9-10%, clearly demonstrating the dominant influence of upwind burning in Punjab and Haryana on downwind receptor concentrations over NCT-Delhi.

Across northern India, residential emissions emerge as the single most important contributor to baseline $PM_{2.5}$, accounting for ~40-50% of total mass and exhibiting limited sensitivity to short-lived activity disruptions. In our scenario framework, a 50% reduction in

residential emissions, representing strong and sustained implementation of PMUY, Unnat Chulha Abhiyan, NCAP, Saubhagya, and allied measures, combined with a complete CRB ban across the airshed lowers $PM_{2.5}$ over NCT-Delhi by ~30%. The simulations further indicate that transport-sector controls can deliver additional benefits, consistent with measures such as strict Bharat Stage compliance, accelerated removal of high-emitting vehicles, restrictions on poor-quality fuels in commercial fleets, and expanded public transport and demand-side interventions, yielding a further ~13% reduction. Industrial-sector mitigation, including fuel switching, adoption of cleaner technologies, enhanced deployment of renewable energy, and consistent application of GRAP-type measures across northern India, contributes an additional ~11% reduction during the high-pollution season. Taken together, these results show that the largest gains come from targeting sectors that simultaneously reduce primary $PM_{2.5}$ and the precursor gases that drive secondary aerosol formation, while also addressing the regional inflow that sustains wintertime background concentrations.

When these measures are implemented coherently and at airshed scale, the improvements are transformative rather than incremental. Under an ambitious yet policy-consistent scenario, 50% reductions in residential, transport, and industrial emissions combined with a complete CRB ban across the NCT-Delhi airshed, NCT-Delhi experiences up to 17 “Good” and 68 “Satisfactory” AQI days within the 153-day study period. Correspondingly, the number of “Very Poor” days declines sharply across NCT-Delhi, Delhi-NCR, Punjab, and Haryana, while the frequencies of “Moderate” and “Satisfactory” days increase. These changes in the NAQI distribution demonstrate that sustained, coordinated inter-state mitigation can fundamentally shift the seasonal exposure regime away from chronic “Very Poor/Severe” conditions toward a substantially cleaner and more health-protective air-quality profile.

The source- and process-oriented diagnostics place these mitigation responses in a mechanistic context. During the October-November CRB period, biomass burning contributes ~50% of surface $PM_{2.5}$ in Punjab, ~36% in Haryana, and ~13% in Delhi-NCR, confirming that CRB control is essential for meaningful reductions in the source states and for reducing transported pollution into NCT-Delhi. Organic aerosols dominate $PM_{2.5}$ composition across northern India, and secondary $PM_{2.5}$ produced from gaseous precursors (NO_x, SO_2, NH_3, and VOCs) accounts for ~57% of total $PM_{2.5}$ over NCT-Delhi during winter. This large secondary fraction highlights why effective policy packages must target not only primary particulate emissions but also precursor gases through multi-sectoral measures. Water-associated aerosol mass and desert dust contribute substantially to the residual category, while BC concentrations increase sharply over Punjab and

Haryana during peak CRB activity. Under prevailing north-westerly flow, these plumes are efficiently transported toward NCT-Delhi, elevating both $PM_{2.5}$ and BC during the most polluted portion of the year.

Consistent with the lockdown analysis, meteorology remains a dominant control on day-to-day $PM_{2.5}$ variability. The most severe episodes coincide with shallow boundary layers, weak winds, low ventilation coefficients, and limited precipitation, all of which suppress dispersion and promote pollutant accumulation. Importantly, however, the modelling experiments show that structural emission reductions retain strong effectiveness even under the least favourable dispersion conditions. Combined 50% reductions in residential, transport, and industrial emissions together with complete elimination of CRB reduce $PM_{2.5}$ by ~40-50% over NCT-Delhi during stagnant conditions. This indicates that, although meteorology modulates the timing and intensity of extremes, robust emission mitigation can substantially lower the baseline burden and meaningfully reduce the frequency and severity of winter episodes rather than relying on transient "cleaning" events driven by weather.

Overall, this chapter demonstrates unequivocally that Delhi cannot clean its air through local measures alone. Persistent winter pollution arises from an airshed-scale coupling of emissions, chemistry, and meteorology, and therefore demands a coordinated, multi-sectoral, multi-state mitigation strategy. The results show that large reductions in wintertime $PM_{2.5}$ are technically achievable through strengthened implementation of existing policies, especially those addressing residential combustion and biomass burning, and that these benefits persist even when dispersion is weakest. Transitioning from city-centric interventions to a scientifically grounded airshed-governance framework is therefore essential. Such an approach would increase the number of "Good" and "Moderate" AQI days across NCT-Delhi while also delivering broader co-benefits for climate mitigation, public health, agricultural productivity, and regional economic development. As India confronts rapid urbanization, rising energy demand, and evolving agricultural practices, an integrated airshed management strategy, supported by improved emissions monitoring, enhanced CRB detection and enforcement, and targeted sectoral policies, represents a critical pathway toward sustained air-quality improvement across the Indo-Gangetic Plain.

Chapter 6: Summary and Scope for Future Work

6.1 Summary

The present thesis demonstrates that a carefully configured and observation-evaluated regional air-quality modelling framework can be used to: (i) reduce major sources of uncertainty in simulated $PM_{2.5}$, (ii) explicitly disentangle the respective influences of emission variability and meteorological variability on observed $PM_{2.5}$ changes, and (iii) quantify the sectoral, chemical, and process-level drivers of severe pollution across North India, with particular emphasis on the NCT-Delhi airshed. By integrating coordinated WRF-Chem sensitivity experiments, the COVID-19 lockdown as a quasi-experimental perturbation, and high-resolution sectoral emission-perturbation simulations, the thesis establishes a coherent mechanistic understanding of persistent $PM_{2.5}$ exceedances over the Indo-Gangetic Plain. Specifically, the results show that chronic and episodic high $PM_{2.5}$ arise from the coupled effects of spatially diffuse, year-round emissions (most notably residential combustion), seasonally intensified episodic sources (especially post-monsoon crop-residue burning), substantial secondary aerosol production from precursor gases, and meteorological regimes that alternately enhance ventilation or promote stagnation and pollutant accumulation. Collectively, these findings provide a process-based foundation for interpreting policy outcomes and demonstrate that sustained improvements in air quality over NCT-Delhi and North India will require coordinated, airshed-scale, multi-sector mitigation, designed with explicit consideration of seasonal meteorology and regional transport pathways.

The National Capital Territory (NCT) of Delhi, situated in the northwestern IGP, exemplifies the severity of this crisis. Like other rapidly growing megacities, Delhi experiences chronically elevated $PM_{2.5}$ levels that adversely impact human health, regional ecosystems, agricultural productivity, and local climate. Current concentrations in Delhi-NCR exceed the 2021 World Health Organization guidelines by more than a factor of 30. Severe haze episodes are most frequent during the post-monsoon (October-November) and winter (December-February) months due to a combination of heightened emissions and unfavourable meteorological conditions, including suppressed boundary-layer heights, weak winds, and temperature inversions. These diverse emission sources, when coupled with seasonal meteorology, collectively drive extreme haze events across northern India. Recent studies consistently identify Indian cities especially those across the IGP as among the world's most prominent $PM_{2.5}$ hotspots.

In this context, the present work advances regional $PM_{2.5}$ modelling over India by evaluating COVID-19 emission reduction impacts and elucidating the mechanisms responsible for

observed declines in pollution levels. We further investigate the dominant sources and chemical composition of surface $PM_{2.5}$ during peak haze episodes over northern Indian states. Finally, this study assesses feasible mitigation pathways to improve air quality and enhance the prospects of achieving clean air across the northern Indian region.

Major Findings of the Thesis:

1. **A physically and chemically robust and optimized WRF-Chem configuration for India** was established through a coordinated sensitivity analysis spanning two contrasting meteorological regimes, monsoon (August 2018) and winter (January 2019). The optimized setup, comprising ERA5 meteorological forcing, the YSU PBL scheme, Lin microphysics, the MOZART–MOSAIC chemical mechanism with VBS-based SOA treatment, SMoG-COALESCE emissions, and moderate grid nudging (0.0005 s^{-1}) above the PBL, substantially improves the realism of both meteorological fields and pollutant concentrations. This configuration provides a robust foundation for subsequent attribution and mitigation experiments (Chapter 2).

2. **Meteorological variability dominates short-term $PM_{2.5}$ fluctuations**, particularly during the COVID-19 period. National-scale $PM_{2.5}$ reductions following lockdown onset were driven primarily by changes in dispersion, mixing, and removal processes rather than by emission reductions alone. This finding demonstrates that apparent air-quality improvements cannot be reliably attributed to emission controls without explicit meteorological normalization (Chapter 3).

3. **Emission reductions during lockdown were highly sectorally asymmetric**. While transport- and industry-related emissions declined sharply, residential emissions increased during the strict lockdown phase, reflecting intensified household energy use. This imbalance explains the non-linear and spatially heterogeneous $PM_{2.5}$ responses observed across regions, even under an extreme, nationwide activity perturbation (Chapter 3).

4. **Residential combustion is the most persistent and influential contributor to baseline $PM_{2.5}$ across North India**, accounting for approximately 40-50% of $PM_{2.5}$ mass over key northern states. Its influence is strongest during winter, when shallow boundary layers and weak ventilation favour pollutant accumulation, highlighting residential energy use as a critical long-term mitigation priority (Chapter 4).

5. **Secondary aerosol formation is a dominant driver of wintertime $PM_{2.5}$**, particularly over major receptor regions. Over NCT-Delhi, secondary $PM_{2.5}$ constitutes roughly 57% of total winter $PM_{2.5}$, indicating that effective mitigation must target precursor gases (NO_x, SO_2, NH_3, and VOCs) in addition to primary particulate emissions (Chapter 4).

6. **Crop-residue burning (CRB) is a major driver of episodic pollution extremes and source-region degradation**. During the post-monsoon period (October-November), CRB contributes ~50% of $PM_{2.5}$ in Punjab, ~36% in Haryana, and ~13% in Delhi-NCR. Biomass-burning-derived organic aerosols dominate the associated mass, and prevailing north-westerly winds efficiently transport both $PM_{2.5}$ and black carbon into NCT-Delhi, intensifying regional haze episodes (Chapters 4-5).

7. **City-centric mitigation is inherently insufficient for NCT-Delhi during high-pollution seasons**. A complete CRB ban applied only within Delhi-NCR yields marginal $PM_{2.5}$ reductions (~2-3%) over NCT-Delhi, whereas extending CRB controls across the full NCT-Delhi airshed (Punjab-Haryana-Delhi-NCR) produces substantially larger benefits (~9-10%), highlighting the dominance of upwind regional sources (Chapter 5).

8. **Airshed-scale, multi-sector mitigation strategies yield transformative rather than incremental improvements**. Under an ambitious yet policy-consistent scenario 50% reductions in residential, transport, and industrial emissions combined with a complete CRB ban across the airshed NCT-Delhi experiences up to 17 “Good” and 68 “Satisfactory” AQI days (out of 153), alongside a pronounced reduction in “Very Poor” days across NCT-Delhi, Delhi-NCR, Punjab, and Haryana (Chapter 5).

9. **Structural emission controls remain effective even under adverse winter meteorology**. Although the most severe pollution episodes coincide with shallow boundary layers, weak winds, low ventilation coefficients, and limited precipitation, combined multi-sector emission reductions together with CRB elimination still lower $PM_{2.5}$ by ~40-50% over NCT-Delhi during stagnant conditions. This demonstrates that emission mitigation can substantially reduce baseline pollution and the intensity of extremes, even when dispersion is least favourable (Chapters 3 and 5).

10. **A central overarching conclusion is that airshed governance represents the scientifically appropriate management framework**. Transboundary transport, regional secondary aerosol formation, and seasonally varying meteorological controls often dominate local $PM_{2.5}$ concentrations. Consequently, effective policy design and evaluation must move beyond administrative boundaries toward coordinated, regionally integrated strategies explicitly aligned with seasonal meteorology and transport pathways (Chapters 4-5).

6.2 Limitations of the Presented Study

While this thesis provides a comprehensive, process-based assessment of $PM_{2.5}$ pollution over North India using a coupled regional modelling framework, several limitations remain. The analysis is temporally constrained by the availability of high-resolution emission inventories, restricting explicit evaluation of post-lockdown emission trends. Model performance and attribution are inherently influenced by uncertainties in sectoral emissions, particularly for residential combustion and crop residue burning, and by limitations in satellite-based fire detection. The focus on $PM_{2.5}$ alone precludes a full assessment of multi-pollutant interactions involving ozone and precursor gases. In addition, the real-world effectiveness of ongoing policy interventions could not be directly quantified due to the lack of validated, policy-specific observational datasets. These limitations motivate several important directions for future research.

6.3 Future scope of work

Although this thesis makes substantial progress toward advancing the science and achieving the objectives of "Assessing Sectoral and Primary Emission Contributions to $PM_{2.5}$ Pollution over North India Using Regional Air Quality Modelling," important uncertainties and emerging research needs remain. Addressing these will strengthen attribution robustness, improve representation of chemical and meteorological processes, and enhance the policy relevance of future air-quality assessments.

1. Strengthening emission constraints using multi-platform observations: Future work should integrate top-down and bottom-up approaches by combining dense ground-based monitoring, chemically speciated aerosol measurements, satellite retrievals (AOD, NO_2, SO_2, NH_3), and activity-based proxies. Such integration is especially critical for reducing uncertainties in residential combustion, informal industry, and open burning, where emissions are spatially diffuse and temporally variable.

2. Improving representation of secondary PM formation processes: Given the dominant role of secondary aerosols during winter, targeted studies are needed to refine nitrate–ammonium partitioning, heterogeneous and aqueous-phase chemistry, and SOA formation pathways, including IVOC and SVOC oxidation. These efforts should be supported by coordinated urban and rural measurements of aerosol composition and precursor gases across the airshed.

3. Advancing meteorology–chemistry coupling and feedback diagnostics: Further research should quantify how aerosol–radiation and aerosol-boundary-layer feedback modify stagnation, boundary-layer evolution, and episode persistence, and how these feedback influence the effectiveness of mitigation strategies across seasons and synoptic regimes.

4. Refining biomass-burning characterization and plume evolution: Improved representation of crop residue burning is needed through better detection of small and obscured fires, refined injection-height assumptions, and explicit treatment of plume chemistry and aging. Higher-resolution fire products and targeted field observations during the post-monsoon season would substantially improve source attribution for the NCT-Delhi airshed.

5. Developing multi-year, multi-season attribution frameworks: Extending sectoral and process-based attribution across multiple years and seasons will help distinguish robust, repeatable controls on $PM_{2.5}$ from year-specific meteorological effects and will allow quantification of interannual variability in mitigation effectiveness.

6. Evaluating policy realism using dynamic activity and compliance scenarios: Future modelling should move beyond idealized emission reductions by incorporating realistic trajectories of policy adoption and compliance, including household energy transitions, vehicle fleet turnover, industrial fuel switching, and enforcement variability. Integrating exposure- and health-based metrics alongside $PM_{2.5}$ mass would further strengthen policy relevance.

7. Expanding monitoring coverage in rural and peri-urban source regions: Finally, improving observational coverage over key upwind regions such as Punjab and Haryana, through calibrated low-cost sensor networks and targeted field campaigns, will be essential for evaluating emissions, boundary-layer processes, and source–receptor transport, which underpin effective airshed-scale management.

References

Afifa, Arshad, K., Hussain, N., Ashraf, M. H., & Saleem, M. Z. (2024). Air pollution and climate change as grand challenges to sustainability. *Science of The Total Environment*, *928*, 172370. https://doi.org/https://doi.org/10.1016/j.scitotenv.2024.172370

Agarwal, P., Stevenson, D. S., & Heal, M. R. (2024). Evaluation of WRF-Chem-simulated meteorology and aerosols over northern India during the severe pollution episode of 2016. *Atmospheric Chemistry and Physics*, *24*(4), 2239–2266. https://doi.org/10.5194/acp-24-2239-2024

Amann, M., Purohit, P., Bhanarkar, A. D., Bertok, I., Borken-Kleefeld, J., Cofala, J., Heyes, C., Kiesewetter, G., Klimont, Z., Liu, J., Majumdar, D., Nguyen, B., Rafaj, P., Rao, P. S., Sander, R., Schöpp, W., Srivastava, A., & Vardhan, B. H. (2017). Managing future air quality in megacities: A case study for Delhi. *Atmospheric Environment*, *161*, 99–111. https://doi.org/10.1016/j.atmosenv.2017.04.041

Ambulkar, R., Govardhan, G., Gavhale, S., Kalita, G., Pande, C., Jat, R., Kulkarni, S., Khare, M., Attri, S. D., & Ghude, S. D. (2025). Crop Residue Burning in North-Western India: Emission Estimation and Uncertainty Quantification. *Journal of Geophysical Research: Atmospheres*, *130*(4), e2024JD042198. https://doi.org/https://doi.org/10.1029/2024JD042198

Anand K A, A., Ganguly, D., Nandi, I., Kajino, M., & Dey, S. (2025). Disentangling the Separate and Combined Effects of Aerosol-Radiation and Aerosol-Photolysis Interactions on Air Quality Over India. *Journal of Geophysical Research: Atmospheres*, *130*(24), e2025JD045316. https://doi.org/https://doi.org/10.1029/2025JD045316

Anchev, N., Jakimovski, B., Spiridonov, V., & Velinov, G. (2020). Temperature Dependent Initial Chemical Conditions for WRF-Chem Air Pollution Simulation Model. In V. Dimitrova & I. Dimitrovski (Eds.), *ICT Innovations 2020. Machine Learning and Applications* (pp. 1–14). Springer International Publishing.

Anderson, R. M., Heesterbeek, H., Klinkenberg, D., & Hollingsworth, T. D. (2020). How will country-based mitigation measures influence the course of the COVID-19 epidemic? *The Lancet*, *395*(10228), 931–934. https://doi.org/10.1016/S0140-6736(20)30567-5

Andreae, M. O., & Rosenfeld, D. (2008). Aerosol–cloud–precipitation interactions. Part 1. The nature and sources of cloud-active aerosols. *Earth-Science Reviews*, *89*(1), 13–41. https://doi.org/https://doi.org/10.1016/j.earscirev.2008.03.001

Apte, J. S., Marshall, J. D., Cohen, A. J., & Brauer, M. (2015). Addressing Global Mortality from Ambient PM2.5. *Environmental Science & Technology*, *49*(13), 8057–8066. https://doi.org/10.1021/acs.est.5b01236

References

Apte, J. S., & Pant, P. (2019). Toward cleaner air for a billion Indians. *Proceedings of the National Academy of Sciences*, *116*(22), 10614–10616. https://doi.org/10.1073/pnas.1905458116

Avolio, E., Federico, S., Miglietta, M. M., Lo Feudo, T., Calidonna, C. R., & Sempreviva, A. M. (2017). Sensitivity analysis of WRF model PBL schemes in simulating boundary-layer variables in southern Italy: An experimental campaign. *Atmospheric Research*, *192*, 58–71. https://doi.org/https://doi.org/10.1016/j.atmosres.2017.04.003

Balakrishnan, K., Dey, S., Gupta, T., Dhaliwal, R. S., Brauer, M., Cohen, A. J., Stanaway, J. D., Beig, G., Joshi, T. K., Aggarwal, A. N., Sabde, Y., Sadhu, H., Frostad, J., Causey, K., Godwin, W., Shukla, D. K., Kumar, G. A., Varghese, C. M., Muraleedharan, P., … Dandona, L. (2019a). The impact of air pollution on deaths, disease burden, and life expectancy across the states of India: the Global Burden of Disease Study 2017. *The Lancet Planetary Health*, *3*(1), e26–e39. https://doi.org/10.1016/S2542-5196(18)30261-4

Balakrishnan, K., Dey, S., Gupta, T., Dhaliwal, R. S., Brauer, M., Cohen, A. J., Stanaway, J. D., Beig, G., Joshi, T. K., Aggarwal, A. N., Sabde, Y., Sadhu, H., Frostad, J., Causey, K., Godwin, W., Shukla, D. K., Kumar, G. A., Varghese, C. M., Muraleedharan, P., … Dandona, L. (2019b). The impact of air pollution on deaths, disease burden, and life expectancy across the states of India: the Global Burden of Disease Study 2017. *The Lancet Planetary Health*, *3*(1), e26–e39. https://doi.org/10.1016/S2542-5196(18)30261-4

Balwinder Singh, McDonald, A. J., Srivastava, A. K., & Gerard, B. (2020). Addendum: Tradeoffs between groundwater conservation and air pollution from agricultural fires in northwest India. *Nature Sustainability*, *3*(11), 972. https://doi.org/10.1038/s41893-020-00632-z

Balzarini, A., Pirovano, G., Honzak, L., Žabkar, R., Curci, G., Forkel, R., Hirtl, M., José, R. S., Tuccella, P., & Grell, G. A. (2015). WRF-Chem model sensitivity to chemical mechanisms choice in reconstructing aerosol optical properties. *Atmospheric Environment*, *115*, 604–619. https://doi.org/https://doi.org/10.1016/j.atmosenv.2014.12.033

Banerjee, T., Kumar, M., Mall, R. K., & Singh, R. S. (2017). Airing 'clean air' in Clean India Mission. *Environmental Science and Pollution Research*, *24*(7), 6399–6413. https://doi.org/10.1007/s11356-016-8264-y

Banks, R. F., Tiana-Alsina, J., Baldasano, J. M., Rocadenbosch, F., Papayannis, A., Solomos, S., & Tzanis, C. G. (2016). Sensitivity of boundary-layer variables to PBL schemes in the WRF model based on surface meteorological observations, lidar, and radiosondes during the HygrA-CD campaign. *Atmospheric Research*, *176–177*, 185–201. https://doi.org/https://doi.org/10.1016/j.atmosres.2016.02.024

Barrero, M. A., Orza, J. A. G., Cabello, M., & Cantón, L. (2015). Categorisation of air quality monitoring stations by evaluation of PM10 variability. *Science of The Total Environment*,

524–525, 225–236. https://doi.org/https://doi.org/10.1016/j.scitotenv.2015.03.138

Beig, G., Sahu, S. K., Singh, V., Tikle, S., Sobhana, S. B., Gargeva, P., Ramakrishna, K., Rathod, A., & Murthy, B. S. (2020). Objective evaluation of stubble emission of North India and quantifying its impact on air quality of Delhi. *Science of The Total Environment*, *709*, 136126. https://doi.org/https://doi.org/10.1016/j.scitotenv.2019.136126

Bekbulat, B., Apte, J. S., Millet, D. B., Robinson, A. L., Wells, K. C., & Marshall, J. D. (2020). PM2.5 and ozone air pollution levels have not dropped consistently across the US following societal covid response. *ISEE Conference Abstracts*, *2020*(1). https://doi.org/10.1289/isee.2020.virtual.O-OS-1692

Bhandari, S., Gani, S., Patel, K., Wang, D. S., Soni, P., Arub, Z., Habib, G., Apte, J. S., & Hildebrandt Ruiz, L. (2020). Sources and atmospheric dynamics of organic aerosol in New Delhi, India: insights from receptor modeling. *Atmospheric Chemistry and Physics*, *20*(2), 735–752. https://doi.org/10.5194/acp-20-735-2020

Bhattu, D., Tripathi, S. N., Bhowmik, H. S., Moschos, V., Lee, C. P., Rauber, M., Salazar, G., Abbaszade, G., Cui, T., Slowik, J. G., Vats, P., Mishra, S., Lalchandani, V., Satish, R., Rai, P., Casotto, R., Tobler, A., Kumar, V., Hao, Y., … Prévôt, A. S. H. (2024). Local incomplete combustion emissions define the PM2.5 oxidative potential in Northern India. *Nature Communications*, *15*(1), 3517. https://doi.org/10.1038/s41467-024-47785-5

Bikkina, S., Andersson, A., Kirillova, E. N., Holmstrand, H., Tiwari, S., Srivastava, A. K., Bisht, D. S., & Gustafsson, Ö. (2019). Air quality in megacity Delhi affected by countryside biomass burning. *Nature Sustainability*, *2*(3), 200–205. https://doi.org/10.1038/s41893-019-0219-0

Borge, R., Alexandrov, V., José del Vas, J., Lumbreras, J., & Rodríguez, E. (2008). A comprehensive sensitivity analysis of the WRF model for air quality applications over the Iberian Peninsula. *Atmospheric Environment*, *42*(37), 8560–8574. https://doi.org/https://doi.org/10.1016/j.atmosenv.2008.08.032

Bowden, J. H., Otte, T. L., Nolte, C. G., & Otte, M. J. (2012). Examining Interior Grid Nudging Techniques Using Two-Way Nesting in the WRF Model for Regional Climate Modeling. *Journal of Climate*, *25*(8), 2805–2823. https://doi.org/10.1175/JCLI-D-11-00167.1

Bran, S. H., & Srivastava, R. (2017). Investigation of PM2.5 mass concentration over India using a regional climate model. *Environmental Pollution*, *224*, 484–493. https://doi.org/https://doi.org/10.1016/j.envpol.2017.02.030

Brown, A. R., Derbyshire, S. H., & Mason, P. J. (1994). Large-eddy simulation of stable atmospheric boundary layers with a revised stochastic subgrid model. *Quarterly Journal of the Royal Meteorological Society*, *120*(520), 1485–1512. https://doi.org/https://doi.org/10.1002/qj.49712052004

References

Cao, F., Zhang, S.-C., Kawamura, K., Liu, X., Yang, C., Xu, Z., Fan, M., Zhang, W., Bao, M., Chang, Y., Song, W., Liu, S., Lee, X., Li, J., Zhang, G., & Zhang, Y.-L. (2017). Chemical characteristics of dicarboxylic acids and related organic compounds in PM2.5 during biomass-burning and non-biomass-burning seasons at a rural site of Northeast China. *Environmental Pollution*, *231*, 654–662. https://doi.org/https://doi.org/10.1016/j.envpol.2017.08.045

Chatterjee, D., McDuffie, E. E., Smith, S. J., Bindle, L., van Donkelaar, A., Hammer, M. S., Venkataraman, C., Brauer, M., & Martin, R. V. (2023). Source Contributions to Fine Particulate Matter and Attributable Mortality in India and the Surrounding Region. *Environmental Science & Technology*, *57*(28), 10263–10275. https://doi.org/10.1021/acs.est.2c07641

Chen, S.-H., & Sun, W.-Y. (2002). A One-dimensional Time Dependent Cloud Model. *Journal of the Meteorological Society of Japan. Ser. II*, *80*(1), 99–118. https://doi.org/10.2151/jmsj.80.99

Chintalapudi, N., Battineni, G., & Amenta, F. (2020). COVID-19 virus outbreak forecasting of registered and recovered cases after sixty day lockdown in Italy: A data driven model approach. *Journal of Microbiology, Immunology and Infection*, *53*(3), 396–403. https://doi.org/https://doi.org/10.1016/j.jmii.2020.04.004

Chowdhury, S., Dey, S., Guttikunda, S., Pillarisetti, A., Smith, K. R., & Di Girolamo, L. (2019). Indian annual ambient air quality standard is achievable by completely mitigating emissions from household sources. *Proceedings of the National Academy of Sciences of the United States of America*, *116*(22), 10711–10716. https://doi.org/10.1073/pnas.1900888116

Cohen, A. E., Cavallo, S. M., Coniglio, M. C., & Brooks, H. E. (2015). A Review of Planetary Boundary Layer Parameterization Schemes and Their Sensitivity in Simulating Southeastern U.S. Cold Season Severe Weather Environments. *Weather and Forecasting*, *30*(3), 591–612. https://doi.org/10.1175/WAF-D-14-00105.1

Cohen, A. J., Brauer, M., Burnett, R., Anderson, H. R., Frostad, J., Estep, K., Balakrishnan, K., Brunekreef, B., Dandona, L., Dandona, R., Feigin, V., Freedman, G., Hubbell, B., Jobling, A., Kan, H., Knibbs, L., Liu, Y., Martin, R., Morawska, L., … Forouzanfar, M. H. (2017). Estimates and 25-year trends of the global burden of disease attributable to ambient air pollution: an analysis of data from the Global Burden of Diseases Study 2015. *Lancet (London, England)*, *389*(10082), 1907–1918. https://doi.org/10.1016/S0140-6736(17)30505-6

Conibear, L., Butt, E. W., Knote, C., Arnold, S. R., & Spracklen, D. V. (2018). Residential energy use emissions dominate health impacts from exposure to ambient particulate matter in India.

Nature Communications, *9*(1), 617. https://doi.org/10.1038/s41467-018-02986-7

Conibear, L., Butt, E. W., Knote, C., Lam, N. L., Arnold, S. R., Tibrewal, K., Venkataraman, C., Spracklen, D. V, & Bond, T. C. (2020). A complete transition to clean household energy can save one–quarter of the healthy life lost to particulate matter pollution exposure in India. *Environmental Research Letters*, *15*(9), 94096. https://doi.org/10.1088/1748-9326/ab8e8a

Cook, P. A., Savage, N. H., Turquety, S., Carver, G. D., O'Connor, F. M., Heckel, A., Stewart, D., Whalley, L. K., Parker, A. E., Schlager, H., Singh, H. B., Avery, M. A., Sachse, G. W., Brune, W., Richter, A., Burrows, J. P., Purvis, R., Lewis, A. C., Reeves, C. E., … Pyle, J. A. (2007). Forest fire plumes over the North Atlantic: p-TOMCAT model simulations with aircraft and satellite measurements from the ITOP/ICARTT campaign. *Journal of Geophysical Research Atmospheres*, *112*(10), 1–20. https://doi.org/10.1029/2006JD007563

Crippa, M, D, G., T, B., T, K., R, W., JW, K., J, K., J, K., S, C., T, M., G, P., J, R., M, M., Z, K., M, P., R, M., BH, H., SJ, S., H, S., … K, F. (2023). The HTAP_v3 emission mosaic: merging regional and global monthly emissions (2000–2018) to support air quality modelling and policies. *EARTH SYSTEM SCIENCE DATA*, *15*(6), 2667–2694. https://doi.org/10.5194/essd-15-2667-2023 (online)

Crippa, Monica, Solazzo, E., Huang, G., Guizzardi, D., Koffi, E., Muntean, M., Schieberle, C., Friedrich, R., & Janssens-Maenhout, G. (2020). High resolution temporal profiles in the Emissions Database for Global Atmospheric Research. *Scientific Data*, *7*(1), 121. https://doi.org/10.1038/s41597-020-0462-2

Dandona, L., Dandona, R., Kumar, G. A., Shukla, D. K., Paul, V. K., Balakrishnan, K., Prabhakaran, D., Tandon, N., Salvi, S., Dash, A. P., Nandakumar, A., Patel, V., Agarwal, S. K., Gupta, P. C., Dhaliwal, R. S., Mathur, P., Laxmaiah, A., Dhillon, P. K., Dey, S., … Swaminathan, S. (2017). Nations within a nation: variations in epidemiological transition across the states of India, 1990–2016 in the Global Burden of Disease Study. *The Lancet*, *390*(10111), 2437–2460. https://doi.org/10.1016/S0140-6736(17)32804-0

Dantas, G., Siciliano, B., França, B. B., da Silva, C. M., & Arbilla, G. (2020). The impact of COVID-19 partial lockdown on the air quality of the city of Rio de Janeiro, Brazil. *Science of The Total Environment*, *729*, 139085. https://doi.org/https://doi.org/10.1016/j.scitotenv.2020.139085

Das, M., Das, A., Sarkar, R., Saha, S., & Mandal, A. (2021). Examining the impact of lockdown (due to COVID-19) on ambient aerosols (PM(2.5)): A study on Indo-Gangetic Plain (IGP) Cities, India. *Stochastic Environmental Research and Risk Assessment : Research Journal*, *35*(6), 1301–1317. https://doi.org/10.1007/s00477-020-01905-x

Dey, S., Purohit, B., Balyan, P., Dixit, K., Bali, K., Kumar, A., Imam, F., Chowdhury, S., Ganguly,

D., Gargava, P., & Shukla, V. K. (2020). A Satellite-Based High-Resolution (1-km) Ambient PM2.5 Database for India over Two Decades (2000–2019): Applications for Air Quality Management. *Remote Sensing*, *12*(23). https://doi.org/10.3390/rs12233872

Di, Z., Gong, W., Gan, Y., Shen, C., & Duan, Q. (2019). Combinatorial Optimization for WRF Physical Parameterization Schemes: A Case Study of Three-Day Typhoon Simulations over the Northwest Pacific Ocean. *Atmosphere*, *10*(5). https://doi.org/10.3390/atmos10050233

Doumbia, T., Granier, C., Elguindi, N., Bouarar, I., Darras, S., Brasseur, G., Gaubert, B., Liu, Y., Shi, X., Stavrakou, T., Tilmes, S., Lacey, F., Deroubaix, A., & Wang, T. (2021). Changes in global air pollutant emissions during the COVID-19 pandemic: a dataset for atmospheric modeling. *Earth System Science Data*, *13*(8), 4191–4206. https://doi.org/10.5194/essd-13-4191-2021

Duarte, H. F., Leclerc, M. Y., Zhang, G., Durden, D., Kurzeja, R., Parker, M., & Werth, D. (2015). Impact of Nocturnal Low-Level Jets on Near-Surface Turbulence Kinetic Energy. *Boundary-Layer Meteorology*, *156*(3), 349–370. https://doi.org/10.1007/s10546-015-0030-z

Duncan, B. N., Logan, J. A., Bey, I., Megretskaia, I. A., Yantosca, R. M., Novelli, P. C., Jones, N. B., & Rinsland, C. P. (2007). Global budget of CO, 1988 - 1997: Source estimates and validation with a global model. *Journal of Geophysical Research Atmospheres*, *112*(22), 1988–1997. https://doi.org/10.1029/2007JD008459

Emmons, L. K. (2003). Budget of tropospheric ozone during TOPSE from two chemical transport models. *Journal of Geophysical Research*, *108*(D8), 8372. https://doi.org/10.1029/2002JD002665

Emmons, L. K., Walters, S., Hess, P. G., Lamarque, J.-F., Pfister, G. G., Fillmore, D., Granier, C., Guenther, A., Kinnison, D., Orlando, J. ., Tie, X., Tyndall, G., Wiedinmyer, C., Baughcum, S. L., & Kloster, S. (2010). Description and evaluation of the Model for Ozone and Related chemical Tracers , version 4 (MOZART-4). *Geoscientific Model Development*, *3*, 43–67. https://doi.org/10.5194/gmd-3-43-2010

Fang, W., Evangeliou, N., Eckhardt, S., Xing, J., Zhang, H., Xiao, H., Zhao, M., & Kim, S.-W. (2023). Increased contribution of biomass burning to haze events in Shanghai since China's clean air actions. *Communications Earth & Environment*, *4*(1), 310. https://doi.org/10.1038/s43247-023-00979-z

Finlayson-Pitts, B. J., & Pitts, J. N. (2000). CHAPTER 1 - Overview of the Chemistry of Polluted and Remote Atmospheres. In B. J. Finlayson-Pitts & J. N. Pitts (Eds.), *Chemistry of the Upper and Lower Atmosphere* (pp. 1–14). Academic Press. https://doi.org/https://doi.org/10.1016/B978-012257060-5/50003-4

Ganguly, D., Jayaraman, A., Rajesh, T. A., & Gadhavi, H. (2006). Wintertime aerosol properties

during foggy and nonfoggy days over urban center Delhi and their implications for shortwave radiative forcing. *Journal of Geophysical Research: Atmospheres*, *111*(D15). https://doi.org/https://doi.org/10.1029/2005JD007029

Ganguly, T., Selvaraj, K. L., & Guttikunda, S. K. (2020). National Clean Air Programme (NCAP) for Indian cities: Review and outlook of clean air action plans. *Atmospheric Environment: X*, *8*, 100096. https://doi.org/https://doi.org/10.1016/j.aeaoa.2020.100096

Gani, S., Bhandari, S., Seraj, S., Wang, D. S., Patel, K., Soni, P., Arub, Z., Habib, G., Hildebrandt Ruiz, L., & Apte, J. S. (2019). Submicron aerosol composition in the world's most polluted megacity: the Delhi Aerosol Supersite study. *Atmospheric Chemistry and Physics*, *19*(10), 6843–6859. https://doi.org/10.5194/acp-19-6843-2019

Gautam, S. (2020). The Influence of COVID-19 on Air Quality in India: A Boon or Inutile. *Bulletin of Environmental Contamination and Toxicology*, *104*(6), 724–726. https://doi.org/10.1007/s00128-020-02877-y

GDB. (2020). Global burden of 369 diseases and injuries in 204 countries and territories, 1990-2019: a systematic analysis for the Global Burden of Disease Study 2019. *Lancet (London, England)*, *396*(10258), 1204–1222. https://doi.org/10.1016/S0140-6736(20)30925-9

Gettelman, A., Mills, M. J., Kinnison, D. E., Garcia, R. R., Smith, A. K., Marsh, D. R., Tilmes, S., Vitt, F., Bardeen, C. G., McInerny, J., Liu, H.-L., Solomon, S. C., Polvani, L. M., Emmons, L. K., Lamarque, J.-F., Richter, J. H., Glanville, A. S., Bacmeister, J. T., Phillips, A. S., … Randel, W. J. (2019). The Whole Atmosphere Community Climate Model Version 6 (WACCM6). *Journal of Geophysical Research: Atmospheres*, *124*(23), 12380–12403. https://doi.org/https://doi.org/10.1029/2019JD030943

Ghoshal Chowdhury, S., Ganguly, D., Khan, A. W., & Dey, S. (2025). Aerosol-Cloud Interactions and Their Role in Modulating Lightning Activity: Evidence From Extreme Events Over India. *Journal of Geophysical Research: Atmospheres*, *130*(23), e2024JD043251. https://doi.org/https://doi.org/10.1029/2024JD043251

Ghude, S. D., Kumar, R., Jena, C. K., Debnath, S., Kulkarni, R. G., Alessandrini, S., Biswas, M. K., Kulkrani, S., Pithani, P., Kelkar, S., Sajjan, V. S., Chate, D. M., Soni, V. K., Singh, S., Nanjundiah, R. S., & Rajeevan, M. (2020). Evaluation of PM2.5 Forecast using Chemical Data Assimilation in the WRF-Chem Model: A Novel Initiative Under the Ministry of Earth Sciences Air Quality Early Warning System for Delhi, India. *Current Science*. https://api.semanticscholar.org/CorpusID:221212334

Goel, V., Hazarika, N., Kumar, M., & Singh, V. (2021). Source apportionment of black carbon over Delhi: A case study of extreme biomass burning events and Diwali festival. *Urban Climate*, *39*, 100926. https://doi.org/https://doi.org/10.1016/j.uclim.2021.100926

Goswami, K., Choudhury, H. K., & Saikia, J. (2012). Factors influencing farmers' adoption of slash and burn agriculture in North East India. *Forest Policy and Economics*, *15*, 146–151. https://doi.org/10.1016/j.forpol.2011.11.005

Govardhan, G. R., Nanjundiah, R. S., Satheesh, S. K., Moorthy, K. K., & Kotamarthi, V. R. (2015). Performance of WRF-Chem over Indian region: Comparison with measurements. *Journal of Earth System Science*, *124*(4), 875–896. https://doi.org/10.1007/s12040-015-0576-7

Grell, G. A., Knoche, R., Peckham, S. E., & McKeen, S. A. (2004). Online versus offline air quality modeling on cloud-resolving scales. *Geophysical Research Letters*, *31*(16). https://doi.org/https://doi.org/10.1029/2004GL020175

Grell, G. a., Peckham, S. E., Schmitz, R., McKeen, S. a., Frost, G., Skamarock, W. C., & Eder, B. (2005). Fully coupled "online" chemistry within the WRF model. *Atmospheric Environment*, *39*(37), 6957–6975. https://doi.org/10.1016/j.atmosenv.2005.04.027

Grell, G., & Baklanov, A. (2011). Integrated modeling for forecasting weather and air quality: A call for fully coupled approaches. *Atmospheric Environment*, *45*(38), 6845–6851. https://doi.org/http://dx.doi.org/10.1016/j.atmosenv.2011.01.017

Guenther, A., Karl, T., Harley, P., Wiedinmyer, C., Palmer, P. I., & Geron, C. (2006). Estimates of global terrestrial isoprene emissions using MEGAN (Model of Emissions of Gases and Aerosols from Nature). *Atmospheric Chemistry and Physics*, *6*(11), 3181–3210. https://doi.org/10.5194/acp-6-3181-2006

Guenther, A., Karl, T., Harley, P., Wiedinmyer, C., Palmer, P. I., Geron, C., Guenther, A., Karl, T., Harley, P., Wiedinmyer, C., & Palmer, P. I. (2006). *Estimates of global terrestrial isoprene emissions using MEGAN (Model of Emissions of Gases and Aerosols from Nature) To cite this version : and Physics Estimates of global terrestrial isoprene emissions using MEGAN (Model of Emissions of Gases and Aer*.

Gulia, S., Mittal, A., & Khare, M. (2018). Quantitative evaluation of source interventions for urban air quality improvement - A case study of Delhi city. *Atmospheric Pollution Research*, *9*(3), 577–583. https://doi.org/https://doi.org/10.1016/j.apr.2017.12.003

Gunwani, P., & Mohan, M. (2017). Sensitivity of WRF model estimates to various PBL parameterizations in different climatic zones over India. *Atmospheric Research*, *194*, 43–65. https://doi.org/https://doi.org/10.1016/j.atmosres.2017.04.026

Gunwani, P., Sati, A. P., Mohan, M., & Gupta, M. (2021). Assessment of physical parameterization schemes in WRF over national capital region of India. *Meteorology and Atmospheric Physics*, *133*(2), 399–418. https://doi.org/10.1007/s00703-020-00757-y

Guo, H, Kota, S. H., Chen, K., Sahu, S. K., Hu, J., Ying, Q., Wang, Y., & Zhang, H. (2018). Source contributions and potential reductions to health effects of particulate matter in India.

Atmospheric Chemistry and Physics, *18*(20), 15219–15229. https://doi.org/10.5194/acp-18-15219-2018

Guo, Hao, Kota, S. H., Sahu, S. K., Hu, J., Ying, Q., Gao, A., & Zhang, H. (2017). Source apportionment of PM2.5 in North India using source-oriented air quality models. *Environmental Pollution*, *231*, 426–436. https://doi.org/https://doi.org/10.1016/j.envpol.2017.08.016

Gupta, M., & Mohan, M. (2013). Assessment of contribution to PM10 concentrations from long range transport of pollutants using WRF/Chem over a subtropical urban airshed. *Atmospheric Pollution Research*, *4*(4), 405–410. https://doi.org/https://doi.org/10.5094/APR.2013.046

Gupta, M., & Mohan, M. (2015). Validation of WRF/Chem model and sensitivity of chemical mechanisms to ozone simulation over megacity Delhi. *Atmospheric Environment*, *122*, 220–229. https://doi.org/https://doi.org/10.1016/j.atmosenv.2015.09.039

Guttikunda, S. K., Dammalapati, S. K., & Pradhan, G. (2025). Assessing air quality during India's National Clean Air Programme (NCAP): 2019–2023. *Atmospheric Environment*, *343*, 120974. https://doi.org/https://doi.org/10.1016/j.atmosenv.2024.120974

Guttikunda, S. K., & Gurjar, B. R. (2012). Role of meteorology in seasonality of air pollution in megacity Delhi, India. *Environmental Monitoring and Assessment*, *184*(5), 3199–3211. https://doi.org/10.1007/s10661-011-2182-8

Guttikunda, S., Ka, N., Ganguly, T., & Jawahar, P. (2023). Plugging the ambient air monitoring gaps in India's national clean air programme (NCAP) airsheds. *Atmospheric Environment*, *301*, 119712. https://doi.org/https://doi.org/10.1016/j.atmosenv.2023.119712

Hariprasad, K. B. R. R., Srinivas, C. V, Singh, A. B., Vijaya Bhaskara Rao, S., Baskaran, R., & Venkatraman, B. (2014). Numerical simulation and intercomparison of boundary layer structure with different PBL schemes in WRF using experimental observations at a tropical site. *Atmospheric Research*, *145–146*, 27–44. https://doi.org/https://doi.org/10.1016/j.atmosres.2014.03.023

Heal, M. R., Kumar, P., & Harrison, R. M. (2012). Particles{,} air quality{,} policy and health. *Chem. Soc. Rev.*, *41*(19), 6606–6630. https://doi.org/10.1039/C2CS35076A

Hoesly, R. M., Smith, S. J., Feng, L., Klimont, Z., Janssens-Maenhout, G., Pitkanen, T., Seibert, J. J., Vu, L., Andres, R. J., Bolt, R. M., Bond, T. C., Dawidowski, L., Kholod, N., Kurokawa, J.-I., Li, M., Liu, L., Lu, Z., Moura, M. C. P., O'Rourke, P. R., & Zhang, Q. (2018). Historical (1750--2014) anthropogenic emissions of reactive gases and aerosols from the Community Emissions Data System (CEDS). *Geoscientific Model Development*, *11*(1), 369–408. https://doi.org/10.5194/gmd-11-369-2018

Hong, S.-Y., Noh, Y., & Dudhia, J. (2006). A New Vertical Diffusion Package with an Explicit

Treatment of Entrainment Processes. *Monthly Weather Review*, *134*(9), 2318–2341. https://doi.org/10.1175/MWR3199.1

Hu, X.-M., Nielsen-Gammon, J. W., & Zhang, F. (2010). Evaluation of Three Planetary Boundary Layer Schemes in the WRF Model. *Journal of Applied Meteorology and Climatology*, *49*(9), 1831–1844. https://doi.org/10.1175/2010JAMC2432.1

III, C. A. P., & Dockery, D. W. (2006). Health Effects of Fine Particulate Air Pollution: Lines that Connect. *Journal of the Air \& Waste Management Association*, *56*(6), 709–742. https://doi.org/10.1080/10473289.2006.10464485

Isaifan, R. J. (2020). The dramatic impact of the Coronavirus outbreak on air quality: Has it saved as much as it has killed so far? *Global Journal of Environmental Science and Management*, *6*(3), 275–288. https://doi.org/10.22034/gjesm.2020.03.01

Jabbari, A., & Bae, D.-H. (2018). Application of Artificial Neural Networks for Accuracy Enhancements of Real-Time Flood Forecasting in the Imjin Basin. *Water*, *10*(11). https://doi.org/10.3390/w10111626

Jacob, D J. (1999). *Introduction to Atmospheric Chemistry*. Princeton University Press. https://books.google.co.in/books?id=14whM9fEOzsC

Jacob, Daniel J., Field, B. D., Li, Q., Blake, D. R., de Gouw, J., Warneke, C., Hansel, A., Wisthaler, A., Singh, H. B., & Guenther, A. (2005). Global budget of methanol: Constraints from atmospheric observations. *Journal of Geophysical Research D: Atmospheres*, *110*(8), 1–17. https://doi.org/10.1029/2004JD005172

Jain, S., & Sharma, T. (2020). Social and Travel Lockdown Impact Considering Coronavirus Disease (COVID-19) on Air Quality in Megacities of India: Present Benefits, Future Challenges and Way Forward. *Aerosol and Air Quality Research*, *20*(6), 1222–1236. https://doi.org/10.4209/aaqr.2020.04.0171

Janjić, Z. I. (1994). The Step-Mountain Eta Coordinate Model: Further Developments of the Convection, Viscous Sublayer, and Turbulence Closure Schemes. *Monthly Weather Review*, *122*(5), 927–945. https://doi.org/10.1175/1520-0493(1994)122<0927:TSMECM>2.0.CO;2

Jethva, H., Torres, O., Field, R. D., Lyapustin, A., Gautam, R., & Kayetha, V. (2019). Connecting Crop Productivity, Residue Fires, and Air Quality over Northern India. *Scientific Reports*, *9*(1), 16594. https://doi.org/10.1038/s41598-019-52799-x

Jia, G., Shevliakova, E., Artaxo, P., N. De Noblet-Ducoudré, Houghton, R., House, J., Kitajima, K., Lennard, C., Popp, A., Sirin, A., Sukumar, R., & Verchot, L. (2019). Land–climate interactions. In P. R. Shukla, J. Skea, E. C. Buendia, V. Masson-Delmotte, H.-O. Pörtner, D. C. Roberts, P. Zhai, R. Slade, S. Connors, R. van Diemen, M. Ferrat, E. Haughey, S. Luz, S. Neogi, M. Pathak, J. Petzold, J. Portugal Pereira, E. H. P. Vyas, K. Kissick, … J. Malley

(Eds.), *Climate Change and Land: an IPCC special report on climate change, desertification, land degradation, sustainable land management, food security, and greenhouse gas fluxes in terrestrial ecosystems* (pp. 131–247). In Press. https://doi.org/https://www.ipcc.ch/srccl/chapter/chapter-2

Jimenez, J. L., Canagaratna, M. R., Donahue, N. M., Prevot, A. S. H., Zhang, Q., Kroll, J. H., DeCarlo, P. F., Allan, J. D., Coe, H., Ng, N. L., Aiken, A. C., Docherty, K. S., Ulbrich, I. M., Grieshop, A. P., Robinson, A. L., Duplissy, J., Smith, J. D., Wilson, K. R., Lanz, V. A., … Worsnop, D. R. (2009). Evolution of Organic Aerosols in the Atmosphere. *Science*, *326*(5959), 1525–1529. https://doi.org/10.1126/science.1180353

Kabiraj, S., & Gavli, N. V. (2020). Impact of SARS-CoV-2 Pandemic Lockdown on Air Quality Using Satellite Imagery with Ground Station Monitoring Data in Most Polluted City Kolkata, India. *Aerosol Science and Engineering*, *4*(4), 320–330. https://doi.org/10.1007/s41810-020-00077-z

Kaiser, J. W., Heil, A., Andreae, M. O., Benedetti, A., Chubarova, N., Jones, L., Morcrette, J.-J., Razinger, M., Schultz, M. G., Suttie, M., & van der Werf, G. R. (2012). Biomass burning emissions estimated with a global fire assimilation system based on observed fire radiative power. *Biogeosciences*, *9*(1), 527–554. https://doi.org/10.5194/bg-9-527-2012

Kalnay, E, Kanamitsu, M., Kistler, R., Collins, W., Deaven, D., Gandin, L., Iredell, M., Saha, S., White, G., Woollen, J., Zhu, Y., Chelliah, M., Ebisuzaki, W., Higgins, W., Janowiak, J., Mo, K. C., Ropelewski, C., Wang, J., Leetmaa, A., … Joseph, D. (1996). The NCEP/NCAR 40-Year Reanalysis Project. *Bulletin of the American Meteorological Society*, *77*(3), 437–472. https://doi.org/10.1175/1520-0477(1996)077<0437:TNYRP>2.0.CO;2

Kalnay, Eugenia. (2002). *Atmospheric Modeling, Data Assimilation and Predictability*. Cambridge University Press. https://doi.org/DOI: 10.1017/CBO9780511802270

Kanawade, V. P., Srivastava, A. K., Ram, K., Asmi, E., Vakkari, V., Soni, V. K., Varaprasad, V., & Sarangi, C. (2020). What caused severe air pollution episode of November 2016 in New Delhi? *Atmospheric Environment*, *222*, 117125. https://doi.org/https://doi.org/10.1016/j.atmosenv.2019.117125

Karambelas, A., Holloway, T., Kiesewetter, G., & Heyes, C. (2018). Constraining the uncertainty in emissions over India with a regional air quality model evaluation. *Atmospheric Environment*, *174*, 194–203. https://doi.org/https://doi.org/10.1016/j.atmosenv.2017.11.052

Karki, R., ul Hasson, S., Gerlitz, L., Talchabhadel, R., Schenk, E., Schickhoff, U., Scholten, T., & Böhner, J. (2018). WRF-based simulation of an extreme precipitation event over the Central Himalayas: Atmospheric mechanisms and their representation by microphysics parameterization schemes. *Atmospheric Research*, *214*, 21–35.

https://doi.org/https://doi.org/10.1016/j.atmosres.2018.07.016

Katoch, V., Kumar, A., Imam, F., Sarkar, D., Knibbs, L. D., Liu, Y., Ganguly, D., & Dey, S. (2023). Addressing Biases in Ambient PM2.5 Exposure and Associated Health Burden Estimates by Filling Satellite AOD Retrieval Gaps over India. *Environmental Science & Technology*, *57*(48), 19190–19201. https://doi.org/10.1021/acs.est.3c03355

Kirkevåg, A., Grini, A., Olivié, D., Seland, Ø., Alterskjær, K., Hummel, M., Karset, I. H. H., Lewinschal, A., Liu, X., Makkonen, R., Bethke, I., Griesfeller, J., Schulz, M., & Iversen, T. (2018). A production-tagged aerosol module for Earth system models, OsloAero5.3 – extensions and updates for CAM5.3-Oslo. *Geoscientific Model Development*, *11*(10), 3945–3982. https://doi.org/10.5194/gmd-11-3945-2018

Knote, C, Hodzic, A., Jimenez, J. L., Volkamer, R., Orlando, J. J., Baidar, S., Brioude, J., Fast, J., Gentner, D. R., Goldstein, A. H., Hayes, P. L., Knighton, W. B., Oetjen, H., Setyan, A., Stark, H., Thalman, R., Tyndall, G., Washenfelder, R., Waxman, E., & Zhang, Q. (2014). Simulation of semi-explicit mechanisms of SOA formation from glyoxal in aerosol in a 3-D model. *Atmospheric Chemistry and Physics*, *14*(12), 6213–6239. https://doi.org/10.5194/acp-14-6213-2014

Knote, Christoph, Tuccella, P., Curci, G., Emmons, L., Orlando, J. J., Madronich, S., Baró, R., Jiménez-Guerrero, P., Luecken, D., Hogrefe, C., Forkel, R., Werhahn, J., Hirtl, M., Pérez, J. L., San José, R., Giordano, L., Brunner, D., Yahya, K., & Zhang, Y. (2015). Influence of the choice of gas-phase mechanism on predictions of key gaseous pollutants during the AQMEII phase-2 intercomparison. *Atmospheric Environment*, *115*, 553–568. https://doi.org/https://doi.org/10.1016/j.atmosenv.2014.11.066

Kota, S. H., Guo, H., Myllyvirta, L., Hu, J., Sahu, S. K., Garaga, R., Ying, Q., Gao, A., Dahiya, S., Wang, Y., & Zhang, H. (2018). Year-long simulation of gaseous and particulate air pollutants in India. *Atmospheric Environment*, *180*, 244–255. https://doi.org/https://doi.org/10.1016/j.atmosenv.2018.03.003

Kroll, J. H., & Seinfeld, J. H. (2008). Chemistry of secondary organic aerosol: Formation and evolution of low-volatility organics in the atmosphere. *Atmospheric Environment*, *42*(16), 3593–3624. https://doi.org/https://doi.org/10.1016/j.atmosenv.2008.01.003

Kulkarni, S. H., Ghude, S. D., Jena, C., Karumuri, R. K., Sinha, B., Sinha, V., Kumar, R., Soni, V. K., & Khare, M. (2020). How Much Does Large-Scale Crop Residue Burning Affect the Air Quality in Delhi? *Environmental Science & Technology*, *54*(8), 4790–4799. https://doi.org/10.1021/acs.est.0c00329

Kumar, A., Imam, F., Dixit, K., Chaudhary, E., Sharma, S., Singh, N., Katoch, V., Agarwal, S., Ganguly, D., & Dey, S. (2025). Sectoral Contributions to Primary and Secondary PM2.5 in

Regional Airsheds of India. *ACS Earth and Space Chemistry*, *9*(4), 806–816. https://doi.org/10.1021/acsearthspacechem.4c00332

Kumar, P., Gulia, S., Harrison, R. M., & Khare, M. (2017). The influence of odd–even car trial on fine and coarse particles in Delhi. *Environmental Pollution*, *225*, 20–30. https://doi.org/https://doi.org/10.1016/j.envpol.2017.03.017

Kumar, P., Hama, S., Omidvarborna, H., Sharma, A., Sahani, J., Abhijith, K. V, Debele, S. E., Zavala-Reyes, J. C., Barwise, Y., & Tiwari, A. (2020). Temporary reduction in fine particulate matter due to 'anthropogenic emissions switch-off' during COVID-19 lockdown in Indian cities. *Sustainable Cities and Society*, *62*, 102382. https://doi.org/https://doi.org/10.1016/j.scs.2020.102382

Kumar, R., Naja, M., Pfister, G. G., Barth, M. C., & Brasseur, G. P. (2012). Simulations over South Asia using the Weather Research and Forecasting model with Chemistry (WRF-Chem): Set-up and meteorological evaluation. *Geoscientific Model Development*, *5*(2), 321–343. https://doi.org/10.5194/gmd-5-321-2012

Kumar, V., Chandra, B. P., & Sinha, V. (2018). Large unexplained suite of chemically reactive compounds present in ambient air due to biomass fires. *Scientific Reports*, *8*(1), 626. https://doi.org/10.1038/s41598-017-19139-3

Kumari, P., & Toshniwal, D. (2022). Impact of lockdown measures during COVID-19 on air quality- A case study of India. *International Journal of Environmental Health Research*, *32*(3), 503–510. https://doi.org/10.1080/09603123.2020.1778646

Lal, R. M., Nagpure, A. S., Anand, A., Maji, S., Tibrewal, K., Gupta, G., Venkataraman, C., & Tong, K. (2025). Transboundary emission contribution to PM2.5 concentrations in Indian cities. *Environmental Research Letters*, *20*(5), 54008. https://doi.org/10.1088/1748-9326/adc147

Lal, S., Venkataramani, S., Naja, M., Kuniyal, J. C., Mandal, T. K., Bhuyan, P. K., Kumari, K. M., Tripathi, S. N., Sarkar, U., Das, T., Swamy, Y. V., Gopal, K. R., Gadhavi, H., & Kumar, M. K. S. (2017). Loss of crop yields in India due to surface ozone: an estimation based on a network of observations. *Environmental Science and Pollution Research*, *24*(26), 20972–20981. https://doi.org/10.1007/s11356-017-9729-3

Lalchandani, V, Srivastava, D., Dave, J., Mishra, S., Tripathi, N., Shukla, A. K., Sahu, R., Thamban, N. M., Gaddamidi, S., Dixit, K., Ganguly, D., Tiwari, S., Srivastava, A. K., Sahu, L., Rastogi, N., Gargava, P., & Tripathi, S. N. (2022). Effect of Biomass Burning on PM2.5 Composition and Secondary Aerosol Formation During Post-Monsoon and Winter Haze Episodes in Delhi. *Journal of Geophysical Research: Atmospheres*, *127*(1), e2021JD035232. https://doi.org/https://doi.org/10.1029/2021JD035232

Lalchandani, Vipul, Kumar, V., Tobler, A., M Thamban, N., Mishra, S., Slowik, J. G., Bhattu, D., Rai, P., Satish, R., Ganguly, D., Tiwari, S., Rastogi, N., Tiwari, S., Močnik, G., Prévôt, A. S. H., & Tripathi, S. N. (2021). Real-time characterization and source apportionment of fine particulate matter in the Delhi megacity area during late winter. *The Science of the Total Environment*, *770*, 145324. https://doi.org/10.1016/j.scitotenv.2021.145324

Lelieveld, J., Evans, J. S., Fnais, M., Giannadaki, D., & Pozzer, A. (2015). The contribution of outdoor air pollution sources to premature mortality on a global scale. *Nature*, *525*(7569), 367–371. https://doi.org/10.1038/nature15371

Lelieveld, J., Gromov, S., Pozzer, A., & Taraborrelli, D. (2016). Global tropospheric hydroxyl distribution, budget and reactivity. *Atmospheric Chemistry and Physics*, *16*(19), 12477–12493. https://doi.org/10.5194/acp-16-12477-2016

Levy, H. (1971). Normal Atmosphere: Large Radical and Formaldehyde Concentrations Predicted. *Science*, *173*(3992), 141–143. https://doi.org/10.1126/science.173.3992.141

Li, L., Chen, Y., Zeng, L., Shao, M., Xie, S., Chen, W., Lu, S., Wu, Y., & Cao, W. (2014). Biomass burning contribution to ambient volatile organic compounds (VOCs) in the Chengdu–Chongqing Region (CCR), China. *Atmospheric Environment*, *99*, 403–410. https://doi.org/https://doi.org/10.1016/j.atmosenv.2014.09.067

Lim, Y.-H., Kim, H., Kim, J. H., Bae, S., Park, H. Y., & Hong, Y.-C. (2012). Air Pollution and Symptoms of Depression in Elderly Adults. *Environmental Health Perspectives*, *120*(7), 1023–1028. https://doi.org/10.1289/ehp.1104100

Liu, P., Tsimpidi, A. P., Hu, Y., Stone, B., Russell, A. G., & Nenes, A. (2012). Differences between downscaling with spectral and grid nudging using WRF. *Atmospheric Chemistry and Physics*, *12*(8), 3601–3610. https://doi.org/10.5194/acp-12-3601-2012

Liu, Y., Chen, X., Li, Q., Yang, J., Li, L., & Wang, T. (2020). Impact of different microphysics and cumulus parameterizations in WRF for heavy rainfall simulations in the central segment of the Tianshan Mountains, China. *Atmospheric Research*, *244*, 105052. https://doi.org/https://doi.org/10.1016/j.atmosres.2020.105052

Lucas-Picher, P., Cattiaux, J., Bougie, A., & Laprise, R. (2016). How does large-scale nudging in a regional climate model contribute to improving the simulation of weather regimes and seasonal extremes over North America? *Climate Dynamics*, *46*(3), 929–948. https://doi.org/10.1007/s00382-015-2623-0

Madala, S., Satyanarayana, A. N. V, & Rao, T. N. (2014). Performance evaluation of PBL and cumulus parameterization schemes of WRF ARW model in simulating severe thunderstorm events over Gadanki MST radar facility — Case study. *Atmospheric Research*, *139*, 1–17. https://doi.org/https://doi.org/10.1016/j.atmosres.2013.12.017

Mahapatra, B., Walia, M., & Saggurti, N. (2018). Extreme weather events induced deaths in India 2001–2014: Trends and differentials by region, sex and age group. *Weather and Climate Extremes*, *21*, 110–116. https://doi.org/https://doi.org/10.1016/j.wace.2018.08.001

Mahato, S., Pal, S., & Ghosh, K. G. (2020). Effect of lockdown amid COVID-19 pandemic on air quality of the megacity Delhi, India. *Science of The Total Environment*, *730*, 139086. https://doi.org/https://doi.org/10.1016/j.scitotenv.2020.139086

Mahoney, K., Swales, D., Mueller, M. J., Alexander, M., Abel, M. R., & Malloy, K. (2018). An Examination of an Inland-Penetrating Atmospheric River Flood Event under Potential Future Thermodynamic Conditions. *Journal of Climate*, *31*(16), 6281–6297. https://doi.org/10.1175/JCLI-D-18-0118.1

Mangaraj, P., Matsumi, Y., Nakayama, T., Biswal, A., Yamaji, K., Araki, H., Yasutomi, N., Takigawa, M., Patra, P. K., Hayashida, S., Sharma, A., Dimri, A. P., Dhaka, S. K., Bhatti, M. S., Kajino, M., Mor, S., Khaiwal, R., Bhardwaj, S., Vazhathara, V. J., … Mor, S. (2025). Weak coupling of observed surface PM2.5 in Delhi-NCR with rice crop residue burning in Punjab and Haryana. *Npj Climate and Atmospheric Science*, *8*(1), 18. https://doi.org/10.1038/s41612-025-00901-8

Manisalidis, I., Stavropoulou, E., Stavropoulos, A., & Bezirtzoglou, E. (2020). Environmental and Health Impacts of Air Pollution: A Review. *Frontiers in Public Health*, *Volume 8*-. https://doi.org/10.3389/fpubh.2020.00014

Mao, J., Jacob, D. J., Evans, M. J., Olson, J. R., Ren, X., Brune, W. H., St. Clair, J. M., Crounse, J. D., Spencer, K. M., Beaver, M. R., Wennberg, P. O., Cubison, M. J., Jimenez, J. L., Fried, A., Weibring, P., Walega, J. G., Hall, S. R., Weinheimer, A. J., Cohen, R. C., … Carouge, C. (2010). Chemistry of hydrogen oxide radicals (HOx) in the Arctic troposphere in spring. *Atmospheric Chemistry and Physics*, *10*(13), 5823–5838. https://doi.org/10.5194/acp-10-5823-2010

Markowski, P., & Richardson, Y. (2010). The Boundary Layer. In *Mesoscale Meteorology in Midlatitudes* (pp. 73–114). John Wiley & Sons, Ltd. https://doi.org/https://doi.org/10.1002/9780470682104.ch4

Mishra, S., Tripathi, S. N., Kanawade, V. P., Haslett, S. L., Dada, L., Ciarelli, G., Kumar, V., Singh, A., Bhattu, D., Rastogi, N., Daellenbach, K. R., Ganguly, D., Gargava, P., Slowik, J. G., Kulmala, M., Mohr, C., El-Haddad, I., & Prevot, A. S. H. (2023). Rapid night-time nanoparticle growth in Delhi driven by biomass-burning emissions. *Nature Geoscience*, *16*(3), 224–230. https://doi.org/10.1038/s41561-023-01138-x

Mohan, M., & Bhati, S. (2011). Analysis of WRF Model Performance over Subtropical Region of Delhi, India. *Advances in Meteorology*, *2011*(1), 621235.

https://doi.org/https://doi.org/10.1155/2011/621235

Mohan, M., & Gupta, M. (2018). Sensitivity of PBL parameterizations on PM10 and ozone simulation using chemical transport model WRF-Chem over a sub-tropical urban airshed in India. *Atmospheric Environment*, *185*, 53–63. https://doi.org/https://doi.org/10.1016/j.atmosenv.2018.04.054

Mohan, M., Kikegawa, Y., Gurjar, B. R., Bhati, S., & Kolli, N. R. (2013). Assessment of urban heat island effect for different land use–land cover from micrometeorological measurements and remote sensing data for megacity Delhi. *Theoretical and Applied Climatology*, *112*(3), 647–658. https://doi.org/10.1007/s00704-012-0758-z

Monforti Ferrario, F., Crippa, M., Guizzardi, D., Muntean, M., Schaaf, E., Banja, M., Pagani, F., & Solazzo, E. (2022). *EDGAR v6.1 Global Air Pollutant Emissions*. https://doi.org/http://data.europa.eu/89h/df521e05-6a3b-461c-965a-b703fb62313e

Morini, E., Castellani, B., Presciutti, A., Anderini, E., Filipponi, M., Nicolini, A., & Rossi, F. (2017). Experimental Analysis of the Effect of Geometry and Façade Materials on Urban District's Equivalent Albedo. *Sustainability*, *9*(7). https://doi.org/10.3390/su9071245

Morrison, H., Thompson, G., & Tatarskii, V. (2009). Impact of Cloud Microphysics on the Development of Trailing Stratiform Precipitation in a Simulated Squall Line: Comparison of One- and Two-Moment Schemes. *Monthly Weather Review*, *137*(3), 991–1007. https://doi.org/10.1175/2008MWR2556.1

Mukhopadhyay, P., Taraphdar, S., Goswami, B. N., & Krishnakumar, K. (2010). Indian Summer Monsoon Precipitation Climatology in a High-Resolution Regional Climate Model: Impacts of Convective Parameterization on Systematic Biases. *Weather and Forecasting*, *25*(2), 369–387. https://doi.org/10.1175/2009WAF2222320.1

Nagar, P. K., Singh, D., Sharma, M., Kumar, A., Aneja, V. P., George, M. P., Agarwal, N., & Shukla, S. P. (2017). Characterization of PM2.5 in Delhi: role and impact of secondary aerosol, burning of biomass, and municipal solid waste and crustal matter. *Environmental Science and Pollution Research*, *24*(32), 25179–25189. https://doi.org/10.1007/s11356-017-0171-3

Nair, V. S., Moorthy, K. K., Alappattu, D. P., Kunhikrishnan, P. K., George, S., Nair, P. R., Babu, S. S., Abish, B., Satheesh, S. K., Tripathi, S. N., Niranjan, K., Madhavan, B. L., Srikant, V., Dutt, C. B. S., Badarinath, K. V. S., & Reddy, R. R. (2007). Wintertime aerosol characteristics over the Indo-Gangetic Plain (IGP): Impacts of local boundary layer processes and long-range transport. *Journal of Geophysical Research: Atmospheres*, *112*(D13). https://doi.org/https://doi.org/10.1029/2006JD008099

Nakanishi, M., & Niino, H. (2006). An Improved Mellor–Yamada Level-3 Model: Its Numerical

Stability and Application to a Regional Prediction of Advection Fog. *Boundary-Layer Meteorology*, *119*(2), 397–407. https://doi.org/10.1007/s10546-005-9030-8

Nandi, I., Kumar, A., Imam, F., Ganguly, D., & Dey, S. (2025). COVID-19 lockdown was insufficient to bring India's PM2.5 levels below national standards. *Environmental Research Communications*, *7*(5), 55005. https://doi.org/10.1088/2515-7620/add3d4

Nandi, I., Srivastava, S., Yarragunta, Y., Kumar, R., & Mitra, D. (2020). Distribution of surface carbon monoxide over the Indian subcontinent: Investigation of source contributions using WRF-Chem. *Atmospheric Environment*, *243*, 117838. https://doi.org/https://doi.org/10.1016/j.atmosenv.2020.117838

Ojha, N., Sharma, A., Kumar, M., Girach, I., Ansari, T. U., Sharma, S. K., Singh, N., Pozzer, A., & Gunthe, S. S. (2020). On the widespread enhancement in fine particulate matter across the Indo-Gangetic Plain towards winter. *Scientific Reports*, *10*(1), 5862. https://doi.org/10.1038/s41598-020-62710-8

Pai, C., Bhaskar, A., & Rawoot, V. (2020). Investigating the dynamics of COVID-19 pandemic in India under lockdown. *Chaos, Solitons & Fractals*, *138*, 109988. https://doi.org/https://doi.org/10.1016/j.chaos.2020.109988

Pai, D. S., Sridhar, L., Rajeevan, M., Sreejith, O. P., Satbhai, N. S., & Mukhopadhyay, B. (2014). Development of a new high spatial resolution (0.25{\textdegree} X 0.25{\textdegree}) Long period (1901-2010) daily gridded rainfall data set over India and its comparison with existing data sets over the region. *MAUSAM*, *65*(1), 1–18.

Panda, J., & Sharan, M. (2012). Influence of land-surface and turbulent parameterization schemes on regional-scale boundary layer characteristics over northern India. *Atmospheric Research*, *112*, 89–111. https://doi.org/https://doi.org/10.1016/j.atmosres.2012.04.001

Pandey, A., Sadavarte, P., Rao, A. B., & Venkataraman, C. (2014). Trends in multi-pollutant emissions from a technology-linked inventory for India: II. Residential, agricultural and informal industry sectors. *Atmospheric Environment*, *99*, 341–352. https://doi.org/https://doi.org/10.1016/j.atmosenv.2014.09.080

Pant, P., Guttikunda, S. K., & Peltier, R. E. (2016). Exposure to particulate matter in India: A synthesis of findings and future directions. *Environmental Research*, *147*, 480–496. https://doi.org/https://doi.org/10.1016/j.envres.2016.03.011

Pant, P., & Harrison, R. M. (2012). Critical review of receptor modelling for particulate matter: A case study of India. *Atmospheric Environment*, *49*, 1–12. https://doi.org/https://doi.org/10.1016/j.atmosenv.2011.11.060

Patel, K., Bhandari, S., Gani, S., Campmier, M. J., Kumar, P., Habib, G., Apte, J., & Hildebrandt Ruiz, L. (2021). Sources and Dynamics of Submicron Aerosol during the Autumn Onset of

the Air Pollution Season in Delhi, India. *ACS Earth and Space Chemistry*, *5*(1), 118–128. https://doi.org/10.1021/acsearthspacechem.0c00340

Patil, R., & Pradeep Kumar, P. (2016). WRF model sensitivity for simulating intense western disturbances over North West India. *Modeling Earth Systems and Environment*, *2*(2), 82. https://doi.org/10.1007/s40808-016-0137-3

Patowary, J., Dutta, S. K., Mahanta, A., & Mantha, T. T. (2024). A Closer Look at the Air Pollution Dynamics during Diwali Festival in India. *EGUsphere*, *2024*, 1–18. https://doi.org/10.5194/egusphere-2024-1594

Pinti, D. L. (2021). Composition of the Earth's Atmosphere. In D. Alderton & S. A. Elias (Eds.), *Encyclopedia of Geology (Second Edition)* (Second Edi, pp. 187–197). Academic Press. https://doi.org/https://doi.org/10.1016/B978-0-08-102908-4.00054-0

Pithani, P., Ghude, S. D., Prabhakaran, T., Karipot, A., Hazra, A., Kulkarni, R., Chowdhuri, S., Resmi, E. A., Konwar, M., Murugavel, P., Safai, P. D., Chate, D. M., Tiwari, Y., Jenamani, R. K., & Rajeevan, M. (2019). WRF model sensitivity to choice of PBL and microphysics parameterization for an advection fog event at Barkachha, rural site in the Indo-Gangetic basin, India. *Theoretical and Applied Climatology*, *136*(3), 1099–1113. https://doi.org/10.1007/s00704-018-2530-5

Purohit, P., Amann, M., Kiesewetter, G., Rafaj, P., Chaturvedi, V., Dholakia, H. H., Koti, P. N., Klimont, Z., Borken-Kleefeld, J., Gomez-Sanabria, A., Schöpp, W., & Sander, R. (2019). Mitigation pathways towards national ambient air quality standards in India. *Environment International*, *133*, 105147. https://doi.org/https://doi.org/10.1016/j.envint.2019.105147

Putaud, J.-P., Van Dingenen, R., Alastuey, A., Bauer, H., Birmili, W., Cyrys, J., Flentje, H., Fuzzi, S., Gehrig, R., Hansson, H. C., Harrison, R. M., Herrmann, H., Hitzenberger, R., Hüglin, C., Jones, A. M., Kasper-Giebl, A., Kiss, G., Kousa, A., Kuhlbusch, T. A. J., … Raes, F. (2010). A European aerosol phenomenology – 3: Physical and chemical characteristics of particulate matter from 60 rural, urban, and kerbside sites across Europe. *Atmospheric Environment*, *44*(10), 1308–1320. https://doi.org/https://doi.org/10.1016/j.atmosenv.2009.12.011

Qian, Z., Chapman, R. S., Hu, W., Wei, F., Korn, L. R., & Zhang, J. (Jim). (2004). Using air pollution based community clusters to explore air pollution health effects in children. *Environment International*, *30*(5), 611–620. https://doi.org/https://doi.org/10.1016/j.envint.2003.11.003

Ragi, A. R., Sharan, M., & Haddad, Z. S. (2017). Objective Detection of Indian Summer Monsoon Onset Using QuikSCAT Seawinds Scatterometer. *IEEE Transactions on Geoscience and Remote Sensing*, *55*(6), 3466–3474. https://doi.org/10.1109/TGRS.2017.2672825

Rai, P., Furger, M., El Haddad, I., Kumar, V., Wang, L., Singh, A., Dixit, K., Bhattu, D., Petit, J.-

E., Ganguly, D., Rastogi, N., Baltensperger, U., Tripathi, S. N., Slowik, J. G., & Prévôt, A. S. H. (2020). Real-time measurement and source apportionment of elements in Delhi's atmosphere. *Science of The Total Environment*, *742*, 140332. https://doi.org/https://doi.org/10.1016/j.scitotenv.2020.140332

Rajeevan, M., Rohini, P., Niranjan Kumar, K., Srinivasan, J., & Unnikrishnan, C. K. (2013). A study of vertical cloud structure of the Indian summer monsoon using CloudSat data. *Climate Dynamics*, *40*(3), 637–650. https://doi.org/10.1007/s00382-012-1374-4

Rajesh, P. V, Pattnaik, S., Mohanty, U. C., Rai, D., Baisya, H., & Pandey, P. C. (2017). Land surface sensitivity of monsoon depressions formed over Bay of Bengal using improved high-resolution land state. *Dynamics of Atmospheres and Oceans*, *80*, 155–172. https://doi.org/https://doi.org/10.1016/j.dynatmoce.2017.10.007

Ramamurthy, P., González, J., Ortiz, L., Arend, M., & Moshary, F. (2023). Corrigendum: Impact of heatwave on a megacity: an observational analysis of New York City during July 2016 (2017 Environ. Res. Lett. 12 054011). *Environmental Research Letters*, *18*(4), 49502. https://doi.org/10.1088/1748-9326/acc541

Rao, N. D., Kiesewetter, G., Min, J., Pachauri, S., & Wagner, F. (2021). Household contributions to and impacts from air pollution in India. *Nature Sustainability*, *4*(10), 859–867. https://doi.org/10.1038/s41893-021-00744-0

Rastogi, N., Singh, A., Singh, D., & Sarin, M. M. (2014). Chemical characteristics of PM2.5 at a source region of biomass burning emissions: Evidence for secondary aerosol formation. *Environmental Pollution*, *184*, 563–569. https://doi.org/https://doi.org/10.1016/j.envpol.2013.09.037

Rathore, J., Ganguly, D., Singh, V., Gupta, M., Vazhathara, V. J., Biswal, A., Kunchala, R. K., Patra, P. K., Sahu, L. K., Gani, S., & Dey, S. (2025). Characteristics of Haze Pollution Events During Biomass Burning Period at an Upwind Site of Delhi. *Journal of Geophysical Research: Atmospheres*, *130*(7), e2024JD042347. https://doi.org/https://doi.org/10.1029/2024JD042347

Reshmi Mohan, P., Srinivas, C. V, Yesubabu, V., Baskaran, R., & Venkatraman, B. (2018). Simulation of a heavy rainfall event over Chennai in Southeast India using WRF: Sensitivity to microphysics parameterization. *Atmospheric Research*, *210*, 83–99. https://doi.org/https://doi.org/10.1016/j.atmosres.2018.04.005

Reyes-Villegas, E., Lowe, D., Johnson, J. S., Carslaw, K. S., Darbyshire, E., Flynn, M., Allan, J. D., Coe, H., Chen, Y., Wild, O., Archer-Nicholls, S., Archibald, A., Singh, S., Shrivastava, M., Zaveri, R. A., Singh, V., Beig, G., Sokhi, R., & McFiggans, G. (2023). Simulating organic aerosol in Delhi with WRF-Chem using the volatility-basis-set approach: exploring model

uncertainty with a Gaussian process emulator. *Atmospheric Chemistry and Physics*, *23*(10), 5763–5782. https://doi.org/10.5194/acp-23-5763-2023

Reyes-Villegas, E., Panda, U., Darbyshire, E., Cash, J. M., Joshi, R., Langford, B., Di Marco, C. F., Mullinger, N. J., Alam, M. S., Crilley, L. R., Rooney, D. J., Acton, W. J. F., Drysdale, W., Nemitz, E., Flynn, M., Voliotis, A., McFiggans, G., Coe, H., Lee, J., … Allan, J. D. (2021). PM1 composition and source apportionment at two sites in Delhi, India, across multiple seasons. *Atmospheric Chemistry and Physics*, *21*(15), 11655–11667. https://doi.org/10.5194/acp-21-11655-2021

Rizwan, S., Nongkynrih, B., & Gupta, S. K. (2013). "Air pollution in Delhi: Its Magnitude and Effects on Health". *Indian Journal of Community Medicine : Official Publication of Indian Association of Preventive & Social Medicine*, *38*(1), 4–8. https://doi.org/10.4103/0970-0218.106617

Rogelj, J., Shindell, D., Jiang, K., Fifita, S., Forster, P., Ginzburg, V., Handa, C., Kheshgi, H., Kobayashi, S., Kriegler, E., Mundaca, L., Seferian, R., & Vilarino, M. V. (2018). Mitigation Pathways Compatible With 1.5°C in the Context of Sustainable Development. In V. Masson-Delmotte, P. Zhai, H. O. Pörtner, D. Roberts, J. Skea, P. R. Shukla, A. Pirani, W. Moufouma-Okia, C. Péan, R. Pidcock, S. Connors, J. B. R. Matthews, Y. Chen, X. Zhou, M. I. Gomis, E. Lonnoy, T. Maycock, M. Tignor, & T. Waterfield (Eds.), *Global Warming of 1.5°C. An IPCC Special Report on the impacts of global warming of 1.5°C above pre-industrial levels and related global greenhouse gas emission pathways, in the context of strengthening the global response to the threat of climate change* (pp. 93–174). In Press. https://doi.org/https://www.ipcc.ch/sr15/chapter/chapter-2/

Saha, A., Pal, S. C., Chowdhuri, I., Ruidas, D., Chakrabortty, R., Roy, P., & Shit, M. (2021). Impact of firecrackers burning and policy-practice gap on air quality in Delhi during Indian's great mythological event of Diwali festival. *Cities*, *119*, 103384. https://doi.org/https://doi.org/10.1016/j.cities.2021.103384

Saha, S., Moorthi, S., Wu, X., Wang, J., Nadiga, S., Tripp, P., Behringer, D., Hou, Y.-T., Chuang, H., Iredell, M., Ek, M., Meng, J., Yang, R., Mendez, M. P., van den Dool, H., Zhang, Q., Wang, W., Chen, M., & Becker, E. (2011). *NCEP Climate Forecast System Version 2 (CFSv2) 6-hourly Products*. Research Data Archive at the National Center for Atmospheric Research, Computational and Information Systems Laboratory. https://rda.ucar.edu/datasets/dsd094000/

Sahu, L. K., Lal, S., Thouret, V., & Smit, H. G. (2011). Climatology of tropospheric ozone and water vapour over Chennai: A study based on MOZAIC measurements over India. *International Journal of Climatology*, *31*(6), 920–936. https://doi.org/10.1002/joc.2128

Sahu, S. K., Sharma, S., Zhang, H., Chejarla, V., Guo, H., Hu, J., Ying, Q., Xing, J., & Kota, S. H. (2020). Estimating ground level PM(2.5) concentrations and associated health risk in India using satellite based AOD and WRF predicted meteorological parameters. *Chemosphere*, *255*, 126969. https://doi.org/10.1016/j.chemosphere.2020.126969

Salmond, J., & McKendry, I. G. (2005). Turbulence in the very stable nocturnal boundary layer: Implications for air pollution. *Progress in Physical Geography*, *29*(2), 171–188. https://doi.org/10.1191/0309133305pp442ra

Samset, B. H., Myhre, G., Forster, P. M., Hodnebrog, Ø., Andrews, T., Boucher, O., Faluvegi, G., Fläschner, D., Kasoar, M., Kharin, V., Kirkevåg, A., Lamarque, J.-F., Olivié, D., Richardson, T. B., Shindell, D., Takemura, T., & Voulgarakis, A. (2018). Weak hydrological sensitivity to temperature change over land, independent of climate forcing. *Npj Climate and Atmospheric Science*, *1*(1), 20173. https://doi.org/10.1038/s41612-017-0005-5

Sathyanadh, A., Prabha, T. V, Balaji, B., Resmi, E. A., & Karipot, A. (2017). Evaluation of WRF PBL parameterization schemes against direct observations during a dry event over the Ganges valley. *Atmospheric Research*, *193*, 125–141. https://doi.org/https://doi.org/10.1016/j.atmosres.2017.02.016

Sawlani, R., Agnihotri, R., Sharma, C., Patra, P. K., Dimri, A. P., Ram, K., & Verma, R. L. (2019). The severe Delhi SMOG of 2016: A case of delayed crop residue burning, coincident firecracker emissions, and atypical meteorology. *Atmospheric Pollution Research*, *10*(3), 868–879. https://doi.org/https://doi.org/10.1016/j.apr.2018.12.015

Schell, B., Ackermann, I. J., Hass, H., Binkowski, F. S., & Ebel, A. (2001). Modeling the formation of secondary organic aerosol within a comprehensive air quality model system. *Journal of Geophysical Research: Atmospheres*, *106*(D22), 28275–28293. https://doi.org/https://doi.org/10.1029/2001JD000384

Schlatter, T. W. (2010). Vertical Structure of the Atmosphere. In *Encyclopedia of Aerospace Engineering*. John Wiley & Sons, Ltd. https://doi.org/https://doi.org/10.1002/9780470686652.eae582

Schnell, J. L., Naik, V., Horowitz, L. W., Paulot, F., Mao, J., Ginoux, P., Zhao, M., & Ram, K. (2018). Exploring the relationship between surface PM$_{2.5}$ and meteorology in Northern India. *Atmospheric Chemistry and Physics*, *18*(14), 10157–10175. https://doi.org/10.5194/acp-18-10157-2018

Seay, B., Adetona, A., Sadoff, N., Sarofim, M. C., & Kolian, M. (2021). Impact of South Asian brick kiln emission mitigation strategies on select pollutants and near-term Arctic temperature responses. *Environmental Research Communications*, *3*(6), 1–11. https://doi.org/10.1088/2515-7620/ac0a66

Seinfeld, J. H., Pandis, S. N., & Noone, K. J. (1998). Atmospheric Chemistry and Physics: From Air Pollution to Climate Change. *Physics Today*, *51*, 88–90. https://api.semanticscholar.org/CorpusID:98232768

Selvam, S., Muthukumar, P., Venkatramanan, S., Roy, P. D., Manikanda Bharath, K., & Jesuraja, K. (2020). SARS-CoV-2 pandemic lockdown: Effects on air quality in the industrialized Gujarat state of India. *Science of The Total Environment*, *737*, 140391. https://doi.org/https://doi.org/10.1016/j.scitotenv.2020.140391

Sharma, A., Srivastava, S., Mitra, D., & Singh, R. P. (2023). Spatiotemporal distribution of air pollutants during a heat wave–induced forest fire event in Uttarakhand. *Environmental Science and Pollution Research*, *30*(51), 110133–110160. https://doi.org/10.1007/s11356-023-29906-7

Sharma, D., & Mauzerall, D. (2022). Analysis of Air Pollution Data in India between 2015 and 2019. *Aerosol and Air Quality Research*, *22*(2). https://doi.org/10.4209/aaqr.210204

Sharma, S., Zhang, M., Anshika, Gao, J., Zhang, H., & Kota, S. H. (2020). Effect of restricted emissions during COVID-19 on air quality in India. *Science of The Total Environment*, *728*, 138878. https://doi.org/https://doi.org/10.1016/j.scitotenv.2020.138878

Shenfeld, L. (1970). Ontario's Air Pollution Index and Alert System. *Journal of the Air Pollution Control Association*, *20*(9), 612. https://doi.org/10.1080/00022470.1970.10469451

Shrivastava, R., Dash, S. K., Oza, R. B., & Sharma, D. N. (2014). Evaluation of Parameterization Schemes in the WRF Model for Estimation of Mixing Height. *International Journal of Atmospheric Sciences*, *2014*(1), 451578. https://doi.org/https://doi.org/10.1155/2014/451578

Sicard, P., De Marco, A., Agathokleous, E., Feng, Z., Xu, X., Paoletti, E., Rodriguez, J. J. D., & Calatayud, V. (2020). Amplified ozone pollution in cities during the COVID-19 lockdown. *Science of The Total Environment*, *735*, 139542. https://doi.org/10.1016/j.scitotenv.2020.139542

Sikder, M. S., & Hossain, F. (2019). Improving operational flood forecasting in monsoon climates with bias-corrected quantitative forecasting of precipitation. *International Journal of River Basin Management*, *17*(4), 411–421. https://doi.org/10.1080/15715124.2018.1476368

Singh, A., Rastogi, N., Kumar, V., Slowik, J. G., Satish, R., Lalchandani, V., Thamban, N. M., Rai, P., Bhattu, D., Vats, P., Ganguly, D., Tripathi, S. N., & Prévôt, A. S. H. (2021). Sources and characteristics of light-absorbing fine particulates over Delhi through the synergy of real-time optical and chemical measurements. *Atmospheric Environment*, *252*, 118338. https://doi.org/https://doi.org/10.1016/j.atmosenv.2021.118338

Singh, K. S., Bonthu, S., Purvaja, R., Robin, R. S., Kannan, B. A. M., & Ramesh, R. (2018). Prediction of heavy rainfall over Chennai Metropolitan City, Tamil Nadu, India: Impact of

microphysical parameterization schemes. *Atmospheric Research*, *202*, 219–234. https://doi.org/https://doi.org/10.1016/j.atmosres.2017.11.028

Singh, N., Agarwal, S., Sharma, S., Chatani, S., & Ramanathan, V. (2021). Air Pollution Over India: Causal Factors for the High Pollution with Implications for Mitigation. *ACS Earth and Space Chemistry*, *5*(12), 3297–3312. https://doi.org/10.1021/acsearthspacechem.1c00170

Singh, R. P., & Chauhan, A. (2020). Impact of lockdown on air quality in India during COVID-19 pandemic. *Air Quality, Atmosphere & Health*, *13*(8), 921–928. https://doi.org/10.1007/s11869-020-00863-1

Singh, T., Biswal, A., Mor, S., Ravindra, K., Singh, V., & Mor, S. (2020). A high-resolution emission inventory of air pollutants from primary crop residue burning over Northern India based on VIIRS thermal anomalies. *Environmental Pollution*, *266*, 115132. https://doi.org/https://doi.org/10.1016/j.envpol.2020.115132

Singh, V., Singh, S., Biswal, A., Kesarkar, A. P., Mor, S., & Ravindra, K. (2020). Diurnal and temporal changes in air pollution during COVID-19 strict lockdown over different regions of India. *Environmental Pollution (Barking, Essex : 1987)*, *266*(Pt 3), 115368. https://doi.org/10.1016/j.envpol.2020.115368

Skamarock, W. C., Klemp, J. B., Dudhia, J., Gill, D. O., Barker, D. M., Duda, M. G., Huang, X.-Y., Wang, W., & Powers, J. G. (2008). A Description of the Advanced Research WRF Version 3. *NCAR Technical Note NCAR/TN-475+STR. June 2008. Mesoscale and Microscale Meteorology Division. National Center for Atmospheric Research. Boulder*, *475*, 1. https://doi.org/10.5065/D68S4MVH

Skamarock, W. C., Klemp, J. B., Dudhia, J., Gill, D. O., Barker, D. M., Duda, M. G., Huang, X.-Y., Wang, W., & Powers, J. G. (2019). *A Description of the Advanced Research WRF Version 4*. https://doi.org/https://doi.org/10.5065/1dfh-6p97 (Original work published 2019)

Smith, S. J., Van Aardenne, J., Klimont, Z., Andres, R. J., Volke, A., & Delgado Arias, S. (2011). Anthropogenic sulfur dioxide emissions: 1850-2005. *Atmospheric Chemistry and Physics*, *11*(3), 1101–1116. https://doi.org/10.5194/acp-11-1101-2011

Srinivas, C. V, Hariprasad, D., Bhaskar Rao, D. V, Anjaneyulu, Y., Baskaran, R., & Venkatraman, B. (2013). Simulation of the Indian summer monsoon regional climate using advanced research WRF model. *International Journal of Climatology*, *33*(5), 1195–1210. https://doi.org/https://doi.org/10.1002/joc.3505

Srinivas, C. V, Yesubabu, V., Hari Prasad, D., Hari Prasad, K. B. R. R., Greeshma, M. M., Baskaran, R., & Venkatraman, B. (2018). Simulation of an extreme heavy rainfall event over Chennai, India using WRF: Sensitivity to grid resolution and boundary layer physics. *Atmospheric Research*, *210*, 66–82.

https://doi.org/https://doi.org/10.1016/j.atmosres.2018.04.014

Srivastava, Shuchita, Behera, S., & Mitra, D. (2024). Distribution of ozone, carbon monoxide and oxides of nitrogen over an urban location in the foothills of the North-Western Himalayas. *Urban Climate*, *55*, 101913. https://doi.org/https://doi.org/10.1016/j.uclim.2024.101913

Srivastava, Sudhakar, Kumar, A., Bauddh, K., Gautam, A. S., & Kumar, S. (2020). 21-Day Lockdown in India Dramatically Reduced Air Pollution Indices in Lucknow and New Delhi, India. *Bulletin of Environmental Contamination and Toxicology*, *105*(1), 9–17. https://doi.org/10.1007/s00128-020-02895-w

Stensrud, D. J. (2011). *Parameterization schemes: Keys to understanding numerical weather prediction models* (Vol. 9780521865). Cambridge University Press. https://doi.org/10.1017/CBO9780511812590

Stull, R. B. (1988). *An Introduction to Boundary Layer Meteorology* (R. B. Stull (ed.); Kluwer Aca). Springer Dordrecht. https://doi.org/https://doi.org/10.1007/978-94-009-3027-8

Thompson, G., Field, P. R., Rasmussen, R. M., & Hall, W. D. (2008). Explicit Forecasts of Winter Precipitation Using an Improved Bulk Microphysics Scheme. Part II: Implementation of a New Snow Parameterization. *Monthly Weather Review*, *136*(12), 5095–5115. https://doi.org/10.1175/2008MWR2387.1

Tibrewal, K., & Venkataraman, C. (2022). COVID-19 lockdown closures of emissions sources in India: Lessons for air quality and climate policy. *Journal of Environmental Management*, *302*, 114079. https://doi.org/https://doi.org/10.1016/j.jenvman.2021.114079

Tibrewal, K., Venkataraman, C., Phuleria, H., Joshi, V., Maithel, S., Damle, A., Gupta, A., Lokhande, P., Rabha, S., Saikia, B. K., Roy, S., Habib, G., Rathi, S., Goel, A., Ahlawat, S., Mandal, T. K., Azharuddin Hashmi, M., Qureshi, A., Dhandapani, A., … Sinha, B. (2023). Reconciliation of energy use disparities in brick production in India. *Nature Sustainability*, *6*(10), 1248–1257. https://doi.org/10.1038/s41893-023-01165-x

Tickell, A., & Ranasinha, R. (2018). Delhi: New writings on the megacity. *Journal of Postcolonial Writing*, *54*(3), 297–306. https://doi.org/10.1080/17449855.2018.1461977

Tie, X., Brasseur, G., Emmons, L., Horowitz, L., & Kinnison, D. (2001). Effects of aerosols on tropospheric oxidants: A global model study. *Journal of Geophysical Research: Atmospheres*, *106*(D19), 22931–22964. https://doi.org/https://doi.org/10.1029/2001JD900206

Tie, X., Madronich, S., Walters, S., Zhang, R., Rasch, P., & Collins, W. (2003). Effect of clouds on photolysis and oxidants in the troposphere. *Journal of Geophysical Research: Atmospheres*, *108*(D20). https://doi.org/https://doi.org/10.1029/2003JD003659

Tobler, A., Bhattu, D., Canonaco, F., Lalchandani, V., Shukla, A., Thamban, N. M., Mishra, S.,

Srivastava, A. K., Bisht, D. S., Tiwari, S., Singh, S., Močnik, G., Baltensperger, U., Tripathi, S. N., Slowik, J. G., & Prévôt, A. S. H. (2020). Chemical characterization of PM2.5 and source apportionment of organic aerosol in New Delhi, India. *Science of The Total Environment*, *745*, 140924. https://doi.org/https://doi.org/10.1016/j.scitotenv.2020.140924

Unger, N., Bond, T. C., Wang, J. S., Koch, D. M., Menon, S., Shindell, D. T., & Bauer, S. (2010). Attribution of climate forcing to economic sectors. *Proceedings of the National Academy of Sciences*, *107*(8), 3382–3387. https://doi.org/10.1073/pnas.0906548107

Upadhyay, A., Dey, S., Chowdhury, S., & Goyal, P. (2018). Expected health benefits from mitigation of emissions from major anthropogenic PM2.5 sources in India: Statistics at state level. *Environmental Pollution*, *242*, 1817–1826. https://doi.org/https://doi.org/10.1016/j.envpol.2018.07.085

Vadrevu, K. P., Ellicott, E., Badarinath, K. V. S., & Vermote, E. (2011). MODIS derived fire characteristics and aerosol optical depth variations during the agricultural residue burning season, north India. *Environmental Pollution*, *159*(6), 1560–1569. https://doi.org/10.1016/j.envpol.2011.03.001

Venkataraman, C, Brauer, M., Tibrewal, K., Sadavarte, P., Ma, Q., Cohen, A., Chaliyakunnel, S., Frostad, J., Klimont, Z., Martin, R. V, Millet, D. B., Philip, S., Walker, K., & Wang, S. (2018). Source influence on emission pathways and ambient PM$_{2.5}$ pollution over India (2015--2050). *Atmospheric Chemistry and Physics*, *18*(11), 8017–8039. https://doi.org/10.5194/acp-18-8017-2018

Venkataraman, C, Habib, G., Kadamba, D., Shrivastava, M., Leon, J.-F., Crouzille, B., Boucher, O., & Streets, D. G. (2006). Emissions from open biomass burning in India: Integrating the inventory approach with high-resolution Moderate Resolution Imaging Spectroradiometer (MODIS) active-fire and land cover data. *Global Biogeochemical Cycles*, *20*(2). https://doi.org/10.1029/2005GB002547

Venkataraman, C, Sagar, A. D., Habib, G., Lam, N., & Smith, K. R. (2010). The Indian National Initiative for Advanced Biomass Cookstoves: The benefits of clean combustion. *Energy for Sustainable Development*, *14*(2), 63–72. https://doi.org/https://doi.org/10.1016/j.esd.2010.04.005

Venkataraman, Chandra, Anand, A., Maji, S., Barman, N., Tiwari, D., Muduchuru, K., Sharma, A., Gupta, G., Bhardwaj, A., Haswani, D., Pullokaran, D., Yadav, K., Sunder Raman, R., Imran, M., Habib, G., Kapoor, T. S., Anurag, G., Sharma, R., Phuleria, H. C., … Singh, V. (2024). Drivers of PM2.5 Episodes and Exceedance in India: A Synthesis From the COALESCE Network. *Journal of Geophysical Research: Atmospheres*, *129*(14), e2024JD040834. https://doi.org/https://doi.org/10.1029/2024JD040834

Villalobos, A. M., Amonov, M. O., Shafer, M. M., Devi, J. J., Gupta, T., Tripathi, S. N., Rana, K. S., Mckenzie, M., Bergin, M. H., & Schauer, J. J. (2015). Source apportionment of carbonaceous fine particulate matter (PM2.5) in two contrasting cities across the Indo–Gangetic Plain. *Atmospheric Pollution Research*, *6*(3), 398–405. https://doi.org/https://doi.org/10.5094/APR.2015.044

Vohra, K., S., M., Chakraborty, A., Shah, H., AS., B., & Pakki, J. (2025). Urgent issues regarding real-time air quality monitoring data in India: Unveiling solutions and implications for policy and health. *Atmospheric Environment: X*, *25*, 100308. https://doi.org/https://doi.org/10.1016/j.aeaoa.2024.100308

Vohra, K., Vodonos, A., Schwartz, J., Marais, E. A., Sulprizio, M. P., & Mickley, L. J. (2021). Global mortality from outdoor fine particle pollution generated by fossil fuel combustion: Results from GEOS-Chem. *Environmental Research*, *195*, 110754. https://doi.org/https://doi.org/10.1016/j.envres.2021.110754

Wallace, J. M., & Hobbs, P. V. (2006). 2 - The Earth System. In J. M. Wallace & P. V Hobbs (Eds.), *Atmospheric Science (Second Edition)* (Second Edi, pp. 25–61). Academic Press. https://doi.org/https://doi.org/10.1016/B978-0-12-732951-2.50007-7

Wang, P., Chen, K., Zhu, S., Wang, P., & Zhang, H. (2020). Severe air pollution events not avoided by reduced anthropogenic activities during COVID-19 outbreak. *Resources, Conservation and Recycling*, *158*, 104814. https://doi.org/10.1016/j.resconrec.2020.104814

Wang, Y., & Akbari, H. (2016). Analysis of urban heat island phenomenon and mitigation solutions evaluation for Montreal. *Sustainable Cities and Society*, *26*, 438–446. https://doi.org/https://doi.org/10.1016/j.scs.2016.04.015

Warner, T. T. (2010). Operational numerical weather prediction. In *Numerical Weather and Climate Prediction* (pp. 358–365). Cambridge University Press.

Wiedinmyer, C., Akagi, S. K., Yokelson, R. J., Emmons, L. K., Al-Saadi, J. A., Orlando, J. J., & Soja, A. J. (2011). The Fire INventory from NCAR (FINN): a high resolution global model to estimate the emissions from open burning. *Geoscientific Model Development*, *4*(3), 625–641. https://doi.org/10.5194/gmd-4-625-2011

Wiedinmyer, C., Kimura, Y., McDonald-Buller, E. C., Emmons, L. K., Buchholz, R. R., Tang, W., Seto, K., Joseph, M. B., Barsanti, K. C., Carlton, A. G., & Yokelson, R. (2023). The Fire Inventory from NCAR version 2.5: an updated global fire emissions model for climate and chemistry applications. *Geoscientific Model Development*, *16*(13), 3873–3891. https://doi.org/10.5194/gmd-16-3873-2023

Xie, Y., Zhou, M., Hunt, K. M. R., & Mauzerall, D. L. (2024). Recent PM2.5 air quality improvements in India benefited from meteorological variation. *Nature Sustainability*, *7*(8),

983–993. https://doi.org/10.1038/s41893-024-01366-y

Yerramilli, A., Challa, V. S., Dodla, V. B. R., Myles, L., Pendergrass, W. R., Vogel, C. A., Tuluri, F., Baham, J. M., Hughes, R., Patrick, C., Young, J., & Swanier, S. (2012). Simulation of surface ozone pollution in the Central Gulf Coast region during summer synoptic condition using WRF/Chem air quality model. *Atmospheric Pollution Research*, *3*(1), 55–71. https://doi.org/https://doi.org/10.5094/APR.2012.005

Yin, L., Du, P., Zhang, M., Liu, M., Xu, T., & Song, Y. (2019). Estimation of emissions from biomass burning in China (2003--2017) based on MODIS fire radiative energy data. *Biogeosciences*, *16*(7), 1629–1640. https://doi.org/10.5194/bg-16-1629-2019

Zaveri, R. A., Easter, R. C., Fast, J. D., & Peters, L. K. (2008). Model for Simulating Aerosol Interactions and Chemistry (MOSAIC). *Journal of Geophysical Research: Atmospheres*, *113*(D13). https://doi.org/https://doi.org/10.1029/2007JD008782

Zaveri, R. A., & Peters, L. K. (1999). A new lumped structure photochemical mechanism for large-scale applications. *Journal of Geophysical Research: Atmospheres*, *104*(D23), 30387–30415. https://doi.org/https://doi.org/10.1029/1999JD900876

Zeyaeyan, S., Fattahi, E., Ranjbar, A., Azadi, M., & Vazifedoust, M. (2017). Evaluating the Effect of Physics Schemes in WRF Simulations of Summer Rainfall in North West Iran. *Climate*, *5*(3). https://doi.org/10.3390/cli5030048

Zhang, A., Wang, Y., Zhang, Y., Weber, R. J., Song, Y., Ke, Z., & Zou, Y. (2020). Modeling the global radiative effect of brown carbon: A potentially larger heating source in the tropical free troposphere than black carbon. *Atmospheric Chemistry and Physics*, *20*, 1901–1920. https://doi.org/10.5194/acp-20-1901-2020

Zhang, H., Wang, Y., Park, T.-W., & Deng, Y. (2017). Quantifying the relationship between extreme air pollution events and extreme weather events. *Atmospheric Research*, *188*, 64–79. https://doi.org/10.1016/j.atmosres.2016.11.010

Zhang, J., Liu, L., Wang, Y., Ren, Y., Wang, X., Shi, Z., Zhang, D., Che, H., Zhao, H., Liu, Y., Niu, H., Chen, J., Zhang, X., Lingaswamy, A. P., Wang, Z., & Li, W. (2017). Chemical composition, source, and process of urban aerosols during winter haze formation in Northeast China. *Environmental Pollution*, *231*, 357–366. https://doi.org/https://doi.org/10.1016/j.envpol.2017.07.102

Zhang, M., Katiyar, A., Zhu, S., Shen, J., Xia, M., Ma, J., Kota, S. H., Wang, P., & Zhang, H. (2021). Impact of reduced anthropogenic emissions during COVID-19 on air quality in India. *Atmospheric Chemistry and Physics*, *21*(5), 4025–4037. https://doi.org/10.5194/acp-21-4025-2021

Zhang, W., Rutledge, S. A., Xu, W., & Zhang, Y. (2019). Inner-core lightning outbreaks and

convective evolution in Super Typhoon Haiyan (2013). *Atmospheric Research*, *219*, 123–139. https://doi.org/https://doi.org/10.1016/j.atmosres.2018.12.028

Zhang, X., Yuan, C., & Zhuang, Z. (2021). Exploring the Change in PM2.5 and Ozone Concentrations Caused by Aerosol–Radiation Interactions and Aerosol–Cloud Interactions and the Relationship with Meteorological Factors. *Atmosphere*, *12*(12). https://doi.org/10.3390/atmos12121585

Zhang, Y. (2008). Online-coupled meteorology and chemistry models: history, current status, and outlook. *Atmospheric Chemistry and Physics*, *8*(11), 2895–2932. https://doi.org/10.5194/acp-8-2895-2008

Zhang, Yang, Wen, X.-Y., & Jang, C. J. (2010). Simulating chemistry–aerosol–cloud–radiation–climate feedbacks over the continental U.S. using the online-coupled Weather Research Forecasting Model with chemistry (WRF/Chem). *Atmospheric Environment*, *44*(29), 3568–3582. https://doi.org/https://doi.org/10.1016/j.atmosenv.2010.05.056

Zhao, Y., Nielsen, C. P., Lei, Y., McElroy, M. B., & Hao, J. (2011). Quantifying the uncertainties of a bottom-up emission inventory of anthropogenic atmospheric pollutants in China. *Atmospheric Chemistry and Physics*, *11*(5), 2295–2308. https://doi.org/10.5194/acp-11-2295-2011

Zhou, M., Xie, Y., Wang, C., Shen, L., & Mauzerall, D. L. (2024). Impacts of current and climate induced changes in atmospheric stagnation on Indian surface PM2.5 pollution. *Nature Communications*, *15*(1), 7448. https://doi.org/10.1038/s41467-024-51462-y

Zittis, G., Bruggeman, A., Hadjinicolaou, P., Camera, C., & Lelieveld, J. (2018). Effects of Meteorology Nudging in Regional Hydroclimatic Simulations of the Eastern Mediterranean. *Atmosphere*, *9*(12). https://doi.org/10.3390/atmos9120470

List of Publication

1. ***Nandi, I.**, Kumar, A., Imam, F., Ganguly, D., & Dey, S. (2025). COVID-19 lockdown was insufficient to bring India's PM2.5 levels below national standards. Environmental Research Communications, 7(5), 55005. https://doi.org/10.1088/2515-7620/add3d4*

2. ***Nandi, I.**, & Ganguly, D. (2026). Toward reliable air quality simulations over India: optimizing WRF-Chem through comprehensive sensitivity analysis of meteorology, physical parameterizations, and emission inventories. Environmental Science: Atmospheres, https://doi.org/10.1039/d5ea00167f*

3. ***Nandi, I.**, Ganguly, D., Habib, G., & Dey, S. (2026). Delhi cannot clean its air alone: airshed-scale mitigation outperforms local controls even under unfavourable winter meteorology. npj Clean Air, https://doi.org/10.1038/s44407-026-00065-6*

4. *Anand K A, A., Ganguly, D., **Nandi, I.**, Kajino, M., & Dey, S. (2025). Disentangling the Separate and Combined Effects of Aerosol-Radiation and Aerosol-Photolysis Interactions on Air Quality Over India. Journal of Geophysical Research: Atmospheres, 130(24), e2025JD045316. https://doi.org/https://doi.org/10.1029/2025JD045316*

5. *Maity, R., **Nandi, I.**, Kumar, A., Singh, V., Ganguly, D., & Kumar, M. (2026). Regional Power Emissions and Heterogeneous Chemistry Drive Extreme Sulfate Levels in Delhi. ACS ES&T Air. https://doi.org/10.1021/acsestair.5c00407*

Conferences

- ***Nandi, I.,** & Ganguly, D. (2023, December). Sensitivity of simulated air pollution levels over India to choices of physical parameterizations, chemistry schemes, and emission inventory using WRF-Chem model. In American Geophysical Union (AGU) 2023 Fall Meeting, (Online).*

- ***Nandi, I.,** Ganguly, D., & Dey, S. (2024, April). Assessing the impacts of emission reduction and meteorology change on India's air quality during COVID-19 lockdown using the WRF-Chem model. In European Geosciences Union (EGU) General Assembly 2024, Vienna, Austria.*

INDRANIL **NANDI**

PH.D. STUDENT AT IIT DELHI. RESEARCH: REGIONAL CLIMATE MODELLING, AIR POLLUTION, DATA ASSIMILATION, REMOTE SENSING, POLLUTANT EMISSION
Centre for Atmospheric Sciences (CAS), Indian Institute of Technology Delhi, Hauz Khas, New Delhi 110016, India.
(+91) 8902005948 | indranilnandi2011@gmail.com / Indranil.Nandi@cas.iitd.ac.in | R^G https://www.researchgate.net/profile/Indranil-Nandi

https://orcid.org/0009-0001-8224-4804

Education

IIT Delhi, Ph.D. (Coursework: Atmospheric Sciences)	CGPA : 9/10	2019-20	*New Delhi, India*
IIRS (ISRO)-AU, M.Tech (Remote Sensing & GIS)	CGPA : 7.64/10	2015-17	*Dehradun, India*
University of Calcutta, M.Sc. (Marine Science)	Percentage: 65.5%	2013-15	*Kolkata, India*
University of Calcutta, B.Sc. (Chemistry Hons.)	Percentage: 56.25%	2010-13	*Kolkata, India*
W.B.C.H.S.E, West Bengal, (Class 12th)	Percentage: 85.2%	2008-10	*Kolkata, India*
W.B.B.S.E, West Bengal, (Class 10th)	Percentage: 82.12%	2006-08	*Kolkata, India*

Publications

2019 Srivastava, S., **Nandi, I.**, Yarragunta, Y., & Kumar, A. S., ***Carbon Monoxide Plume over Northwestern Himalaya: A Remote Sensing and Modeling Approach.*** R. R. Navalgund et al. (Ed.), *Remote Sensing of Northwest Himalayan Ecosystems*. Singapore: Springer Nature Singapore Pte Ltd. 2019. Retrieved from *https://doi.org/10.1007/978-981-13-2128-3_15*

2020 **Nandi, I.,** Srivastava, S., Yarragunta, Y., Kumar, R., & Mitra, D., ***Distribution of surface carbon monoxide over the Indian subcontinent: Investigation of source contributions using WRF-Chem. Atmospheric Environment,*** *243*, 117838. *https://doi.org/https://doi.org/10.1016/j.atmosenv.2020.117838*

2023 **Nandi, I.,** & Ganguly, D. (2023, December). Sensitivity of simulated air pollution levels over India to choices of physical parameterizations, chemistry schemes, and emission inventory using WRF-Chem model. **In *American Geophysical Union (AGU) 2023 Fall Meeting*, (Online).**

2024 **Nandi, I.,** Ganguly, D., & Dey, S. (2024, April). Assessing the impacts of emission reduction and meteorology change on India's air quality during COVID-19 lockdown using the WRF-Chem model. **In *European Geosciences Union (EGU) General Assembly 2024*, Vienna, Austria.**

2025 **Nandi, I.,** A. Kumar, F. Imam, D. Ganguly, and S. Dey (2025), **COVID-19 Lockdown Was Insufficient to Bring India's $PM_{2.5}$ Levels Below National Standards.** ***Environmental Research Communications*,** *https:doi.org/10.1088/2515-7620/add3d4*

2026 **Nandi, I.**, & Ganguly, D. (2026). **Toward reliable air quality simulations over India: optimizing WRF-Chem through comprehensive sensitivity analysis of meteorology, physical parameterizations, and emission inventories.** Environmental Science: Atmospheres, *https://doi.org/10.1039/d5ea00167f*

2026 **Nandi, I.**, Ganguly, D., Habib, G., & Dey, S. (2026). **Delhi cannot clean its air alone: airshed-scale mitigation outperforms local controls even under unfavourable winter meteorology.** npj Clean Air, *https://doi.org/10.1038/s44407-026-00065-6*

2026 Maity, R., **Nandi, I.,** Kumar, A., Singh, V., Ganguly, D., & Kumar, M. (2026). **Regional Power Emissions and Heterogeneous Chemistry Drive Extreme Sulfate Levels in Delhi.** ACS ES&T Air. *https://doi.org/10.1021/acsestair.5c00407*

Current Position

Centre for Atmospheric Sciences, IIT Delhi — *New Delhi, India*

PURSUING REGULAR PH.D. UNDER MOE, GOVT.OF INDIA FELLOWSHIP SCHEME **(Thesis Submitted on 19-12-2025)** — *July 2019 to Present*

- **Thesis Title: ASSESSING SECTORAL AND PRIMARY EMISSION CONTRIBUTIONS TO $PM_{2.5}$ POLLUTION OVER NORTH INDIA USING REGIONAL AIR QUALITY MODELLING**
- **Supervisor: Prof. Dilip Ganguly (CAS, IIT Delhi)**

Scholastic Achievements

Jan 2018 to Jun 2019

Worked as **Junior Research Fellow** (JRF) under MoEFCC sponsored project entitled, **"National Carbonaceous Aerosol Programme (NCAP) working Group III"** at Centre for Atmospheric Sciences, Indian Institute of Technology Delhi under the supervision of project **PI: Prof. Dilip Ganguly** (Centre for Atmospheric Sciences, IIT Delhi, India).

Worked as a **Project Assistant** under ISRO GBP sponsored project entitled **"Study of air pollutant over the Indian**

Jun 2016 to Aug 2017	**subcontinent: Investigation of source regions"** under the supervision of project **PI: Dr. Shuchita Srivastava** (Atmospheric Sciences Department, Indian Institute of Remote Sensing, ISRO, Dehradun, India).
2015-2017	Awarded **Golden Jubilee Fellowship** from Indian Institute of Remote Sensing, ISRO, Dehradun, India.
2010-2015	Achieved **Inspire Scholarship for Higher Education (SHE)** From Dept. of Science and Technology, Govt. of India.

Skills

Programming	**MATLAB, R , PYTHON**
Operating Systems	**Linux, Mac, Windows with experience to work with High Performance Parallel Computing System (HPCs)**
Modelling	**Regional Climate Modelling using WRF / WRF-Chem (v4.2.2), Proficiency with Four-Dimensional Data Assimilation (FDDA, Grid Nudging), Global Climate Modelling using MOZART – 4, CESM2 and Pollution Dispersion Modelling using AERMAP, AERMET, AERMOD. Global and Regional Sector Specific Primary Pollutant Emission Preparation and Emission Contribution Analysis.**
Visualization	**NCAR Command Language (NCL), NCO, CDO, ERDAS, ENVI, ArcGIS, QGIS, SIGMA PLOT**

Professional Summary

- **Capable in Numerical Weather Hindcast and Forecast experiments and Regional Climate Modelling applications in fields of Atmospheric Science. Air Quality Modelling with full interaction of Chemical Species. Prediction of Primary Pollutants like Carbon Monoxide (CO), Sulfur Dioxide (SO_2), Nitrogen Oxides (NOx), Secondary Pollutants like Ozone (O_3), Sulfate (SO_4) as well as Aerosol Species like Particulate Matter (PM_{10} and $PM_{2.5}$), Dust, Sea Salt, Nitrate Aerosols etc.**

- **Proficient in satellite retrievals and atmospheric remote sensing product processing, I specialize in developing thorough statistics and scoreboards to ensure meticulous evaluation of models and experimental outcomes, prioritizing robustness and accuracy. My deep understanding of satellite retrievals and atmospheric sensing principles allows me to effectively mentor and support team members, promoting collaboration and knowledge sharing.**

- **Equally productive on solo projects or as part of a team. Flexible when faced with changing priorities. Willingness to quickly adapt to new Environments & Technologies.**

Personal Details

Permanent Address:	**West Das Para (Vidyasagar Sarani), Sonarpur, Kolkata:700150, West Bengal, India.**
Present Address:	**Room No. 311, Centre for Atmospheric Sciences, Block 6, IIT Delhi, Hauz Khas, New Delhi: 110016, India**
Date of Birth:	**11-07-1992 (DD-MM-YYYY)**
Marital Status:	**Married**

I hereby declare that above-mentioned information is correct to the best of my knowledge and belief.



Indranil Nandi